Heinrich Heine
Universität Düsseldorf

Individualised Medicines by Pharmaceutical Inkjet Printing onto Orodispersible Films

Inaugural-Dissertation

zur Erlangung des Doktorgrades
der Mathematisch-Naturwissenschaftlichen Fakultät
der Heinrich-Heine-Universität Düsseldorf

vorgelegt von

Olga Kiefer (geb. Kapelnikova)
aus Charkiw

Düsseldorf, Januar 2022

aus dem Institut für Pharmazeutische Technologie und Biopharmazie
der Heinrich-Heine-Universität Düsseldorf

Gedruckt mit der Genehmigung der
Mathematisch-Naturwissenschaftlichen Fakultät der
Heinrich-Heine-Universität Düsseldorf

Berichterstatter:

1. Prof. Dr. Jörg Breitkreutz
2. Prof. Dr. Anne Seidlitz

Tag der mündlichen Prüfung: 03.03.2022

Es scheint unmöglich. Bis Du es machst.

- Hornbach -

Publications

Parts of this doctoral thesis have already been published in peer-reviewed journals or at conferences:

Peer-reviewed Papers

Tian Y., Orlu M., Woerdenbag H. J., Scarpa M., Kiefer O., Kottke D., Sjöholm E., Öblom H., Sandler N., Hinrichs W. L. J., Breitkreutz J., Visser J. C., 2019. *Oromucosal films: from patient centricity to production by printing techniques*, Expert Opin Drug Deliv 16, 981–993

Personal contribution: 10%

OK contributed to one quarter to the development of the study design. The idea for this manuscript originates from CV. OK wrote the paragraph about pharmaceutical inkjet printing and participated in the discussion. She also contributed to the manuscript revision.

Visser J. C., Wibier L., Kiefer O., Orlu M., Breitkreutz J., Woerdenbag H. J., Taxis K., 2020. *A Pediatrics Utilization study in The Netherlands to identify active pharmaceutical ingredients suitable for inkjet printing on orodispersible films*, Pharmaceutics 12 (2), 164.

Personal contribution: 15%

OK contributed to the development of the study design together with CV who was responsible for the main manuscript idea. OK contributed more than a third to the writing and revision of the manuscript.

Kiefer O., Breitkreutz J., 2020. *Comparative investigations on key factors and print head designs for pharmaceutical inkjet printing*, Int J Pharm 586, 119561.

DOI: 10.1016/j.ijpharm.2020.119561

Personal contribution: 90%

OK was responsible for the idea and study design of this manuscript. She carried out the experimental implementation and data evaluation. JB gave support in the creation of the concept and evaluation of the results. OK wrote and corrected the manuscript independently. JB supervised the work and revised the manuscript.

Kiefer O., Fischer B., Breitkreutz J., 2021. *Fundamental investigations into metoprolol tartrate deposition on orodispersible films by inkjet printing for individualised drug dosing*, Pharmaceutics 13 (2), 247.

DOI: 10.3390/pharmaceutics13020247

Personal contribution: 80%

OK developed the idea and study design in cooperation with BF and JB. OK performed the experimental work and data evaluation with support of BF regarding the confocal Raman microscopy and images. OK wrote and corrected the manuscript independently with support of BF. JB supervised the work and revised the manuscript.

Oral Presentations

Kiefer O., Fischer B., Breitkreutz J., 2021. *Investigations on inkjet printed metoprolol tartrate orodispersible films for paediatric application*, virtual 12th PBP World Meeting.

Kiefer O., Breitkreutz J., 2019. *From wet to dry thickness of oral films*, 13th Annual Meeting of the PSSRC, Düsseldorf (Germany).

Kiefer O., Breitkreutz J., 2019. *Inkjet printing for pharmaceutical applications*, IMI Europe Inkjet Ink Development Conference, Hamburg (Germany), *invited talk*.

Kiefer O., Breitkreutz J., 2018. *Pharmaceutical inkjet printing – dream or reality?*, The Inkjet Conference, Neuss (Germany).

Poster Presentations

Kiefer O., Breitkreutz J., 2019. *Comparison of two print heads for pharmaceutical inkjet printing*, 3rd European Conference on Pharmaceutics, Bologna (Italy).

Combined Oral and Poster Presentations

Kiefer O., Breitkreutz J., 2018. *Orodispersible films with absorbents for pharmaceutical inkjet printing*, 10th European Paediatric Formulation Initiative, London (UK).

Other Publications (not Used in this Thesis)

Inoue M., Kiefer O., Fischer B., Breitkreutz J., 2020. *Raman monitoring of semi-continuously manufactured orodispersible films for individualized dosing*, J Drug Deliv Sci Technol, 102224

DOI: 10.1016/j.jddst.2020.102224

Personal contribution: 10%

MI was responsible for the conceptualization and experimental methods and performed the experimental work with support of BF and OK. OK contributed to the writing and revision of the manuscript. JB was the supervisor and performed the revision of the final manuscript.

Table of Contents

List of Abbreviations

ADA	advanced drop analysis
ADI	accepted daily intake
ANOVA	analysis of variance
API	active pharmaceutical ingredient
a.u.	arbitrary unit
AUC	area under the curve
AV	acceptance value
BCS	biopharmaceutics classification system
bw	body weight
CCD	charge-coupled device
CI	confidence interval
CIJ	continuous inkjet
CPP	critical process parameter
CQA	critical quality attribute
CU	content uniformity
DAD	diode-array detector
DCPA	dicalcium phosphate anhydrous
DMC	Dimatix® materials cartridge
DoD	drop-on-demand
DoE	design of experiments
d	diameter
dpi	dots per inch
DF	degrees of freedom
DFT	dry film thickness
DVS	dynamic vapour sorption analysis
EFSA	European Food Safety Authority
EMA	European Medicines Agency
EtOH	ethanol
FDA	Food and Drug Administration
GMP	good manufacturing practice
h	height
HMI	human machine interface
HPB	head personality board
HPMC	hydroxypropyl methylcellulose
HPLC	high performance liquid chromatography
ICH	International Council of Harmonisation
IJP	inkjet printing
in	inch
IR	infrared
KM	Konica Minolta print head
L_s	length after strain
LAC	lactose
LD_{50}	median lethal dose
LT	L-thyroxine
LVER	linear viscoelastic region
MACO	maximum allowable carry over
MB28	Millijet® blue 28
MBS	minimum batch size
MCC	microcrystalline cellulose
MPT	metoprolol tartrate
MST	micrometre screw thickness
MxCMC	Parteck® ODT
n.d.	not determined
No.	number
NOEL	no observed effect level
ODF	orodispersible film
oTH	optical thickness
p.a.	per analysis
PAT	process analytical technology
PC	powder cellulose
PEG	polyethylene glycol
PHA	print head assembly
Ph. Eur.	European Pharmacopoeia
PIP	paediatric investigation plan
pTH	physical thickness
PVA	polyvinyl alcohol
PZT	lead zirconate titanate
Q^2	coefficient of prediction
QbD	quality by design
r	radius
R	regression coefficient
R^2	coefficient of determination
RH	relative humidity
RI	refractive index
RSD	relative standard deviation
SC	solvent-casting
SD	standard deviation
SEM	scanning electron microscopy
SF	safety factor
sMCC	silicified microcrystalline cellulose
SP	Spectra print head
t_n	time point n
TDD	total daily dose
TGME	tri (ethylene glycol) monoethyl ether
TIJ	thermal inkjet
UV/Vis	ultraviolet and visible light
vs.	versus
w	width
WHO	World Health Organization
WFT	wet film thickness
xPVP	crospovidone

1 Introduction

1.1 Individualised Medicine(s)

With the increasing advances in diagnostic procedures, identification of biomarkers and the study of human physiology, the understanding evolved that the idea of *one-size-fits-all* is no longer appropriate in modern pharmacotherapy. This paradigm shift has been addressed by the development of better adapted therapeutical concepts. The terms "individualised" [1, 2], "personalised" [3, 4], "P4" [5], "precision" [4, 6], "stratified" [4, 7], "age-appropriate" [8, 9] and "patient-centred" [10] medicine gradually arose in the literature. Each has a slightly different emphasis, so there is no general definition of the single patient-oriented approach. In the present work, "individualised medicine" is used as an umbrella term that encompasses all aspects of these definitions. Since human genomics [2, 11], age [12, 13], sex [14] and recently microbiome diversity [15] are in the focus for the individual pharmacotherapy concept, a wide range of interdisciplinary factors are to be considered. The common objective is the optimisation of patient care regarding safety, efficiency and effectiveness [16]. The incidence of mostly dose-dependant side effects [17] and the associated additional hospital stays are intended to be reduced by means of individually tailored therapy. Furthermore, the improvement of patients' acceptance and adherence regarding frequency of intake, mechanical handling, swallowability, palatability and medication identification should lead to more reliable medication [12, 18]. Additionally, the cultural influence on the acceptance of administration routes and dosage forms should not be underestimated. Patients' preferences have been shown to vary strongly according to geographical and cultural origin [8].

The approach of individual pharmaceutical preparations is not new. In the community pharmacy, the compounding of individual prescriptions adapted for the special needs of patients was the main activity of pharmacists until the introduction of industrial mass production. Today, compounding is still conducted in the community and hospital pharmacies to provide customised dermal, pain, substitution or oncological therapy, active and placebo samples for clinical trials, orphan drugs and adapted medicines for paediatric patients [19]. In Germany alone, 13 million compounded medicines were produced for patients of the statutory health insurance in 2020 [20]. However, the regulatory monitoring of quality level of the medicines is different than in the pharmaceutical industry. There is no

harmonisation of compounding regulations so that there are clear differences in quality between pharmacies all over the world [19, 21]. Even within one country there are serious variations. For instance, only 68% of participating German pharmacies correctly prepared the anionic dexamethasone cream during a ring trial. Failures were identified in declaration of API (active pharmaceutical ingredient) and its dosage, API identity, homogenous API distribution, API over- and underdosing, particle size and galenic consistency [22].

To overcome the supply gap for paediatric patients in the pharmaceutical industry, the European Union introduced the regulations on medicinal products for paediatric use [23] about 10 years after a similar publication by the US Food and Drug Administration (FDA) [24]. Since then, the submission of a paediatric investigation plan (PIP) is obligatory for pharmaceutical companies which develop a new medical product. PIPs detail all the measures that will be implemented to demonstrate the quality, safety and efficacy in target child age group. This fundamental element led already to some available medicines for children and more information for clinicians [25, 26]. Nevertheless, there are still gaps in supply, so that on-demand compounding remains necessary and plays an important role in paediatric care [27]. On the other hand, the steady rise in human life expectancy poses particular challenges for the health care system. Patients' multimorbidity and polypharmacy shall be considered during product development [13]. To improve the medication for older patients EMA established the Geriatric Medicines Strategy [28]. Moreover, a reflection paper on the pharmaceutical development for elderly was recently published to illustrate the current status and to emphasise the importance of a patient-centric approach. The advantages and disadvantages of different dosage forms and administration routes are discussed [29].

In this context, the term "patient-centric pharmaceutical drug product design" [10] arose, connecting the individual patients' characteristics of any origin and the characteristics of pharmaceuticals including among others the type of dosage form, functionality of packaging and user information. To meet the requirements of flexible and patient-oriented dosing, manufacturing technologies, dosage forms and dosing devices have to be developed further [30].

One example of successful industrially manufactured individualised medicines is Kymriah® from Novartis. The advanced immunocellular therapy of acute lymphoblastic leukaemia by tisagenlecleucel is the first FDA-approved gene therapy entering the US market. The infusion

dispersion is manufactured from the patient's own T cells which are genetically re-engineered outside the body and re-infused in order to recognize and eliminate CD19 expressing cells [31]. Less complex manufacturing concepts of tailored dosage forms are more practicable in community and/or hospital pharmacies than in the industrial mass production scale. These institutions are closer to the patients and can react more flexible to their special needs. Potent APIs with a narrow therapeutic window, with the requirement of gradual dosing and/or characterised by known inter- and intraindividual pharmacokinetic and -dynamic variabilities are particularly candidates for a tight therapeutic drug monitoring (TDM). Since flexible individual step-wise adjustments of the dose strength are required, appropriate on-demand medicines supply that meet this are needed. This requirement is age independent and can occur in paediatric, adult or geriatric patients.

Without the development of new manufacturing technologies and dosage forms, the concept of individualised medicine cannot be fully realised. Innovative approaches focus on oral drug delivery, as it is the most acceptable administration route. Exact dosing must be ensured. Liquid dosage forms can be tailored volumetrically or by counting the single drops by the patient. Multiparticulate solid dosage forms like mini-tablets can be flexibly counted to achieve the target dosage. However, the final dosing is usually controlled by the patient himself, its legal guardians or the medical staff. This can still lead to administration errors due to the human factor. With increasing digitalisation and automation of processes as well as upcoming E-prescribing in the health care sector [32], manufacturing technologies have also to be adapted. Additive manufacturing, which has increasingly found its way into the medical field, enables the individualisation already during the production step monitored by pharmacists in collaboration with the attending physician. With the help of computer-based information, spatial objects, in this case dosage forms are built up layer by layer. That can be compared with compounded medicines with the advantage that automated pre-dosing can reduce manufacturing errors by the operator and administration errors such as incorrect tablet splitting by the patient, without losing flexibility. Usually only 3D-printing is described with the term "additive manufacturing" [33]. But there are further build-up deposition techniques, classified as 2D-printing, that are in focus of research for customised solid oral dosage forms, such as flexographic [34, 35], stencil [36] and inkjet printing [37-41]. However, the boundaries between 2D and 3D are often fluid. These new approaches to fabricate individualised

medicines are no longer only topics in academic research, but hospital pharmacy, clinical trial sites and pharmaceutical industry are also showing increased interest [42-47].

1.2 Inkjet Printing Technology

1.2.1 Industrial Inkjet Printing

Inkjet printing is a digital rapidly advancing printing technology based on precise, contactless application of large number of individual drops that build up the target image on a substrate. The drop volume is typically in the range of 1-100 pl. Depending on how many ink dots are placed within one inch (1 in = 2.54 cm) a different print resolution results, expressed in dots per inch (dpi).

With development of the first inkjet printers end of the 1960s, flexible automated marking and coding of products was made possible for the first time [48]. The used operation principle was continuous inkjet printing (CIJ) which is based on the Plateau-Rayleigh instability [49]. This describes that a perturbed liquid cylindrical body breaks up into drops driven by capillary force.

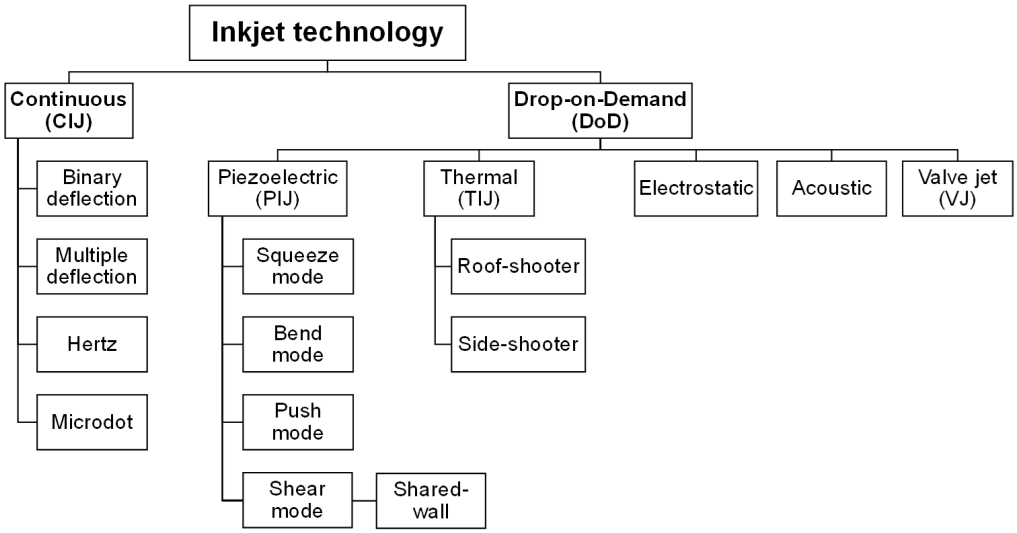

Figure 1: Overview of inkjet technologies modified according to Le et al. [48]

In CIJ print heads, a continuous ink stream from pressurised ink supply breaks up initiated by a transducer. The formed drops are deflected in an electrostatic field so they land on the target substrate location (Figure 2). The higher the charge, the higher is the deflection degree. Not required ink drops are led into a gutter and recycled [50]. There are binary and multiple

deflection systems as well as some special systems (Figure 1). The benefit of CIJ is that high frequencies and fast-drying inks can be used. The maintenance demand and risk of nozzle clogging is lowered due to pressure control and a continuous liquid jet. This allows a high throughput to be achieved.

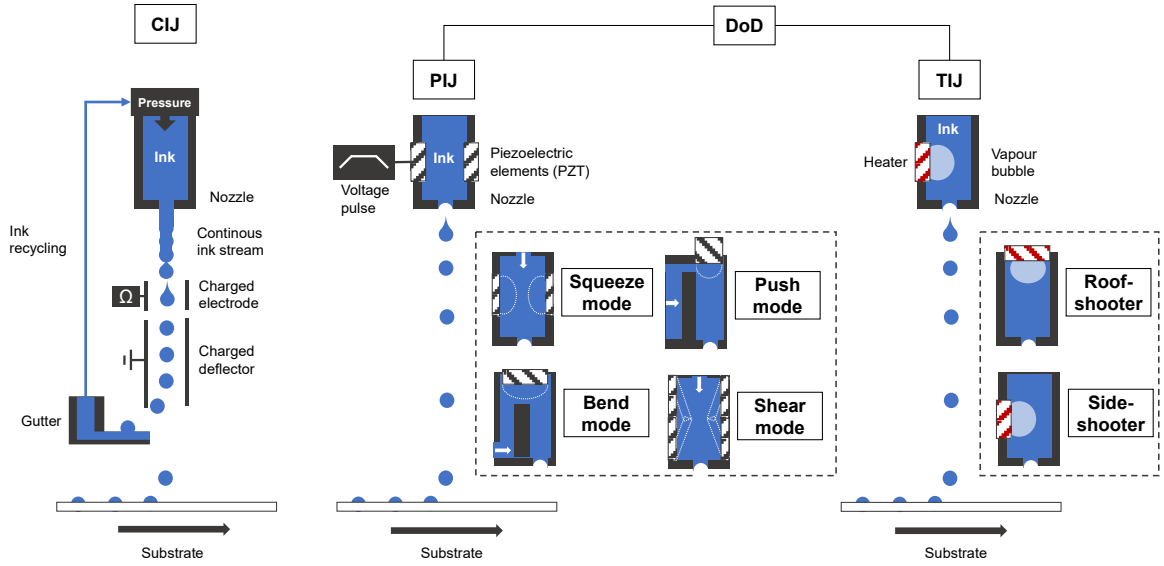

Figure 2: Schematic illustration of the drop generation principles by the main inkjet systems [51, 52]

Besides, drop-on-demand inkjet (DoD) technology has been developed and became the most commonly used system which allowed to print text and graphics also for home and office applications. DoD is characterised by impulsive ejection of drops only when they are needed. This includes two different techniques, the thermal inkjet (TIJ) and piezoelectric inkjet (PIJ). In case of piezoelectric operation, electric driving voltage pulse, is converted to a mechanical deformation of channels made of piezo elements. As a result, an acoustic pressure wave within the ink generates defined drops leaving the nozzles (Figure 2) [53]. The way how the voltage pulses are arranged is described by the so-called waveform, a key element of PIJ. There are four main print head operation principles: squeeze, bend, push and shear mode, as well as the sub-mode of the last: shared-wall. They differ in the manner the piezoelectric elements are deformed [48, 54]. In a TIJ print head, the pressure for drop ejection is thermally built up by an expanding vapour bubble, which is created by heating the ink using electronic resistors. Finally, the cavitation collapses, thereby drawing in further ink [53]. Depending on the location of the heater in relation to the nozzle, there are roof-shooter and side-shooter systems (Figure 2). In addition, there are special DoD ejection technologies: electrostatic, acoustic and valve jet (VJ) (Figure 1). VJ can be used to dispense higher drop volumes and higher ink viscosities, but

with lower frequencies than TIJ and PIJ [55]. The nozzles are connected with valves that can be individually accessed by relatively low, pneumatically or piezoelectrically generated pressure.

Generally, the major advantage of DoD is the possibility of high print resolutions due to smaller nozzle spacing than CIJ. Moreover, CIJ requires larger ink quantities than DoD, which can be a drawback when using expensive ink components. PIJ can process a wider range of inks than TIJ because there is no dependence on vaporisation capability. Volatile solvents as well as sensitive materials are not negatively affected by the ejection technique. Therefore, printing of functional materials for micro-manufacturing purposes is often performed by PIJ although TIJ print heads are simpler and cost-effective in production [53]. For this reason, the focus of this work is on the PIJ technology.

The ink types in conventional industrial printing can be classified in aqueous, solvent, oil, energy-curable, hot-melt and hybrid inks [56]. The selection of the print head technology as well as the substrate type determines the ink type. Depending on this, appropriate supplements have to be added to achieve properties providing ink printability. "Printability" is a broadly defined term describing the reliable ink performance that leads to high-quality printed images. It is determined especially by the critical physicochemical fluid properties dynamic viscosity η, surface tension γ and density ϱ. The ultimate goal is to develop inks that perform stable and precisely with a wide range of printing systems. But this is challenging to implement due to the complexity of the system's variability and inter-relationships. Fromm [57] used the ratio of dimensionless indicators Reynolds number *Re* (Equation 1) and Weber number *We* (Equation 2) $Re/We > 2$ to predict a stable drop formation in a DoD printing system.

$$Re = \frac{\rho v d}{\eta} \qquad \text{(Equation 1)}$$

$$We = \frac{\rho v^2 d}{\gamma} \qquad \text{(Equation 2)}$$

Here, v is the fluid velocity and d a characteristic length, usually the nozzle diameter. However, specific limit values were not defined in Fromm's study. The idea was resumed by Derby et al. [58]. They used the dimensionless Ohnesorge number *Oh* (Equation 3), respectively inverse Ohnesorge number Z (Equation 4), to propose an operating range for printable inks of $1 \leq Z \leq 10$ by computerised modelling (Figure 3).

$$Oh = \frac{\sqrt{We}}{Re} = \frac{\eta}{\sqrt{\gamma \rho d}} \quad \text{(Equation 3)}$$

$$Z = \frac{1}{Oh} = \frac{Re}{\sqrt{We}} = \frac{\sqrt{\gamma \rho d}}{\eta} \quad \text{(Equation 4)}$$

If Z decreases below 1, drop formation is prevented by too high dynamic viscosity. With Z values above 10, secondary drops, so-called satellites, occur. Considering further printing characteristics, Jang et al. adjusted the critical limits to $4 \leq Z \leq 14$ [59]. Thus, there are differently defined regions for printable fluids (Figure 3) in industrial inkjet printing.

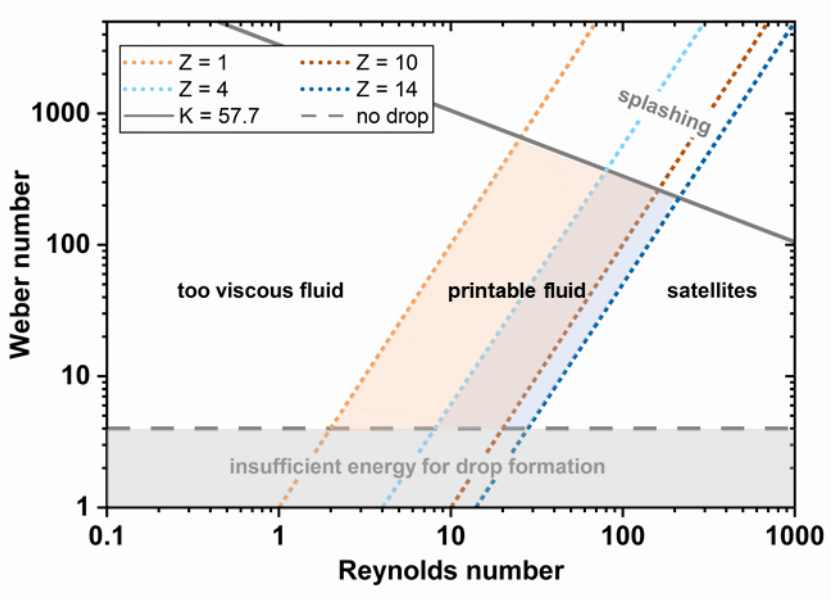

Figure 3: Schematic diagram showing parameter space for stable drop formation during DoD inkjet printing, modified according to Derby et al. [60]

Drop formation requires a sufficiently high kinetic energy, but too high energy input combined with an inconvenient constellation of fluid properties leads to splashing on the substrate. Drop velocity and substrate roughness play an important role here. The dimensionless splash value K describes the critical limit for the onset of splashing depending on the function of surface roughness R (Equation 5) [61, 62]. For flat and smooth surfaces, the empirical threshold is above > 57.7 (Figure 3) [62].

$$K = \sqrt{We\sqrt{Re}} = f(R) \quad \text{(Equation 5)}$$

Paper of various qualities is the classically used substrate for inkjet printing. With advancement of inkjet printers and inks, diverse materials such as polymeric foils, textiles, glass, ceramics and food have been imprinted [50]. By additives and physical and/or chemical

treatment, substrates are often modified to achieve target characteristics. Wetting, spreading, coalescence, absorption, fixation and drying of ink depend strongly on the type of substrate [63]. These interactions determine the final image quality.

It becomes clear that the main elements of printing equipment, ink and substrate cannot be considered independently of each other. Altogether, they determine the process window. This interaction is often illustrated by the "golden triangle" of inkjet printing (Figure 4).

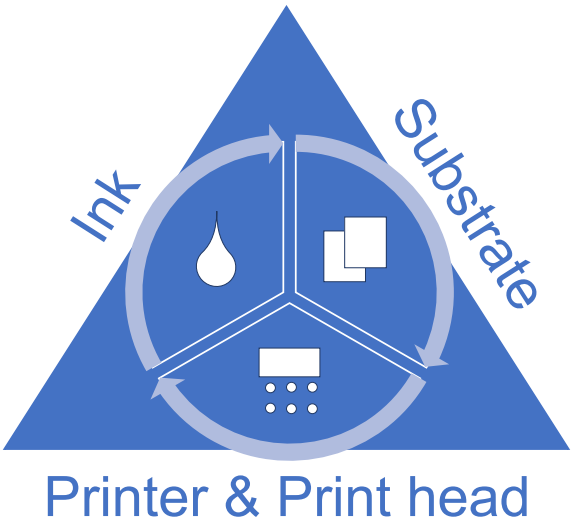

Figure 4: The golden triangle of inkjet printing showing the interdependencies of ink formulation, substrate where the ink is deposited and the used equipment

1.2.2 Pharmaceutical Inkjet Printing

In the pharmaceutical field, inkjet printing was originally used for labelling of secondary and primary packages with batch numbers and expiry dates. In recent years, marking with security QR-codes and direct imprinting of the single dosage forms has become an important part of improving anti-counterfeiting and identification of medication [64, 65]. This also requires a highly flexible printing technology. Besides laser printing, this is often realised by inkjet technology [66-68]. In Japan, many tablets are imprinted by inkjet, as tablets are usually offered in individual, transparent bags for a single dosing [69, 70]. At the same time, innovative approaches to use inkjet printing as deposition tool for high-throughput gene and drug screenings [71, 72], functional coatings of implants, stents or microneedles as well as drug-loading of oral dosage forms [73-76] emerged. The main advantage of inkjet printing for biotechnology and pharmaceutical applications is its contactless, precise, flexible and fast operation. Smallest quantities can be reliably dispensed minimising production waste and

process time and thus costs. With the use of inkjet printing for pharmaceutical purposes, there are further quality requirements in addition to the known technological challenges. To distinguish from usual industrial application (section 1.2.1), it has been referred to as pharmaceutical inkjet printing in this work.

The greatest milestone for pharmaceutical inkjet printing so far is that Spritam® from Aprecia® Pharmaceuticals, has been approved for the market by the FDA in 2015 [77]. It is produced using the ZipDose® technique, in which a three-dimensional porous tablet is built up by inkjet printing of a drug-free binder solution onto a moving powder bed [46]. The powder bed consists of the API levetiracetam and excipients which, together with the binder solution, build up the tablet matrix. This production technique was chosen for the commercial production of a high-dose but rapidly disintegrating dosage form to improve the patients' adherence. The next step is to use its further potential and establish pharmaceutical inkjet printing as a tool for on-demand production individualised dose strengths on site (section 1.1).

Before an API can be deposited by inkjet printing onto a substrate, it has to be transferred into a suitable ink formulation. The challenge of pharmaceutical inks compared to conventional industrial inks (section 1.2.1) is that the composition is highly dependent on the target API and has to comply with the requirements of pharmacopoeias regarding quality, efficacy and safety. Since the printed dosage forms are intended primarily for oral and parenteral application, there are particular restrictions on the excipients used in the ink formulations that have to be consider. Several APIs were already tested in inkjet printers for preparation of oral solid dosage forms (Table 1). However, they often played the role of model drugs and were not therapeutically effective at the dose-strength prepared. Due to the low-dose deposition of inkjet technology, the maximum printed dose until now are 12.1 mg montelukast sodium [78]. In particular, only sodium picosulfate (9 mg) and warfarin (2.5 mg) were in the range of therapeutic doses.

Table 1: Overview of the APIs, their maximum printed dose per unit (means, rounded to three decimal digits) on film substrates for oral drug delivery and the used inkjet equipment

API	Dose/unit [mg]	Printer / Print head	Type	Ref.
caffeine	0.437 1.272	Canon IP 1300 Dimatix DMP-2800 / DMC-11610	TIJ PIJ	[79, 80]
cannabinoids	0.567	Epson XP-8500	PIJ	[81]
ciprofloxacin	0.003	MicroFab MJ-AL-01	PIJ	[82]
clonidine	0.253	HP Deskjet 460	TIJ	[83]
diclofenac sodium	2.408	HP Deskjet D4260	TIJ	[84]
enalapril maleate	0.500	PixDro JS 20 / Spectra SE-128 AA	PIJ	[85]
furosemide	6.700	PixDro LP50 / Spectra SL-128 AA	PIJ	[86]
glimepiride	1.920	SMLD 300G micro-valve	VJ	[87]
haloperidol	4.100	PixDro LP50 / Spectra SL-128 AA	PIJ	[78]
indomethacin	0.068 0.703	Epson Stylus SX400 SMLD 300, SMLD 300G micro-valve	PIJ VJ	[88, 89]
L-thyroxine sodium	0.180 0.859	HP Deskjet 5940 PixDro LP50 / Spectra SL-128 AA	TIJ PIJ	[90, 91]
lidocaine hydrochloride	2.840	PixDro LP50 / Spectra SL-128 AA	PIJ	[92]
liothyronine	0.050	HP Deskjet 5940	TIJ	[90]
loperamide hydrochloride	2.431	Dimatix DMP-2800 / DMC-11610	PIJ	[80]
melatonin	0.351	HP Deskjet 5940	TIJ	[93]
metformin hydrochloride	0.720	sciFLEXARRAYER S3 / SciDROP Pico	PIJ	[94]
metotoprolol tartrate	5.012	PixDro LP50 / Spectra SE-128 AA	PIJ	[41]
montelukast sodium	12.100	PixDro LP50 / Spectra SL-128 AA	PIJ	[78]
paracetamol	0.720	SMLD 300, SMLD 300G micro-valve	VJ	[89]
sodium picosulfate	9.000	sciFLEXARRAYER S3 / SciDROP Pico SciDROP Nano	PIJ VJ	[95, 96]
prednisolone	1.951	PixDro LP50 / Spectra SL-128 AA	PIJ	[91]
propranolol hydrochloride	4.100	Canon Pixma iP7250 PixDro LP50 / Spectra SL-128 AA	TIJ PIJ	[78, 97]
ramipril diketopiperazine	1.970	SMLD 300G micro-valve	PIJ	[87]
rasagiline mesylate	1.030	Canon Pixma MP495	TIJ	[98]
salbutamol sulphate	0.798	HP Deskjet D1660	TIJ	[99]
warfarin sodium	2.500	HP Deskjet 5940	TIJ	[100]

Note: Prerequisite for the selection was that the substrate was edible and the liquid deposition equipment was based on inkjet principles

Recently, 34 suitable API candidates for pharmaceutical inkjet printing on orodispersible films were identified and discussed within a paediatric utilisation study in the Netherlands. It has been found that despite the large number of candidates, it may be ambitious to achieve the sufficient dosage [101]. Furthermore, PIJ-printed orodispersible films were produced by Öblom et al. in the hospital pharmacy environment intended for future use in the children's

hospital. They were directly compared with 3D-printed films and conventionally compounded oral powders and showed promising results [45]. Since 2020, the university hospital of Heidelberg researches on inkjet printing of patient-centred medicines in collaboration with the start-up company DiHeSys with Harro Höfliger company as strategic engineering partner. The 2D/3D-pharmaprinter developed in-house is used for this purpose [42]. These activities demonstrate that there is an increased interest in inkjet printing as pharmaceutical manufacturing technology, particularly in hospital setting. However, it is still the advanced initial phase of development into an established technology. There is still a lack of sufficient process understanding and strong formulation experience including deep knowledge about the physicochemical properties of pharmaceutical inks. Additionally, commercially available off-the-shelf inkjet printers are not yet designed for operation at Good Manufacturing Practice (GMP) conditions and there are no elaborated quality control guidelines yet.

Besides pipette-like automated dispensing systems, commercially available TIJ, PIJ and VJ printers, partially modified, were misappropriately used for the production of solid oral dosage forms (Table 1). In the field of research inkjet printers, PixDro LP50 (Meyer Burger) and DMP-2800 (Fujifilm Dimatix) are the most frequently used systems. Since they were originally developed for functional printing applications such as photovoltaics, displays, printed electronics, the printers do not necessarily meet pharmaceutical quality requirements using unsafe organic solvents and other materials. DMP-2800 is working with a disposable cartridge system. This requires only low ink amounts and is able to avoid cross-contamination by using one separate cartridge per API. The benefit of PixDro LP50 is that it has exchangeable print heads of different manufacturers and may also use the cartridges of DMP-2800. This opens the possibility of more flexible dosage form manufacturing process development.

In the first trials to apply active ingredient by means of inkjet printing, often non-edible substrates from the industrial inkjet field like paper, plastic foil and glass were used [37, 38, 102-104]. Following, oral films, in particular orodispersible film preparations were used (Table 1). Tablets and capsules have also been considered as pharmaceutical substrates, but almost only for liquid deposition techniques other than inkjet technology [105-108].

1.3 Orodispersible Films

Orodispersible films (ODFs) are a relatively novel dosage form and are included in the European Pharmacopeia (Ph. Eur.) since 2012 as part of the monograph "oromucosal preparations". They are roughly defined as "single- or multi-layer sheets of suitable materials, to be placed in the mouth where they disperse rapidly" [109].

The basis of ODFs are polymers. They form the film matrix and co-determine the critical quality attributes (CQA) disintegration time, API release, mechanical strength, chemical stability and organoleptic characteristics [110, 111]. The predominant manufacturing technology of ODFs is the solvent-casting method. Thereby, the polymer mass containing dissolved or dispersed API is coated onto a release liner using a coating knife or roller. To achieve the orodispersible properties, water-soluble cellulose ethers, polyvinyl alcohol and polyvinylpyrrolidone (povidone) grades of low molecular weights as well as maltodextrins and pullulan are the most used polymers [112]. As there is no specification about the exact disintegration time in the pharmacopoeias, orodispersible tablets which must disintegrate within 180 s according to Ph. Eur. [113] or 30 s according to a FDA guideline [114] serve as guidance for formulation development. Other important excipients of ODFs are plasticisers such as glycerol, polyethylene glycol 400 and triethyl citrate. They are used to modulate the mechanical film properties towards greater flexibility. The dried polymer sheets are finally cut into pieces of 1 to 6 cm^2 and pouched in moisture-proof package due to their sensitivity to humidity [115]. Since there are no defined ranges of mechanical properties and no standardised testing devices for film-type dosage forms, it is challenging to compare the results of different scientific publications. The "suitable mechanical strength to resist handling without being damaged" according to Ph. Eur. [109] must be determined by the manufacturer on his own [116]. As administered, ODFs already disintegrate or even dissolve in the oral cavity, taste agents or maskers may be therefore essential to cover the often bitter taste of APIs and thus improve patients' adherence.

Beginning with the breath freshener strips Listerine® PocketPaks® from Pfizer and LTS Lohmann launched in 2001, Zuplez® from Strativa Pharmaceuticals and MonoSol Rx containing ondansetron base was the first ODF approved by the FDA in 2010 [117, 118]. Since then, the portfolio has expanded significantly in the pharmaceutical area, although only few products have actually remained on the market. The reasons for that are manifold. ODFs are

still a niche product, unknown to many patients and physicians, and more expensive than conventional oral dosage forms. The water and/or organic solvents must be removed by evaporation which requires high energy input and heat exposure for APIs. Temperature-sensitive APIs often cannot be processed. Usually, the dose of ODFs is determined by the film thickness and area. As main disadvantage, the drug-load limitation to about 50 mg per film piece and with that to low-dose potent APIs is often mentioned [119]. However, this can be also seen as an advantage, as ODFs offer a formulation platform for low-dose APIs. In addition, as part of the concept of individualised medicine, there is a growing attention in the community and hospital pharmacies because of their simple manufacturing, flexibility in customisation and good swallowability [45, 119, 120]. ODFs combine the benefits of liquid and solid dosage forms. The fast disintegration ensures a rapid release of the API if absorption is rapid from the oromucosal area. Since the acceptability of ODFs in children of different ages has been demonstrated, these patient groups should benefit from these opportunities [121, 122].

In the meantime, several advanced concepts were realised such as instant ODF formulations [123], nanoparticle- and micropellets-loaded ODFs [124, 125], solid foams [126], ODFs prepared by electrospinning [127], freeze drying [126], semi-solid 3D-printing [45], hot-melt extrusion [128] and finally ODFs loaded with APIs by several printing techniques [35, 36, 98]. New areas of application are also being developed. ODFs are proposed as carriers for vaccines [129, 130] and veterinary medicines [131, 132].

1.4 Model Drugs

1.4.1 Metoprolol Tartrate

Metoprolol is a relatively selective β_1-adrenoceptor antagonist. It is indicated for the treatment of arterial hypertension, coronary heart disease, cardiac arrhythmia, hyperkinetic heart syndrome and for the acute treatment of heart attack. Another field of application is reinfarction and migraine prophylaxis. Depending on the level of sympathetic tone, the metoprolol lowers the frequency and contractility of the heart, the AV-conduction velocity and plasma renin activity [133]. There are three different salts of metoprolol on the market:

fumarate, succinate and tartrate [134], whereby metoprolol tartrate (MPT) was used in the present work. Therefore, all quantity information refers to this metoprolol salt.

MPT (Bis[(2*RS*)-1-[4-(2-methoxyethyl)phenoxy]-3-[(1-methylethyl)amino]propan-2-ol]-(2*R*,3*R*)-2,3-dihydroxybutanedioate) is a racemate of two enantiomers and is used in a cation : anion ratio of 2:1 (Figure 5).

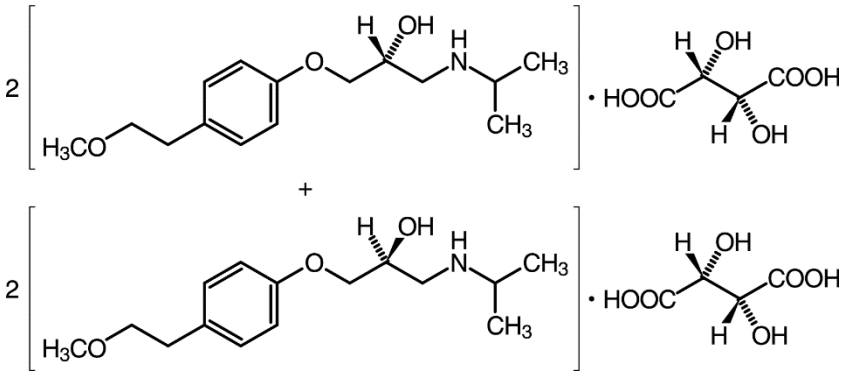

Figure 5: Chemical structural formula of MPT [135]

It is characterised by a very good solubility in water of > 1000 g/l at 15–25 °C [135] and is a representative of BCS (Biopharmaceutics Classification System) class I due to its additionally high permeability [136]. The therapeutic dose depends on the indication and is between 50 and 200 mg per day in adult patients [134]. Beta-blockers like MPT are essential not only for treatment of heart diseases in adults but also in premature infants, new-borns and children. Since safety and effectiveness in paediatric patients have not been established yet, it is used off-label [137-140].

After oral application, the non-retarded MPT is almost completely and rapidly absorbed from the entire small intestine and colon. It is predominantly metabolised by the enzyme cytochrome P450 2D6 (CYP2D6). In case of CYP2D6 polymorphism, there are four phenotypes: ultra-rapid, extensive, intermediate and poor metaboliser showing significantly different MPT pharmacokinetics [133, 141]. In particular, for extensive metabolisers, there is an additional age dependency for children with regard to the MPT clearance [142]. For that purpose, an exact dosing is necessary to allow gradually increase from the individual initial to final dosage, especially because of the unknown metaboliser status [139]. There are several finished drug products, mostly solid oral dosage forms that are not suitable for paediatric patients. Up to now, capsules or solutions are extemporaneously prepared to fill this gap [140, 143]. For treatment of hypertension, initial doses of 1–2 mg/kg bw/day distributed over two

single doses are reported. Maximum doses are indicated as 6-8 mg/kg bw/day up to a maximum of 200 mg total dose per day. Twice daily administration of 0.1–0.2 mg/kg bw is recommended for treatment of heart failure. The dose may be doubled every two weeks if the patient is in stable condition until the target dose of 1–2.5 mg/kg bw is reached [144, 145].

In summary, there is a need for appropriate dosage forms containing therapeutically reasonable dose strengths of MPT for paediatric use. To improve the quality and safety of paediatric cardiac oral drug therapy advanced manufacturing techniques are crucial to be established. In addition, precise low initial doses may be required for titration of adults and geriatric patients.

1.4.2 L-Thyroxine

L-thyroxine (LT) is indicated for substitution therapy of hypothyroidism, hyperthyroidism as accompanying therapy to thyrostatic treatment, benign goitre, after removal of goitre to prevent recurrence and for malignant thyroid changes as suppression or substitution therapy after thyroidectomy. Synthetic LT is not distinguished from the naturally occurring hormone T_4 and is converted in the organism into the more effective thyroid hormone liothyronine (T_3) [146].

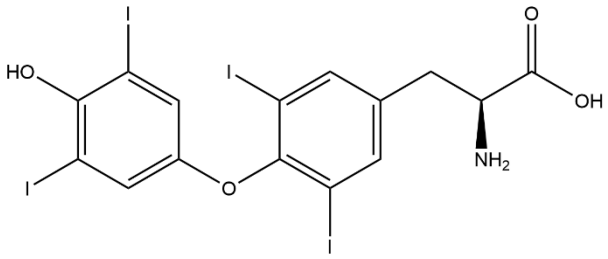

Figure 6: Chemical structural formula of LT

LT is usually administered as sodium salt because it shows better gastrointestinal absorption than the free-acid [147]. It is light sensitive, shows a very slightly water solubility of 0.15 g/l at 25 °C and is nevertheless a representative of BSC class III [148, 149]. When taken fasting, up to 80% is absorbed in the upper small intestine via intestinal active transporters. However, absorption is influenced by many factors such as coffee consume, time interval to a meal and intake of inorganic salts. Since only LT was available as raw drug substance, this was used in this work.

LT is classified as a narrow therapeutic index drug requiring a stepwise dose titration. Overdosing leads to serious toxicities some of which are irreversible whereas underdosing results in insufficient treatment. Therefore, a TDM based on serum TSH (thyroid-stimulating hormone) and total or free T_4 levels is crucial for a safe and successful therapy [146]. The therapeutic dose depends on the indication, weight, age and comorbidities of the patients. For adults, it is between 25 and 200 µg/day. There are mainly tablets on the market due to the limited shelf life, especially for liquid formulations [150]. For individual dosing, tablet splitting may be necessary but not all LT tablets can be divided. A comparable bioavailability of tablets and liquid formulations was shown [146]. However, serious issues regarding interchangeability of LT products of different formulations and brands have to be considered [147].

In newborns and children with congenital hypothyroidism requiring rapid substitution, an initial dose of 10 to 15 µg/kg bw/day is recommended for the first three months. After that the dose should be adjusted individually based on clinical findings. In children with acquired hypothyroidism, an initial dose of 12.5 to 50 µg/kg bw/day is recommended. The dose should be gradually increased every two to four weeks based on measured thyroid hormone and TSH levels until the dose required for complete substitution is reached. Consequently, a highly flexible dosing is mandatory. For paediatric patients, it is suggested to administer the LT tablets as freshly compounded oral suspension or drops [146]. Alternatively, capsules can be produced from tablets or raw drug substance and opened before use [148].

It is one of the most prescribed APIs in Germany and the United States [151, 152]. Due to the high demand on the one hand and the necessity of individualised adaption and close monitoring of low-dose regimen, LT was selected as model drug for the present work.

2 Aims and Outline

This work focuses on inkjet printing of APIs onto orodispersible films (ODFs) for individualised therapy. Metoprolol tartrate (MPT) and L-thyroxine (LT) have been chosen as model drugs as they differ in their solubility properties, dosage and target patient groups. Thus, a wide application could be covered.

In detail, the main aims of the present thesis were:

- Development of pharmaceutical ink formulations and characterisation methods thereof
- Expanding process understanding of the inkjet printing technology with regard to pharmaceutical applications, including fundamental investigation of the influence of key factors on the printed quantities and on different drug dosing strategies
- Mechanistic investigations on solvent-casting process of ODFs regarding substrate thickness as important parameter for mechanical resistance and development of suitable substrates for pharmaceutical inkjet printing with addition of functional excipients
- Elaboration of a generalised concept of pharmaceutical printing process including a rational workflow from API selection to final formulation with established manufacturing process

3 Results and Discussion

3.1 Development and Characterisation of Pharmaceutical Inks

Parts of this section have already been published in peer-reviewed journals. The content was linguistically and graphically adapted. Further data have been added.

- Kiefer O., Breitkreutz J., 2020. *Comparative investigations on key factors and print head designs for pharmaceutical inkjet printing*, Int J Pharm 586, 119561.
  DOI: 10.1016/j.ijpharm.2020.119561
- Kiefer O., Fischer B., Breitkreutz J., 2021. *Fundamental investigations into metoprolol tartrate deposition on orodispersible films by inkjet printing for individualised drug dosing*, Pharmaceutics 13(2), 247.
  DOI: 10.3390/pharmaceutics13020247

3.1.1 Introduction and Objectives

The first aim of this work was to establish a general formulation development process for pharmaceutical inks. This was performed with drug-free prototypes spiked with a blue dye for visual control and later quantitative content examination of printing results. Since ink, printer and substrate cannot be considered as completely independent of each other, two different print heads and a standard substrate were initially used to investigate the ink performance. The print heads KM512SHX (KM) and Spectra SE-128 AA (SP) were used as test systems, whereby a detailed view at the equipment will be discussed in the following chapter. As standard substrate a frequently used ODF composition based on hypromellose (HPMC) was used (section 1.3). In the second step, two APIs with different physicochemical properties and therapy regimens, metoprolol tartrate (MPT) and L-thyroxine (LT), were selected. On this basis, specialised ink formulations were developed. Methods for ink characterisation before, during and after printing were established and evaluated. Finally, pharmaceutical inks were put in context of the dimensionless numbers used to predict printability (section 1.2.1).

To establish a general formulation development process, basic requirement criteria for pharmaceutical inks were defined first. The most important aspect in the selection of

excipients is safety for all patient age groups. Since most ink components used in industrial inkjet printing processes are not suitable for an oral uptake by humans, pharmaceutical alternatives have to be found. The safety assessment of pharmaceutical excipients is usually carried out on the basis of precedence of use in commercial pharmaceutical products or as food additives [153]. However, special care is required of paediatric or geriatric patients because they differ in pharmacokinetics and pharmacodynamics from the average adult [12].

In addition, the physicochemical properties of the API and the overall ink formulation have to be taken into account, since the concentration and stability of the API in the solution, rheological behaviour, surface tension, density, volatility and wetting of the substrate have a significant influence on the processability in the printer and with that on the final dosage.

3.1.2 Drug-free Model Ink

3.1.2.1 Selection of Excipients

As starting point for formulation development, the test inks for KM and SP print heads suggested by printer manufacturer Meyer Burger were used as references with regard to their physicochemical properties.

For KM, the single-component-system triethylene glycol monoethyl ether (TGME, R1) and, for SP, the multi-component-system XL30 blue (R2) were recommended by Meyer Burger. TGME is a colourless, hygroscopic, little volatile liquid which is miscible with water (Figure 7). In the industrial inkjet printing it is used as solvent, humectant and wetting agent like other glycol ethers. XL30 consists of propylene glycol (PG) as viscosity enhancer, propylene carbonate as solvent and Millijet® blue 28 (MB28) as polymeric dye, whereby there is no precise information available on the quantitative composition [154].

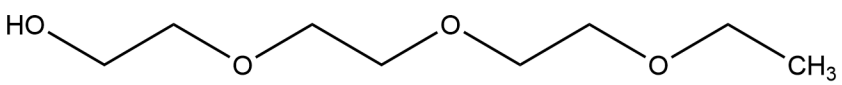

Figure 7: Chemical structural formula of triethylene glycol monoethyl ether (TGME)

As a basic requirement in the development of pharmaceutical inks, it was specified that all components have to be safe in the quantities used for all patient age groups.

Looking into the previously published literature (Table 2), it became obvious that only limited options are available.

Table 2: Overview of excipients used in ink solutions for oral application and their regulatory status, status until March 2017

Excipients	Function	ADI*/PDE** [mg/kg bw]	MDE*** [mg]	Ref.
acetone	(co)solvent	50 (class 3)	-	[103]
L-arginine	stabiliser	-	25	[104]
dimethyl sulfoxide (DMSO)	solvent	50 (class 3)	-	[102-104]
erythrosine	dye	0–0.1	-	[105]
ethanol (EtOH)	(co)solvent	50 (class 3)	1	[34, 76, 80, 91, 102, 103, 105, 155-158]
glycerol	cosolvent, viscosity enhancer, humectant, recrystallisation inhibitor	not specified	31536	[34, 76, 83, 97, 99, 158-161]
lactic acid	salt-former, cosolvent	not limited	132	[105]
methanol	(co)solvent	30 (class 2)	-	[83]
poly (lactic-co-glycolic acid) (PLGA)	viscosity enhancer, controlled release, recrystallisation inhibitor	-	-	[103]
polyethylene glycol (PEG) 400 / 3000 / 8000	cosolvent, viscosity enhancer, humectant, recrystallisation inhibitor	0–10	24000	[95, 156, 159, 162]
propylene glycol (PG)	viscosity enhancer, humectant, recrystallisation inhibitor	0–25	27120	[34, 37, 80, 92, 98, 104]
povidone (PVP) K28 / K30 / K90	viscosity enhancer, recrystallisation inhibitor	0–50	2828	[102-104, 155, 157]
sodium desoxycholate	permeation enhancer, surfactant	-	-	[161]
sodium dodecyl sulfate (SDS)	surfactant, solubiliser	-	600	[162]
water, purified	solvent	-	-	[34, 37, 76, 80, 83, 92, 95, 97-99, 158-161]

*Not*e: *acceptable daily intake [163]; **permitted daily exposure [164]; ***maximum daily exposure for oral route [165]

Based on the literature research, a selection of most used pharmaceutical acceptable excipients was made. Ethanol, water, glycerol, polyethylene glycol 400 and propylene glycol were chosen for the formulation screening of the drug-free model ink.

EtOH serves as solvent and indirectly for adjustment of surface tension. As EtOH is evaluated as uncritical additive as long as it is used in accordance with good manufacturing practice (GMP) to keep the residual solvents below 50 mg/kg bw [166]. Water is the most used solvent and dispersing agent in liquid dosage forms. However, a potential hazard is bacterial growth during storage. Aqueous inks have therefore to be prepared with purified water according

Ph. Eur. and utilised within 24 h at ambient temperature or within one week if refrigerated. An addition of preservatives has to be evaluated with regard to target patient group.

Glycerol 85% (G85%), PEG 400 and PG serve as viscosity enhancers and humectants minimising quick solvent evaporation and thus ink drying at the nozzles [167]. PG can additionally be used as preservative in 20% concentration based on the water phase. In medicinal products, quantities even up to 500 mg/kg bw per day are tolerated for adults based on clinical data. However, EMA limited it to 50 mg/kg bw per day in children less than 5 years old and to 1 mg/kg bw per day in pre-term and newborns due to their immature metabolism [168]. The reduced capacity of alcohol dehydrogenase could lead to potential toxic accumulation of PG especially with co-administration of EtOH. Therefore, PG should be only used in paediatric medicinal products if it is required. In case of inkjet printing, this risk is considered to be less relevant, as the applied quantity is small.

Liquid components that are miscible with each other were preferred to minimise the risk of precipitation or recrystallisation and therefore nozzle blockage. However, polymers of low-molecular weight like hypromellose (HPMC), hydroxypropyl cellulose (HPC) and povidone (PVP) in low concentrations were also tested as alternatives to modify the dynamic viscosity of the inks. High-molecular weight or high-concentration polymer solutions could hinder the drop pinching-off from nozzles due to their viscoelasticity [169]. In general, non-ionic surfactants as well as polymers were preferred to minimise later potential interactions with APIs.

3.1.2.2 Formulation Screening

The dynamic viscosities (section 5.5.1.1) and surface tensions (section 5.5.2) of the ink formulations were measured as key properties for fluid dynamics and drop formation (Table 3). Since the used inkjet printer PixDro LP50 has only integrated heating units in the print heads, an active cooling was not possible in case of an increased ambient temperature. Therefore, a print head temperature of 30 °C, close to the upper limit of the possible ambient temperature, was defined for all subsequent examinations. Thus, the physicochemical properties of developed inks had to be determined at 30 °C. The recommended dynamic viscosity limits of inks for KM are 8–12 mPa·s and for SP are 8–20 mPa·s at jetting temperature.

The surface tension should stay between 24 and 36 mN/m for SP, for KM it is not explicitly specified [170, 171].

First, the selected base fluids were investigated as potential standalone carriers for APIs in pharmaceutical inks (Table 3, T1–T5). In the next step, the base fluids were combined into dual (T14–T17) and triple mixtures (T6–T10) whereby the surfactant polysorbate 20 (PS20) was used to decrease the surface tension (T15). Aqueous solutions of low-molecular weight polymers in low concentrations were finally tested in small quantities (T11–T13).

Table 3: Ink formulations for composition screening and their physicochemical properties at 30 °C; dark green: met recommendation; yellow: too low; red: too high; orange and light green: intermediate regions (mean ± SD, n = 3)

Ink	Composition	Dynamic viscosity at 1000 s^{-1} [mPa·s]	Surface tension [mN/m]
R1	TGME (KM test ink)	5.6 ± 0.0	33.6 ± 0.1
R2	XL30 blue (SP test ink)	12.0 [172]	35.6 ± 0.0* [40]
T1	EtOH	1.0 ± 0.0	21.9 ± 0.1
T2	H_2O	0.8 ± 0.0	70.1 ± 0.6
T3	G85%	61.0 ± 1.5	65.2 ± 0.3
T4	PEG 400	64.9 ± 0.3	45.3 ± 0.2
T5	PG	29.2 ± 0.3	36.0 ± 0.1
T6	H_2O_EtOH_G85% (1:1:1)	3.6 ± 0.0	30.2 ± 0.2
T7	H_2O_EtOH_PEG400 (1:1:1)	4.7 ± 0.1	30.6 ± 0.2
T8	H_2O_EtOH_PG (1:1:1)	3.2 ± 0.1	30.6 ± 0.1
T9	EtOH_PEG400_G85% (1:1:1)	12.9 ± 0.2	30.3 ± 0.3
T10	EtOH_PG_G85% (1:1:1)	9.9 ± 0.1	29.7 ± 0.2
T11	HPC-L_H_2O (0.03:1)	10.7 ± 0.1	42.9 ± 0.2
T12	HPMC606_H_2O (0.03:1)	8.6 ± 0.1	44.2 ± 0.3
T13	PVP-K30_H_2O (1:9)	4.8 ± 0.1	45.0 ± 0.4
T14	PEG400_H_2O (1:1)	8.3 ± 0.1	43.5 ± 0.3
T15	PEG400_H_2O_PS20 (1:1:0.02)	8.3 ± 0.1	32.0 ± 0.3
T16	PEG400_EtOH (3:2)	6.3 ± 0.3	27.6 ± 0.2
T17	PEG400_EtOH (3:1)	13.5 ± 0.6	32.1 ± 0.4

*at ambient conditions

Considering only the dynamic viscosity and surface tension, it becomes clear that it is difficult to meet both properties with one formulation. For the simplest formulation consisting of a base fluid, EtOH could be an option, as the remaining candidates exceed the advised ranges. T10, T15 and T16 were the only mixtures that met the required properties. These were observed by the drop view system of the printer (section 5.5.7) using static jetting (section 5.3.3) by KM

print head. The KM print head with the smaller nozzles was chosen, as it was assumed that it would lead to more precise printing results. Jetting T10, ejected drops were visible in the drop view (section 5.5.7). However, if test printing T10 on non-edible foil substrate, no print traces and with that no drop ejection could be detected visually. The rational reason for that could not be identified. Jetting of T14, consisting of PEG and H_2O, led to an unstable drop formation which included jetting and no-jetting phase although Thabet et al. has shown printing feasibility of a similar ink composition by SP print head [85]. It was assumed that the high-shear rates within the print head led to lower hydration of PEG so that it resulted in locally short-termed increase of viscosity and with that to jetting failures. Water forms two hydrogen bridges to two different ether oxygen atoms of PEG stabilising its helical structure. Few water molecules that are not directly associated with PEG are sufficient to trigger a stiffening effect and reduced contraction of PEG molecules [173]. Jetting (section 5.3.3) of T15 was feasible but also instable so that the decrease of surface tension by PS20 did not lead to an improvement in comparison to T14. Therefore, mixtures of H_2O and PEG 400 were considered as not suitable as base fluids for pharmaceutical inks. Raijada et al. have already tested different mixtures of EtOH and PEG 400, but with a different printing system [156] so that a direct comparison is not possible. However, jetting of T16 showed also no issues using KM print head, increasing the PEG 400 quantity from 60 to 75% (w/w) led to the limits of the system due to higher viscosity of 13.5 ± 0.5 mPa·s. To jet T17, a print head temperature of 35 °C was required which was not within the intended temperature range. Since EtOH is only able to form a single hydrogen bond, it does not lead to locally abrupt increased viscosities in case of segregation effects due to high-shear rates [173]. For further investigations the mixtures of EtOH and PEG 400 as basic ink formulations were used as it was demonstrated that they were stably jettable and printable.

After performing the preliminary trials, two approaches of ink formulation development became conceivable. Excipients could be combined until the range of properties for viscosity and surface tension recommended by the print head manufacturers are exactly hit. However, this is still no guarantee that the developed formulation will actually be printable over a longer period of time and in a reproducibly stable manner. Solutions mixed with various excipients show a much wider range of complex interactions. Density, transmission of the sound wave through the ink, viscoelasticity, dynamic surface tension, rheological stress of the ink before passing the nozzles, ink chemistry in general, dissolved gases and more contribute to final

droplet formation. This includes print head geometry and adjusting print settings in concert with target formulation. It could be a time-consuming and less promising formulation strategy.

Alternatively, only the upper limit of the recommended ranges could be considered as a guidance not to be exceeded. Liquids that are too viscous with high surface tension result in missing drops because the ejection energy per se is insufficient. No process adjustment can be performed in this case. Physicochemical properties that are too low carry the risk of producing satellites (section 1.2.1) that are difficult to control, but enable drops to be ejected in general. For the printing industry, it is essential to avoid these, as they reduce the quality of the printed image. However, whether the satellites are a relevant challenge in the pharmaceutical production of uniform doses remains to be clarified. Further additions and parallel adjustment of the print settings could achieve the target result more efficiently and systematically.

3.1.2.3 Model Lead Formulations and Their Physicochemical Properties

Following the first formulation screening, a more systematic investigation into the interactions between physicochemical properties of the ink and the potential printing systems should be carried out. In order to achieve different properties with minimum number of components, three ink formulations based on EtOH and PEG 400 were chosen (section 5.2.2.1). Millijet® blue 28 (MB28) that is usually used for industrial inkjet applications [154, 174], was used as model substance because of its good colouring and solubility characteristics but had no pharmaceutical relation.

The objective was that the ink properties stayed below the recommended upper limit of print head manufacturers as previously proposed (section 3.1.2.1). The higher the ratio of PEG 400 within the ink formulation, the higher are the dynamic viscosities, surface tensions and the densities of the tested samples (Table 4). Since the physicochemical properties could not be adjusted independently, it was not feasible to produce inks of foreseen values to fulfil the experimental design by using only the two components. Dynamic viscosity was chosen as representative factor for the follow-up design of experiments (DoE) (section 5.4.1.1) investigations because it was more sensitive towards changes of the system. The minimum and maximum possible surface tension differed between the inks by factor 2 and density even smaller, the difference between the viscosities was approximately a factor of 65.

Table 4: Results of investigations on physicochemical properties at 30 °C (mean ± SD, n = 3)

Ink	Composition [v/v % ǀ w/v %]					Dynamic viscosity at 1000 s^{-1} [mPa·s]	Surface tension [mN/m]	Density [kg/m^3]
F1	EtOH_MB28	100		ǀ	2	1.0 ± 0.0	22.0 ± 0.1	748.4 ± 9.1
F2.1						4.3 ± 0.2	26.1 ± 0.1	894.8 ± 0.6
F2.2	EtOH_PEG400_MB28	50	50	ǀ	2	4.4 ± 0.1	26.1 ± 0.0	887.3 ± 0.1
F2.3						4.4 ± 0.1	26.5 ± 0.1	903.1 ± 1.2
F3	EtOH_PEG400_MB28	40	60	ǀ	2	6.7 ± 0.2	27.7 ± 0.2	917.0 ± 3.7

Due to reported high shear forces up to 10^6 s^{-1} during a printing process [175], the flow properties of the inks were additionally determined by the optical high-shear rheometer (section 5.5.1.2). The investigations on the rheological characteristics showed that the produced ink F1 was a Newtonian fluid even at high shear rates, however, F2 and F3 showed different curve progressions (Figure 8). F2 showed a slight downward trend from 4.7 to 4.2 mPa·s. Regarding F3, shear thinning could be observed from a shear rate of 7,300 s^{-1} and was partially repealed at 140,000 s^{-1}. Since these were single measurements obtained at an external laboratory, it was difficult to make a general statement. Nevertheless, the 10 recorded values of F1 and F2 had a very small analytical standard deviation whereas F3 showed higher scattering and with that a less stable system. This reinforced the hypothesis of a shear rate-dependent deviation from Newtonian flow behaviour due to presence of increasing amount of PEG 400.

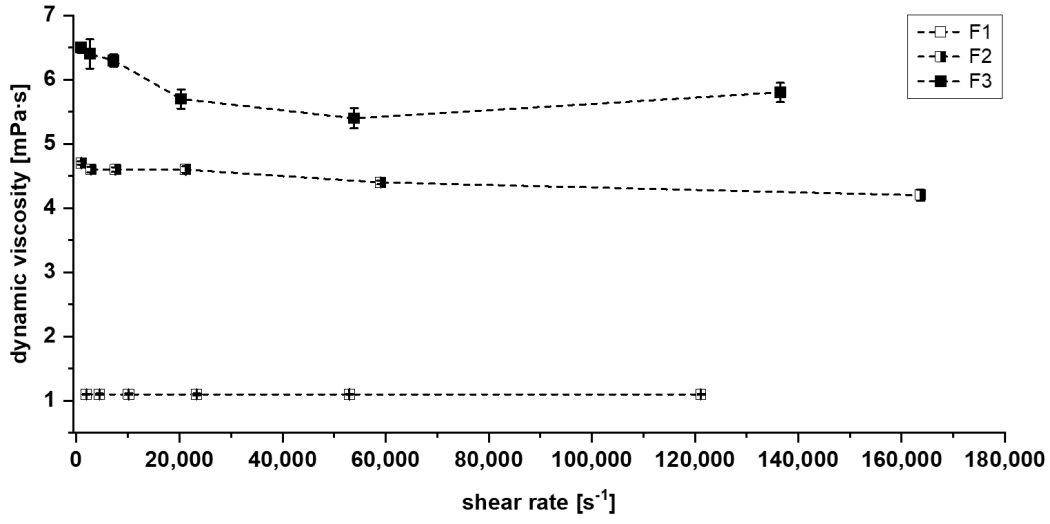

Figure 8: Flow characteristics of the ink compositions F1–F3 measured by Fluidicam RHEO at six different shear rates (mean ± analytical SD, n = 1) (modified from Kiefer et al. [176], by courtesy of Elsevier)

3.1.2.4 Printability and Drop Properties

In order to be more broadly positioned, two different printing systems, KM and SP print head, were considered with regard to the printability of the inks, in contrast to the initial screening process (section 3.1.2.1).

The inverse Ohnesorge number *Z* (section 1.2.1) for each ink formulation and the respective print head was calculated and placed in context of theoretical evaluation of printability in literature [58, 59]. F1 with *Z* of 18.1 (KM) and 24.0 (SP) is expected to be accompanied by satellite drops. F2 with *Z* of 5.0 (KM) and 6.6 (SP) can be evaluated as a printable fluid. Finally, F3 with *Z* of 3.4 (KM) and 4.5 (SP) is on the borderline between printable and too-viscous fluid and could probably show jetting failures.

The default settings for each print head, pre-set by the printer manufacturer, were used to record the ink in flight by the drop view camera (section 5.3.1 and 5.5.7). Comparing the resulted drop images (Figure 9) with the theoretical performance prediction, the assumption for F1 can be confirmed. The low viscosity and surface tension led to satellites for both KM and SP, whereby the drop applied by SP appeared even more consistent. In case of F2, KM ejected an elongated drop due to acceleration and SP a two-part drop consisting of an elongated ligament and leading spherical drop. The latter will probably merge together with the main drop due to different speeds. For this purpose, images taken at different distance from the nozzle plate, so-called LED delay, have to be considered in later examinations. This is the preferred approach to determine the change in drop dynamics during flight depending on the covered distance.

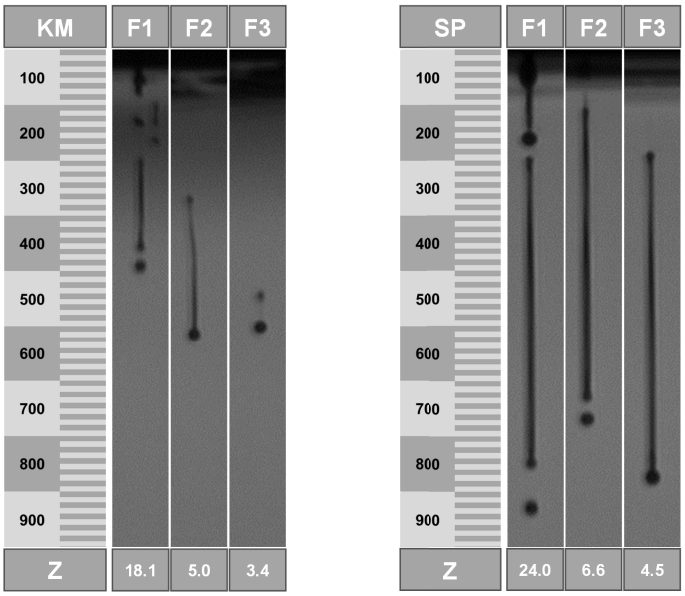

Figure 9: Drop view images of ink formulation F1, F2 and F3 jetted by KM and SP print head at 30 °C, depicted with corresponding calculated Ohnesorge numbers (*Z*), records at various LED delays; images cut from original

It became apparent that the physicochemical ink properties are not sufficient to characterise the drop performance during the printing process in general, since the print settings also highly influence the ink printability. This will be discussed in more detail in the following section 3.2.

First printing experiments were conducted. On closer examination of imprinted ODFs by the light microscopy (Figure 10), differences could be identified between the used ink formulations, but also the applied print heads. F1 covered the film substrate so that the single drop pattern was no longer visible after evaporation of EtOH. Since the applied ink volume was higher, the colour intensity of the prints by SP print head appeared stronger.

With addition of PEG 400, the morphology of the printed ODFs changed. Single drops became visible, whereby a higher percentage of PEG 400 resulted in less wetting of the film and less coalescence of the ink. At the same time, the drying of the ink was not sufficient so that the ink containing PEG 400 could be easily smudged on the film substrate. Finally, missing lines could be seen when using ten nozzles of KM print head. This showed first deficiencies of the system.

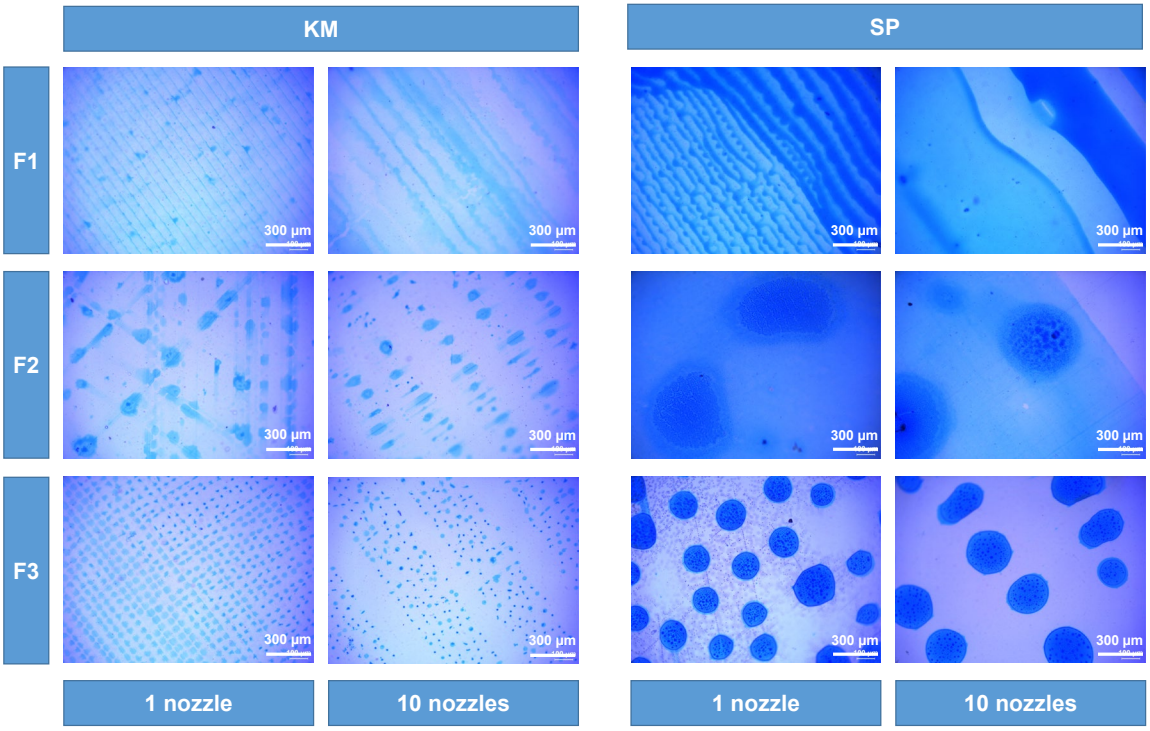

Figure 10: Light microscopic images of printed areas (500 dpi) by one or ten nozzles on HPMC-based ODFs (used from Kiefer et al. [176], by courtesy of Elsevier)

3.1.2.5 Drying Behaviour

The drying time of ink formulations on the substrate is a key parameter for fast processing. Drying means in that case that the liquid ink components are removed by evaporation. During the first printing experiments (section 3.1.2.4) it has become apparent that inks containing PEG 400 did not dry in an appropriate process time of few hours and could still be wiped off after three days. To analyse the drying behaviour of the inks, a thin ink layer was dried in an oven at constant temperature and weighed at selected time points (section 5.5.5). Imprinted film substrates were not investigated because of only small amounts of deposited fluid volume. Considering all ink formulations after 6 h no significant change in weight was observed (Figure 11). F1 showed the largest decrease to 2.5% (w/w) of original weight which matches the proportion of MB28 in the ink. EtOH was completely evaporated. On the contrary, 52.8% (w/w) of F2 and 64.9% (w/w) of F3 were left approximately corresponding to the PEG 400 and the dye MB28 amount in the ink. This behaviour could be explained by the low vapour pressure of PEG 400 of < 0.1 hPa at 20 °C [177]. Therefore, PEG 400 was expected to accumulate soluble APIs like the model dye on the surface and act as an additional plasticiser for polymer films due to its low volatility.

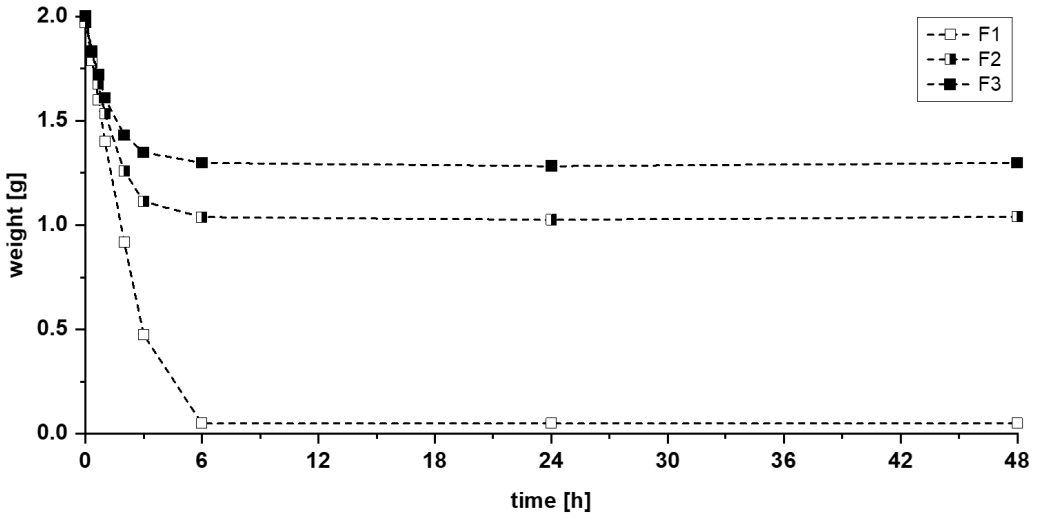

Figure 11: Drying process of the ink compositions F1–F3, loss of weight during drying time at 30 °C (n = 1) (modified from Kiefer et al. [176], by courtesy of Elsevier)

It could be concluded that PEG 400 is not suitable of large proportions for an ink formulation printed on HPMC-based substrates which lack absorption into the film matrix. Because of extended drying time the films could not be processed and packed. Nevertheless, the formulations containing PEG 400 were acceptable as model inks for further investigations regarding inkjet process understanding (section 3.2.2).

3.1.3 Metoprolol Tartrate Ink

3.1.3.1 Formulations and Their Physicochemical Properties

As MPT is highly soluble in water according to Ph. Eur., deionised water was chosen as carrier fluid for the ink. The advantage of water for drug-loaded inks for printing is that it is a non-toxic solvent. A potential hazard, however, is bacterial or fungi growth during storage. As preservatives should be avoided for use as ink for the paediatric population, especially neonates [12], the formulations are intended for processing within 24 h. An addition of preservatives could be considered for older children only.

A surfactant has to be used because water shows a surface tension of 71.2 ± 0.6 mN/m at 30 °C, which is too high for stable inkjet printing [178]. Poloxamer 407 (P407) was selected at a concentration of 0.1% (w/w) due to its non-ionic character so that less interactions with ionic APIs could occur. As jetted fluids can be accompanied by satellites, 1% HPMC 615 was added to modulate the ink viscosity and stabilise the drop ligament [52]. HMPC of higher molecular weight than in section 3.1.2.2 was used to reduce the quantity from 3% to 1% (w/w) achieving

a comparable dynamic viscosity at the same time. Additionally, 10% glycerol (G85%) was used as a viscosity enhancer but mainly as a humectant to prevent too-fast water evaporation.

To investigate the influence of the individual components on the ink properties, drug-free solutions (I1–I4) were analysed in addition to MPT-containing formulations (I5–I9) (Table 5). An ink based on an EtOH-water mixture (E) was produced for comparison purposes. With an EtOH mole fraction of 0.236, a maximum dynamic viscosity at 30 °C can be achieved without additional viscosity enhancer [179]. Water (R) served as a reference. SP print head was planned as printing system.

Table 5: Composition of investigated drug-free (I1–I4, R) and MPT-containing (I5–I9, E) ink formulations (w/w %) and the results of investigations on physicochemical properties dynamic viscosity, surface tension and density at 30 °C (mean ± SD, n = 3)

Ink	P407 [%]	G85% [%]	HPMC615 [%]	MPT [%]	H_2O [%]	EtOH [%]	Dynamic viscosity at 1000 s^{-1} [mPa·s]	Surface tension [mN/m]	Density [kg/m^3]
R	-	-	-	-	100	-	0.8 ± 0.0	70.1 ± 0.6	995.7 [180]
I1	0.1	-	-	-	99.9	-	0.8 ± 0.0	39.8 ± 0.3	998.2 ± 3.4
I2	0.1	10.0	-	-	89.9	-	1.0 ± 0.0	39.7 ± 0.4	1019.4 ± 1.6
I3	0.1	-	1.0	-	98.9	-	3.1 ± 0.1	40.3 ± 0.6	1000.4 ± 2.1
I4	0.1	10.0	1.0	-	88.9	-	4.1 ± 0.1	39.7 ± 0.5	1019.7 ± 3.4
I5	0.1	-	-	10.0	89.9	-	1.2 ± 0.0	38.3 ± 0.5	1013.7 ± 2.5
I6	0.1	-	1.0	10.0	88.9	-	5.2 ± 0.1	38.7 ± 0.7	1007.6 ± 12.1
I7	0.1	10.0	1.0	10.0	78.9	-	6.2 ± 0.1	39.4 ± 0.4	1040.3 ± 2.2
I8	0.1	-	-	20.0	79.9	-	1.8 ± 0.0	38.8 ± 0.3	1038.6 ± 1.7
I9	0.1	-	-	41.0	58.9	-	6.7 ± 0.1	37.2 ± 0.2	1082.3 ± 1.2
E	-	-	-	10.6	49.9	39.5	2.4 ± 0.0	29.9 ± 0.1	937.4 ± 6.5

Regarding the key properties of the prepared inks, it is noticeable that surface tensions of the inks I1–I9 were quite similar at about 40 mN/m (Table 5) and mainly depend on the use of surfactant P407. Only the addition of EtOH in E led to a decreasing value. Dynamic viscosity, on the contrary, was clearly influenced by the total ink composition. The addition of MPT resulted in a greater change of ink viscosity if HPMC was already present in the solution. This could be described by the solvation of dissociated MPT salt. Fewer water molecules are available for the hydration of HPMC chains so that the dynamic viscosity increases. Glycerol 85% as a liquid with dynamic viscosity of 61 ± 1.5 mPa·s at 30 °C leads to a further increase. Finally, the fluid density is affected by the solid content as well as by the amount of glycerol.

In summary, all components have a certain impact on the physicochemical ink characteristics, which makes a systematic ink development more complex.

The investigations on flow behaviour of MPT inks at high shear rates confirmed Newtonian flow behaviour for inks I5, I7, I8 and E (Figure 12). The first measured value deviated slightly from the second value in each case. This could be explained by the fact that the dynamic viscosity of the samples is low and the target shear rate of 1000 s^{-1} cannot be reached due to still existing turbulent flows. Laminar flow only occurs at a higher flow rate. Since I7 contained 1% (w/w) HPMC 615, it was a pseudoplastic fluid showing shear thinning with increasing shear rate. Higher MPT quantity of I8 led to significant higher viscosity compared to I5.

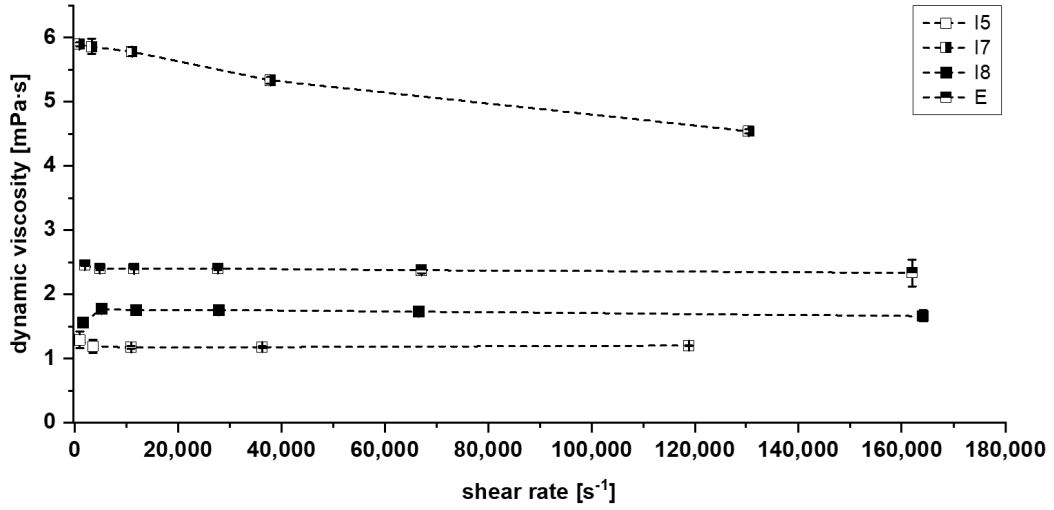

Figure 12: Flow characteristics of the ink compositions I5, I7, I8 and E measured by Fluidicam RHEO at different shear rates (mean ± analytical SD, n = 1)

3.1.3.2 Printability and Drop Properties

Further to the previously used implemented drop analysis tool of the HMI software (section 3.1.2.4), the advanced drop analysis (ADA) add-on was applied to determine the general printability of ink formulations. For that purpose, the long-term drop stability was determined at varying LED delays at fixed waveform (section 5.3.1.2). The formulations R, I1, I2, I4, I5, I7 and E could be jetted stably during the investigated period. Inks I4 and I7 which contained HPMC 615 were printable but wiping of the nozzle plate and purging between trials was necessary to regain a stable jetting. The polymer probably dried in some areas despite the promise of glycerol. Therefore, it has been decided to skip I3 and I6 which did not contain glycerol at all to avoid the risk of blocked nozzles and process failures due to HPMC.

The inverse Ohnesorge number Z (section 1.2.1) for each ink formulation was calculated. R ($Z = 61.8$), I1 ($Z = 46.6$), I2 ($Z = 37.6$) and I5 ($Z = 30.7$) are expected to be accompanied by satellite drops. I4 ($Z = 9.2$), I7 ($Z = 6.1$) and I9 ($Z = 5.6$) can be evaluated as fluids in the printable region. Finally, E is borderline between printable and too-low viscous fluid and could probably show some satellites.

Regarding the drop images at a LED delay of 50 µs (Figure 13), the ejected ink drops look similar. All inks, except I4 and I7, showed a fast leading satellite in front of the main drop due to exceeding a critical acceleration at the nozzle [181]. That was not predicted by calculated Z value. At this point, the surface tension forces were not sufficient to hold the ink together according Wijshoff et al. The surface tension of R was much higher than the one of I4 and I7, but did not prevent the formation of leading satellite. Therefore, it was assumed that the viscosity has a higher impact in this case. All inks formed long tails with a leading spherical head whereby E has been stretched so far that the head is barely visible. Only when images at a LED delay of 75 µs were considered, it could be noticed that the tails broke-up in small drops in case of R, I1 and I2. Additionally, slower satellites were formed from the tail of the drop as predicted. Only the ink I7 and I9 remained as coherent drops. The leading edge of E was so fast that after 75 µs the drop exceeded the limits of the image area.

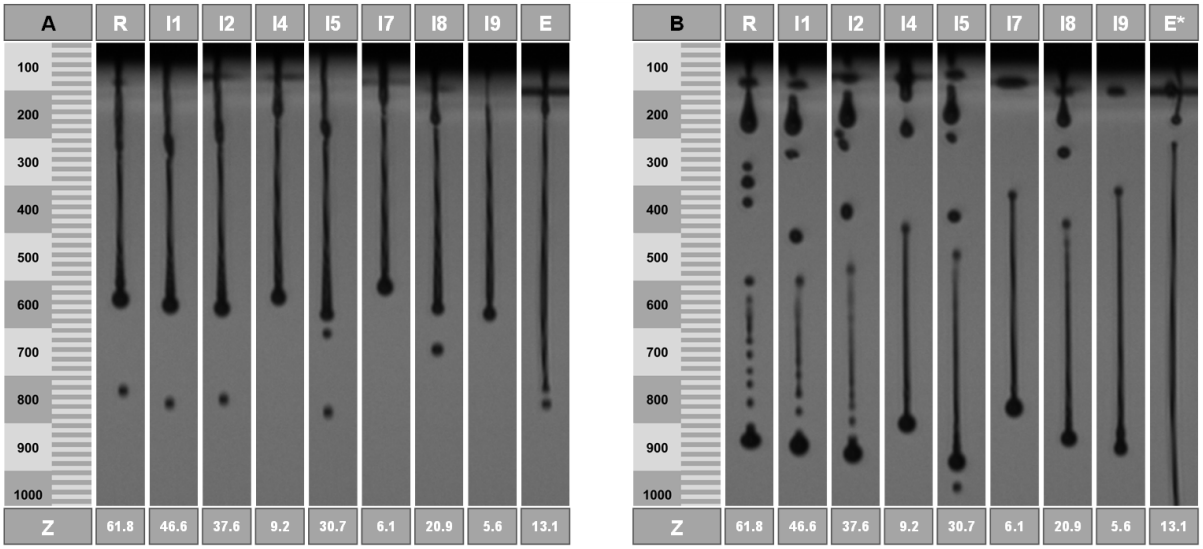

Figure 13: Drop view images of jetted ink formulations by SP at 30 °C, pulse voltage of 100 V (90%) and a pulse timing of 2–5–2 µs at LED delays 50 µs (A) and 75 µs, exceptionally 60 µs for E* (B); depicted with corresponding Ohnesorge numbers (Z)

A preselection of ink formulations was performed on the basis of the jetting behaviour. With the help of a drop analysis method, I5 and I7 were identified as the most promising

formulations. I8 and I9, differ from I5 only in the MPT content, were also suitable inks and will further discussed in section 3.2.4.3 as part of different dosing concepts.

3.1.3.3 Selection of Lead Formulation

To figure out the most suitable composition on a discrimination basis, the distribution of MPT after printing I5 and I7 was investigated. Already, visually, a difference between I5 and I7 could be detected. ODFs imprinted by I5 showed a regular line pattern (Figure 14, A), whereas the ones imprinted by I7 (Figure 14, B) showed a blurred structure. Counting the lines of I5-ODF, however, the theoretical number of 500 deriving from the set resolution was not reached, and only 38 lines could be recovered. This could indicate that the drop diameters are larger than the swath width, but it still does not explain why I5 and I7 resulted in different print patterns.

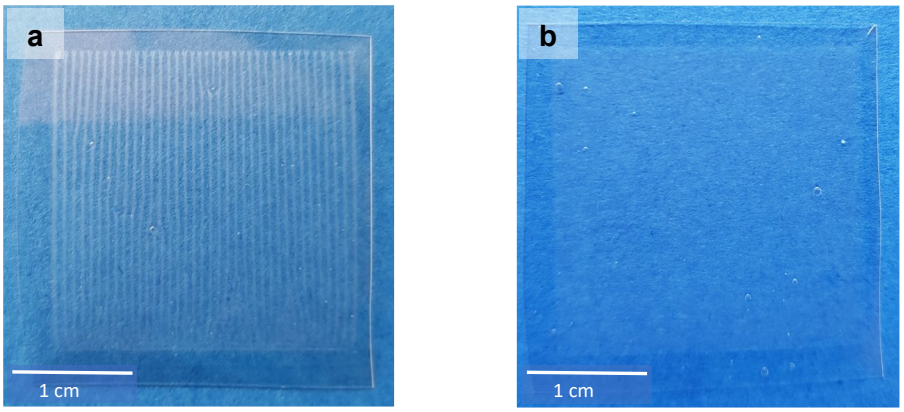

Figure 14: Ink formulations I5 (a) and I7 (b), printed on HPMC-ODFs using a resolution of 500 dpi, resulting in 500 × 500 drops on an area of 1 inch² (≈ 6.45 cm²) (modified from Kiefer et al. [41])

To examine the observed differences in more detail, confocal Raman microscopy (section 5.5.20.3) was used. In the dark field, the previously mentioned line pattern of I5-ODF turned out to be a featherlike structure (Figure 15a). This strengthened the hypothesis of an unequal distribution of MPT. The explanation could be found in the partial line-by-line dissolving of the film surface by the water-based ink during printing, but it does not reflect the mismatch of visible line number and set resolution.

For Raman mapping, a characteristic peak had to be found for MPT which is not influenced by the second main component HPMC. After analysis of the spectra of pure substances, the MPT peak at 1615 cm^{-1} (Figure 15b) was chosen.

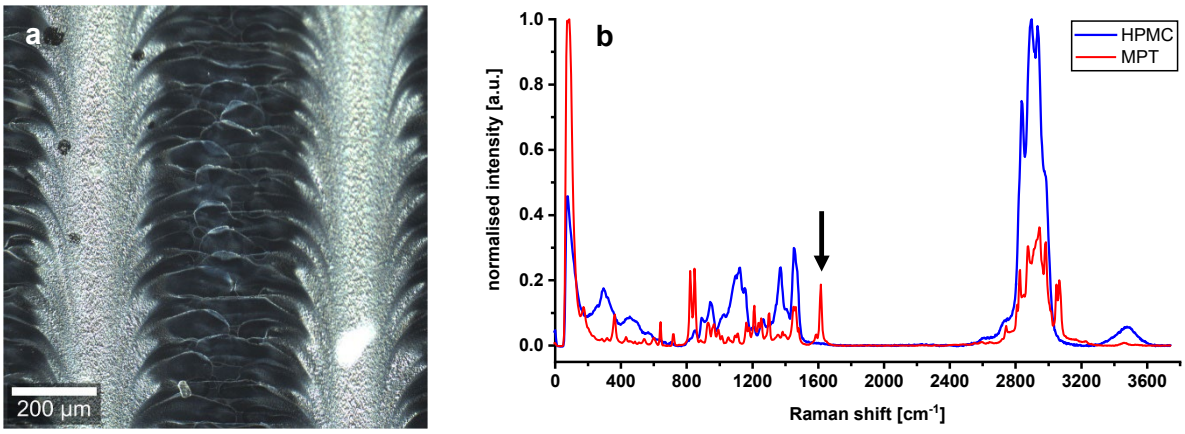

Figure 15: Dark field image of ODF imprinted by I5 (a) and Raman spectra of pure substances HPMC and MPT (b) with a characteristic peak at 1615 cm^{-1} and 10 s exposure time, normalisation to the intensity of respective maximum peak in arbitrary unit (a.u.) (modified from Kiefer et al. [41])

Raman measurements of a freshly manufactured sample stored for one day in a desiccator at 18 °C were performed. 17 points were selected along a line of 800 µm so that the light and dark feather-like structures could be captured (Figure 16). Small-stepped scans were performed at each point with a spatial resolution of 0.5 µm and 10.0 s exposure time along a depth of 20 µm. Since the measurements could not always start exactly at the same distance from the ODF surface, the first measurable Raman intensity maximum was defined as surface (depth = 0 µm). In total, 577 Raman spectra were recorded along 17 µm depths, which are about half the thickness of the film. With increasing depth, the Raman intensity decreased due to the decreasing MPT concentration and not due to the increasing deflection of the laser. This was confirmed by a two-point measurement of the film back side, which resulted in no presence of MPT. Furthermore, an intensity profile corresponding to the surface structures becomes obvious. There is a higher MPT concentration in the light areas of the dark field image than in the darker areas. This actually means that the regular deposited ink drops coalesce on the ODF before drying and that the drops have not been deposited regularly at all. This topic is discussed in more detail in the following section. After short storage of one day at low relative humidity (RH) and temperature (15–30% RH, 18 °C) directly after printing, the diffusion of MPT was limited to the upper half of the ODF (Figure 16a). After a further storage of the sample in polyethylene-sachet at room conditions with higher temperature and relative humidity (40–60% RH, 22–25 °C) for 2.5 months, the diffusion took place throughout the entire film thickness. This led to a homogenous MPT distribution but smaller Raman intensities due to lower concentration per film volume (Figure 16b).

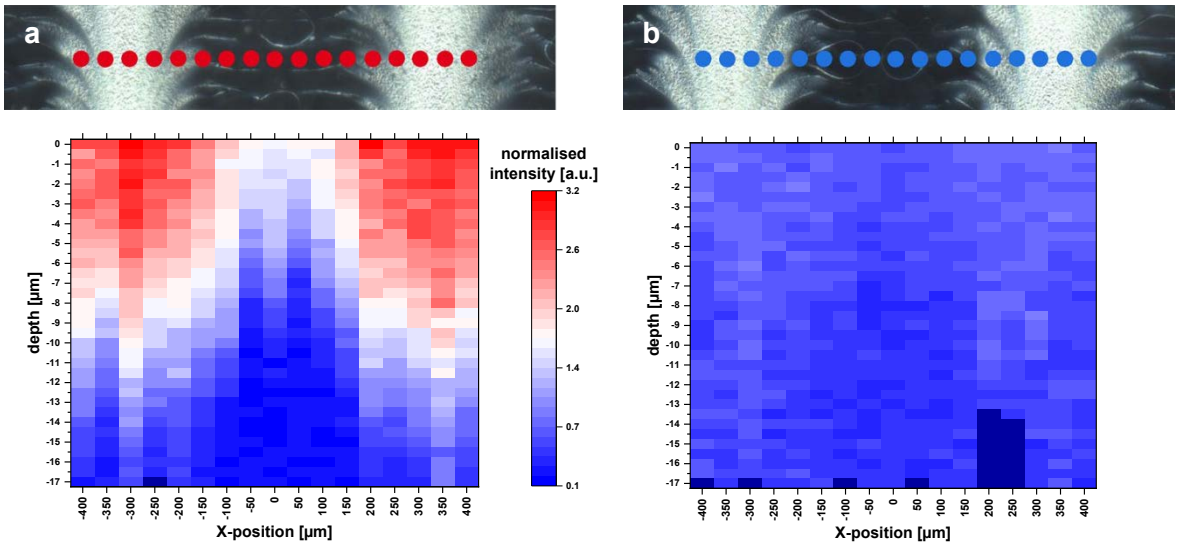

Figure 16: Dark field images and corresponding heatmaps of single-point depth scans (17 positions) at 1615 cm^{-1} recorded with spatial resolution of 0.5 µm and 10.0 s exposure time (a) one day after printing and (b) 2.5 months after printing, normalisation related to the HPMC peak at 1370 cm^{-1}; red: high intensity, blue: low intensity, dark blue: no data available (modified from Kiefer et al. [41])

In contrast, I7 ink stayed partially on the surface of the ODF and accumulated the dissolved MPT (Figure 17a). The ink could be easily wiped off by rubbing, touching or packaging of the ODF. The reason is that glycerol did not evaporate completely within an appropriate process time and was not completely incorporated into the film matrix. Porous or functionalised substrates could be an opportunity to solve this issue [98, 126]. A depth scan (Figure 18) was performed along the yellow line (Figure 17a). The printed side was placed upwards. By analysing the Raman spectra (Figure 17b), a qualitative assignment of the components could occur. The red marked area displays a mixture of glycerol, HPMC and MPT, and the blue marked area a mixture of HPMC and MPT. For an accurate quantitative statement, a further calibration step should be carried out. It can be noticed that glycerol drops containing MPT are located on the ODF surface. Since the drops deflected the Raman signal, there are black unassigned spaces. To verify that the whole film consists mainly of HPMC, the film sample was turned over so that the printed side was facing down. As it is challenging to find exactly the same spot again, the investigated area was slightly shifted. Nevertheless, a drop of glycerol is visible on the bottom side. The black area is replaced by a continuous blue one because of the smooth surface, and only a small air bubble in the film matrix can be anticipated. By performing Raman mapping, it was feasible to determine the localisation of MPT after printing of two potential ink formulations and draw further conclusions based on this.

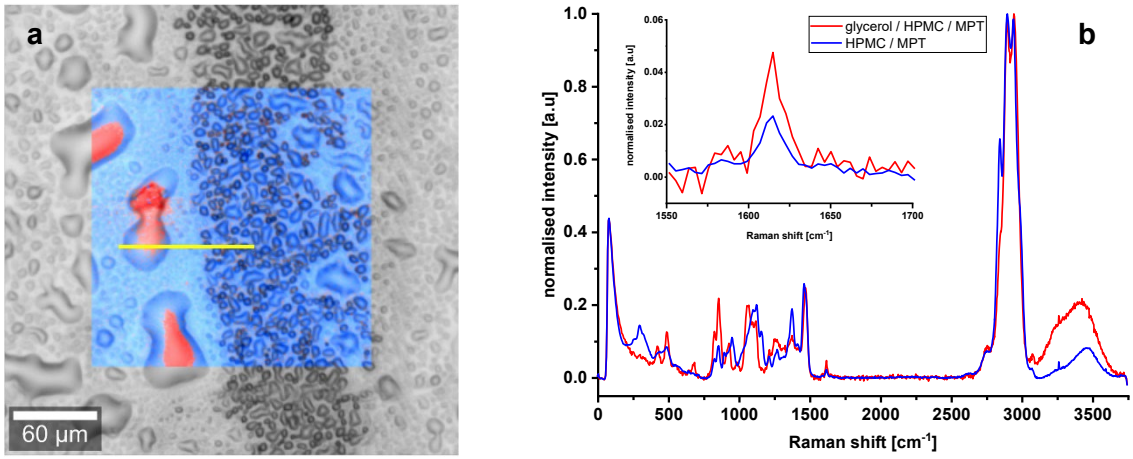

Figure 17: Raman microscope surface scan of ODF imprinted by I7 (a) with an area of 200 × 200 µm, spatial resolution of 1 µm and 0.05 s exposure time. Average normalised Raman spectra of the surface scan (b) with magnified characteristic MPT peak at 1615 cm^{-1}; HPMC and MPT; blue: mixture of HPMC and MPT (modified from Kiefer et al. [41])

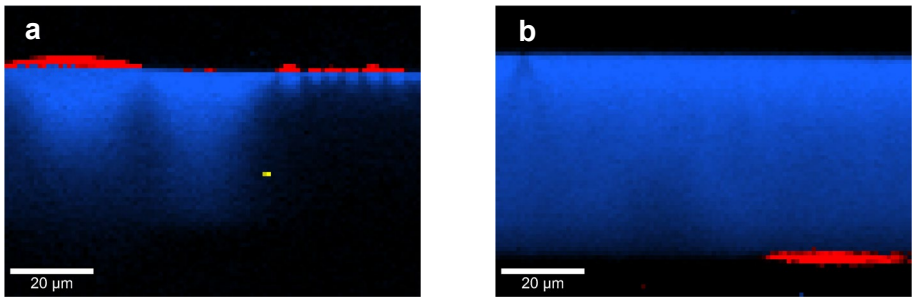

Figure 18: Depth scan of the cross-section from top (a) and bottom side (b) of the ODF with an area of 100 × 70 µm along the yellow line in Figure 17, spatial resolution of 1 µm and 0.2 s exposure time; red: mixture of glycerol, HPMC and MPT; blue: mixture of HPMC and MPT (modified from Kiefer et al. [41])

In case of ODFs which disintegrate rapidly and are being swallowed with saliva flow, the distribution of API and ink excipients within the film matrix after inkjet printing and during storage primarily serves to differentiate between suitable and unsuitable ink formulations. Regarding further film application like mucoadhesive buccal films for oromucosal drug delivery, however, the uncontrolled API diffusion could be crucial if unidirectional drug release towards the oral mucosa has to be assured. There could be a risk of undesirable co-dissolving of the directly subsequent protecting backing layer during printing of high ink quantities onto the mucoadhesive film layer. Confocal Raman microscopy offers a helpful tool to investigate and evaluate these phenomena on a small scale.

A series of formulations were investigated with the aim of developing printable drug-loaded inks for manufacturing of individual-dose ODFs with metoprolol tartrate. It was found that glycerol is not suitable as an excipient with the function to prevent drying at the nozzles for inks printed on ODFs based only on HPMC. Due to a lack of penetration into the substrate

and evaporation, an API loss-free handling and packaging cannot be ensured. A more absorbent film substrate has to be developed to overcome this issue. Finally, an unexpected feather-like surface structure of imprinted ODFs was detected. Further investigations were carried out to find out the rational cause. These will be discussed in the following section 3.2.3 on the topic of process understanding.

3.1.4 L-Thyroxine Ink

3.1.4.1 Formulations and Their Physicochemical Properties

According to Ph. Eur., the sodium salt of LT is with 0.15 g/l very slightly soluble in water and with 4 g/l slightly soluble in EtOH 96%. Since no sodium salt form was available for the present experiments, the LT classified as insoluble in water and alcohols according to the safety data sheet was used [182]. There is a manufacturing instruction for compounded preserved aqueous drops [148] of a concentration of 0.25 µg/ml including 40% (v/v %) anhydrous glycerol which could be used as starting point for ink formulation development. However, the concentration of the ink should be high enough to ensure dosage application in therapeutic range. As the application by inkjet printing is rather in the microlitre range, this approach could not be used.

In published literature [90, 91], polar aprotic dimethyl sulfoxide (DMSO) in high proportion was used in pharmaceutical inks as cosolvent for LT. Although it is classified as solvent of low toxic potential (class 3) with PDE of up to 50 mg according ICH guideline Q3C(R8) [164], there are many controversial discussions about the safety in humans. There are hints that DMSO can induce changes in cellular processes [183] and show dose- and application-route-dependent adverse effects [184]. Since there are no approved oral medicines containing DMSO and it is not recognised as safe, caution is advised during use, especially in children.

In the present study, the developed ink formulation for LT was based on the eluent mixture used by Alomari et al. for HPLC analysis [90]. DMSO, EtOH and H_2O were mixed in the ratio 30:30:40 (v/v %) (section 5.2.2). The light sensitivity and poor solubility elaborated the test setup. Since the use of DMSO could not be avoided, the theoretical and actual quantity of DMSO should be determined in order to evaluate the potential risk for patients.

The dynamic viscosities and surface tensions of drug-free (L1) and LT-containing ink (L2) were determined (Table 6). No significant differences were expected due to low concentration of LT. This could be confirmed.

Table 6: Results of investigations on physicochemical properties at 30 °C (mean ± SD, n = 3)

Ink	Dynamic viscosity at 1000 s^{-1} [mPa·s]	Surface tension [mN/m]
L1	2.2 ± 0.0	33.4 ± 0.2
L2	2.2 ± 0.0	33.9 ± 0.2

DMSO is sparingly volatile with 0.55 hPa at 20 °C [185]. Therefore, it is assumed that its ratio in the ink remains the same after printing. During drying on the film substrate, EtOH and H_2O are expected to evaporate almost residue-free, while DMSO is expected to remain unchanged.

3.1.4.2 Printability and Drop Properties

As the drug-free ink formulation L1 has been shown the same physicochemical properties as LT-containing L2 ink, it was used to check the general printability avoiding the printer contamination with potent drug. Based on the gained experience from previous trials, the jetted L1 ink was observed by drop view at different LED delays (Figure 19) (section 5.3.1.2 and 5.5.7). After 10 µs no drop has been released. This delay could be explained by a slower build-up of the pressure wave within the ink after contraction of the channel walls. The ejected drop was elongated but stayed a coherent drop consisting of a long tail and small leading spherical head. Only after its pinch-off from the nozzle, a slow satellite from the tail was formed.

The long-term drop stability was determined. L1 could be jetted stable during the investigated period. After printing on an HPMC-based film substrate, the ink seemed to be absorbed by the film matrix. No residuals could be manually wiped off.

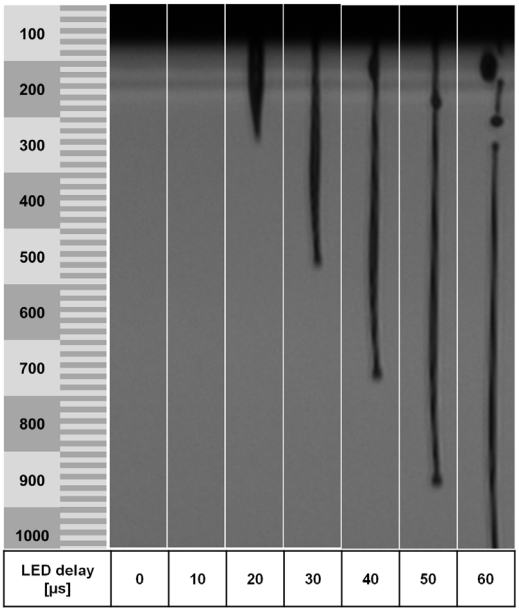

Figure 19: Jetted L1 ink by SP print head at print head temperature of 30 °C and pulse voltage of 100 V (90%) and a pulse timing of 2–4–2 µs at different LED delays

3.1.5 Summary and Conclusion

After an excipient selection, drug-free and API-containing pharmaceutical inks were developed and characterised. On the basis of the gained experiences, the formulation development process could be optimised. Confocal Raman microscopy was established as a tool to detect API and excipients distribution and location within the imprinted films. It could be shown that API diffuses over time into the ODF matrix. Besides, it turned out that high quantities of glycerol and PEG 400 led to insufficient drying of ink on film substrate surface and with that to an accumulation of API or dye. All pre-selected formulations were printable but they showed various drop shapes while jetting. The dimensionless Z numbers could predict whether the ejected drops were consistent or accompanied by satellites. Nevertheless, a drop view system is required as additional quality control tool to evaluate the actual device dependent jetting performance. The ink drops have to be recorded at different distances from the nozzle plate to catch the drop dynamics.

3.2 Process Understanding of Pharmaceutical Inkjet Printing

Parts of this section have already been published in peer-reviewed journals. The content was linguistically and graphically adapted. Further data have been added.

- Kiefer O., Breitkreutz J., 2020. *Comparative investigations on key factors and print head designs for pharmaceutical inkjet printing*, Int J Pharm 586, 119561.
  DOI: 10.1016/j.ijpharm.2020.119561
- Kiefer O., Fischer B., Breitkreutz J., 2021. *Fundamental investigations into metoprolol tartrate deposition on orodispersible films by inkjet printing for individualised drug dosing*, Pharmaceutics 13(2), 247.
  DOI: 10.3390/pharmaceutics13020247

3.2.1 Introduction and Objectives

In order to extend the process understanding, selected subjects of the inkjet printing technology were considered with regard to the pharmaceutical application. Now that the ink formulation development has been discussed (section 3.1), the main focus was on the inkjet equipment and the associated settings.

Two piezoelectric driven print heads working in shear rate, KM512SHX (KM) and Spectra SE-128 AA (SP) were compared within a systematic approach. The print heads differ in their nozzle diameter and number as well as in the piezoelectric actuation units (Figure 20).

SP has 128 nozzles in single row (Figure 20a, SP) with a diameter of 35 µm ejecting respectively a nominal drop volume of 30 pl. It operates in shear mode whereby the perpendicular applied electrical field to the polarisation direction leads to shear deformation of the two independent piezoelectric ceramic (PZT) slices A and B. They are located at the back of channels and are controlled by one trapezoidal pulse voltage divided into rising/falling and a dwell phase (Figure 20b, SP). The ink can be ejected simultaneously from all nozzles. KM has 512 nozzles in two rows, R and L, ejecting respectively a nominal drop volume of 4 pl (Figure 20a, KM). It operates by the shared-wall principle, a special case of the shear mode. The channels themselves are made of PZT and two adjacent nozzles share one channel wall so that the ink can be only ejected successively (Figure 20b, KM). It is driven by a high and a low pulse voltage

(ON V, OFF V) which are held for a defined time period. The high voltage causes ink ejection by channel contraction and the low voltage leads to ink refilling into the channels by moving the channel walls outwards.

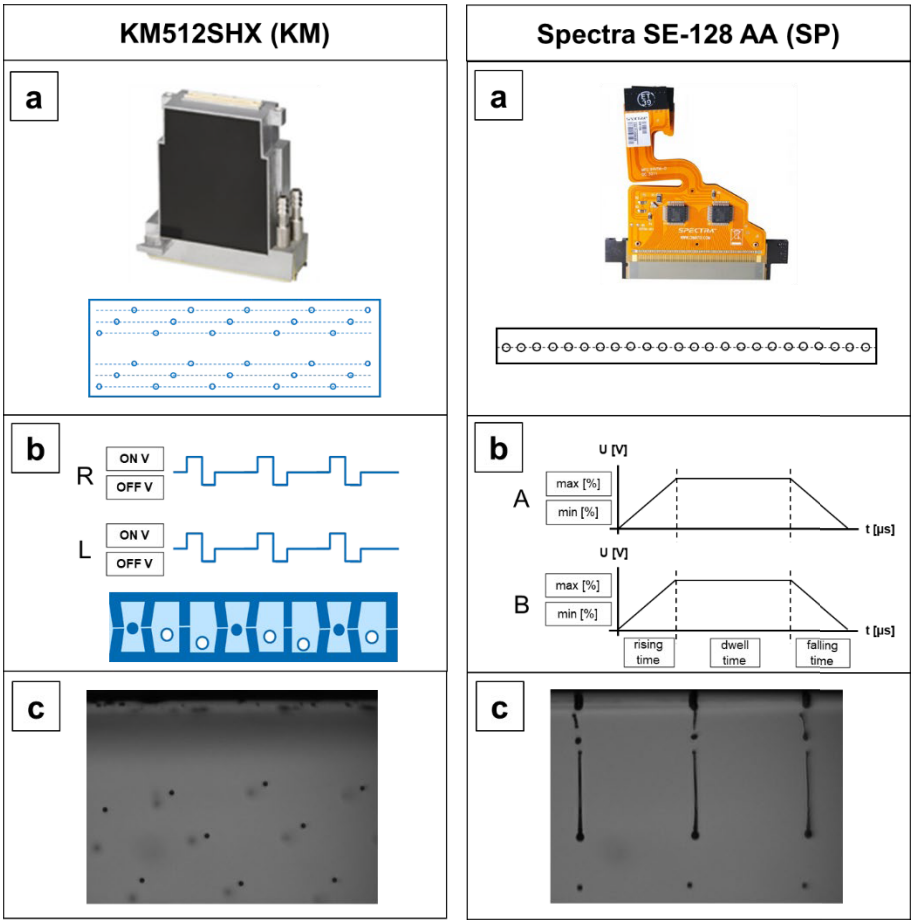

Figure 20: Print head designs with zoomed nozzle plate (a), typical waveforms (b) and resulting drop view (c) of KM512SHX (KM) and Spectra SE-128 AA (SP) (modified according [170, 176, 186, 187])

The objective was to demonstrate the influence of key factors on the printed quantities and to find out which features were advantageous for pharmaceutical application. Hereby, the drug-free inks containing MB28 were used (section 3.1.2.3). The effect of their different physicochemical properties on printed quantities was taken into account.

After selecting a print head for all further examinations based on the results, the influence of print settings on the morphologic structure of ODFs used as substrates was investigated.

Moreover, different drug dosing strategies have been tested. The API dosage can be controlled by means of ink API concentration [99], number of layers, printed area and resolution. All adjustments have individual advantages and disadvantages. The ink concentration is limited by the API solubility in case of solutions. As long as the API remains dissolved, different

concentrated inks could serve as bulk product. The number of layers is not freely selectable due to limited mechanical stability of the film substrate and especially the prolongation of process time. But printing several layers enables an easy adjustment of the dose without an ink exchange and cleaning step. By pre-setting different template areas, the physiological facts of target patients have to be considered. The oral cavities of newborns, children and adults differ significantly in surface area [188]. As the ODFs have to be cut with excess to the sides of the printed area to ensure no loss of API, the final size has to be rationally defined. Using different printing resolutions allows the increase of API dose without changing the ink and expanding the production time if selecting a high-resolution inkjet print head. Inks containing the APIs MPT or LT, as representatives of BCS class I and III drugs, were used to achieve different dose strengths adjusting a wide range of resolutions. A newborn, as a particularly critical patient group, with a body weight of 3.5 kg was selected as an example patient for treatment by MPT. For the potential treatment by LT, no special kind of patient was chosen. In case of MPT as freely water-soluble API, the ink concentration and the print resolution were varied. Hereby, a proof-of-concept of additive inkjet printing on ODFs loaded by fixed MPT dose was conducted.

Finally, the print head cleaning process and potential cross-contamination risk was critically discussed.

3.2.2 Comparative Investigations on Print Head Designs

3.2.2.1 Preliminary Studies

The dependence of printed quantity on single print parameters was investigated. For this purpose, driving voltage, firing frequency, print head distance to the substrate, number of layers and print resolution were selected. To keep the influence of the ink constant, the ink formulation F1 containing MB28 was used (section 5.2.2). Inkjet printing (section 5.3) and static jetting process (section 5.3.3) were combined.

Varying the applied voltage on the PZTs at fixed firing frequency of 5000 Hz (section 5.3.1), KM achieved mean MB28 quantities between 33 and 93 µg. The adjusted pulse voltage and the jetted MB28 quantity showed an exponential correlation with increasing scattering (Figure 21).

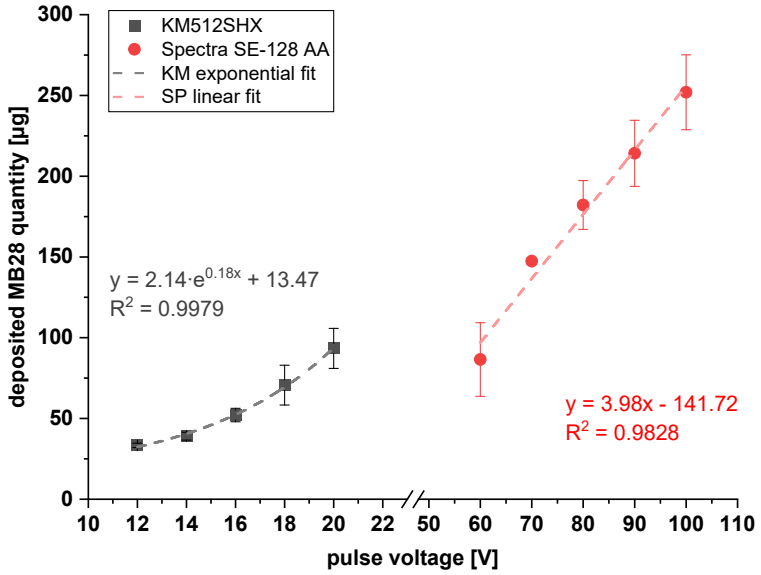

Figure 21: Blue dye (MB28) quantities resulting of varying driving pulse voltage and print heads, F1 ink (mean ± SD, n = 3)

Since a linear relationship is described in the literature for shear mode print heads [40, 170, 189], it was assumed that an additional factor influenced the quantity course. The fact that the jetting experiment order was not randomised and took place for a relatively long time period of 300 s could lead to a locally increased temperature in the nozzles. Higher temperature resulted in lower ink viscosities and with that in non-linearly increased drop volumes. This assumption could be confirmed in a repeat experiment. A randomised order, lower firing frequency of 3000 Hz and shorter jetting time of 180 s were set. In this case, the dye MB28 quantity linearly correlated with the used pulse voltage.

After the first experiences with KM print head, the experimental setup for SP was adapted accordingly. SP print head achieved mean quantities between 87 and 252 µg after jetting for 60 s at a firing frequency of 5000 Hz. The adjusted pulse voltage and the jetted dye MB28 quantity show a linear correlation (Figure 21).

After demonstrating that the developed drug-free inks F1, F2 and F3 are generally printable (section 3.1.2.4) using the SP and KM print heads, it should be investigated which influence the applied driving voltage has on the drop characteristics. With the help of the Analyze tool (section 5.5.7), volume, speed and flight angle of the jetted drops were determined. Additionally, the aspect ratio (AR) of the main drop defined as major distance divided by the minor distance of an approximated ellipse was calculated. Only the main drop respectively

was taken into account because the drop view tool often did not detect smaller or non-spherical drops reliably.

The drop view results (Table 7, Figure 22) illustrate the influence of the chosen print head and set printing parameters in combination with the ink properties.

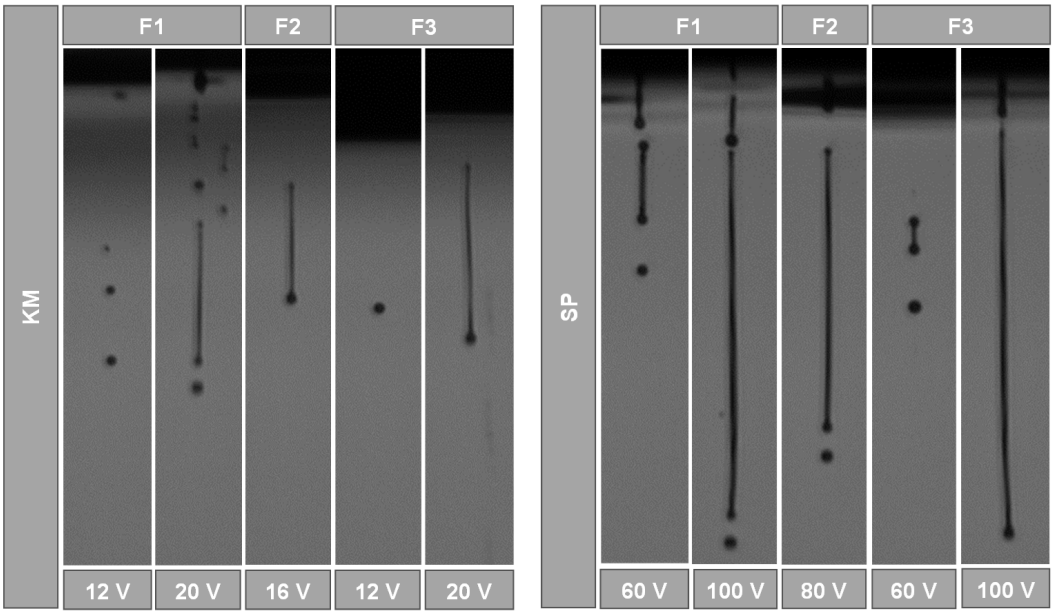

Figure 22: Drop view images of inks F1-F3 at jetting frequency of 1000 Hz and print head temperature of 30 °C, KM512SHX (left) and Spectra SE-128 AA (right) (used from Kiefer et al. [176], by courtesy of Elsevier)

Table 7: Drop view analysis results of the main drops (n = 1)

Print head	Ink	Pulse voltage [V]	Speed [m/s]	Volume [pl]	Angle [°]	AR
KM	F1	12	6.84	2.5	0.37	1.03
		20	31.84	5.0	-0.84	32.23
	F2	16	17.83	5.8	0.07	24.35
	F3	12	4.59	3.4	-0.62	1.04
		20	15.41	6.9	0.55	35.42
SP	F1	60	3.93	10.9	2.03	11.50
		100	7.16	36.7	0.87	54.39
	F2	80	7.71	21.6	0.54	42.21
	F3	60	3.50	7.4	0.40	4.52
		100	6.00	36.6	0.36	61.35

The drop volumes of SP were in total larger than of KM due to the bigger nozzle diameters of 35 µm. Comparing low and high voltage levels jetting F1 and F3 inks, it can be noticed that an increase in driving voltage led to an increase in the main drop volume. This supports the previously presented results on deposited MB28 quantities. Application of high voltages led

to increased speed of drops and with that to longer tails and greater AR in both cases. Moreover, the lower the dynamic viscosity, the higher the number of satellites was which separated from the main drop. These outcomes were consistent with findings in the literature [52]. For the pharmaceutical implementation, this means that the driving voltage in connection with physicochemical ink properties is one of the control elements for drug dosing. Consistent drops are advantageous as their trajectory as well as volume is easier to control for precise inkjet printing. However, if the total volume of the satellites is reproducible, this should not have a negative impact on the dosage.

Regarding the results of varying firing frequencies, a linear correlation for both print heads was observed during jetting (Figure 23a). The slopes differ due to different drop volumes. Calculating the mean quantity ejected per drop, the results vary by 0.09 ng/drop ± 14.7% using KM and 0.21 ng/drop ± 4.7% using SP for the set frequencies without a particular trend. The reason is that print heads with smaller nozzles are more sensitive to the smallest irregularities at the nozzle plate like drying of ink or adhering dust particles.

Comparing single-pass and multiple-pass printing at constant resolution of 175 dpi, the measured MB28 quantity increased linearly with the number of layers using both print heads (Figure 23b). In literature, increasing standard deviations with increasing number of layers are reported which are associated with higher chance of direct contact with the print head [98, 99]. This was not observed in the present study due the different design of the substrate feed of the used printer. In the present case, the film substrate is fixed on a horizontally moving substrate table at a defined distance to the print head whereas it was moved in the reports by rollers through the printer.

Mounting the KM and SP print head at different distances from the film substrate, no clear dependency of MB28 quantities could be found (Figure 23c). Only a slight downward trend with increasing distance is suggested. It could be noticed visually that the edges of the printed squares were blurred at a print head distance of 10 mm. However, since the printed squares were cut with protruding edges, the actual print area misplacement could not be determined to the fullest extent. Increasing distance to the moving substrate led to extended time-of-flight and with that to effects on the main drop and satellites trajectory [190, 191].

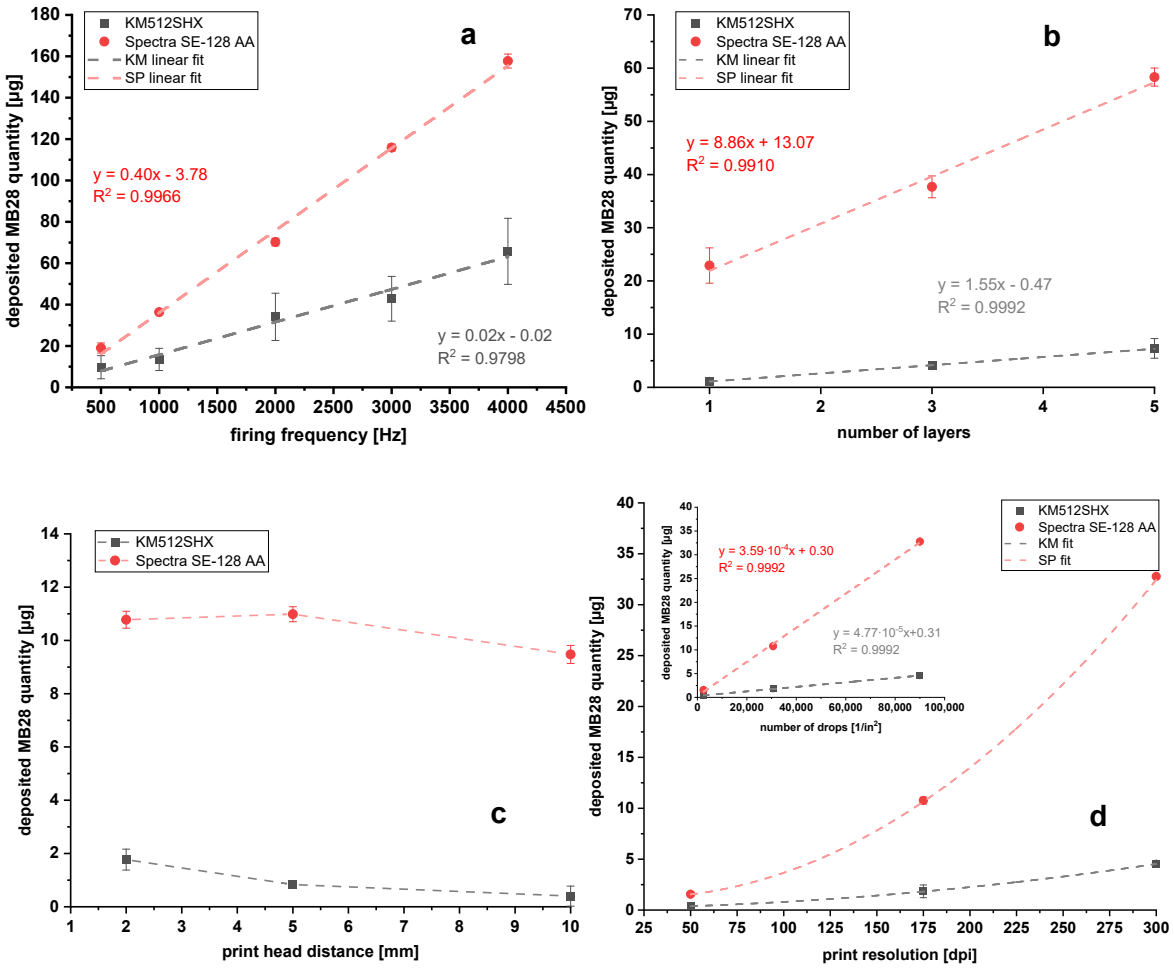

Figure 23: Deposition of MB28 resulting of varying the firing frequency (a), number of layers (b), print head distance to the substrate (c) and print resolution (d); squares of 1 in² printed with one nozzle on an HPMC-ODF or jetted into a watch glass, F1 ink (mean ± SD, n = 3)

Applying print resolutions between 50 and 300 dpi, the MB28 quantity raised with increasing dots per inch following a quadratic function (Figure 23d). To transform it to a linear function, the set resolution in dpi was recalculated to the theoretically printed number of drops per area. Due to different drop volumes, KM and SP print head showed different quantity levels.

First effects of print settings and resulting printed quantities could be shown. To identify the significance and interactions of the key factors, a statistical experimental design was implemented and will be presented section 3.2.2.4.

3.2.2.2 Negative Pressure

During preliminary printing studies, it has been noticed that there were difficulties using SP print head at the default negative pressure of -15 mbar. PEG 400-containing ink was leaking of the nozzles so that no printing was possible. Using the KM print head, there were no such

issues. To find out the reason for this and to determine if there are any MB28 quantity variations by setting different negative pressures, the target ink formulations were tested (section 5.5.5).

According the recommended calculation (Equation 12), the optimum p_{set} is between -16 and -28 mbar depending on the used value for the negative meniscus pressure and height of ink level. It would be more practical if one set negative pressure that works in all experiments could be found and kept constant to prevent further effects. Furthermore, the constructional difference between KM and SP is not explained by this equation.

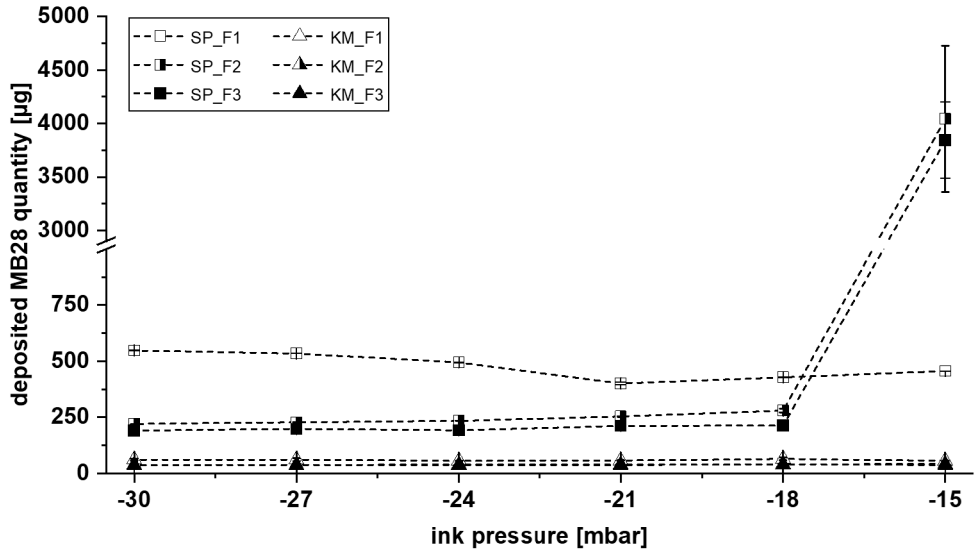

Figure 24: Applied negative pressure to the ink reservoir of SP and KM print head and resulting jetted MB28 quantities (mean ± SD, n = 3) (modified from Kiefer et al. [176], by courtesy of Elsevier)

The negative pressure has no influence on the ejected fluid amount in case of KM print head, whereas if using the SP print head, it is not freely selectable and there are larger differences between the inks (Figure 24). This could be explained by the Bond number or Eötvös number (Equation 6) which describes the ratio between the gravitational and surface forces, also expressed as hydrostatic and capillary pressures. The height of the liquid column is given by Jurin's law (Equation 7) with the condition of an ideal wetting of the capillary wall ($\theta = 0$).

$$Bo = Eo = \frac{\rho g L^2}{\gamma} = \frac{\rho g h r}{2\gamma} \qquad \text{(Equation 6)}$$

$$h = \frac{2\gamma}{\rho g r} \qquad \text{(Equation 7)}$$

Where γ is surface tension, ϱ density of fluid, g gravitational acceleration, L characteristic length, h filling level and r nozzle radius responsible for capillary pressure.

The negative pressure set to the ink container has to support the capillary pressure to overcome the hydrostatic pressure to avoid the ink running out of the nozzles in an uncontrolled way. In case of KM print head, it does not matter which value is adjusted in the range of -15 and -30 mbar. The smaller ink channel and nozzle diameter leads to higher capillary pressure so that a negative pressure of -15 mbar is already sufficient to hold the meniscus (Equation 6). On the contrary, SP print head needs at least -18 mbar to reach a constant ejected fluid amount using inks with higher densities (F2, F3). For the following experiments -18 to -21 mbar for KM and -21 mbar for SP were used in order to have a safety margin to the upper limit.

3.2.2.3 Printed Geometries

Before the API is printed, the operator has to think about the set process parameters but also about the design of the target geometry. The most optimal shape for printing on an ODF is a square because it makes the best use of the available cut rectangular area and thus minimises grid waste. However, it can be beneficial to switch to another design if additional dye is used to make the dosage form more patient-friendly or distinctive. First printing concepts including line-, point- and surface covering prints, bar codes, serialisation labelling, were already reported and realised [33, 40]. To ensure that the selected geometry of the printed dosage form has later no impact on the API content, three different shapes of the same area of 6.45 cm^2 were printed by KM and SP. Simplified a square (h: 2.54 cm, w: 2.54 cm), circle (r: 1.43 cm) and an equilateral triangle (length of sides: 3.86 cm) were chosen and printed in this order (Figure 25). At the same time, the printing process of inks F1, F2 and F3 by one and ten nozzles was compared.

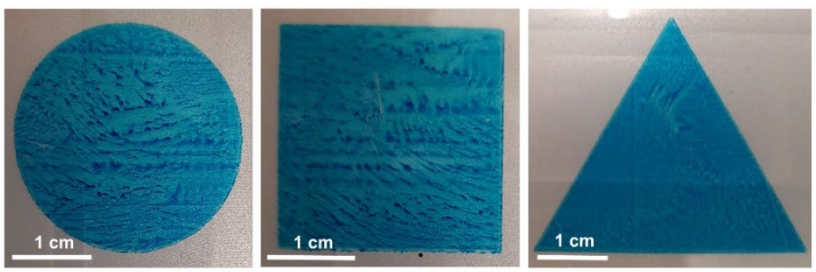

Figure 25: Exemplary illustration of printed geometries from F1 ink using SP print head (used from Kiefer at al. [176], by courtesy of Elsevier)

Regarding the results (Figure 26), in the case of KM, there is a decreasing trend of F1 ink to deposit volumes from square to triangle. That could be explained by increasing amount of

dried ink at the nozzles during the advanced printing process time as the experiment order was square, circle and finally triangle. Partial clogging led to lower MB28 quantities on the ODFs. Comparing the SP outcomes, no trends could be detected. SP print head has a bigger nozzle diameter and with that larger contact area with fresh ink. Consequently, the deposited MB28-containing ink did not dry as fast as in the KM print head. Two-way analysis of variance (ANOVA) confirmed that there are statistically significant differences in MB28 quantities between the printed geometries using KM whereas no differences can be shown using SP. It can be seen that ten nozzles printed slightly lower quantities than one nozzle. That may be related to inter-nozzle deviations or failing nozzles. This phenomenon was more pronounced for the KM print head. The influence of the used ink compositions was significant ($p < 0.05$) for both print heads. With higher PEG 400 content the MB28 quantity decreased. This is investigated and discussed in more detail in the subsequent section.

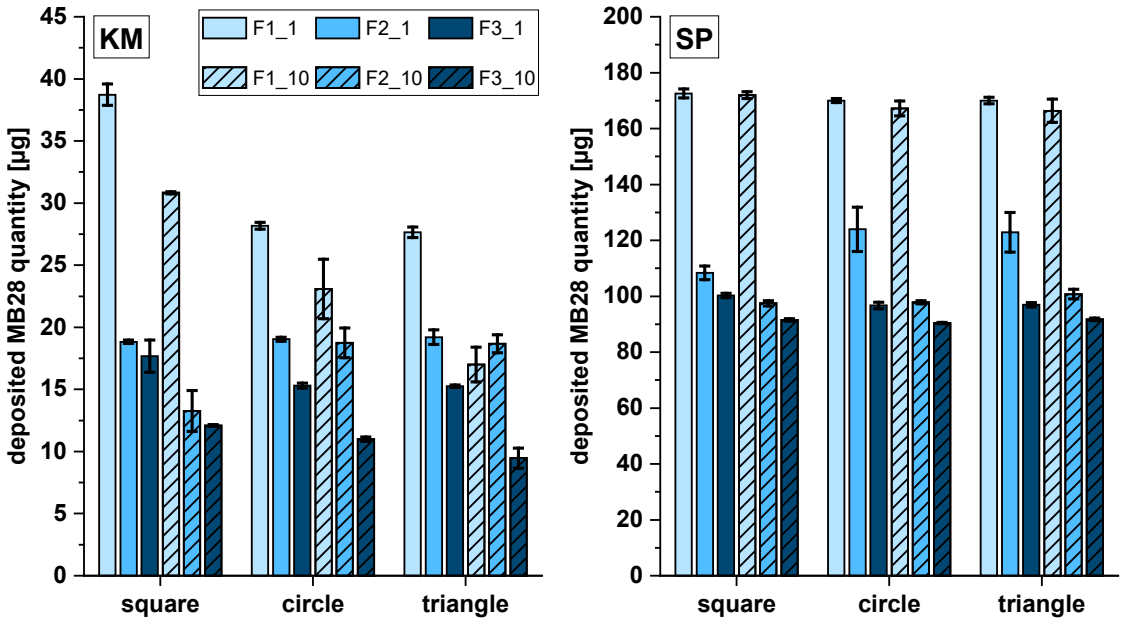

Figure 26: Different geometries (1 in² ≈ 6.45 cm²) printed by KM with nozzle Nr. 70 and nozzles Nr. 1–10 (left) and by SP with nozzle Nr. 68 and nozzles Nr. 62–73 (66) (right) (mean ± SD, n = 3) (modified from Kiefer et al. [176], by courtesy of Elsevier)

In summary, it could be demonstrated that the printed geometry has no effect on the deposited quantities, whereas ink properties and number of used nozzles have a significant effect. More complex geometries, such as child-friendly figures, intricate patterns, or letters, may still be challenging, as the calculation of the surface area may be more difficult and finer areas may be more error-prone for printing.

3.2.2.4 Influencing Parameters and Design of Experiments

After the first conclusions, the influence and interactions of the critical printing process variables and ink compositions on the printed quantities should be statistically evaluated by design of experiments (DoE) (section 5.4.1.1). As factors, the previously individually examined pulse voltage (V), print resolution (dpi), number of layers (lay) and print head distance from the substrate (phd) were chosen. Additionally, dynamic viscosity (η) as representative parameter for the ink properties was taken into account in the model. To achieve comparable MB28 quantities with both print heads, the print resolutions were adapted to each other assuming that the KM print head generates 4 pl and SP print head 30 pl drops (Table 8).

Table 8: Calculation of theoretically applied number of drops and ink volumes

Print head	Resolution [dpi]	Number of drops/ODF per 1 in²	Calculated total volume [pl]
KM	600	360,000	1 440,000
	900	810,000	3 240,000
	1200	1 440,000	5 760,000
SP	220	48,000	1 440,000
	330	108,000	3 240,000
	440	192,000	5 760,000

It has to be kept in mind that increasing the resolution using the same print speed leads to higher firing frequencies. The frequency f can be calculated based on the print resolution R_p and speed v_s taking the set quality factor QF (section 5.3) into consideration (Equation 8).

$$f = \frac{R_p \times v_s}{25.4 \times QF} \qquad \text{(Equation 8)}$$

That can lead to lack of time to refill ink into the pump chambers, especially if the channels are smaller and the viscosity of the ink is higher simultaneously. In order to avoid this issue, the print speed was adapted in further investigations to keep the frequency constant. In the present setup, it cannot be distinguished whether resolution or frequency revealed the observed effect. It is probably a mixture of both.

Regarding the quantity results of the factor level combinations N1 to N19 (section 6, Table 36 and Table 37), SP print head showed overall lower relative scattering (Figure 27). This could be explained by the different time-of-flight of the drops from the nozzle to the substrate as already assumed in section 3.2.2.1. Larger drop volumes produced by SP arrived faster at the

substrate than the smaller ones ejected from KM because of the higher weight force. While the drop was still in flight the substrate table was already moving forward. This caused drop landing in a slightly different position than intended. If the print head has a bigger distance the time-of-flight increases. Additionally, the drop can be deflected by the airflow between the print head and substrate table.

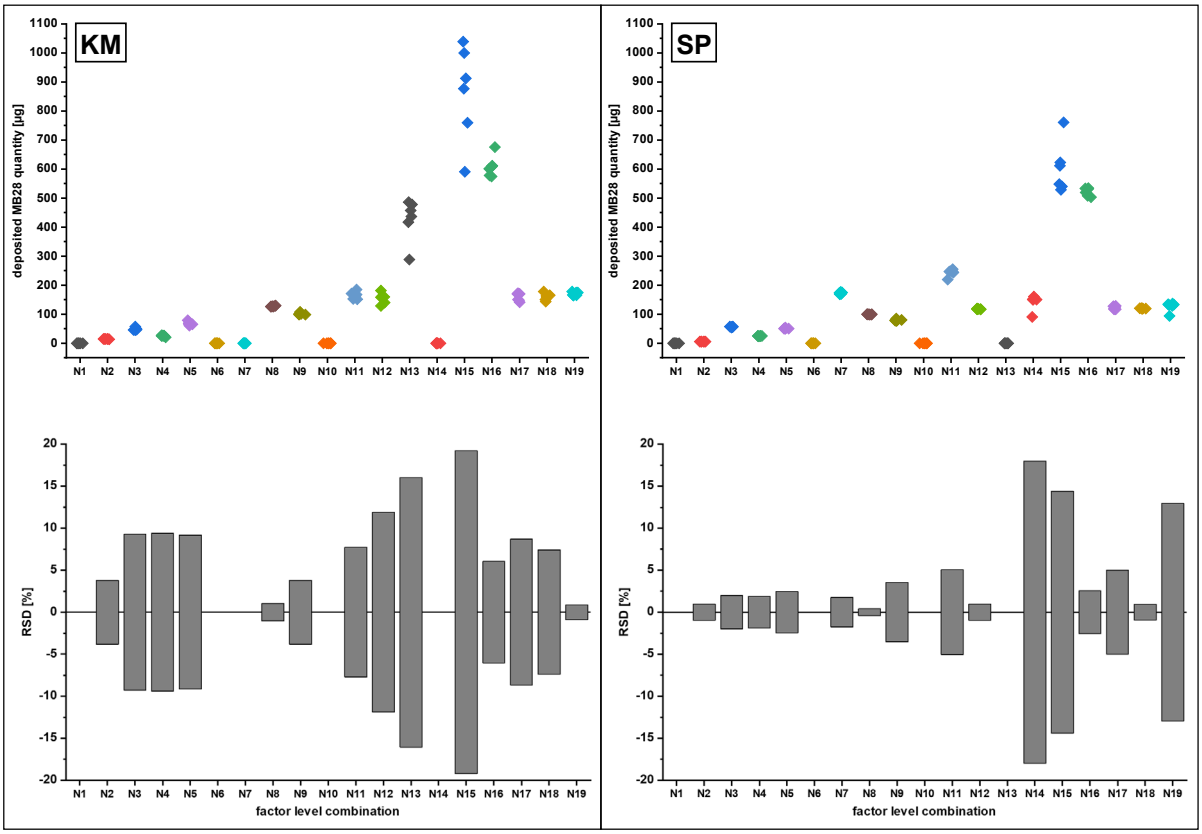

Figure 27: Single values for the deposited MB28 quantities (n = 6) and the related relative standard deviations (RSD in %) of the factor level combinations N1–N16 and the three experimental runs of the centre point N17–N19 (modified from Kiefer et al. [176], by courtesy of Elsevier)

Particularly striking was the factor level combination N15. In this specific case, the extreme values of all investigated factors were present: high viscosity, low pulse voltage, high number of layers, high resolution and with that high frequency. This combination represented the worst-case, however, it at least resulted in deposited ink quantities. For future inkjet printing of API inks, it is crucial that the content uniformity according Ph. Eur. 2.9.40 test specifications is given. Large variations on quantities could lead to deviations from the label claim and thus to exceeding the acceptance value of 15 and insufficient quality for batch release.

The coefficient plots (Figure 28) show that in case of KM all factors, except the combination of viscosity and number of layers, interact significantly with each other which means that no investigated parameter can be considered independently of each other. Both print heads had

in common that with increasing dynamic viscosity (as well as surface tension and density) and distance from the substrate the MB28 quantity decreased. In contrast, if pulse voltage, resolution or firing frequency and number of layers increased, respectively, the MB28 quantity achieved higher values, too.

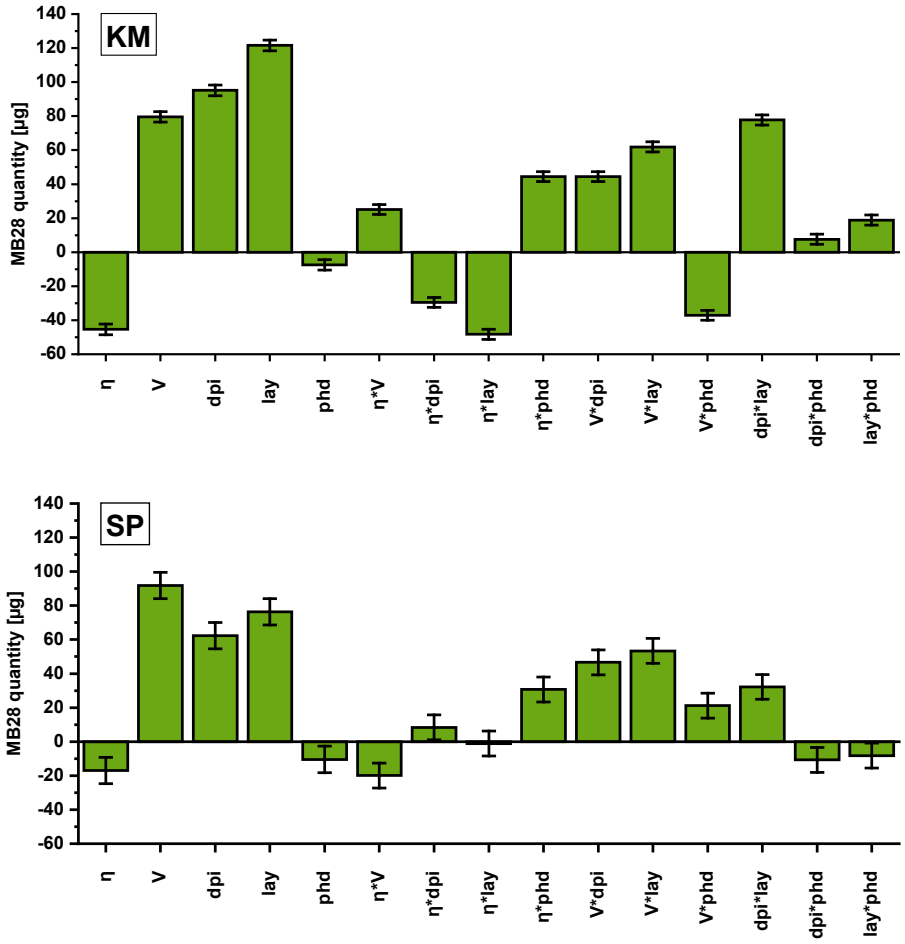

Figure 28: Coefficient plots for KM (R^2 = 0.9999, Q^2 = 0.8187) and SP (R^2 = 0.9998, Q^2 = 0.6499), scaled and centred (coefficient ± CI: 95%); factors: dynamic viscosity (η), pulse voltage (V), print resolution (dpi), number of layers (lay), print head distance from the substrate (phd) (modified from Kiefer et al. [176], by courtesy of Elsevier)

However, the factors with the strongest effects were different for both print heads and the interactions between the factors had partly divergent effect orientation. The interaction between the set pulse voltage and chosen number of layers had the greatest influence using SP and the resolution and number of layers using KM.

Evaluating the contour plots (Figure 29), it is apparent that with higher resolution the effect of number of layers becomes higher using KM and with increasing number of layers the effect of voltage is higher using SP. This can be confirmed by the drop view analysis (Table 7, section 3.2.2.1). The main drop volume increased by factor 3 to 5 and for KM only by factor 2 changing

the voltage from low to high level. This may be related to the different channel geometries [192].

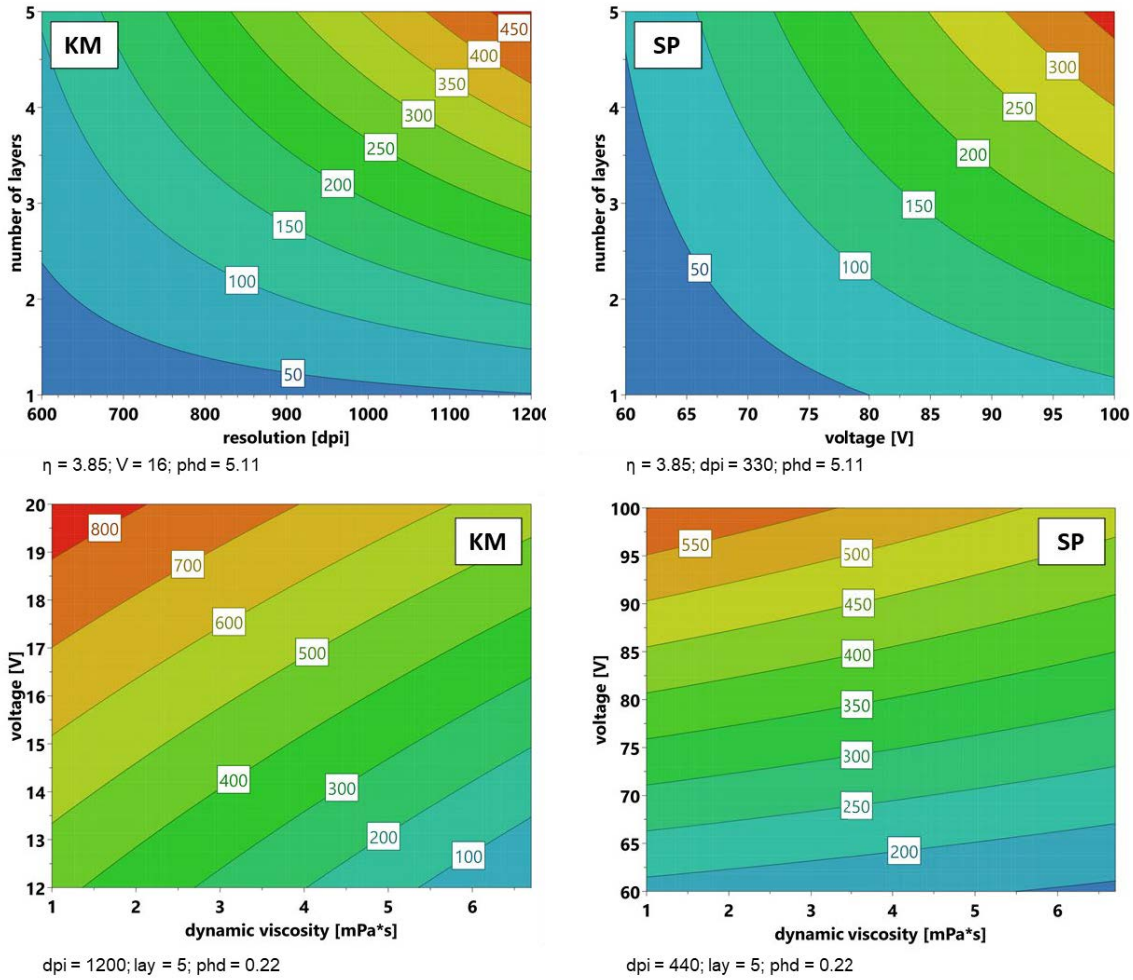

Figure 29: Contour plots for the deposited MB28 quantities (modified from Kiefer et al. [176], by courtesy Elsevier)

Using both print heads, it was most effective maximising the printed quantity by increasing the resolution and number of layers simultaneously. Low viscosity of the ink at high voltage, high resolution and number of layers and small substrate-print head distance led to higher quantity.

For further experiments, it was decided to use the SP print head due to its larger nozzle diameter and with that more efficient deposition of API ink as well as a lower susceptibility to errors.

3.2.3 Influence of Print Settings on Morphologic Structure of ODFs

Besides the observed influence on the drop trajectory, the printing settings also seem to have an influence on the pattern of the imprinted area. First indications were already given during the MPT ink screening (section 3.1.3.3). Although this does not necessarily have any pharmaceutical relevance, the influencing factors have to be understood and assessed in order to evaluate the quality of printed dosage forms. Furthermore, uncontrolled patterns on the applied ODF could confuse the patients and potentially have an impact on their compliance and therapy adherence.

Two options should be considered. The ink formulation F1 was tested as a composition which contains a dye, evaporates fast and does not dissolve the ODF. ODFs imprinted by F1 were examined with regard to the influence of adjusted resolution on the print pattern. The ink formulation I5 was tested as a composition which is transparent, evaporates more slowly and partially dissolves the ODF. ODFs imprinted by I5 were analysed regarding the influence of varying print speed, direction and angle.

Looking at the light microscope images of film substrates imprinted at varying resolutions, there are visible differences (Figure 30). At low resolution of 50 dpi, isolated dried drops in regular spacing can be seen. Their shape is not round, they seem to consist of two or three parts that have merged together. This is due to the formation of the satellites seen in the drop view (section 3.1.2.4). Setting a resolution of 127 dpi, the drops are placed closer together and form a kind of fish scale pattern. The blue dye as non-evaporating component is mainly transported outwards to the edges of the drops during drying, which is described in the literature as coffee-ring effect [193, 194]. The evaporation of the solvent, in this case EtOH, causes thermal and concentration gradients within the single deposited drops. These local differences in turn lead to a surface-tension gradient and the so-called Marangoni flows [195]. This pattern is replaced by wavy parallel lines of dark blue with light blue intermediate spaces if a resolution of 254 dpi is adjusted. This was identified as “scalloped lines” described by Soltman et al. analysing inkjet printed lines depending on the drop spacing and substrate temperature [196]. Finally, the increase of resolution to 500 dpi led to overflowing of the area. A line pattern is still recognisable, but loses its regularity and straightness.

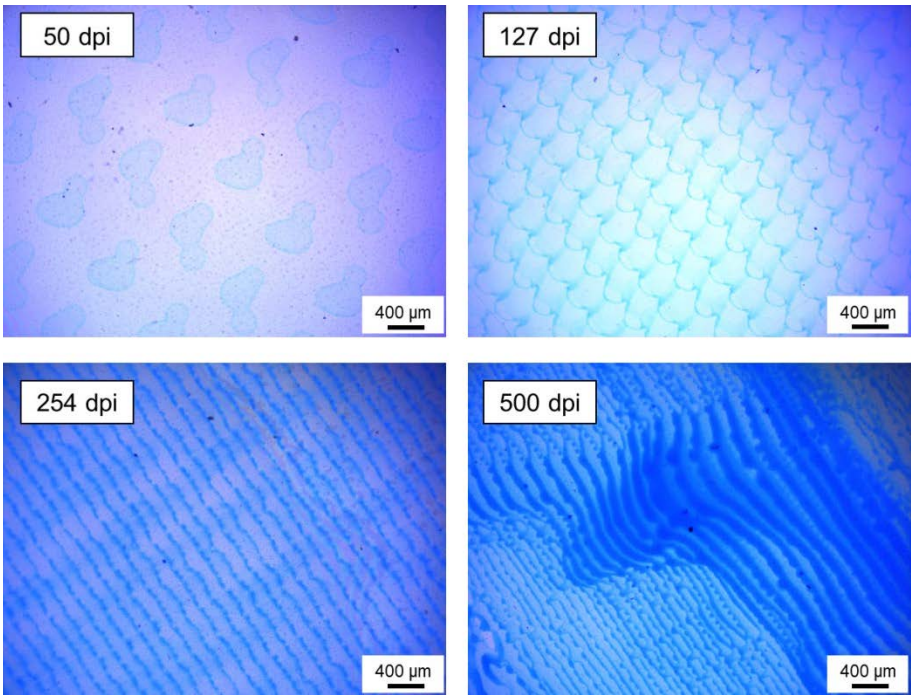

Figure 30: Light microscope micrographs of F1 ink imprinted (Y-normal, bi-directional) by SP print head at different resolutions, pulse voltage of 80 V (90%), print speed of 200 mm/s

After systematically varying the print settings speed, direction and angle (section 5.3.1), the samples imprinted by I5 were viewed under the confocal Raman microscope in the dark field. This enabled a defined visualisation of the surface structures even without coloured ink.

Figure 31 displays the generated images. All have the regular stripe pattern in common as already observed in experiments with the F1 ink. X-normal print angle resulted in 40 parallel and Y-normal print angle 12 perpendicular stripes referring to the front edge of the substrate table. Relating this to the whole printed area of 2.54 × 2.54 cm, then in both cases a stripe width of exactly 50 µm is obtained. This means that a width of 2.54 cm includes approximately 500 stripes, which corresponds to the set resolution of 500 dpi and with that to the number of printed swaths.

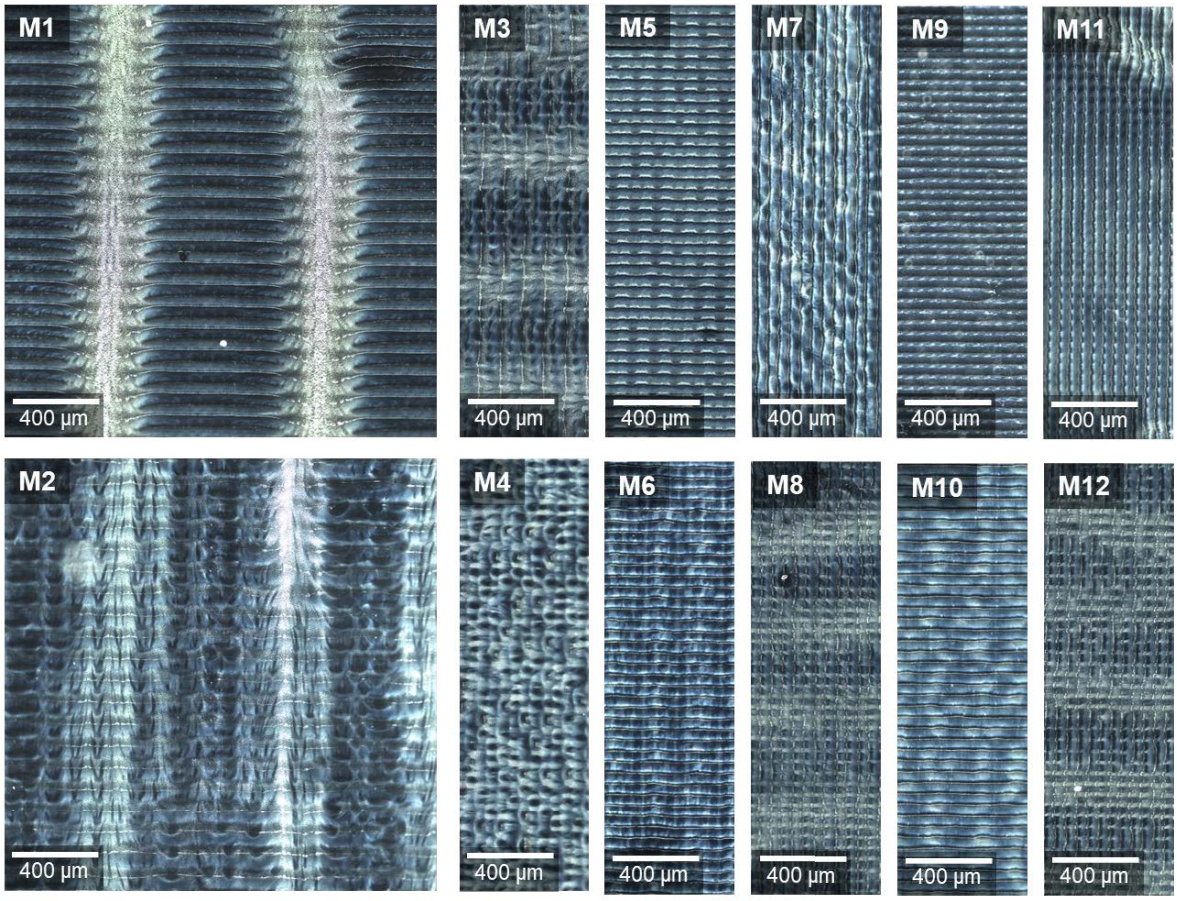

Figure 31: Dark field micrographs of ODFs imprinted at varying print settings (defined in section 5.3.1) stitching images of an area 2000 × 2000 µm (M1, M2, M3 cut) and 2000 × 600 µm (M4–M12), rotated by 90° for observation under the microscope (used from Kiefer et al. [41])

Comparing the low- and high-speed samples, it can be noticed that the 100 mm/s (Figure 31, even numbers) led to more diffuse pattern than 50 mm/s (Figure 31, odd numbers). This may be caused by more turbulent air flows in the gap between the moving print head and substrate table at higher speed. The feather-like pattern appears clearly only with bi-directional inkjet printing (M1, M2). In M3, M8 and M12 only blurred light areas perpendicular to the printed swaths are visible.

The preceding experiments (section 3.1.3.3) showed that the light areas contain a higher MPT concentration directly after the printing process. The jet from a nozzle usually consists of main drops and satellites. The latter are undesirable, but can often only be reduced and not completely avoided. Due to their small volume and with that mass, secondary droplets in particular can be deflected by eddy flows [190, 197]. Since the used substrate was an HPMC-based ODF, the surface was dissolved by the water-based ink drops which coalesce to lines. Each dried partially before an adjacent swath was printed. Depending on the printing movement settings, the drops flew at different angles on the substrate creating feather-like

three-dimensional surface structures. The additional ink deposition on the areas already printed with main drops led to a structural change and higher MPT content.

Considering the edges of the printed surface provides further insights (Figure 32). The drops that formed the tips were smaller than those that coalesce to the spaces in between. Using higher resolutions and with that tighter drop deposition would lead to a stepwise loss of the pattern. A closed surface is expected.

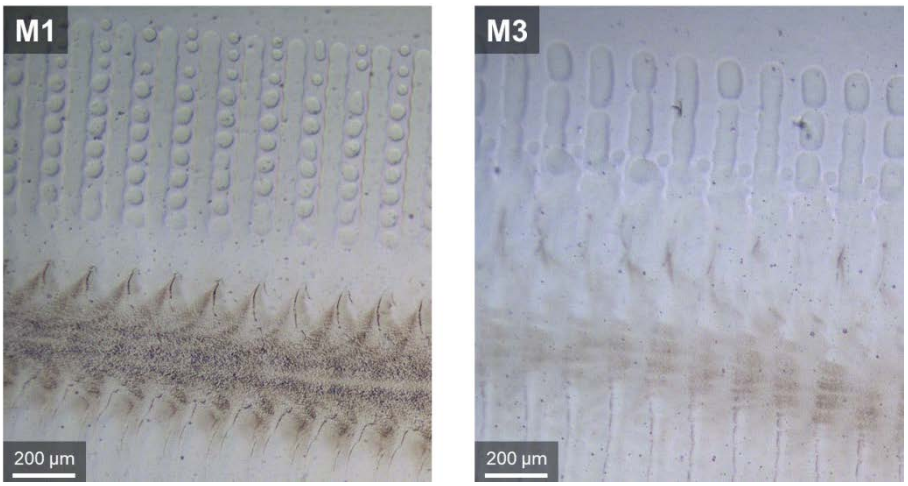

Figure 32: Magnification from light microscope micrographs of the edges of the samples M1 and M3, printed bi-directionally at a speed of 50 mm/s

3.2.4 Drug Dosing Concepts

3.2.4.1 Calibration of Content by Print Resolution

After investigating the influence of varying print resolutions on qualitative properties of ODFs, this should be used as concept for drug dosing control. To obtain a usable dosing range, a calibration series with MPT ink I5 was performed at resolutions of 250 to 2000 dpi.

In order to achieve a linear and not a quadratic relationship (section 3.2.2.1), the resulting MPT content was related to the number of drops building the printed area (Table 9). Preliminary studies have shown that the maximum used resolution of 2000 dpi is limited in terms of printing speed and thus firing frequency. At speeds of 70 or 100 mm/s, printing stopped in the middle of the process. Consequently, the print speed was adjusted according to resolution to keep a constant frequency of 2000 Hz. Thus, a potential effect of frequency on the printed quantity could be excluded.

Table 9: Used resolutions for calibration and corresponding calculated required print speed and number of drops related to an imprinted area of 1 cm^2

Print resolution [dpi]	Print speed [mm/s]	Number of drops [1/cm^2]
250	200	9,688
500	102	38,750
750	68	87,188
1,000	51	155,000
1,250	41	242,188
1,500	34	348,751
1,750	29	474,688
2,000	25	620,001

For the production of paediatric tailored MPT dosages, downscaling of printed area to an appropriate child-friendly size of 1 cm^2 was performed. The ink concentration of 111.2 mg/ml ink allowed this reduction. The resulting MPT contents could be described by a linear function with a coefficient of determination of 0.999 (Figure 33).

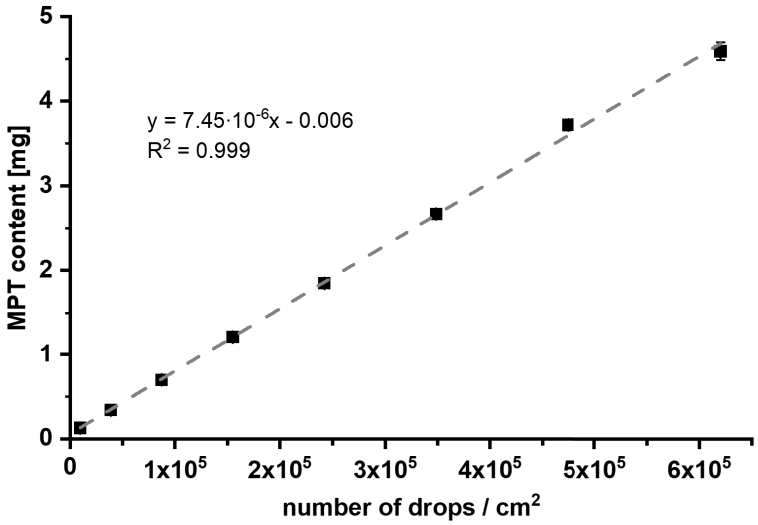

Figure 33: I5 ink calibration series of print resolutions at pulse voltage of 100 V (90%) and pulse timing of 2–5.8–2 µs (mean ± SD, n = 3) (modified from Kiefer et al. [41])

Although MPT is administered off-label to children only, there are some dose recommendations, e.g. from formula notes of NRF (section 1.4.1). As for the present trials, a newborn of 3.5 kg was exemplary chosen as target patient simulating a very low-dose regimen, single dosages of 0.35 to 0.7 mg for initial heart failure treatment and 1.75 to 3.5 mg are indicated for maintenance therapy.

The linear equation was used to calculate the required resolutions to accomplish the recommended initial single MPT dosages for a 3.5 kg newborn 0.35 mg and 0.7 mg for heart

failure as well as by 1.75 mg or 3.5 mg per unit for treatment of hypertension. All batches achieved the target doses showing low AV for the pharmacopoeial specified limit of 15 at L1 [198] (Figure 34). Compared to other solid dosage forms, these low AV demonstrate that the inkjet printing process is reliable enabling a very precise dosing so that production of consistent dose units is feasible.

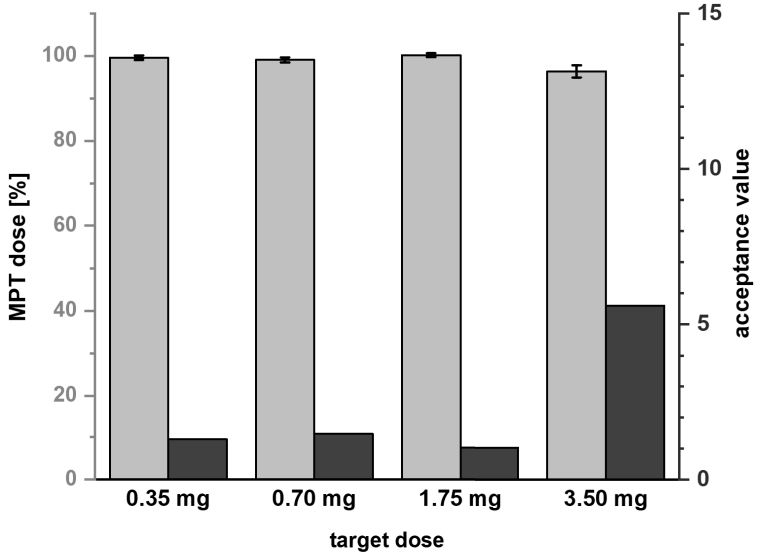

Figure 34: Resulting MPT dose as percentage of label claim of printed units (mean ± SD, n = 10) and corresponding acceptance values (AV) (modified from Kiefer et al. [41])

3.2.4.2 Transfer of Concept to Low-Dose API

After it could be shown that the print resolution concept works well with MPT as an easily soluble API, this should be transferred analogue to the more demanding drug substance LT regarding dose strength, solubility and stability. Since the concentration of the selected L2 ink (section 3.1.4) is comparably low with 1 mg/ml but the dose regimen is in the microgram range, a printed area of 2 × 3 cm had to be adjusted to achieve reasonable LT dosages. Thus, a child-friendly size of 1 cm^2 was not feasible to realise. Consequently, the present approach is more suitable for an individualised therapy of adult patients. This was the first limitation factor.

Adjusting the resolutions of 250 to 2000 dpi, LT contents of 3.9 to 103.1 µg per ODF were achieved (Figure 35). The relationship could be described by a linear equation with a coefficient of determination of 0.995. The therapeutically reasonable dose range begins at 12.5 µg for children and ends at maximum 200 to 300 µg per day for adults depending on the diagnosed disease [199]. To achieve 12.5 µg/ODF, resolutions below 615 dpi

(377,669 drops/6 cm²) are not appropriate for the predetermined ink concentration and printing area. Moreover, printing of three layers at a resolution of 1815 dpi or an application of three ODFs of one printed layer are required to achieve the daily high dose of 300 µg.

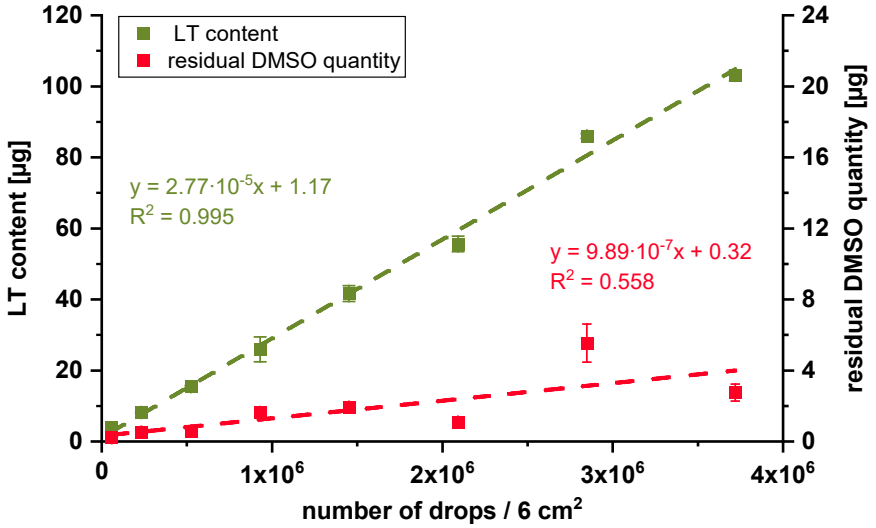

Figure 35: L2 ink calibration series of printing resolutions and the corresponding recovered residual DMSO quantities at a pulse voltage of 100 V (90%) and a pulse timing of 2–4–2 µs (mean ± SD, n = 3)

The L2 ink contained DMSO as cosolvent for the API (section 3.1.4.1). According to ICH, residual solvents of class 3 like the included DMSO are solvents with low toxic potential and can be regarded as safe for adults if the PDE of 5000 ppm or 0.5% is not exceeded [164]. A DMSO peak was visible in the HPLC chromatogram at a wavelength of 225 nm (section 5.5.21.3) so that a simultaneously quantification with LT was possible. After ensuring the linear relationship between the HPLC signal and the DMSO quantity (section 5.5.21.3), the chromatograms were evaluated according to the resulting linear equation. The samples were measured one day after the production.

In contrast to the LT contents, the recovered residual DMSO quantities unexpectedly showed a poor correlation to the number of deposited drops per ODF (Figure 35). This could be due to diffusion through the film matrix, so that DMSO residues may have remained undetected on the process liner. The coefficient of determination was only 0.558. However, the course of the mean values is analogous to the corresponding LT mean values. In particular at higher resolutions, the variation of DMSO increases. Since the experimental order was randomised, it was not a trend phenomenon. The reason for this behaviour could be the very low quantities.

The residual DMSO in a single ODF was between 4 and 111 ppm and with that clearly below the limit of 5000 ppm. Therefore, up to 45 pieces per day theoretically would be allowed for

administration to adults regarding only the DMSO quantity. Since no residual solvents limits for paediatric patients are defined, no evidence-based assessment can be made in this case.

Table 10: Residual DMSO quantities for a weight of a single ODF of 50 mg (mean ± SD, n = 3)

Resolution [dpi]	Number of drops per 6 cm² ODF	Residual DMSO quantity [µg]	DMSO in 50 mg ODF [ppm]
250	58,115	0.21 ± 0.12	4
500	232,854	0.53 ± 0.09	11
750	523,626	0.58 ± 0.01	12
1000	929,447	1.63 ± 0.03	33
1250	1,452,384	1.92 ± 0.25	38
1500	2,092,732	1.08 ± 0.17	22
1750	2,848,326	5.55 ± 1.08	111
2000	3,720,150	2.76 ± 0.48	55

The LT contents were predicted using the theoretical ink concentration based on the weights and the determined drop volumes using the drop view Analyze tool (section 5.5.7). The residual DMSO quantities were predicted based on the percentage of 30% (v/v %) in the ink (section 3.1.4.1). Figure 36 shows the corresponding predicted vs. observed plots. In a perfect prediction, the slope would be around 1 and coefficient of determination would be ≥ 0.999. Looking at the resulted slope of 0.66, it is obvious that the LT contents were slightly overestimated (Figure 36a). The reason for that could be the uncertainty by using the drop view camera for determination of the real drop volume during printing.

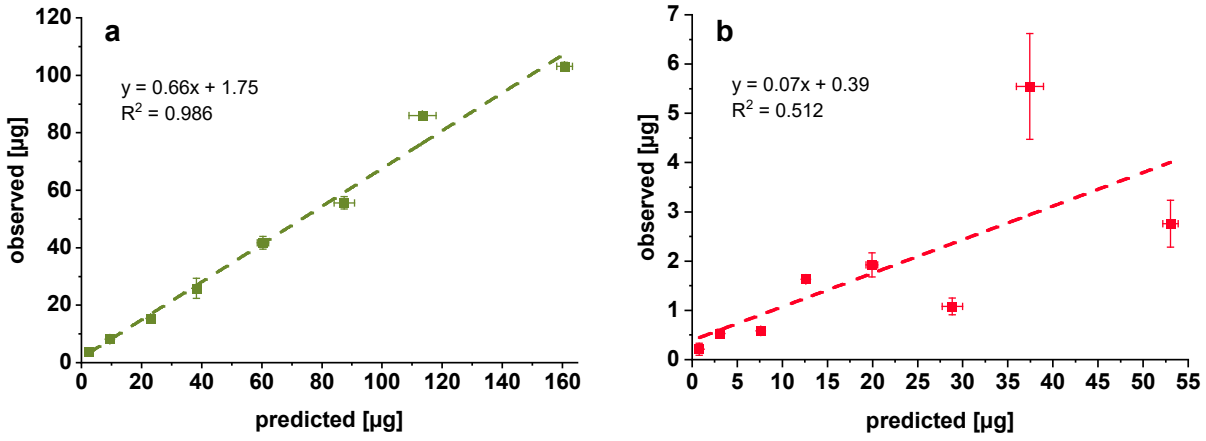

Figure 36: Predicted vs. observed plot (mean ± SD, n = 3) for prediction of LT contents (a) and residual DMSO quantities (b)

In case of DMSO, the slope was 0.07 and the coefficient of determination was poor with 0.512 (Figure 36b). The residual DMSO quantities were clearly overestimated. Since DMSO is hardly

volatile, it was not able to evaporate in such scale. The actual reason for this difference could not be determined with certainty.

In principle, the concept of print resolution could be transferred to the low-dose LT for treatment of patients of different age groups. Nevertheless, the used ink formulation L2 needs further optimisation regarding the LT concentration enabling a broader dosage range by administration of only one ODF piece of an age-appropriate size. For that purpose, a solvent mixture has to be found which enables higher LT concentration in the ink without remaining in the final product in unacceptable quantities after drying.

3.2.4.3 Variation of API Concentration

Increasing API concentration in the ink is an opportunity of controlling the dosage of printed single doses. The target ink formulation I5 containing 111.2 mg/ml MPT was compared to two further inks I8 and I9 (section 5.2.2.2) containing 250.3 mg/ml and 703.9 mg/ml MPT, respectively. These high loadings are only possible due to the very good water solubility of the API. To find out the dosage range using the same resolutions as for I5, the inks I8 and I9 were also used to print squares of 1 cm^2 adjusting 250 to 2000 dpi. The resulting MPT contents also followed linear functions, only the corresponding slopes differed (Figure 37a). The maximum dose that could be achieved was 9.51 mg per ODF using I9 at 2000 dpi. The predicted factors for the content increases from I5 to I8, I5 to I9 as well as I8 to I9 were calculated on the basis of the concentration ratios to each other. It is striking that the increase in the content with increasing ink concentration does not correspond to the predicted factor using the respective resolution (Figure 37b).

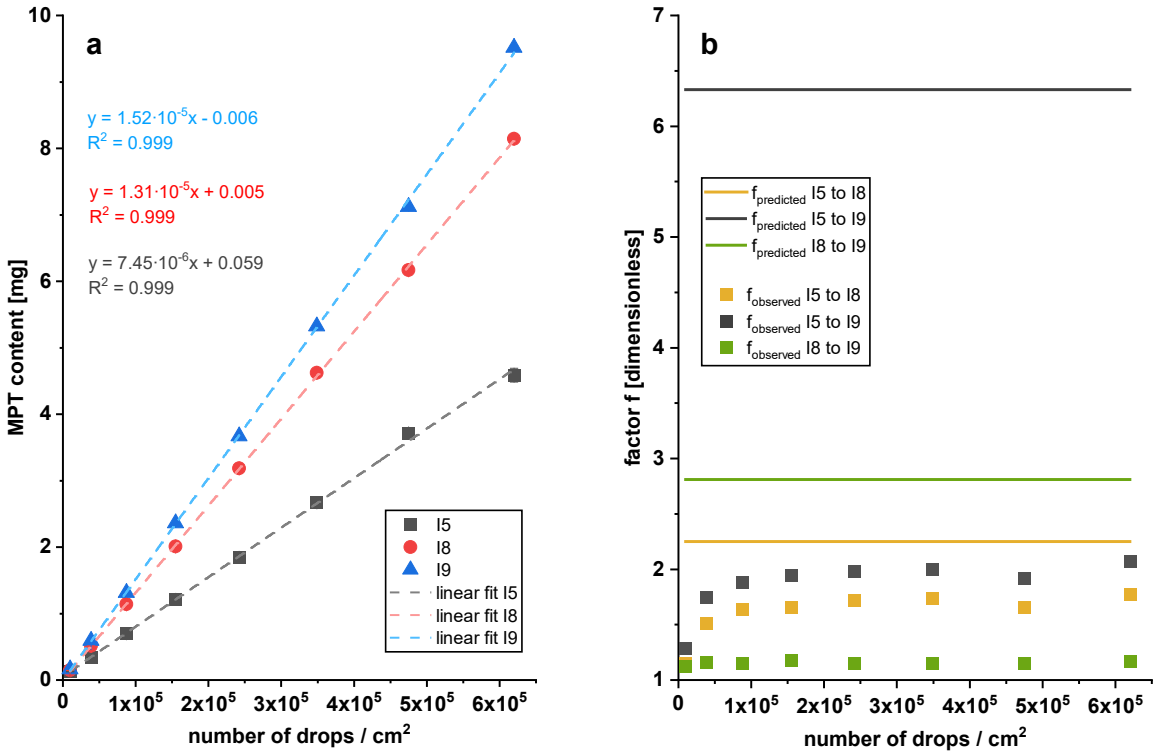

Figure 37: I5, I8 and I9 ink calibration series of print resolutions at a pulse voltage of 100 V (90%) and a pulse timing of 2–5–2 (mean ± SD, n = 3) (a), corresponding predicted and actual content factors (b)

The mismatch may be related to the different physicochemical properties of the ink formulations (section 3.1.3.1). Due to the significant increase of solid content and with that also dynamic viscosity, the drop volume decreased with higher MPT concentration in the ink. This occurred non-linearly. During the examination, it was noticed that the imprinted areas dry much slower as if using I5 ink and that after three days crystals are visible under the microscope. Printed ODFs by I8 showed first crystals at a resolution of 750 dpi after three days of storage at ambient conditions (Figure 38a). The crystal size increased in the sample printed at 2000 dpi, also the crystal habit changed. Printed ODFs by I9 already showed recrystallisation at 500 dpi (Figure 38b). It can be assumed that there is a limited amount of MPT that can be dissolved in the polymer film matrix. If the capacity is exceeded, supersaturated areas arise due to the evaporation of the solvent water. Here, crystal nuclei can be formed and grow into larger crystals. The solid state of the API can be crucial for its physicochemical properties and with that solubility. For MPT, two polymorphs are described in literature [200, 201]. Both polymorphs have similar properties. As the ODFs disintegrate very fast and are swallowed by the patient, the recrystallisation is more an optic issue in this case. Nevertheless, the growing crystals could separate themselves from the ODF by physical contact so that the correct dose could not be guaranteed.

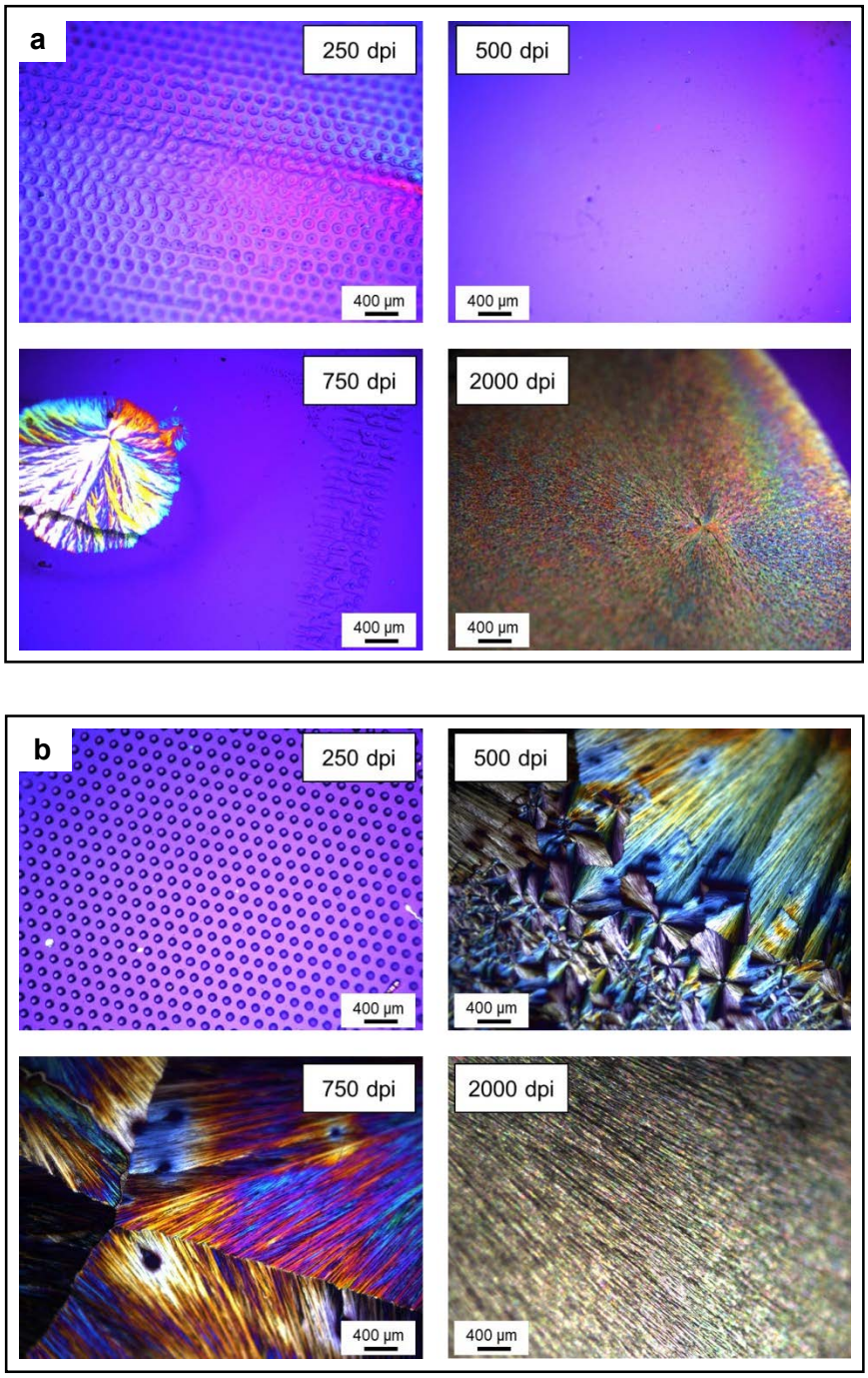

Figure 38: Polarised light microscope micrographs of imprinted ODFs by I8 (a) and I9 (b) after three days of storage at ambient conditions

The efficiency of the ink concentration as a dosage control element is limited, in case of good soluble APIs, by the change in ink properties. In the present study, an increase in ink concentration of an already high concentrated ink I8 by a factor of 2.8 led only to an increase in dose by a factor of 1.2. If the limits of a system are well-known, it offers the possibility to use lower resolutions for a target dosage. This could help to reduce the mechanical impact on the film substrate and to save the process time since higher resolutions result in increasing liquid deposition per area and prolonged printing time.

3.2.4.4 Additive Dose Printing

The aim was to prepare an ODF sheet with a target dose of 0.35 mg/cm² by solvent-casting method and additively imprint it with squares of 0.35 mg/cm² so that a total single dose of 0.70 mg/cm² is produced. To achieve this, a calibration step was performed comparable to the print resolution calibration (section 3.2.4.1). A solution of HPMC containing 8.3 mg/ml MPT was prepared and cast adjusting different gap widths of the coating knife (section 5.2.1.3). With the help of the resulting linear equation (Figure 39), the target gap width of 562 µm could be calculated.

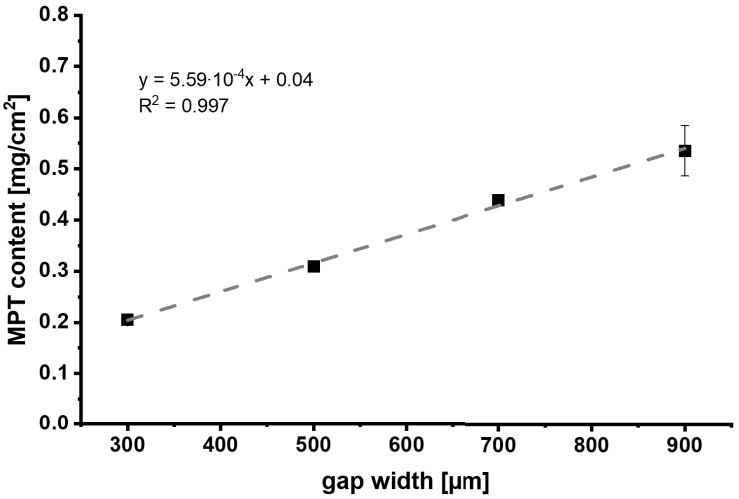

Figure 39: Calibration series of different coating knife gap widths (mean ± SD, n = 3)

For comparative purposes, the content uniformity of the automatically cut (section 5.2.1.4) cast MPT-containing ODF sheet and of an imprinted drug-free ODF sheet adjusting the resolution to 507 dpi (section 3.2.4.1) was investigated (section 5.5.22). All single units of the cast batch showed a higher MPT contents than 0.35 mg/cm² (Figure 40) so that the predicted gap width was slightly overestimated. However, the AV was with 5.9 clearly below the pharmacopoeial specified limit of 15. On the contrary, the single units of the printed batch showed unexpectedly lower MPT contents and an AV of 14.3 although this was significantly lower in the previous study (section 3.2.4.1). Hereby, the predicted print resolution seemed to be underestimated.

Finally, the additional dose was printed on the cast MPT-containing ODF sheet. Since the content measurement by HPLC is a destructive method, further samples had to be printed on an adjacent film surface. The single units varied around the total target dose of 0.70 mg (Figure 40). The CU was determined and an AV of 10.4 resulted.

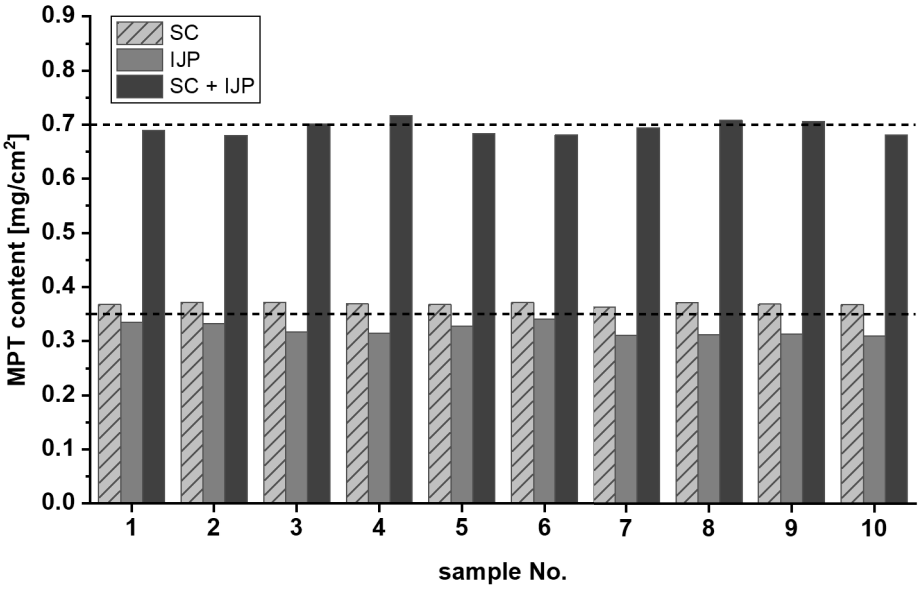

Figure 40: MPT contents of solvent-cast ODFs (SC), imprinted ODFs (IJP) and additively printed ODFs (SC + IJP); single samples for analysis of content uniformity according to Ph. Eur. 2.9.40 (n = 10)

Unlike printing on drug-free ODFs, where a protruding safety margin is possible during cutting, the cut-out of the printed API-containing ODFs has to be very precise. An incorrect cut could lead directly to a wrong dose and with that deviating AV. In the present study, manual cutting of the imprinted squares using a scalpel was carried out. Therefore, minimal offcuts could not be excluded. For the future, an automated coordinate-aligned cutting process should be implemented. Nevertheless, the samples fulfilled the requirements of an AV ≤ 15 and with that the successful implementation of additive dose printing could be demonstrated.

3.2.5 Dosage Reliability

Following the identification of deviating contents (section 3.2.4.4), it was decided to preform regular re-calibration steps. The initial calibration (section 3.2.4.1) was defined as time point t_0. With the results displayed in Figure 41, it could be confirmed that the MPT dose varied over time. The resolution of 250 dpi led to quantities between 73 and 127 µg and 2000 dpi to quantities between 4 and 5 mg. However, the coefficient of determination was at each time point $R^2 \geq 0.999$. As the used HPLC method was validated and since different nozzle numbers (No.) were used for inkjet printing, it was assumed that there could be an inter-nozzle variation in terms of drop volume.

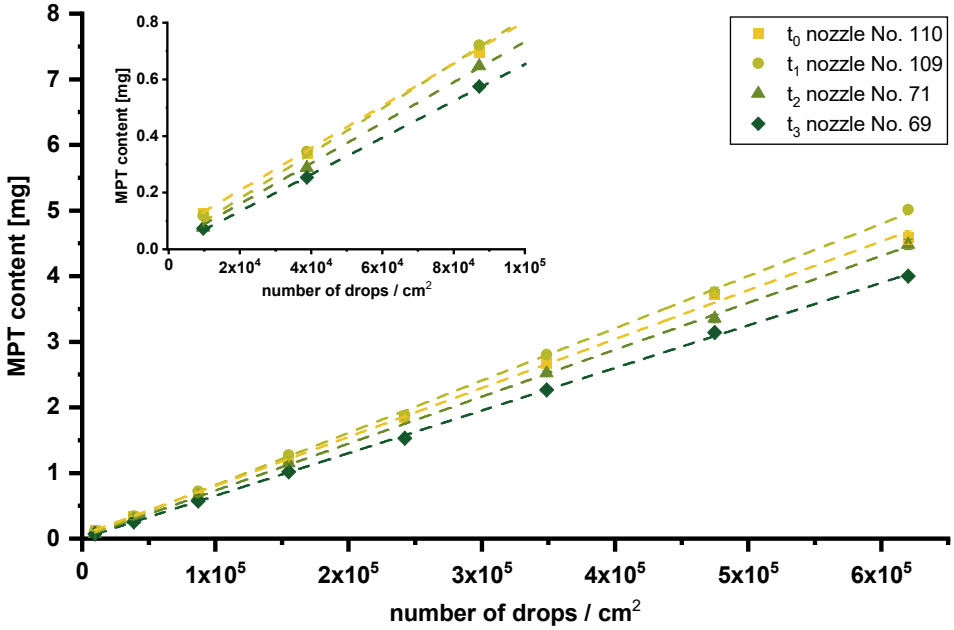

Figure 41: Calibration series of print resolution at different time points (t_0–t_3) distributed over five months (mean ± SD, n = 3) (modified from Kiefer et al. [41])

To verify this, samples were printed with respectively one of ten nozzles distributed over the entire print head width at time point t_3. The resolution of 1000 dpi was chosen as setting that is located approximately in the centre of the analysed print resolution range (section 3.2.4.1). The production was performed in one day. The resulted mean MPT contents are shown in Figure 42. As already implied by the figure, only nozzle No. 1 differed significantly from any other used nozzles according to the performed Tukey test (section 5.4.2 and 6, Figure 99. The remaining mean values showed non-significant differences and were around 1 mg.

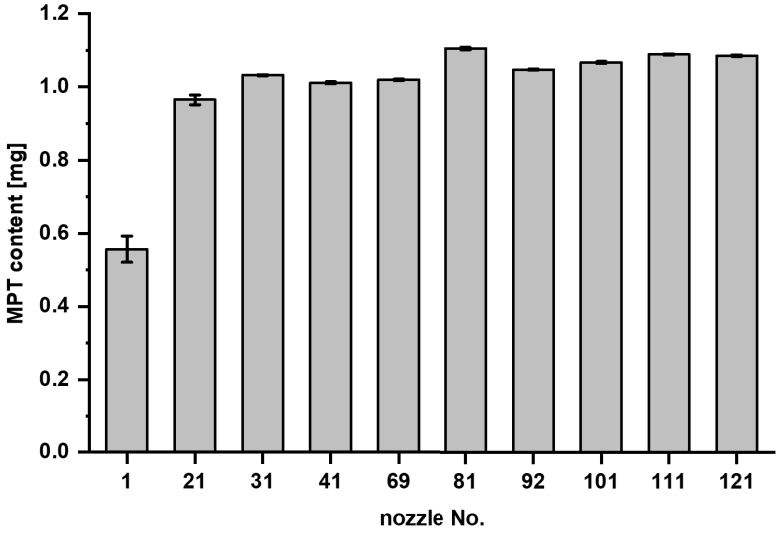

Figure 42: MPT content of samples printed at 1000 dpi with ten different nozzles on the same day in randomized order (mean ± SD, n = 3) (modified from Kiefer et al. [41])

If, however, the means of the respective resolutions printed at different days during five months (Figure 41) were compared by the Tukey test (section 5.4.2) it turned out that almost all were significantly different from each other. Only three mean differences of t_0 and t_1 of a total of 45 combinations were non-significant (section 6, Figure 98). Looking at the values in the course of the time from t_0 to t_3, a decreasing MPT content trend is apparent. For this reason, a general inter-nozzle variation was considered less relevant than the nozzle aging and the associated blockage over time. There are many conceivable causes for nozzle aging. They can wear out by incompatible ink, dried ink, mechanical strain of the PZTs, thermal stress, scratching due to physical action of wiping cloths in combination with dust and/or force of wipe, insufficient maintenance, exposure to UV-light or just due to long-term operation [171]. For the pharmaceutical inkjet printing, it means that a calibration series in the target range before each printing process is crucial, especially, after a long manufacturing break. Each time, the resolutions for target API strengths have to be recalculated using a recent calibration series. If this is assured, then the inkjet printing is not only very precise but also accurate in its dosage.

3.2.6 Cleaning Process of Print Head Assembly (PHA)

Over the course of the SP print head's operating time, it was noticed that the wiping cloth turned blue during purging of pure solvents through the PHA after longer breaks in operation. The only source of this could be previously used MB28-containing inks. However, these inks have not been used for six months at that point. Since no blue ink could be found visually in the ink container or at the nozzle plate, it was decided to disassemble the PHA completely into individual parts. The origin has now been clearly localised. The transition piece between ink container and the ink-tube leading to the heater bar as well as the interspace between the heater bar and the carbon array body showed blue and still liquid ink traces (Figure 43). As the components were not evaporated and build a smeary layer, it was concluded that it could be only residuals of PEG 400 containing MB28. Purging with pure solvents water, EtOH and isopropanol was not sufficient for complete cleaning. Even after six months, ink components from previous experiments could be found. The spreading properties of PEG 400 led to distribution of it into parts which could not be reached by usual maintenance. It becomes obvious that already the ink flow path consists of many dead spaces, interspaces and difficult-to-reach angles. These are high-risk areas for potential contamination. As the regular

disassembling of the whole construction has been avoided in order not to introduce dust into the system and to avoid wear of the plastic parts, this contamination was not detected for a long time period. Moreover, no impurity peaks were detected during the assay investigations of following experiments with MPT because of the different measuring wavelengths.

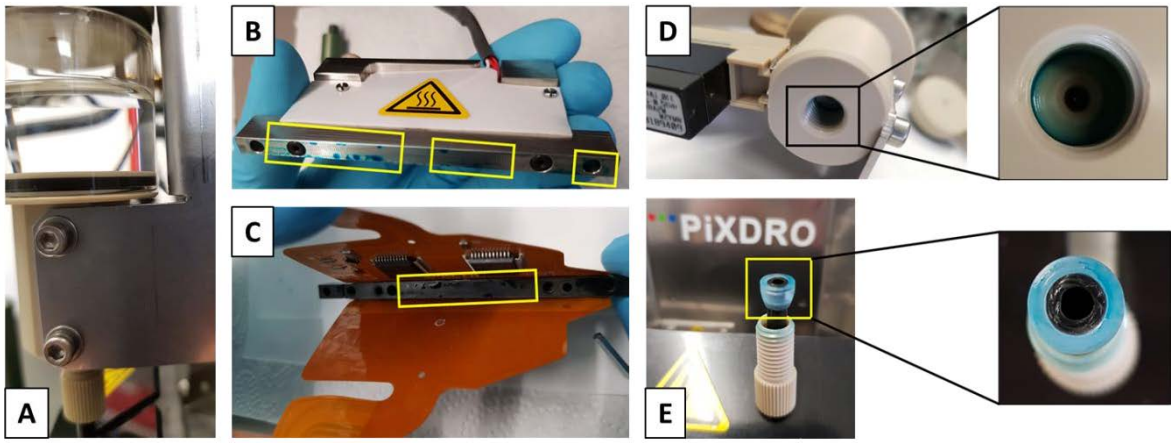

Figure 43: Pictures of the clean ink supply containing EtOH (A), heating block (B), carbon array body (C), ink container exit (D) and transition piece with ink tube (E) contaminated by MB28 ink

This cleaning issue could be only discovered due to the blue dye diffusing in the direction of lower concentration in the cleaning solvent. If an ink is transparent like the used MPT-containing ink, there is no chance to detect visually insufficient cleaning or cross-contaminations of other APIs printed by the same print head. Therefore, a comprehensive cleaning process design is required.

An investigation was started regarding the minimum volume of solvent required to meet the acceptance criteria for clean equipment after printing MPT-containing ODFs for paediatric patients. Current guidelines were used for orientation purposes. First, the sampling method and acceptance criteria had to be established. There are two sampling methods commonly used in the pharmaceutical industry: swab and solvent rinse method [202]. Since the PHA parts with which the ink has the only direct contact are mostly hidden or difficult to reach, it was decided to use the solvent rinse method.

To set the acceptance criteria, there are different approaches depending on the available information about the API. According to current EMA guideline [203], it should be based on the health-based exposure limits (HBEL) including permitted daily exposure (PDE) or the acceptable daily exposure (ADE). In the case that no data is accessible, the median lethal dose (LD_{50}) can be used as rational basis for estimation [204]. The LD_{50} for MPT is in the range

3470 to 4670 mg/kg bw for oral administration in rats [205]. For the worst-case scenario, the lower value was selected. With that information, the no-observed-effect level (NOEL) could be calculated (Equation 9). NOEL is required for determination of the maximum allowable carry over (MACO) to the next product. In context of the production of paediatric dosage forms, it was evaluated as not appropriate to insert the usually used standard adult body weight (bw) of 50 kg [203]. Therefore, a body weight of 3.5 kg was exemplarily taken so that a NOEL of 6.07 mg resulted.

In order to be able to calculate MACO (Equation 10), the minimum batch size (MBS) and therapeutic daily dose (TDD) of the next product batch had to be defined. The ink supply filling of 1 g was set as MBS and the recommended daily MPT dosages of 0.7 mg and 3.5 mg (section 1.4.1) were set as TDD. For oral administration, the safety factor (SF) is usually 1000. This led to a MACO of 8.7 mg and 1.7 mg depending on TDD. That means that the higher the TDD, the smaller is MACO.

$$NOEL\ [mg] = \frac{LD_{50} \times bw}{2000} \qquad \text{(Equation 9)}$$

$$MACO\ [mg] = \frac{NOEL \times MBS_{next}}{SF \times TDD_{next}} \qquad \text{(Equation 10)}$$

In order to determine the required solvent volume, the PHA with integrated SP print head was rinsed by water in fractions after printing with inks I5, I8 and I9 respectively. Water was selected as cleaning solvent due to the good solubility of MPT in it. Per fraction, a volume of 10 ml was purged into a watch glass underneath the print head. The content of the watch glass was quantitatively transferred, weighed and analysed. The initial fraction No. 0 was the pure ink itself. After each emptying, the ink supply was re-filled with fresh water. In this way, a total of 150 ml of water distributed to 15 fractions were passed through the PHA.

The resulted MPT quantities per fraction are shown in Figure 44. Depending on the ink concentration, the starting point at fraction No. 0 is different. After the first rinse fraction, a sharp decrease in MPT could be detected. Depending on the ink concentration, different minimum rinse volumes were required to meet the previously established acceptance criteria. The second fraction showed a MPT quantity below MACO of 8.7 mg for I5 ink and only the third fraction for I8 and I9. To fall below MACO of 1.7 mg, three fractions for I5 and even four fractions for I8 and I9 were required. It was noticeable that the quantity of MPT in the PHA became less with each fraction, but only asymptotically approached the zero value. That

means that small residues remained in the system and that with increasing number of fractions the cleaning result became more inefficient.

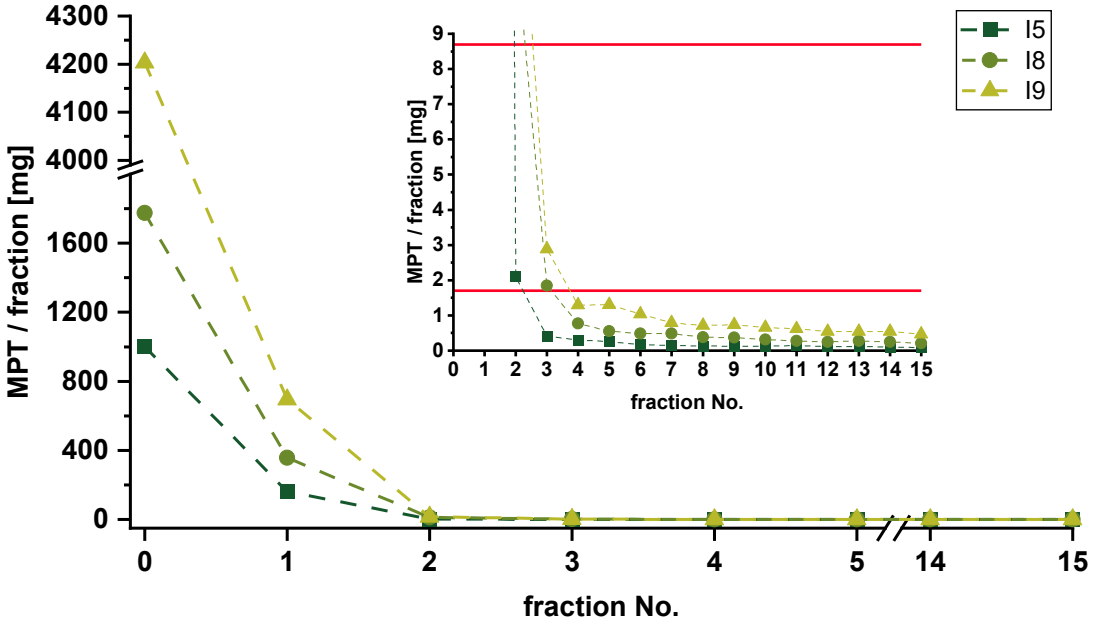

Figure 44: MPT quantities in single rinse fractions (n = 1), MACO of 8.7 mg and 1.7 mg are displayed as red line in the zoom-in.

For commercial manufacturing of printed ODFs, a complete cleaning validation of the printing process has to be performed to ensure product safety. In case of solvent casting of API-containing substrates (section 3.2.4.4), this process has to be also taken into account. However, this can only be limited to PHA, as it is the only part in direct contact with the ink as intermediate product. This is the advantage of inkjet printing as contactless technology. A potential contamination of the substrate table by temporarily dissolving of the film during printing is prevented by an intermediate liner separating the substrate table from the ODF sheet. The present study is only the first step towards cleaning process design including residues understanding and development of a strategy for cleaning process control [204].

To avoid the risk of cross-contaminations, disposable cartridges or dedicated PHAs for each processed API should be preferred for pharmaceutical applications. Additionally, development of more suitable printers and print heads superior by more simple construction and exclusion of inaccessible regions have to be accelerated.

3.2.7 Summary and Conclusion

In the course of comparing two industrial print heads, it became clear that the SP print head with larger nozzle diameter and a smaller number of nozzles is at an advantage for pharmaceutical application. It was less susceptible to temperature effects due to prolonged operation and was able to deposited more effective ink volumes. Even though it has been suspected that smaller nozzles will lead to more precise doses, it could be shown that smaller nozzles are more prone to clogging. The choice of print head was evaluated as crucial for the printing result. Furthermore, the dynamics of print head and substrate table has an impact on the morphological structure of film substrates. Special print heads adapted to pharmaceutical requirements would be preferable. To avoid cross-contaminations of APIs and minimise the hazard risk for patients, a cleaning validation should be performed for the final equipment. Only the parts of the printer that are in direct contact with the product are relevant. Due to the contactless process, only the PHA is a critical equipment part.

All selected drug dosing concepts were successfully established and critically evaluated. An increase in ink concentration only leads to an increase in dose up to a certain point. If a significant change in physicochemical properties of the ink is reached, the effectiveness of this method levelled off. Print resolution shown to be a useful parameter for dose controlling. In this context, dose calibration before each print campaign was found to be essential due to print head aging over time. However, the degree to which the resolution can be freely set is limited by the number of nozzles of a print head. After the mechanistic consideration with one nozzle, the next step should be a scale-up to a use of multiple nozzles.

3.3 Development of Appropriate Substrates for Inkjet Printing

3.3.1 Introduction and Objectives

Knowledge and process understanding of inkjet printing as a liquid deposition technique is of little use without a selection of suitable substrates of pharmaceutical quality for the target application. In the past, the first pharmaceutical inkjet printing experiments were carried out on non-edible paper sheets or foils until later mainly oral films and edible icing sheets were used as substrates [80, 98, 206]. The substrate properties are crucial for the performance of the final dosage form und have to be designed target oriented. In the present work, so far, a commonly used solvent-cast ODF composition based on HPMC was used as universal drug-free substrate. This has been sufficient for the purpose of investigations on inkjet printing process, but unintended physical deformations and dissolving of the film as well as ink coalescence on the surface could be observed. Comparable issues have already been addressed in the literature. One of the promising solutions was to develop porous substrates by electrospinning [92] or by freeze-drying of foams [126] to increase the absorption capacity of the films. Another approach was to add soluble, fibrous and porous additives to achieve an adequate adhesion of the printing ink to the substrate surface in addition to complete absorption [207].

On this basis, one aim of the study was to carry out further investigations into the use of functional excipients. Using characterisation methods developed accordingly, the extent to which these can change the absorption and mechanical properties of the substrates should be examined. Hereby, the substrates should still keep the orodispersible characteristics [113, 114]. Ink compositions developed in the course of the present work were used as test inks.

Furthermore, a deeper mechanistic understanding into the solvent-casting process itself should help to control the substrate thickness as important parameter for mechanical resistance of ODFs. The gap width is often used as adjustment tool for the film thickness to achieve a target API dosage [208, 209]. It has already been shown that the actual wet film thickness (WFT) does not correspond to the set gap width of the coating knife, both in small-scale production and in continuous production [210]. In case of pharmaceutical inkjet printing, the substrates are usually drug-free. However, the initial WFT has an impact on final

dry film thickness (DFT) which could be crucial for the mechanical resistance of the substrates to the printed inks. Moreover, printing of an additional dose onto an ODF containing a certain API dose is conceivable and was already shown to be feasible (section 3.2.4.4). For that purpose, knowledge about the required WFT for the target dose per unit is necessary. To overcome the thickness mismatch, an empirical factor or a generalised API excess of 30% was added in the past [211-213]. For continuous film production, a chromatic confocal optical sensor has proven itself as process analytical tool (PAT) to monitor and adjust in-line the WFT [214]. As the small-scale production could play an important role for community and hospital pharmacies [215], the method was transferred to a lab-scale film applicator and further developed.

The dynamically changing layer thickness of the polymer solution during film casting and the associated drying process was investigated. For this purpose, an optical probe was mounted into a developed XYZ-frame above the film applicator (section 5.5.11.2). A linear dependence of API content on the film thickness has already been shown [214] so that it was not in the focus. Therefore, drug-free polymer solutions based on two different HPMC and PVA grades were used as model systems. The optical thickness converted to physical thickness served as surrogate parameter for the drying progress and its temporal course was used to describe the drying kinetics. The effects and interactions of set parameters on WFT and DFT during the solvent-casting of ODFs were examined within the framework of a DoE (section 5.4.1.2).

3.3.2 Functional Films Containing Absorbing Additives

3.3.2.1 Selection of Additives

Initially, a pre-selection of additives was conducted. Seven different excipients were selected because their properties were expected to have a positive effect on the absorption of ink. Formerly used additives could not lead to a significantly improved absorption [207]. Therefore, other excipients and/or grades were considered. The requirement was that they were not soluble or only poorly soluble in the target polymer mass to ensure the physical interaction with the ink. Powdered cellulose (Arbocel® P290, PC), silicified microcrystalline cellulose (Prosolv® SMCC 50, sMCC) and microcrystalline cellulose (Vivapur® 105, MCC105) were chosen as representatives of fibrous materials with potential wicking effect. As absorbing powders of huge specific surface, mesoporous silica gel of different particle size distributions

was tested (Parteck® SLC, pSLC and Silica gel 60, SG60). Finally, a spray-dried α-lactose monohydrate grade (FlowLac® 100, fLAC) and functionalised dicalcium phosphate anhydrous (Fujicalin®, fDCPA) were selected as representatives of porous spheres. The raw materials were investigated by a scanning electron microscope (SEM) (section 5.5.20.2) regarding their particle shape characteristics and surface structures (Figure 45).

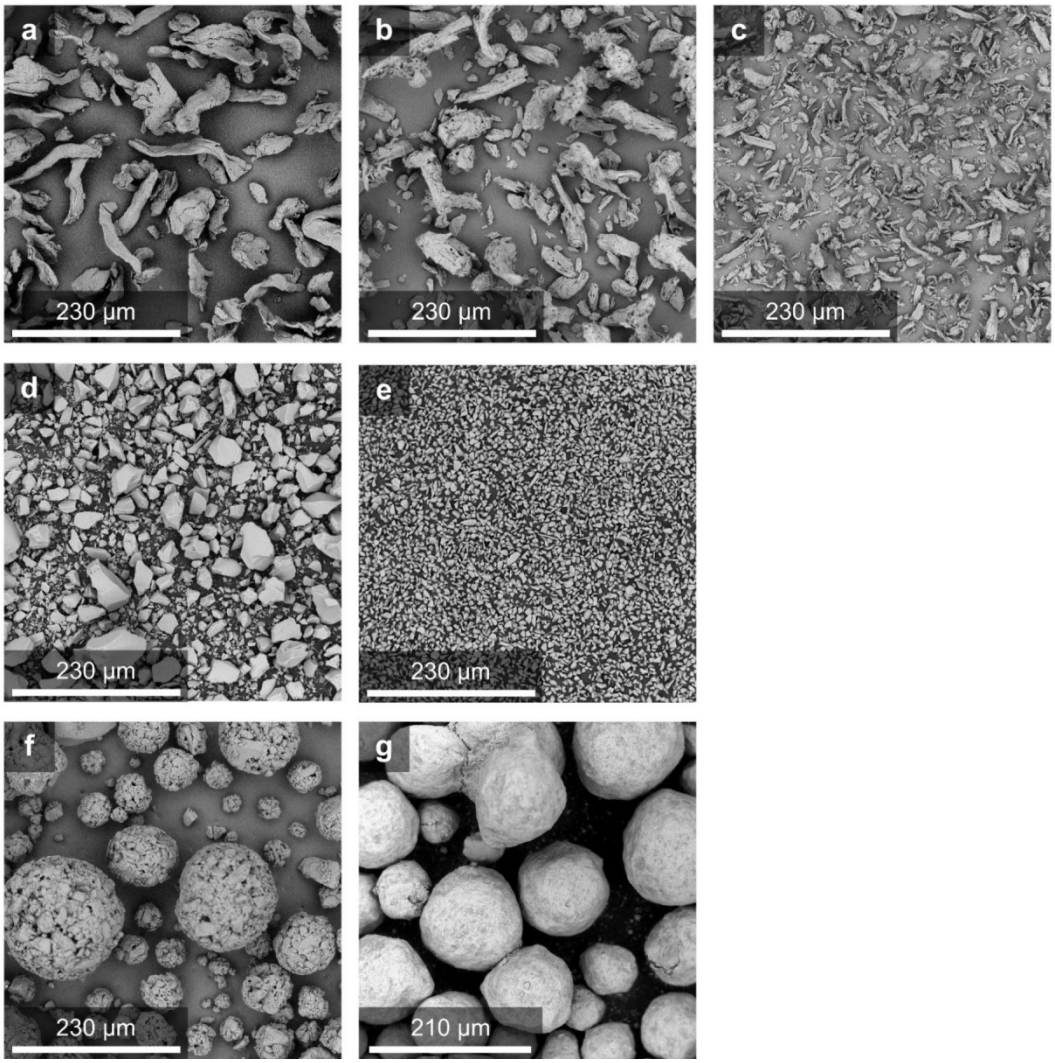

Figure 45: SEM images of PC (a), sMCC (b), MCC105 (c), pSLC (d) SG60 (e), fLAC (f) and fDCPA (g)

PC has a coarse fibre structure with consistent surface (Figure 45a). The co-processed MCC with colloidal silicon dioxide showed a more loose and porous structure providing a larger specific surface area (Figure 45b). MCC of a very fine grade produced by grinding still showed the fibrous origin (Figure 45c). The angular silica particles pSLC and SG60 were morphologically comparable (Figure 45d, e). They differed only in the particle size. FLAC showed typical spherical particle shape that is generated by the spray-drying process (Figure 45f). However, it is visible that the spherical agglomerates were built of single particles due to

the use of a suspension of milled lactose crystals in a lactose solution [216]. In comparison, the spray-dried fDCPA agglomerates had a smoother surface structure (Figure 45g) due to finer primary particles obtained by restrictive crystal growth [217].

The corresponding particle size distributions of the selected additives (section 5.5.19) are displayed in Figure 46. These were relevant for the preparation of the film-forming suspensions. To achieve stable and processable suspensions, the particle size distribution of the additives has to be ideally narrow [218]. The measurement results supported the microscopically determined differences in particle size. SG60 had the smallest particles with mean x_{50} of 6 µm and dDCPA had the biggest particles with mean x_{50} of 124 µm. It was expected that if the viscosity of the film-forming solution would be not sufficiently high, the dispersed fDCPA particles would sediment quickly. Furthermore, predetermined breaking points in the dried film could occur faster due to bigger imperfections.

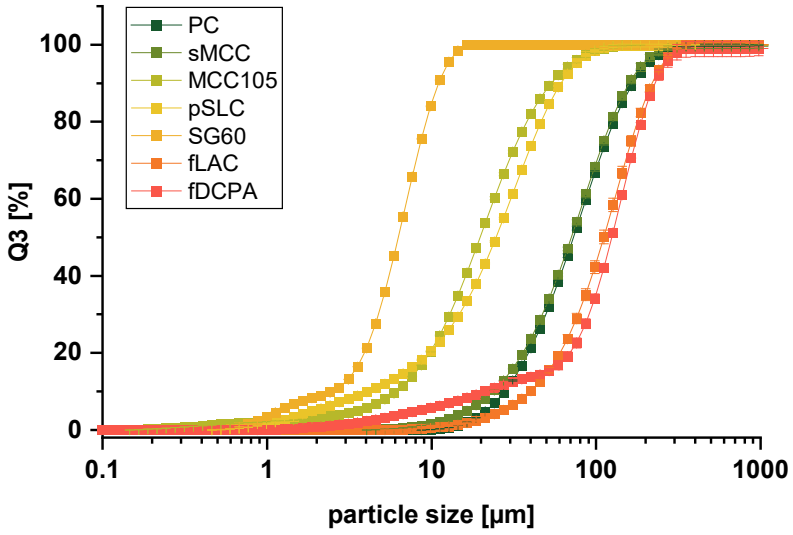

Figure 46: Cumulative particle size distribution (Q3) of the raw materials (mean ± SD, n = 3) measured by laser diffraction

Table 11: Particle size characteristics of the used additives (mean ± SD, n = 3)

Additives	x_{10}	x_{50}	x_{90}
PC	28 ± 0	73 ± 1	168 ± 3
sMCC	24 ± 0	71 ± 1	159 ± 4
MCC105	6 ± 0	20 ± 0	54 ± 1
pSLC	4 ± 0	25 ± 0	61 ± 1
SG60	2 ± 0	6 ± 0	11 ± 0
fLAC	40 ± 1	111 ± 3	219 ± 7
fDCPA	21 ± 2	124 ± 1	229 ± 7

3.3.2.2 Preliminary Studies on Film Manufacturing Method

The objective was to find a manufacturing process that would ensure an even distribution of the particles while maintaining their functionality. Two different methods of incorporating the selected additives were considered. Firstly, they should be dispersed in the drug-free polymer pre-solution before casting and coated as a suspension. Secondly, they were intended to be dispensed by gravity onto the finished cast, but still wet film to ensure that the single particles would not be covered completely by the polymer mass. The resulting rough surface would be determined only by the particle characteristics of the additives.

For the gravity-based procedure, a HPMC-based film sheet was cast by the automated film applicator and directly sprinkled with the respective additives through fine sieves with mesh sizes of 250 to 180 µm. For that purpose, the entire sieve bottom was covered by the weighed additive and distributed as evenly as possible over the film by means of manual shaking motion. It was challenging to apply a defined powder quantity per area. For the suspension method, each additive was dispersed in the polymer pre-solution and stirred so that the powder was wetted and homogeneously distributed in the mass. This was carried out until shortly before casting so the particles had little time to sediment.

Comparing the two methods for modification of the substrates for inkjet printing, it was noticed that the suspension method led already visually to more uniform films. The gravity-based method offered few control options and resulted in an uneven distribution of the additives. Furthermore, loose non-adhered powder remained in some areas of the film sheets. This might later lead to contamination of the inkjet printer and low patient compliance due to powdery mouthfeel. An electrostatic powder coating as used in the food and pharmaceutical industry [219, 220] would be more suitable in this case. Consequently, it was decided to continue with the film suspension manufacturing method.

3.3.2.3 Formulation Development and Characterisation

Since HMPC 606 was used as the film-forming polymer in the previous experiments, this was also chosen for preparation of the polymer pre-solutions for functional films. Some components such as lactose were expected to dissolve and others to swell in an aqueous system. Therefore, two types of polymer pre-solutions were prepared. The one type was completely water-based and the other was based on EtOH 70% (w/w). A reference without

any additive was produced respectively (Table 12, R1, R2). Since in the past an additive quantity of 1.5% (w/w) did not show an appropriate effect on the ink absorption [207], it was decided to increase it to 5% in relation to the total weight of the liquid mass. The films were cast adjusting the gap width of the coating knife to 500 µm, regardless of the particles size distribution of the single additives.

Table 12: Functional film formulations based on aqueous and ethanolic HPMC pre-solutions and their characteristics, grammage, micrometre screw thickness (MST, section 5.5.11.1) and disintegration time (mean ± SD, n = 6)

Formulation	Polymer pre-solution	Additive	Processability	Grammage [g/m²]	MST [µm]	Disintegration time [s]
R1	aqueous	-	✓	65 ± 2	84 ± 4	9 ± 1
R2	ethanolic	-	✓	53 ± 1	83 ± 5	6 ± 1
S1	aqueous	PC	✓	83 ± 4	163 ± 2	6 ± 1
S2		sMCC	✓	84 ± 4	163 ± 6	8 ± 1
S3		MCC105	✓	82 ± 7	115 ± 6	11 ± 2
S4		pSLC	✘	n.d.	n.d.	n.d.
S5		SG60	✘	n.d.	n.d.	n.d.
S6		fLAC	✓	92 ± 7	125 ± 8	13 ± 2
S7		fDCPA	✓	82 ± 4	214 ± 19	6 ± 1
S8	ethanolic	PC	✓	69 ± 2	162 ± 10	5 ± 1
S9		sMCC	✓	72 ± 3	168 ± 9	4 ± 1
S10		MCC105	✓	70 ± 2	122 ± 5	7 ± 1
S11		pSLC	✘	76 ± 1	204 ± 48	5 ± 2
S12		SG60	✘	75 ± 2	210 ± 55	6 ± 1
S13		fLAC	✓	70 ± 2	245 ± 8	4 ± 1
S14		fDCPA	✓	69 ± 2	232 ± 12	3 ± 0

Casting the formulations S4 and S5 containing silica grades pSLC and SG60, the film sheets got a large number of cracks and partly detached from the intermediate liner during drying (Figure 47a, b). Formulations S11 and S12 behaved similarly but were slightly less cracked so that samples could be cut out (Figure 47c, d). However, this could only be done manually using a scalpel and not with the cutting plotter. The particularly water-absorbent property of silica caused that it was no longer available as a plasticiser for HPMC. The film became brittle. Moreover, a kind of inverse siliconisation took place. The free surface energies of the film and liner differed so far that there were no appropriate interfacial adhesion forces any more [221].

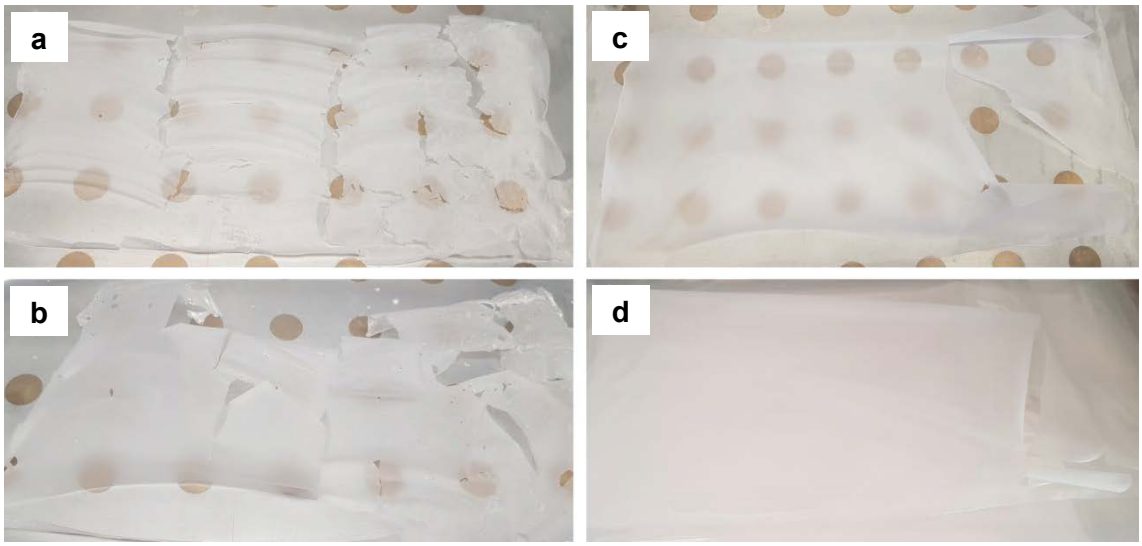

Figure 47: Images of cracked film sheets of formulation S4 (a), S5 (b), S11 (c) and S12 (d) directly after preparation

The formulations S4 and S5 as well as S11 and S12 have been excluded for further investigations since they were non-processable and hence, useless for imprinting. Only their water sorption results were used for comparison. All other formulations could be manufactured without any issues. In case of S6, an irregularity was observed. The embedded lactose dissolved almost completely in the polymer pre-solution so that no consistent particles, like in formulation S13, were in the final film. Despite this, the S6 was further examined in order to capture the influences on the printing results.

The film thickness measured by micrometre screw gauge (MST, section 5.5.11.1) is represented by the thickest point of the film and is particularly influenced by incorporated particles. Additives with smaller particles are able to arrange themselves in multilayers, whereas additives with larger particles have a higher probability of forming a particulate monolayer within the film matrix. In this case, the grammage was more meaningful. Due to the additives, the mass per area of all functional films (S1–S14) increased in comparison to the references (R1, R2). Moreover, water-based formulations (R1, S1–S7) showed about 20% higher average grammage than films produced of ethanolic pre-solution (R2, S8–S14) which is also reflected in the longer disintegration time (Table 12). This can be explained on the one hand by the lower density of 863 kg/m^3 (section 5.5.3) of the ethanolic polymer pre-solution in comparison to the aqueous one with 1000 kg/m^3. Adjusting the gap of the coating knife to the same width resulted in the same coated volume, but not the same mass per volume. Furthermore, if there is more water in the wet polymer layer, higher quantities of residual water can remain in the films after drying and make them heavier. Nevertheless, all samples demonstrated the

characteristics of ODFs with a disintegration time of clearly below 30 s [114] or rather 180 s [113]. It should be noted, however, that the used apparatus (section 5.5.17) is of limited suitability for determining differentiated disintegration times of ODFs. The relatively high medium volume of 900 ml and strong sample movement lead to usually faster disintegration than other methods [222].

Water sorption isotherms of the films were obtained using dynamic vapour sorption (DVS, section 5.5.12). All samples showed an exponential progression (Figure 48). An initially nearly constant water uptake at a low rate was followed by a steep increase from a critical relative humidity (RH) value of 70%. This behaviour could be explained by the Brunauer-Emmett-Teller (BET) theory [223]. First the water is adsorbed to the film surface in a monomolecular layer. In a second step, multilayer adsorption took place until a complete solubilisation of the polymer chains occurred. The latter led to a partial dissolving of the matrix and with that to lowering the diffusion barrier for the water molecules [224, 225]. Then the process can be described as water absorption.

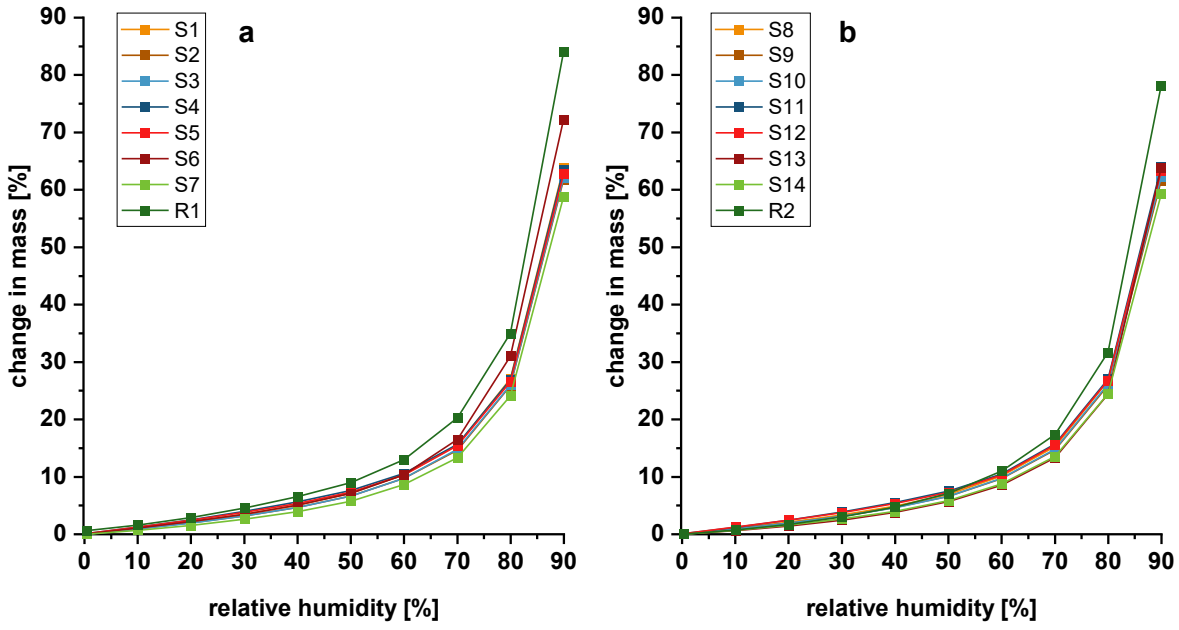

Figure 48: Water sorption isotherms of the functional films based on aqueous (a) and ethanolic (b) polymer pre-solutions and the corresponding references at equilibrium (n = 1)

Comparing the behaviour of the different formulations with the references, it became obvious that the water sorption capacity is mainly determined by HPMC and glycerol and not by the incorporated additives or the used solvent for the polymer pre-solutions. The functional films absorbed water at 90% RH in total up to 64.0%. S6 was an exception and will be discussed later. In contrast, the water uptake of the references R1 and R2 was up to 84.1% at 90% RH so

that they showed a higher sensitivity to climatic changes (Figure 48a, b). The undissolved additives led to the difference. An impact caused by the type of additive could not be detected. Since the additives replaced proportionally the HPMC quantity, a lower polymer content per film piece was present in comparison to the references. The water uptake capacity of the polymer was additionally limited by the particles act as occupancy of free interaction sites for water molecules. The number of available polar groups decreased so that the interaction with water was reduced [225]. Furthermore, the particles prolonged the diffusion distance for the water molecules so that their mobility was restricted. The case of the dissolved lactose in S6 supported this assumption. There were no powder particles in the film matrix but imperfections due to incorporated lactose molecules between the polymer chains. The change in mass was below the references and above the formulations containing dispersed additives (Figure 48a). Despite the rather small differences in the water sorption isotherms, the impression was gained during practical work that the ODFs including additives were easier to handle and adhered less to the operator's fingers.

To investigate the effect of the additives on the mechanical film properties before and after inkjet printing, the functional films were used as substrates for the MPT-containing ink I5 (section 3.1.3). Related to previous experiments (section 3.2.4.1), an area of 1 cm^2 was imprinted adjusting the print resolution to 1000 and 2000 dpi. As references, pure HPMC-based films R1 and R2 (Table 12) were used. For practical reasons, the films were cut to pieces of 2 × 3 cm to perform mechanical tests (section 5.5.16). The key parameters, puncture strength and elongation at break, were calculated. The corresponding results are depicted in Figure 49. The incorporated powders interacted with the polymer chains of HPMC so that no homogenous polymer matrix could be formed. The defective points resulted in lower cohesion force between the HPMC chains. Consequently, all functional films had a lower puncture strength in comparison to the references.

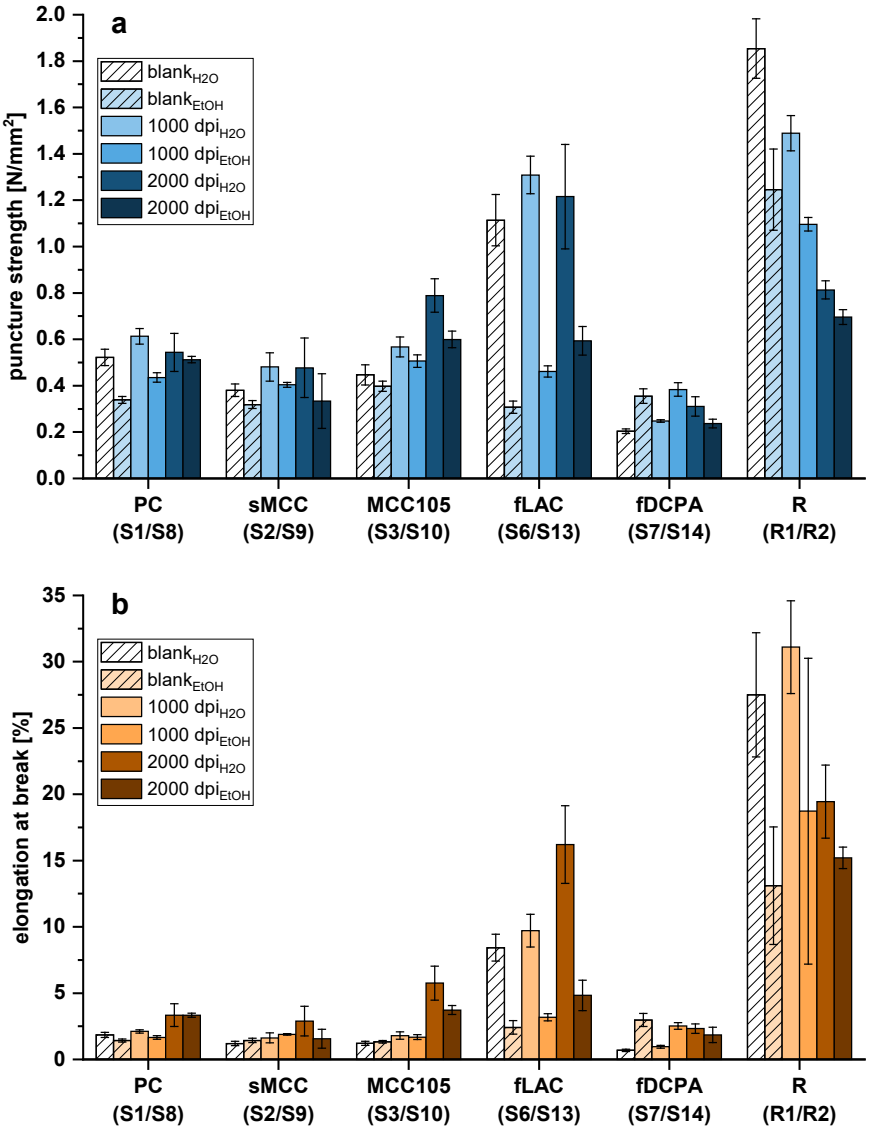

Figure 49: Puncture strength (a) and elongation at break (b) of blank and imprinted* functional films by the ink I5 determined by Texture Analyser, R: reference HPMC-based film (mean ± SD, n = 6, *n = 3)

In general, the formulations based on aqueous polymer pre-solutions often showed a higher mechanical resistance and flexibility than the ones based on ethanolic pre-solutions. This could be related to the different grammage values and the different water content. The water content of the films was indirectly determined calculating the difference between initial net weights and the ones at RH of 0% during the water sorption investigations. Generally, the functional films based on ethanolic polymer pre-solution showed with 2.7% to 3.2% a slightly lower water content than the films based on aqueous polymer pre-solution with 3.0% to 3.6%. The reference films R1 included 5.6% and R2 3.8% water. Its plasticising effect is reflected in the higher values for elongation at break.

The puncture strength increased in the most cases after printing, both for ethanolic and water-based samples. The water in the MPT ink played the role of additional plasticiser and partially dissolved the polymer film and rearranged it. This led to more flexible parts and the need of higher force to push through the film. The results of S6 and the reference deviated again. The puncture strength of S6 samples was quite high, presumably because the additive was almost completely dissolved whereas it stayed particulate in the ethanolic polymer pre-solution (Figure 50). Therefore, it had fewer predetermined breaking points. The puncture strength of the reference film decreased after imprinting because of the already visible change of the film structure. Comparing the appearance of imprinted references with imprinted functional films, it could be determined that the reference films deformed to a bulge-shape after drying (Figure 50). The functional films stayed flatter. However, the particles were washed away to the edges after imprinting, especially at a resolution of 2000 dpi, so that a clear rectangle appeared. This also explained the increase in puncture strength mentioned previously. A coherent polymer matrix area was formed so the cohesion between the polymer chains and with that the mechanical resistance increased.

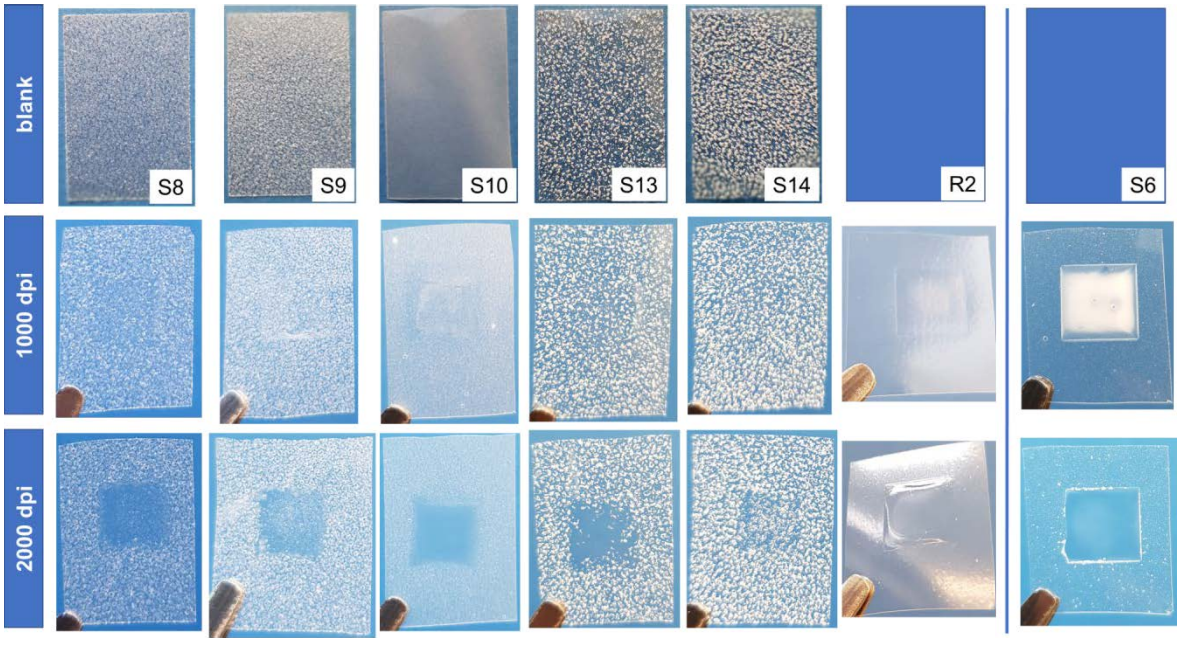

Figure 50: Photographs of blank and imprinted films of 6 cm^2, not available for blanks of R2 and S6

3.3.2.4 Optimisation of Silica-containing Formulations

As the HPMC-based functional films including silica particles cracked during the production (section 3.3.2.3) they were not suitable as substrates for inkjet application. But before silica was completely excluded as an ink-absorbing additive, attempts were made to optimise the

formulation. For that purpose, the polymer polyvinyl alcohol (PVA) in grade 4-88 was chosen as film-forming agent because, in preliminary studies, PVA-based films were shown to be more plastically deformable. In contrast formulations in section 3.3.2.3, only 5% (w/w) of PVA were used. Moreover, two different quantities, 5% and 12%, of the additive SG60 were incorporated. For comparison, references R3 and R4 were each prepared with 5% (w/w) polymer. The film characteristics are listed in Table 13.

Table 13: Functional film formulations based on aqueous polymer pre-solutions of PVA or HPMC and their characteristics, grammage, micrometre screw thickness (MST, section 5.5.11.1) and disintegration time (mean ± SD, n = 6)

Formulation	Polymer	Additive	Processability	Grammage [g/m²]	MST [µm]	Disintegration time [s]
R3	PVA 4-88	-	✓	179 ± 13	165 ± 9	16 ± 5
R4	HPMC 606	-	✓	77 ± 4	67 ± 6	5 ± 1
S15	HPMC 606	5% SG60	✗	n.d.	n.d.	n.d.
S16	PVA 4-88	5% SG60	✓	146 ± 3	139 ± 4	17 ± 1
S17		12% SG60	✓	131 ± 17	104 ± 13	n.d.

Unlike HPMC-based film sheets, the resulting PVA-based sheets did not crack immediately after casting (Figure 51a). However, a wavy white line was formed in the middle during drying of the wet film containing 5% SG60 at each manufacturing (Figure 51b). On the contrary, the films containing 12% SG60 had a more regular structure but they detached from the intermediate liner (Figure 51c). The orodispersible characteristic was given in all measured cases. Despite prolonged disintegration times in comparison to HPMC-based samples, the limit of 30 s [114] or rather 180 s [113] was not exceeded.

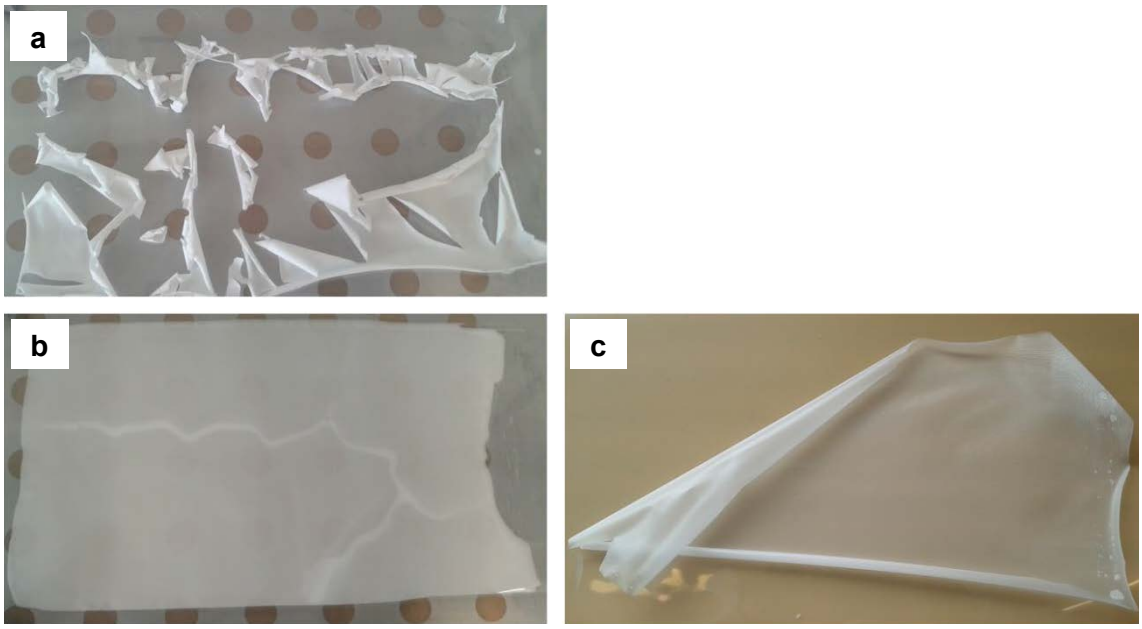

Figure 51: Photographs of film sheets (22 × 40 cm) based on polymer pre-solutions prepared of 5% HPMC 606 containing 5% SG60 (S15, a) and prepared of 5% PVA 4-88 containing 5% SG60 (S16, b) and 12% SG60 (S17, c), percentages in w/w %

The mechanical properties of the processable functional films S16 and S17 as well as the references were investigated (section 5.5.16). The results can be seen in Figure 52. It is obvious that the addition of SG60 led to a drastic decrease of the elongation at break in comparison to the pure film (R3). A higher proportion of silica particles paradoxically led to a higher mechanical resistance.

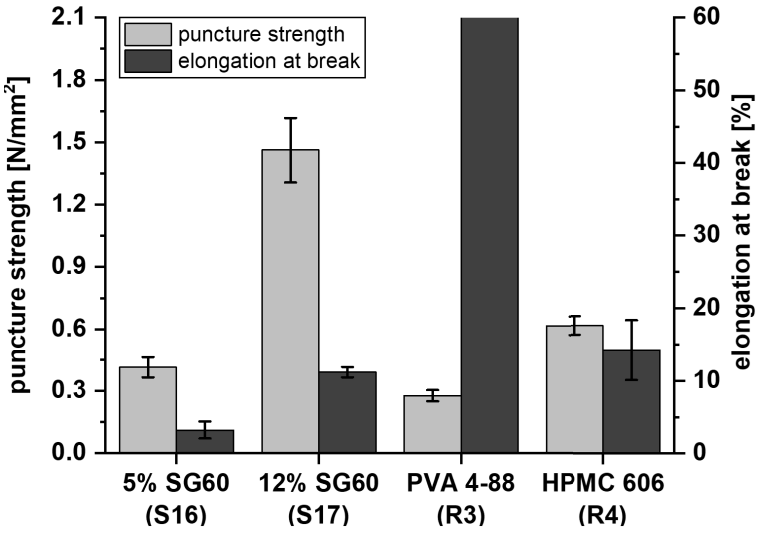

Figure 52: Puncture strength and elongation at break of blank functional films determined by Texture Analyser (mean ± SD, n = 6), 60% was the maximum measurable elongation at break (section 5.5.16)

Since the uncut S16 film sheet cracked and coiled up partly after two weeks of storage at ambient condition, it could not be imprinted anymore. Printing on S17 at 1000 and 2000 dpi

did not have a high impact on the mechanical properties. Although the silica particles were washed away like other embedded additives before (section 3.3.2.3), the mean puncture strength was 0.55 N/mm² in both cases and the mean elongation at break between 2% and 6%. By replacing the polymer, it was feasible to produce more stable film sheets. However, further formulation optimisation should be taken into account.

3.3.2.5 Absorption Behaviour

The attempts already made to quantify the absorption capacity of substrates using paraffin oil under vacuum [226] have been evaluated to be insufficient to describe the real case. The target applications involve mostly alcoholic or aqueous inks that have to be absorbed by the substrate. Dissolving and deformation processes could not be realistically demonstrated using paraffin oil. Since it is challenging to determine the differences in absorption capacity quantitatively, imaging methods were used in model experiments. In order to gain a better insight into the processes at the small-scale level, the absorption process was observed using the Drop Shape Analyzer (DSA, section 5.5.4) in side view and stereo microscope (section 5.5.20.1) in top view. For these investigations, only processable formulations based on ethanolic polymer pre-solutions (section 3.3.2.3) and the optimised PVA-based films including SG60 as additive (section 3.3.2.4) were used.

Figure 53 and Figure 54 show the behaviour of a coloured water drop on the different substrates recorded at different time points by the stereo microscope camera (section 5.5.20.1). Already after 5 min, the reference film R2 no longer resisted the drop and tore so that the liquid was spread under the film (Figure 53). The other functional films remained consistent, however, the drop seemed not to be absorbed but only to dry. The difference to the broken films seemed to be the different wetting and with that the wetted surface area. Although the deposited drop size was not always exactly the same, variations could be already suspected in the present top view. During the experimental performance, it was noticed that the drop behaviour applied on the formulation S16 differed depending on the used film side. The film side facing the air (top) behaved like the previously mentioned formulations (Figure 54). But the drop on the side facing the intermediate liner (bottom) had a kind of fringes instead of a clear drop edge which indicated a capillary effect. Formulation S17 did not show this effect.

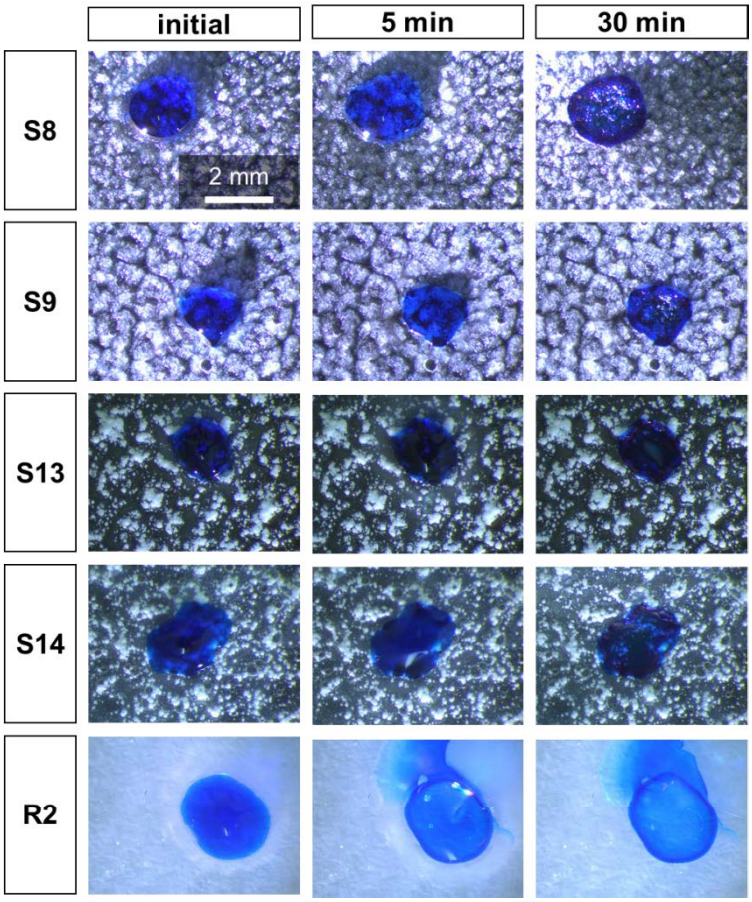

Figure 53: Stereo microscope micrographs of a selection of functional films, based on ethanolic HPMC 606 pre-solution, with applied drop of water (~10 µl) coloured by MB28 at different time points (S10 n.d.); R2 for better visibility with white paper background

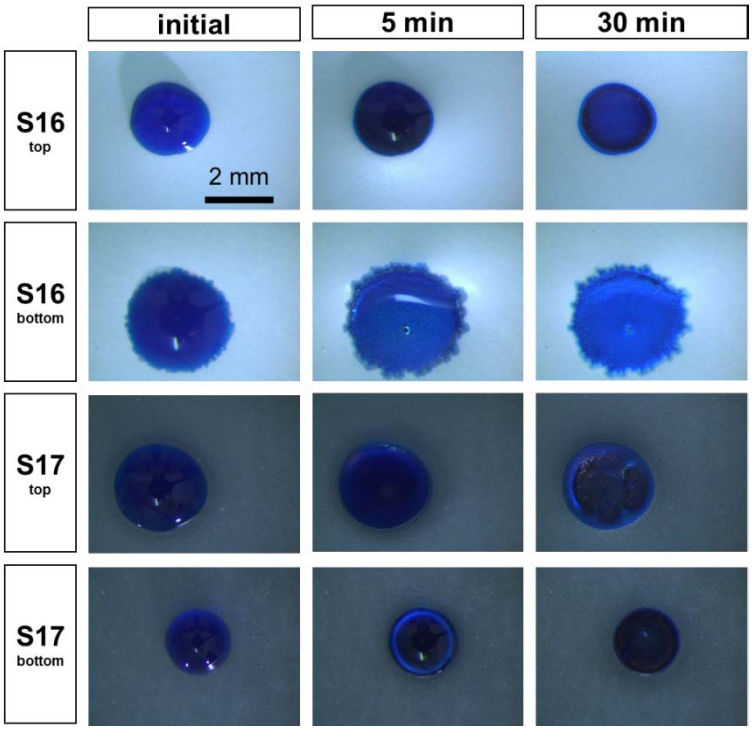

Figure 54: Stereo microscope micrographs of a selection of functional films, based on PVA 4-88, with applied drop of water (~10 µl) coloured by MB28 at initial time point, after 5 and 30 min

The absorption process could be monitored more detailed using the drop shape analysis. Since smaller volumes of 1 µl were applied here, there was less risk of the test liquid flooding the film. Besides, this experimental setup was closer to reality of inkjet printing than the previous one. Selected images recorded at 1 s, 30 s, and 120 s after deposition onto the film substrate are displayed in Figure 55. After 120 s, only S8 and S10 completely absorbed the drop. The drop on R2 remained almost unchanged, the drop was slightly reduced in height due to evaporation. On the small-scale, the contact angle did not seem to have any influence on the dissolving or absorption processes as suggested before although it did show clear differences.

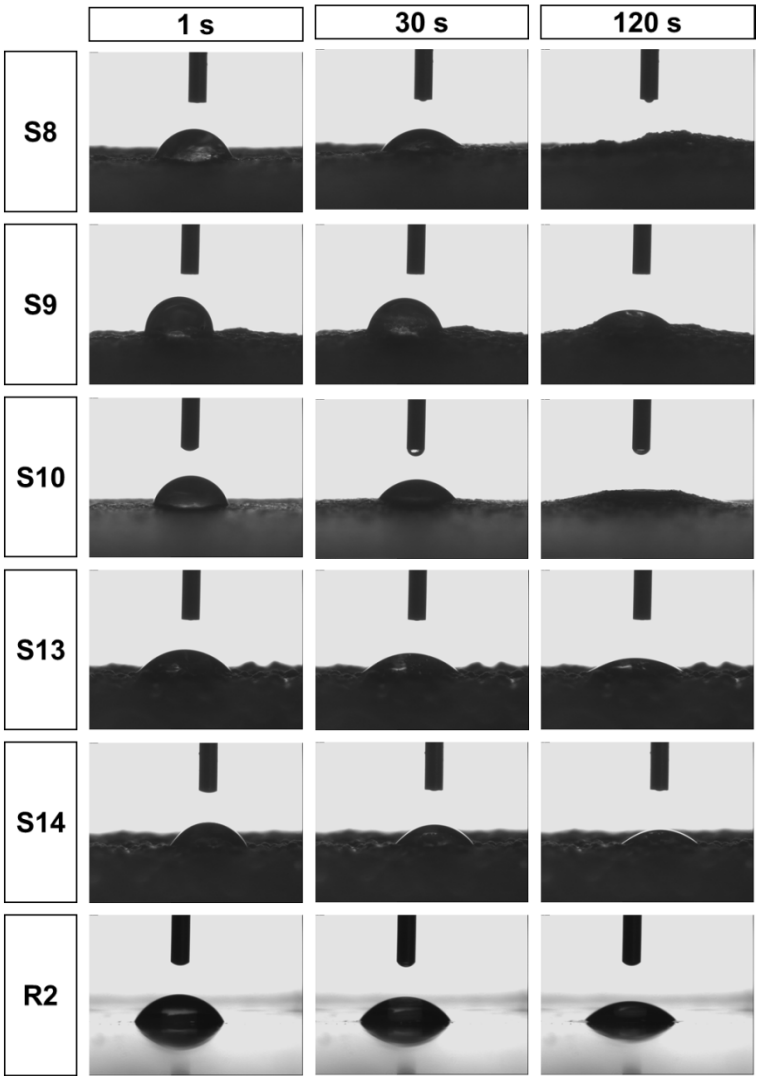

Figure 55: DSA images of a selection of functional films, based on ethanolic HPMC 606 pre-solution, with applied drop of water (1 µl) at different time points

Looking at the DSA images of S16 and S17 (Figure 56), it becomes clear that the film sides must indeed have different surface properties because the deposited drop did not behave in identical way. The drop on the top side of S16 led only to swelling of the film matrix after 120 s,

whereas on the bottom side, the drop disappeared already after 30 s. In contrast, S17 showed inverse absorption behaviour.

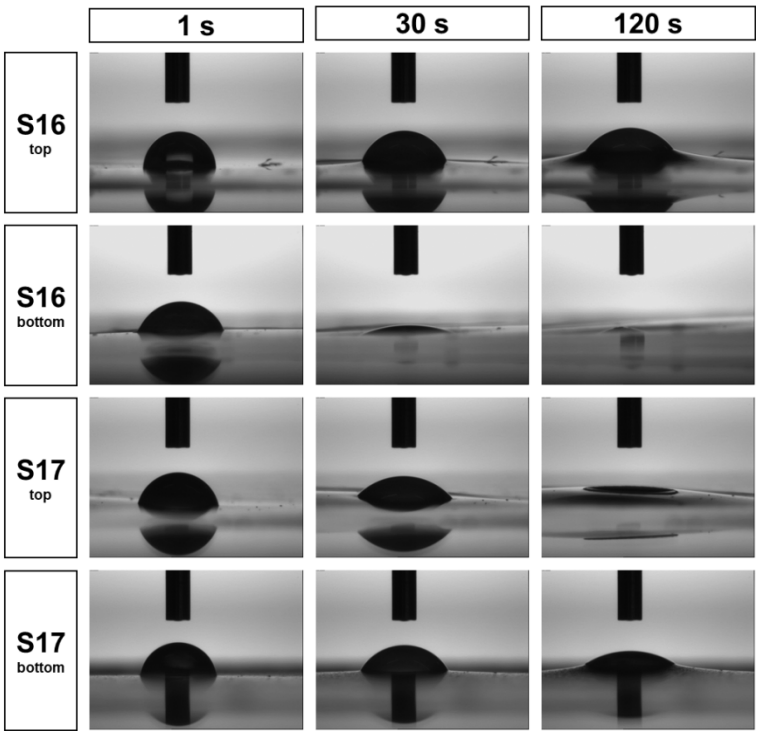

Figure 56: DSA images of functional films from the side facing the air (top) and the side facing the liner (bottom), based on PVA 4-88 pre-solution, with applied drop of water (1 µl) at different time points

To support the assumption, the surface morphology of the functional films was examined by SEM (section 5.5.20.2). The images of the HPMC-based functional films S8, S9, S10, S13 and S14 are depicted in Figure 57. In all cases, the incorporated particles were covered by a thin polymer layer. Caused by the big particle size and spherical shape, polymer-rich gaps are visible when looking at S13 and S14 (Figure 57d.1, e.1). Although the total mass percentages of the additives were the same, the particle number per volume was different due to varying particle sizes. This could have an influence on the distribution in the film and with that on the absorptive properties. The fibrous additives were arranged more closely to each other with increasing homogeneity with decreasing particle size (Figure 57a, b, c). Looking at the cross-sections, it is noticeable that they kept their fibrous structure despite of partial swelling.

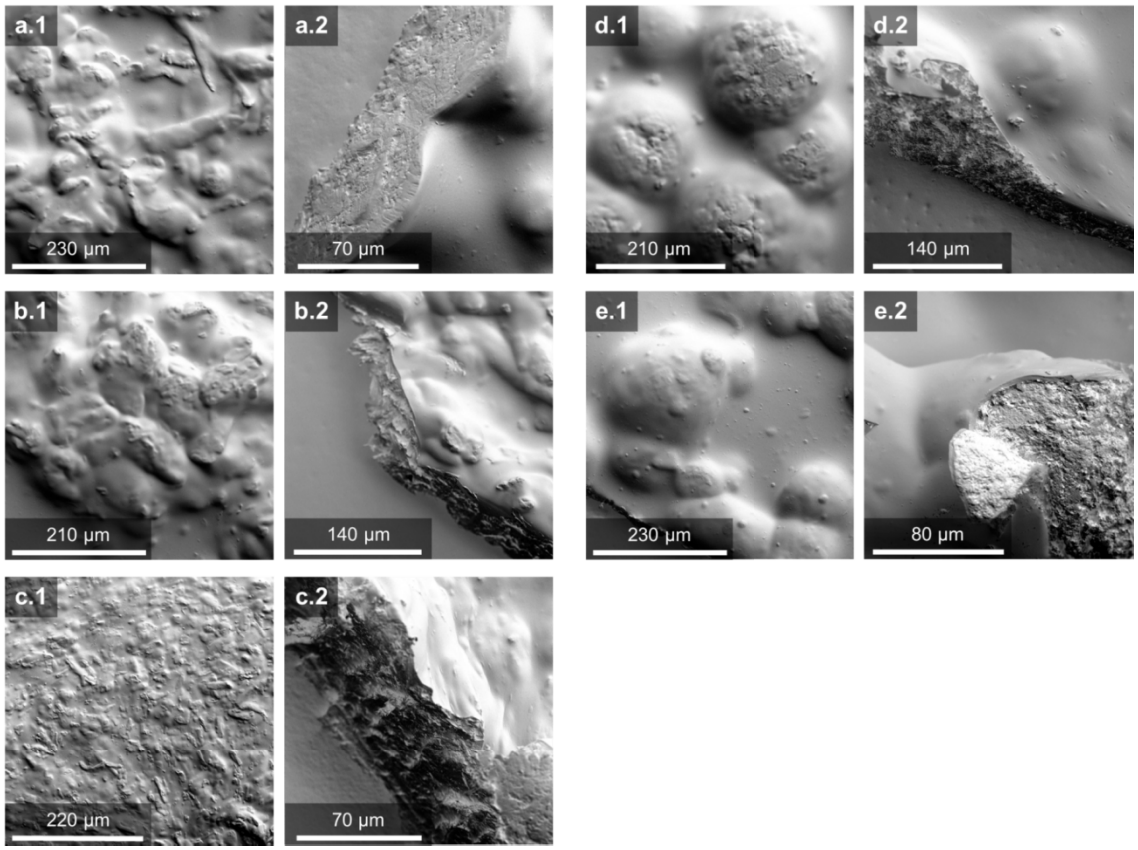

Figure 57: SEM images of S8 (a), S9 (b), S10 (c), S13 (d) and S14 (e); overview of the surfaces (1) and detailed cross-sections (2)

In general, the small particle size of SG60 led to an irregular brick wall-like arrangement of the particles within the polymer matrix regarding the formulations S16 and S17 (Figure 58). The top side of S16 was identified as a continuous smooth polymer layer (Figure 58a.1). Contrary, the bottom side was predominantly particulate (Figure 58b).

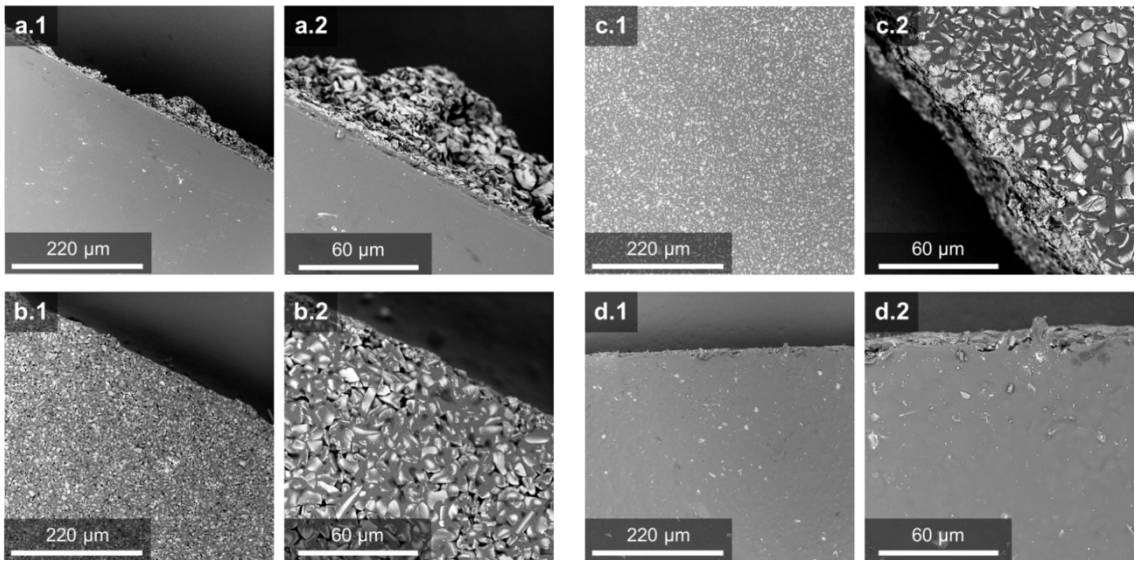

Figure 58: SEM images of S16 top (a) and bottom side (b), S17 top (c) and bottom side (d); focus on the surfaces (1) and detailed cross-sections (2)

In case of S17, the top side was particle-rich (Figure 58c) whereby more polymer-rich areas in dark grey could be detected than at S16. The bottom side was smooth (Figure 58d). That means that using higher quantities of SG60 made the particles sediment less than using lower additive quantities. This could be explained by the fact that with higher silica quantities the absorption of water out of the polymer solution increased. Consequently, the viscosity of the polymer phase increased so that the sedimentation was slowed down. These observations were consistent with the results of the DSA measurements. A particulate surface is more beneficial for ink absorption than a polymer-rich surface. Therefore, the initial approach to sprinkle the additives on the wet film layer was not unreasonable. For the future, it will be a challenge to develop such substrates without losing the elastic film properties.

For proof-of-concept, direct-compressed tablets as an example for particulate substrates were manufactured (section 5.2.3). The punch diameter was chosen as large as possible so that there would be enough surface area to print on later. As fillers, commonly used lactose monohydrate (Tabletose® 80, tLAC) and microcrystalline cellulose grades (Vivapur® 102, MCC102) were chosen. Furthermore, a ready-to-use excipient for orodispersible tablets consisting of mannitol and sodium croscarmellose (Parteck® ODT, MxCMC) was used. Crospovidone (Kollidon® CL, xPVP) was used as disintegrant and fumed silica (Aerosil® 200, SiO_2) to improve the powder flowability. The tablets were produced at three different compression forces (4.5 kN, 8 kN and 15 kN) to investigate the influence on the absorption behaviour. The applied compression pressure (section 5.2.3) was calculated. Disintegration time of the tablets (section 5.5.17) and the tensile strength (section 5.5.18) were determined to describe the mechanical characteristics (Table 14).

Table 14: Tablet formulations, the calculated mean compression pressure and the mechanic properties (mean ± SD, n = 50, *n = 10, **n = 6)

Formulation	Composition	Compression pressure [MPa]	Tensile strength* [MPa]	Disintegration time** [s]
C1	tLAC80 + MCC102 + xPVP	44.9 ± 3.5	1.0 ± 0.1	16 ± 1
		82.0 ± 3.5	2.7 ± 0.7	17 ± 5
		152.4 ± 4.9	4.9 ± 0.2	25 ± 5
C2	MCC102 + xPVP	41.5 ± 5.2	1.7 ± 0.3	25 ± 7
		88.0 ± 8.4	4.2 ± 0.6	27 ± 4
		142.7 ± 10.1	6.4 ± 0.5	48 ± 9
C3	MCC102 + SiO_2	46.1 ± 1.6	1.9 ± 0.1	61 ± 20
		80.3 ± 3.3	4.2 ± 0.2	114 ± 26
		173.3 ± 10.7	8.5 ± 0.7	> 180
C4	MxCMC	48.3 ± 1.2	0.6 ± 0.0	38 ± 19
		83.1 ± 1.7	1.5 ± 0.1	25 ± 8
		150.2 ± 2.7	3.4 ± 0.2	31 ± 6

The absorption behaviour was comparable for all formulations. Therefore, only the DSA images of C1 and C4 are shown in the following (Figure 59). The other images can be found in the appendix (section 6, Figure 100). The same recording time points like the functional films could not be met because the tablets absorbed the water drop within few seconds. The process could be divided into three parts: wetting, absorbing and swelling. The higher the adjusted compression pressure, the greater was the initial contact angle and the final swelling dimensions of the tablet. But it had no visible impact on the rapid absorption rate. The initial contact angle and the swelling process at corresponding set manufacturing parameters were determined by the used excipients. Unlike the functional films, the tablets had a larger volume so that there was more material to absorb the drop.

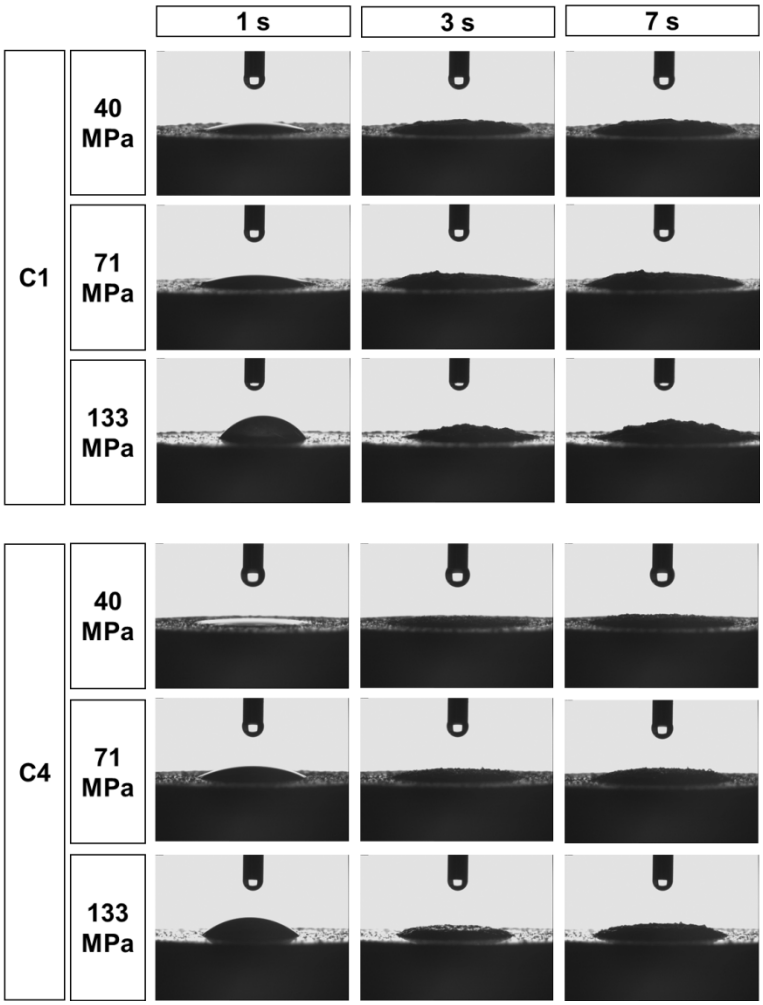

Figure 59: Exemplary DSA images of the tablet formulations C1 and C4 (section 5.2.3) with applied drop of water (5 µl) at different time points and compression pressures

Regarding the SEM images of the tablets (Figure 60a.1, b.1, c.1), the intended particulate and fibrous morphology is visible. Formulations based on MCC102 and xPVP (Figure 60a.2, b.2) showed deep cracks at wetted areas due to swelling processes. C3 had clearly less pronounced cracks due to the fact that no xPVP acting as disintegrant was included (Figure 60c.2). Wetted formulation C4 showed partially dissolved mannitol particles connected with partially dissolved xCMC particles (Figure 60d.2). No cracks could be identified but increased number of pores between the single particles. This formulation also showed the smallest contact angle and the least swelling during the DSA investigations.

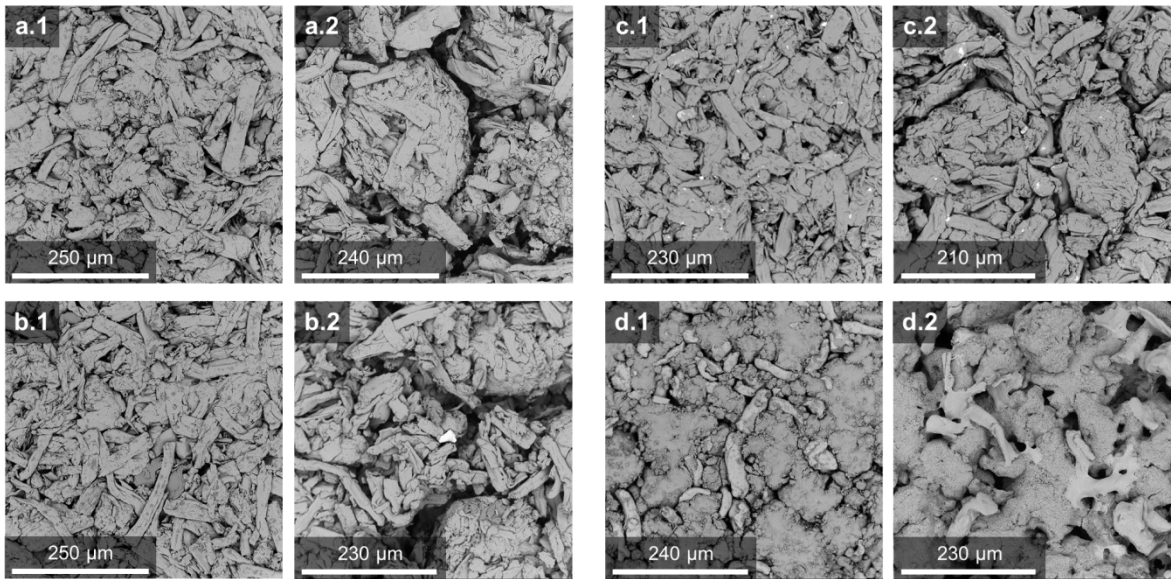

Figure 60: SEM images of the tablet formulations C1 (a), C2 (b), C3 (c) and C4 (d) produced at a compression pressure of 4.5 kN; non-wetted (1) and wetted areas by applied water drop during the DSA measurements

In summary, it has been shown that absorption of water-based fluids is improved when the substrate consists of only compressed particles. However, tablets of usual dimensions are probably not suitable for pharmaceutical printing due to a small printable surface area. Increasing the dimensions would lead to inappropriate dosage forms for varying patient groups so that it is a limitation factor in this case. If the inks consist of other components, especially solvents, further investigation regarding absorption behaviour have to be performed.

Alternatively, according to the most recent publications [227], the film-forming polymer covering the functional particles could be completely avoided by using ODFs produced of homogenised cellulose only. This paper-like substrates showed an acceptable mechanical strength and, in case of 10% MCC101 and respectively 100% (w/w) PC, also an appropriate disintegration time for orodispersible dosage forms within 30 s or 180 s [227]. Since this manufacturing technique does not require any additional polymer the absorption barrier could be excluded. This is reminiscent of first pharmaceutical inkjet printings which were performed on ordinary, non-edible copy paper sheets [80, 98, 206].

3.3.3 Fundamental Investigations on Factors Influencing the Film Thickness

3.3.3.1 New XYZ-Frame for Optical Sensor Mounting

Objective of this study was to monitor the solvent-casting process on a small production scale, as it might be implemented in a public or hospital pharmacy of the future, in terms of film thickness as key parameter for film production. For this purpose, an optical probe with a measuring range of 3 mm (section 5.5.11.2) was used. Consequently, it had to be mounted above the cast sample so that it was positioned within this range still ensuring enough flexibility along the z-axis. The probe had to be fixed perpendicular to the sample avoiding incorrect prolongation of thickness due to diagonal angle of LED light incidence. To measure the polymer layer thickness at different positions of the film applicator, additionally mobility of the probe in x- and y-direction was necessary. To realise this, a customised XYZ-frame was built (section 5.5.11.2).

Since it is a sensitive optical system, dovetail rails were used to enable smooth and precise displacement. The probe holder was made from an aluminium block with a recess milled to the exact diameter of the optical probe (d = 49.0 mm) and two plastic screws for fixing it (Figure 61b, B). An adhesive measuring tape was attached so that positions could be approached at clearly defined coordinates. Finally, the film applicator was positioned on the base crossbars and levelled together with the frame.

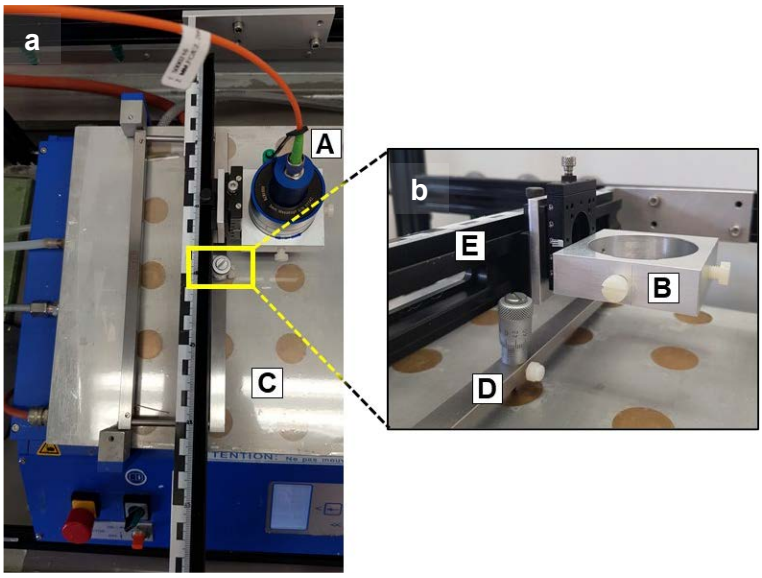

Figure 61: Top view of the optical probe (A) mounted in the aluminium holder (B) above the casting area of the film applicator (C) (a) and detailed image of the coating knife (D) in front of the crossbar (E) (b)

The movable parts were easy to fix and demount, so that the measuring probe could be moved flexibly to any point in the casting area of the film applicator. The only restriction was the micrometre screw of the coating knife (Figure 61b, D). The screw was protruding so that the probe-bearing crossbar (Figure 61b, E) was restricted in its freedom of movement. It was not possible to mount it higher than this, as the probe would otherwise leave its measuring range. Alternatively, coating frames with fixed gap width could be used if other positions should be investigated. These have the advantage that they do not have a disturbing micrometre screw.

3.3.3.2 From Wet to Dry Film Thickness

The solvent-casting process was monitored by the optical probe directly after pouring the polymer solution onto the intermediate liner fixed on the heating plate of the film applicator (section 5.2.1.3). The measuring principle of the chromatic confocal optical sensor is described in detail in section 5.5.11.2.

To calculate the physical thickness (pTH) from the optical thickness (oTH) data recorded in the chromatic thickness measurement mode, knowledge of the refractive index (RI) of the measured sample was required (section 5.5.11.2). However, the RI of a polymer solution changes dynamically with the progress of drying which could not be determined directly. Furthermore, the temperature and the wavelength of the incident light influence the RI. The use of a fixed measured RI of the polymer solutions was not useful and led to incorrect values. To work around this issue, instead of oTH, the also recorded distance to the first interface during the casting of the polymer solution was subtracted from the distance to the first interface of the process liner recorded before the casting process (section 5.5.11.2). Therefore, RI was no longer necessary. Instead, a method was found to indirectly retrospective determine the dynamic changing RI by calculating as ratio of recorded oTH and calculated pTH. In the following, the term thickness always refers to the physical thickness, unless otherwise specified.

Preliminary, film thickness profiles of HPMC 606-based solution were recorded during drying and repeating characteristics have been noticed. In general, the profile could be subdivided into four segments: initial lamella, rising wave, falling branch and plateau (Figure 62).

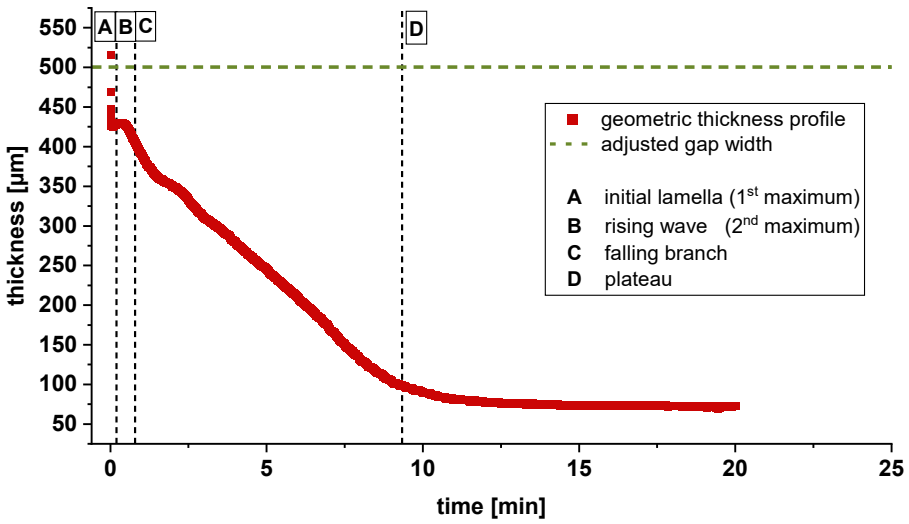

Figure 62: Example geometric thickness profile of HPMC 606 solution cast at 30 °C adjusting the gap width to 500 µm; subdivided segments initial lamella (A), rising wave (B), falling branch (C) and plateau (D)

The linearly falling branch (Figure 62C) or "constant rate period" and the plateau (Figure 62C) or the end of the "falling rate period" are also typical phases during a drying process of porous particulate material where first the unbound then the stronger bound water is removed until the equilibrium moisture content is achieved [228]. The drying mechanism of polymer solutions can be described also by the three phases [229, 230]. First, the temperature rises within the polymer layer by heat transfer. In the second phase, the incorporated water evaporates with constant rate unhindered by the polymer. The vapor pressure corresponds to the pure water [230]. The constant reduction in thickness due to the water loss could be also determined during the confocal chromatic sensor measurements. The slope of the resulting line was defined as shrinking rate (shR). This allowed indirect conclusions to be drawn about the drying kinetics of the polymer films (section 5.5.15). Finally, the polymer molecules come closer together due to the loss of water. As consequence, the residual water evaporates diffusion-controlled by the polymer network so that the evaporation rate reduces asymptotically until the equilibration moisture is achieved and a continuous film is formed [231, 232]. In case of present film thickness measurements, no significant change in thickness was detectable anymore in the plateau. The dry film thickness (DFT) was defined as mean of last 20 values of the plateau (section 5.5.15). Instead defining a transition phase between the first and third stage, the time point of the intersection of falling branch and plateau was set as drying time (dryT). Usually, the drying rate is determined by measuring the moisture content or weight loss versus time. This requires the destructive use of sample material. Using the

optical probe, it is possible to indirectly measure the drying progress on-line, contactless and with that non-destructive.

To my best knowledge, the first two segments of the thickness profile have not been described in literature yet. The initial lamella (= first maximum, Figure 62A), which was formed by polymer solution rising up the coating knife (Figure 63a), disappeared after a split second as the coating knife continued to move forward. Wetting behaviour and viscoelastic properties were assumed to be the cause of this phenomenon. The poured polymer solution accumulated in front of the coating knife and was forced through its narrow gap. This could lead to locally different shear rates, hydrostatic pressures and a macroscopically recognisable rolling movement of the viscous solution, which was finally drawn into the gap [233]. After leaving the gap, the polymer chains relax and escape in the energetically more favourable direction, in this case the z-direction. There, the solution met the front of the coating knife and adhered due to the wetting. The suggested microscopic cross-section of the lamella at the coating knife is shown in the schematic Figure 63b.

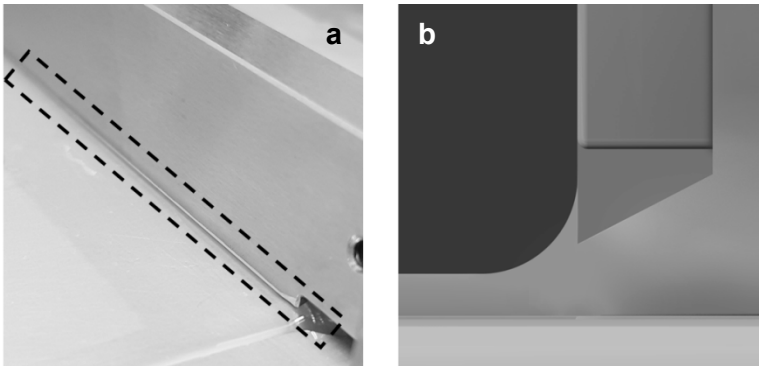

Figure 63: Photograph of cast polymer solution with visible lamella at the coating knife highlighted by black dashed box (a), schematic 3D computer graphic of a cross-section with zoom on the lamella formation at the coating knife (b)

It became clear that the optical sensor is sensitive to disruptive factors. The smallest movements in the film-liner-association, e.g. due to changes in the vacuum, were mapped as waves. In the course of the experiments, it turned out that a wave (= second maximum) rebounded shortly after the lamella (Figure 62B). The reason for this will be discussed later in this chapter.

Because of the lamella, it was difficult to define a certain value for the WFT. It was observed that from the first second the change in thickness slowed down to below 1 µm/s so that the arithmetic mean of second 1 to 3 was calculated and defined as WFT.

3.3.3.3 Effects of Process Parameters on Thickness Profile of ODFs

To identify the important factors and investigate the influence of set process parameters, polymer types and grades for ODF manufacturing, two DoEs were performed (section 5.4.1.2). As quantitative factors of influence, the adjusted gap width, casting speed and temperature of the heating plate were selected. The polymers HPMC 606 and HPMC 615 and PVA 4-88 and PVA 18-88 served as qualitative factors. In the appendix, all factor level combinations are summarised (section 6, Table 38 and Table 39). Since ODFs are sensitive to humidity [234, 235], which could not be controlled during the experiments, the ambient conditions were measured at the beginning and end with the help of a data logger. The ambient temperature during the production of the HPMC-based ODFs was between 20.8 and 25.5 °C and RH between 45.7 and 62.3%. The temperature during the production of the PVA-based ODFs was between 21.9 and 24.5 °C and RH between 44.8 and 60.0%.

For film preparation, the heating plate was adjusted to 30 °C, 40 °C and 50 °C. Since the resulting thickness profiles of samples dried at the same temperature were similar, only example profiles will be discussed in the following (Figure 64). All measurements showed the same profile as mentioned before (section 3.3.3.2). It was striking that the higher the temperature was, the bigger was the rising wave after the initial lamella. At 30 °C (Figure 64a), it was even hardly measurable. It could be assumed that higher temperatures led to faster water evaporation and with that polymer chains got more abrupt closer together. The result was a contraction of the whole polymer mass which caused a measurable increase of thickness.

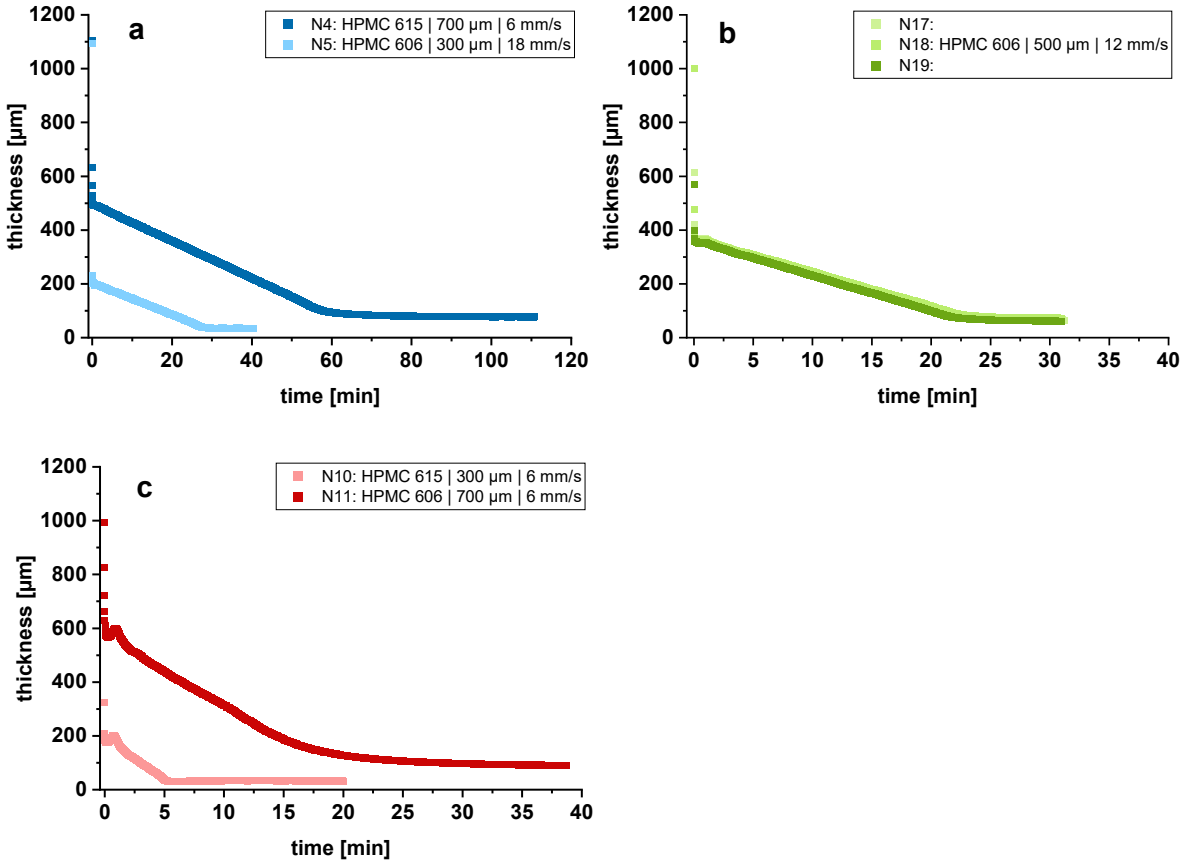

Figure 64: Exemplary thickness profiles of cast HPMC-based solutions dried at 30 °C (a), 40 °C (b) and 50 °C (c), measured by optical sensor at scan rate of 2000 Hz, 200 values averaged

To determine the drying kinetics, the lamella and second maximum, if applicable, as well as the plateau segment were cut off (section 5.5.15). Performing a linear fit, a coefficient of determination of $R^2 \geq 0.999$ for the falling branch was achieved in all cases so that zero-order kinetics could be considered. The shrinking rate depends on the applied temperature and type of drying. In case of the film applicator, it is conductive drying. The heating plate had no direct contact to the cast polymer solution, as the intermediate liner was in-between.

Thermography

To test how the real heat distribution was, the film applicator was examined by an IR camera (section 5.5.14) at the three set temperatures. Looking at Figure 65, the thermographic contour plots with corresponding temperature profiles of the film applicator only covered by the intermediate liner are demonstrated. In all cases, the temperature values along the horizontal and vertical lines in the region of interest (ROI) were 4.0% to 5.8% higher than set. With increasing temperature, the profiles took a convex shape so at the edges the temperature was lower than in the centre.

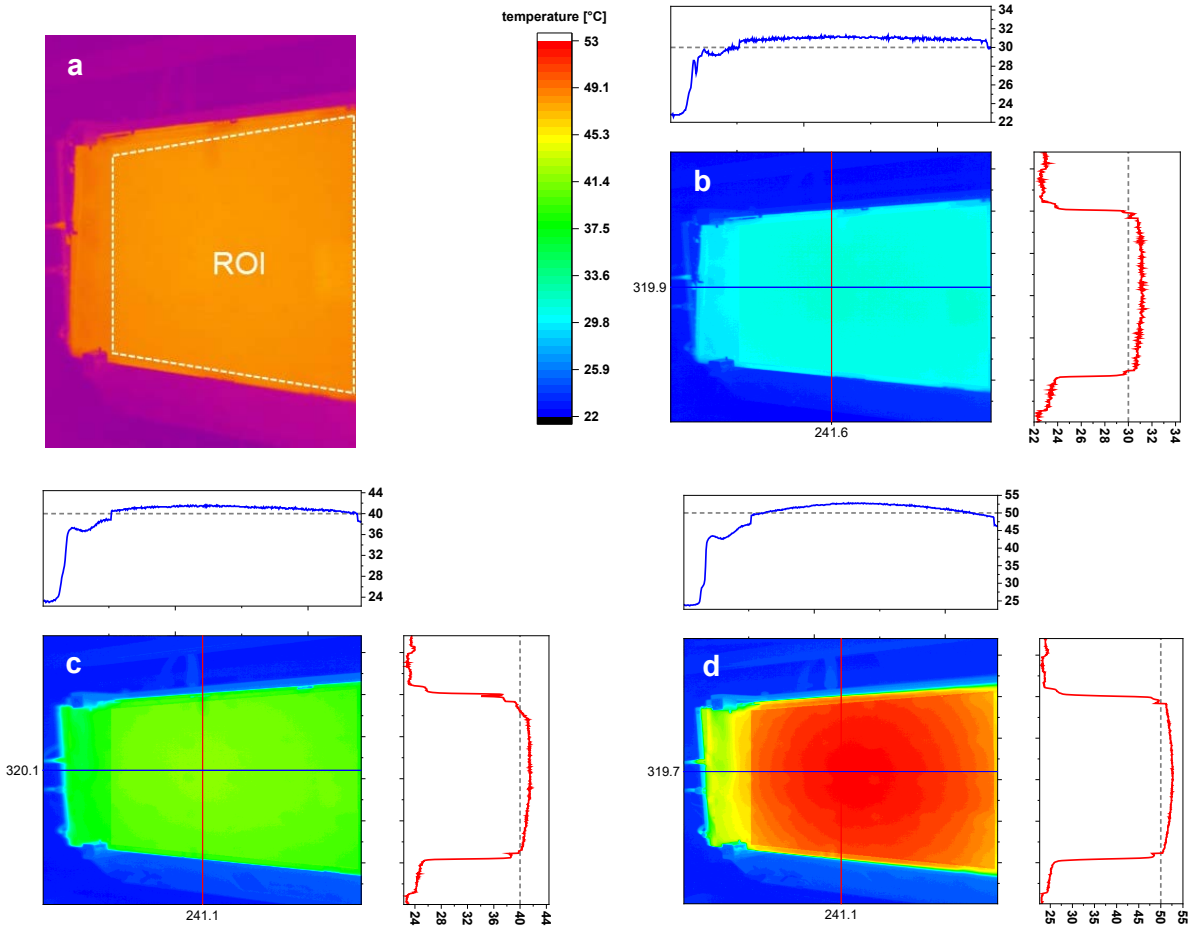

Figure 65: Original IR camera image of film applicator covered by the intermediate liner exemplary at 30 °C with highlighted region of interest (ROI) (a) and thermographic contour plot at 30 °C (b), 40 °C (c) and 50 °C (d) with corresponding temperature profiles determined at pixel positions 320 (horizontal) and 241 (vertical)

The temperature equilibration of the polymer mass during the casting process should be fast, so that the set temperature of the heating plate could correspond to the actual temperature effecting the mass. This was verified evaluating the IR camera records of casting in the most extreme conditions using a high gap width of 700 µm and setting a low temperature of 30 °C. The temperature of the just poured polymer mass was compared to the temperature of the thin polymer layer generated by the moving coating knife (Figure 67). The results confirmed that the temperature of the heating plate was achieved in the cast polymer solution at least after 10 s (Figure 66). It can also be seen that due to the slower coating speed of 6 mm/s (Figure 66a), the cast polymer mass warms up before coating and is thus two degrees warmer than with a faster coating speed of 18 mm/s (Figure 66b).

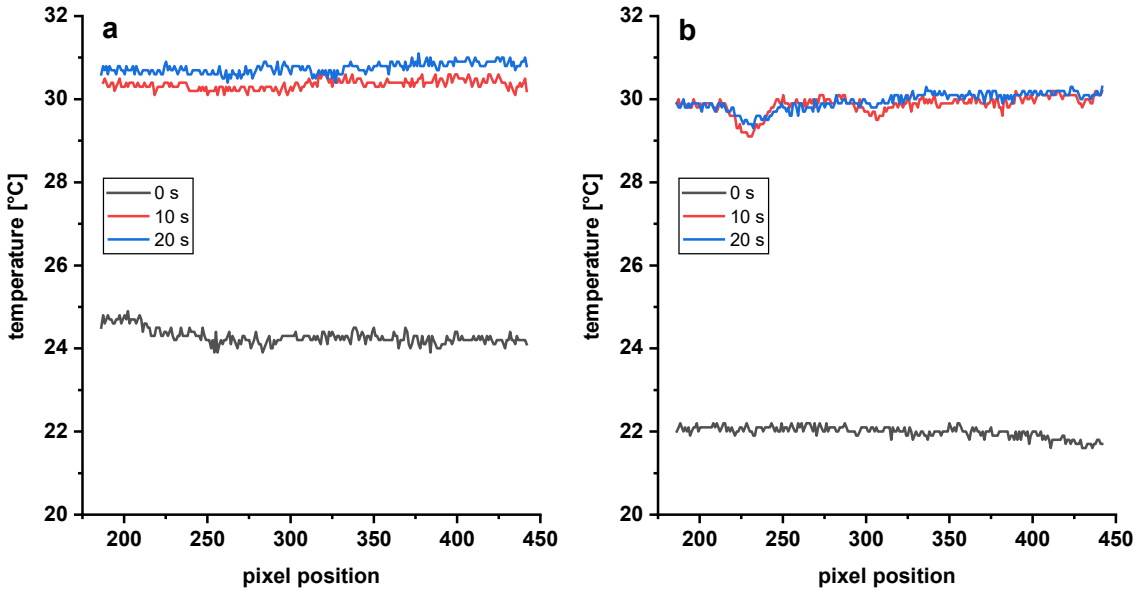

Figure 66: Temperature profiles of HPMC 606-based solution along the black line (Figure 67) using a gap width of 700 µm at a speed of 6 mm/s (a) and 18 mm/s (b); recorded directly (0 s), 10 s and 20 s after starting the solvent-casting at 30 °C

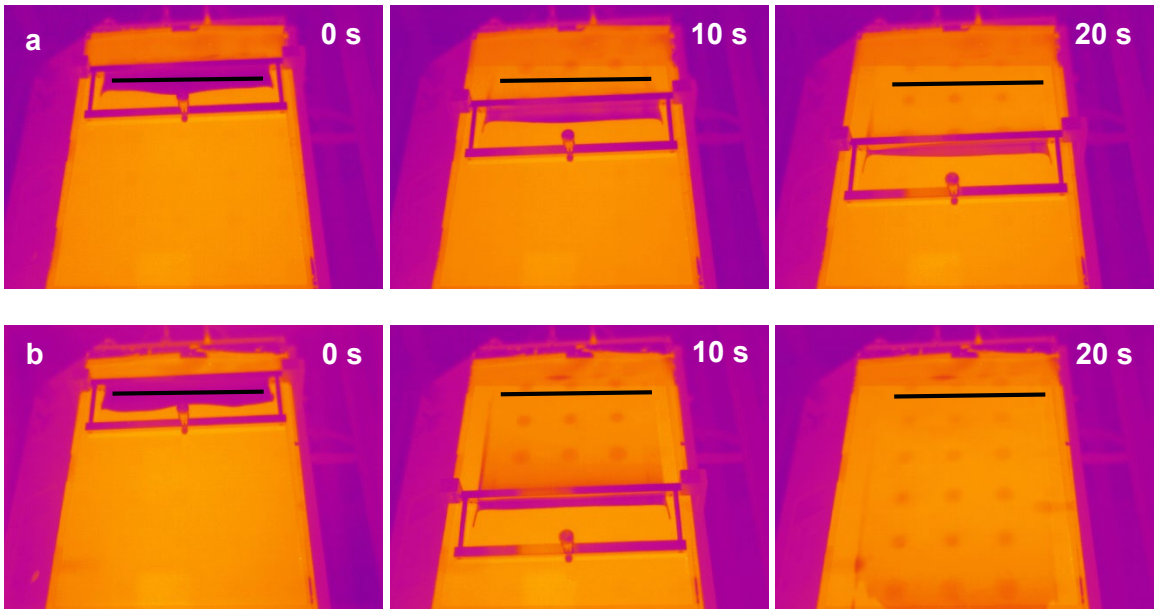

Figure 67: IR camera images of the solvent-casting process of HPMC 606-based solution using a gap width of 700 µm at a speed of 6 mm/s (a) and 18 mm/s (b), black line outlines the localisation of the evaluated temperature profile

Model Evaluation of DoE

The DoE results were connected by means of a mathematical interaction model and fitted using multiple linear regression (MLR) to estimate the coefficients of the terms. To evaluate if it is a good or poor model, the summary of fit plots (Figure 68) were considered. In both experiments, the responses showed R^2 values of 0.963–0.999 and Q^2 values of 0.637–0.996. Two

exceptions were the responses lamella and wave length (WL) in case of HPMC-based solutions (Figure 68a). The responses lamella and WL even showed a negative Q^2 which was an indication of a bad model or insignificant terms. Drying time (dryT) showed a low and shrinking rate (shR) even a negative model validity due to high reproducibility of 0.998 and 0.999 respectively that did not represent the true experimental error. This led to a significant but artificial lack of fit. Additionally, the model describing the lamella was insufficient. In the case of PVA-based solutions, the response dryT had a negative and shR a low model validity for the already aforementioned reasons (Figure 68b). Apart from that, good models were generated.

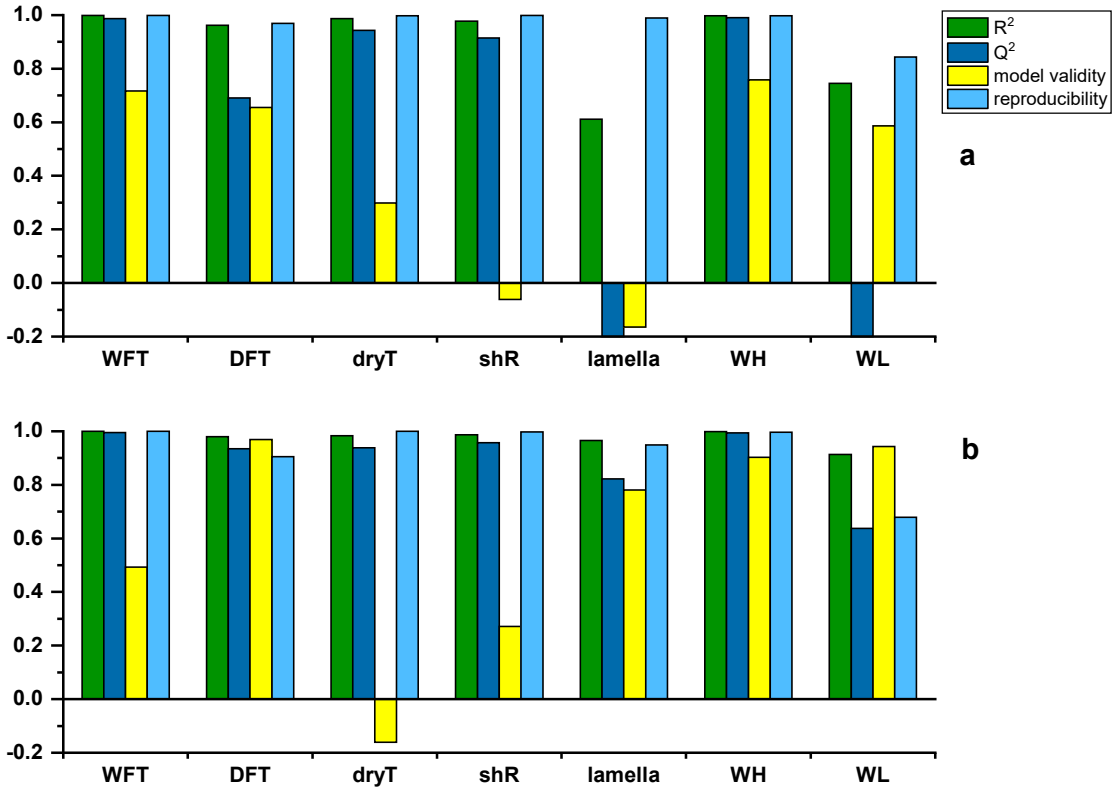

Figure 68: Summary of fit plots, HPMC-based (a) and PVA-based (b) solutions (N = 19, DF = 8); responses: wet film thickness (WFT), dry film thickness (DFT), drying time (dryT), shrinking rate (shR), thickness of initial lamella/1st maximum (lamella), wave height (WH), wave length/2nd maximum (WL)

Lamella and Wet Film Thickness

Starting with the lamella, it could be noticed that cast HPMC-based solutions showed higher thickness than PVA-based solutions in almost all experimental runs (Figure 69). Furthermore, it became apparent that the lamella was not always higher than the adjusted gap width. In some cases, it was just below. Statistical analysis showed, however, no significant effects or interactions between factors regarding the lamella.

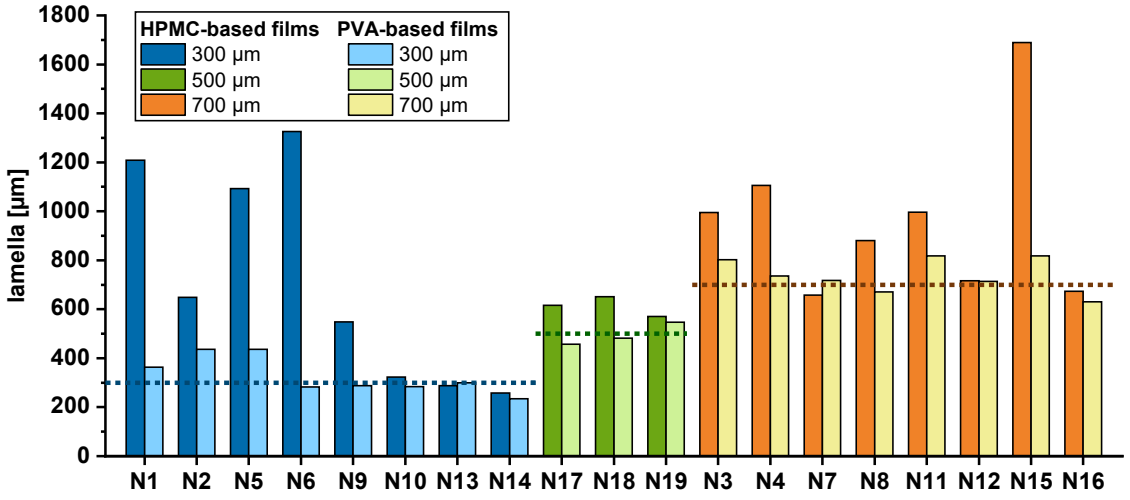

Figure 69: Measured lamella thickness of HPMC- and PVA-based solutions (n = 1) arising during the casting process, experimental runs (section 6) ordered by actual used gap width of the coating knife (dashed lines)

Despite the different lamella dimensions, the resulting WFT using different polymers seemed to be hardly distinguishable from each other (Figure 70). With larger gap width the absolute difference between target and real WFT increased. Due to higher weight force than internal resistance of the solution and laterally unlimited area, spreading in all directions took place immediately after leaving the gap [236]. This caused a downward deviation of WFT from the adjusted gap width of the coating knife. However, if considering the percentage difference, the real WFT deviated between 12.7% and 39.9% for HPMC and between 19.9% and 38.5% for PVA from the target WFT. The extent of the deviation was not significantly dependent on the gap width.

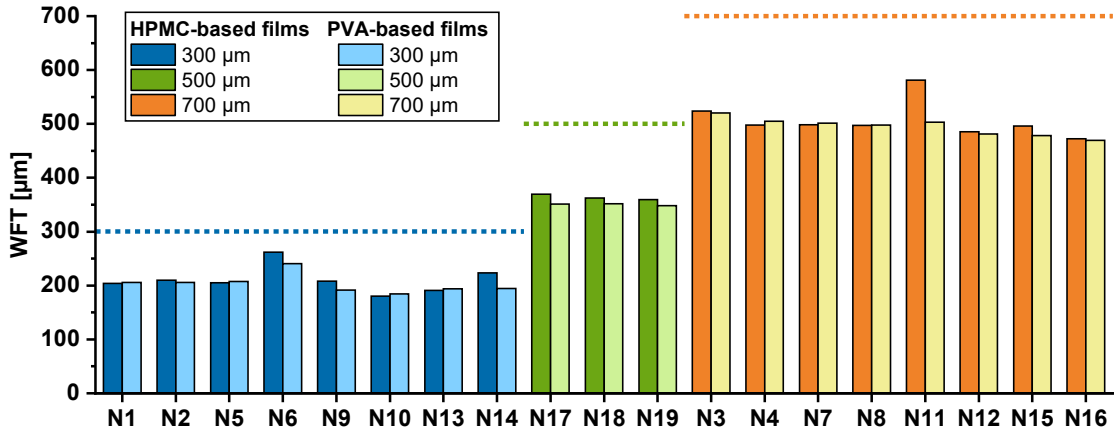

Figure 70: Measured WFT of HPMC- and PVA-based films (n = 1), experimental runs (section 6) ordered by used gap width of coating knife (dashed lines)

Dry Film Thickness and Grammage

Plotting the DFT against the WFT, the relationship could be described by a linear regression with R^2 of 0.900 (Figure 71a). Relating the WFT to the grammage defined as ratio of sample weight and area (section 5.5.11.1), a higher goodness of data prediction was given with R^2 of 0.993 (Figure 71b). This could be due to the fact that during the optical measurement only one spot with a diameter of 12 µm was examined in a single measurement. In contrast, a six-fold determination of the grammage was carried out by weighing samples with a size of 4 cm^2. The occurring scattering showed that there were variations within the film sheets produced at different settings. These can be better captured with more area-wide measurement. There are optical line- or area-scan sensors [237, 238] which would be even more meaningful for in-line thickness monitoring of film substrates.

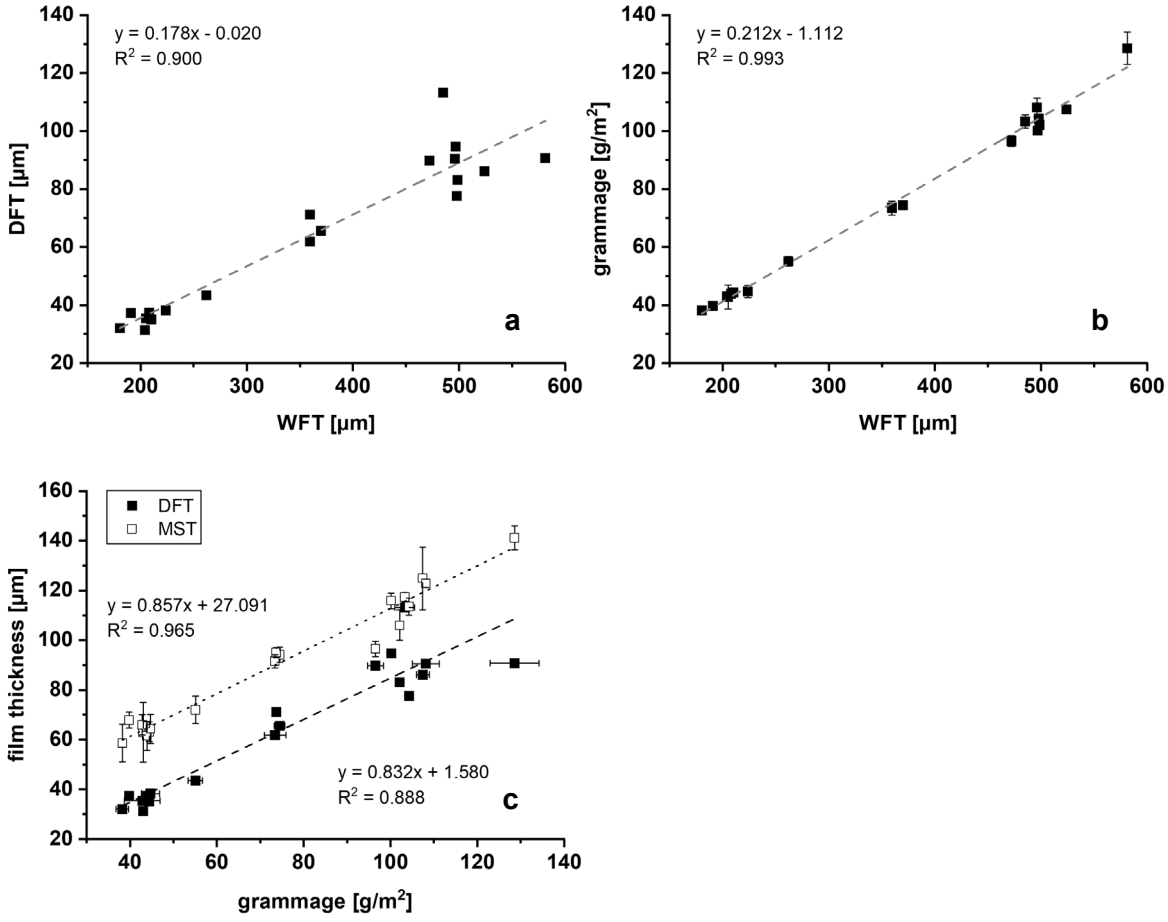

Figure 71: DFT plotted against WFT (n = 1) (a), grammage (mean ± SD, n = 6) plotted against WFT (n = 1) (b), DFT (n = 1) and MST (mean ± SD, n = 6) plotted against grammage (mean ± SD, n = 6) (c), representative data of HPMC-based films

Besides the grammage, the thickness of dry films is an in-process control parameter usually measured at-line mechanically, the results of the optical sensor and the mechanical

measurement by a modified micrometre screw were compared. It was expected that with higher film thickness the grammage will increase. Both DFT and micrometre screw thickness (MST) plotted against the grammage showed a linear relationship (Figure 71c). It was noticeable that the resulting balance lines did not overlap, but were shifted in parallel by about 25 µm. MST consistently had higher values than DFT. Only in the range around 100 g/m² did the values of DFT and MST scatter greatly and overlapped partly. A growing trend of scattering with increasing grammage [214], however, could not be detected. Since the micrometre screw with flat jaws always measured the thickest part of the film piece, it overestimated the average thickness of the piece. Whereas, the optical sensor randomly measures only one spot out of the material. Consequently, the coefficient of determination is poorer for DFT with $R^2 = 0.888$ than for MST with $R^2 = 0.965$. As the overestimation of MST was relatively uniform, it may be assumed to be a systematic error due to a dead space of about 25 µm between the micrometre screw jaws in zero position.

Regarding the coefficient plot of WFT (Figure 72), the adjusted gap width had by far the greatest and most relevant effect. Nevertheless, there were further significant interactions between the polymer grade and gap width, casting speed and drying temperature that had an effect on the WFT. Their effect was comparatively low but influenced the difference between the target and real WFT.

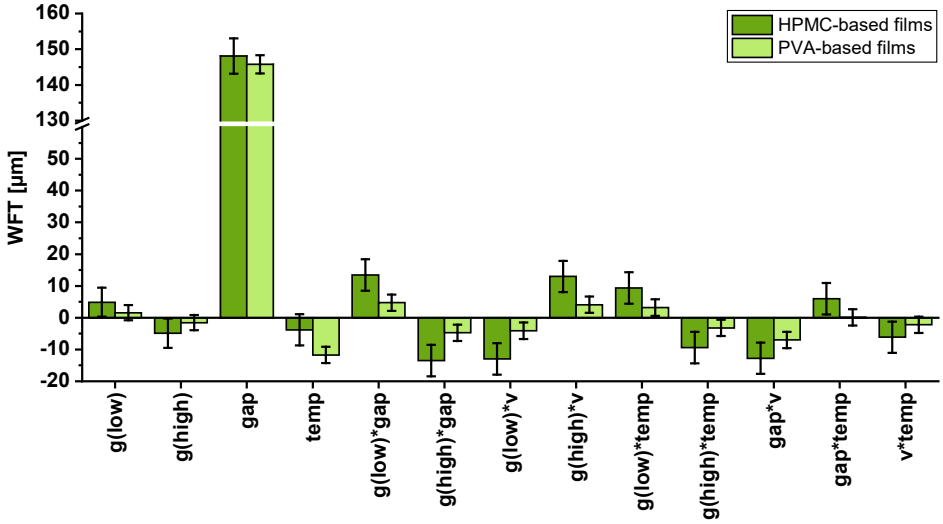

Figure 72: Coefficient plots of WFT, scaled and centred (± CI: 95%), illustrating results as soon as one of the polymer types showed a significant effect; g = polymer grade, gap = gap width, v = coating speed, temp = drying temperature

Comparing the low and high grade of the respective polymer, it became obvious that they behaved contrary to each other. High grades led to smaller and low grades to higher WFT in

case of the interaction with the gap width and temperature. Decreasing gap width means higher applied pressure on the sample. Increasing temperature, on the other hand, led to faster evaporation of water and thus increased stiffness of the polymer chains. As a consequence, the already existing stiffness effect caused by longer polymer chains of the high polymer grades was enhanced.

Using higher casting speed and high polymer grade at the same time resulted in higher WFT. These effects were always lower when analysing PVA-based solutions. The different viscoelastic properties were assumed to be the reason. Higher casting speed also means higher applied shear stress to the sample. The theoretical calculated shear rates varied from 8.6 s^{-1} (700 µm, 6 mm/s) to 60.0 s^{-1} (300 µm, 18 mm/s). Therefore, a special attention was paid to the rheological properties of the polymer solutions.

Rheologic Investigations

Dynamic viscosity profiles at changing shear rates and oscillation experiments at different temperatures were conducted. Considering the dynamic viscosity of HPMC and PVA, it was found that HPMC showed a pseudo-plastic and PVA a Newtonian-like flow behaviour at shear rates of 0.1 to 100 s^{-1}. Increase of the dynamic viscosity at higher temperatures is unusual. At 40 °C, the samples seemed to dry at the edges of the cone geometry of the rotary viscosimeter and this may have led to measurements errors when a dried-on part became detached. This is illustrated for the example of PVA 18-88 in Figure 73. The measurements at 50 °C were not feasible at all because the equilibrium could not be reached thus the measurement time has been constantly extended.

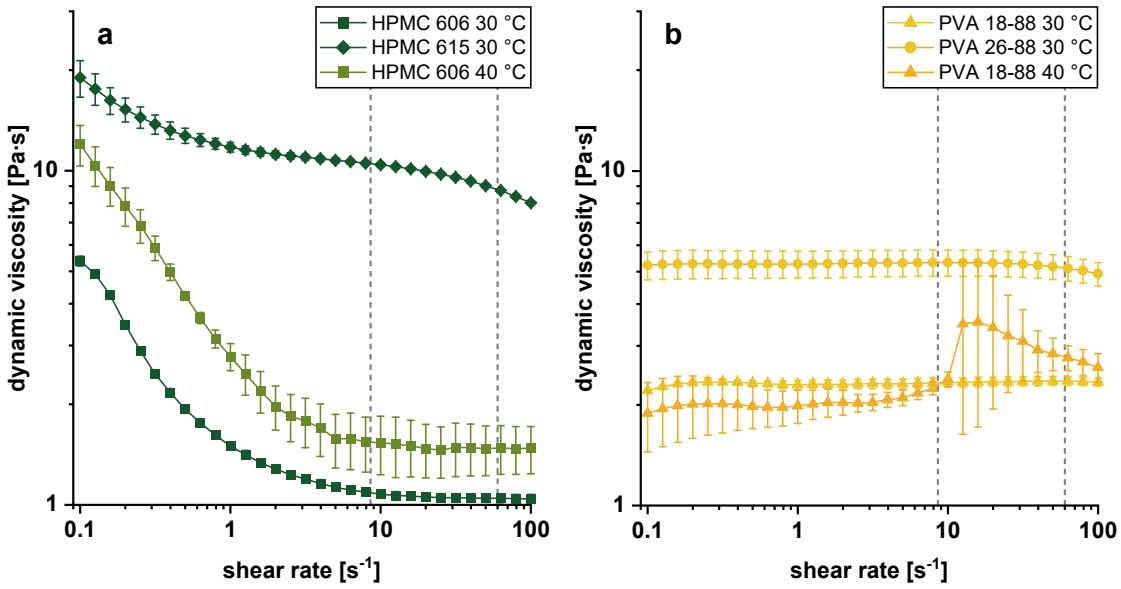

Figure 73: Flow curves of HPMC-based (a) and PVA-based solutions (b) over a logarithmic range of shear rates at 30 °C and 40 °C (mean ± SD, n = 3)

The oscillation measurements, on the other hand, could be carried out without any problems. In order to find out the relation between elastic and viscous part of the polymer solutions, the loss factor (tanδ = G''/G') was plotted against decreasing oscillation frequency (Figure 74). The determination was performed using constant strain of $\gamma = 1\%$ which is in the linear viscoelastic range (LVER) of all samples. For ideal elastic behaviour the value of tanδ is zero, storage modulus G' dominates completely over loss modulus G''. For ideally viscous behaviour the value for tanδ approaches infinity since it has to be divided by zero, G'' dominates over G'. If G' and G'' are in equilibrium, then tanδ is 1.

For both polymers, tanδ decreased towards zero with rising temperature due to increasing elastic part. The polymer chains were more rigid and can therefore follow the motion less. The HPMC-based solutions remained in the elastic region with tanδ of 0.2 to 5.7 over the whole frequency range. PVA-based solutions, on the contrary, showed a clear maximum in low frequency range < 1 Hz. With decreasing oscillation frequency, the entangled polymer network gained more flexibility and mobility. The polymer chains moved relatively to each other and the deformation energy is lost by frictional heating effects so that the viscous part becomes predominant [239]. Thus, the formation of a smaller lamella than HPMC-based solutions during film casting could be explained as previously assumed.

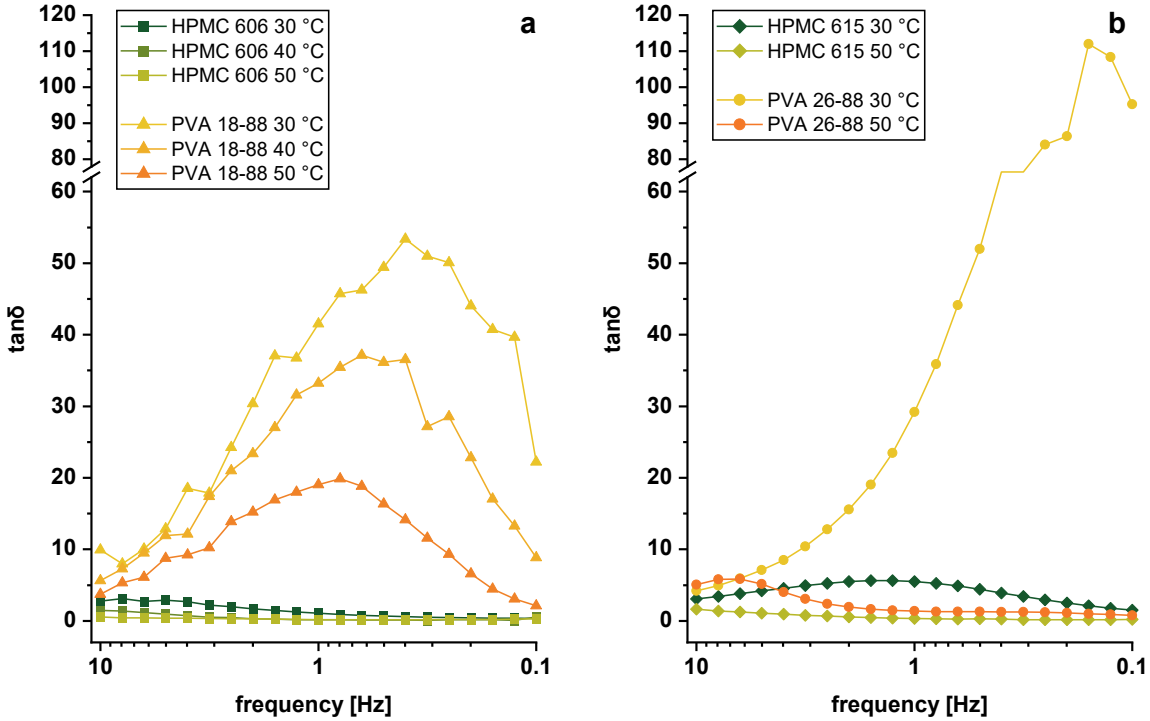

Figure 74: Loss factor tanδ (dimensionless) against decreasing oscillation frequency 10–0.1 Hz at different temperatures (n = 1), low polymer grades (a) and high polymer grades (b)

Drying Time and Shrinking Rate

The drying time was significantly affected by the adjusted gap width and set heating plate temperature (Figure 75). The higher the temperature was, the faster the polymer solution reached the plateau and with that the final DFT. Both factors could not be considered separately because there was a significant interaction. There were no differences between the two polymer types.

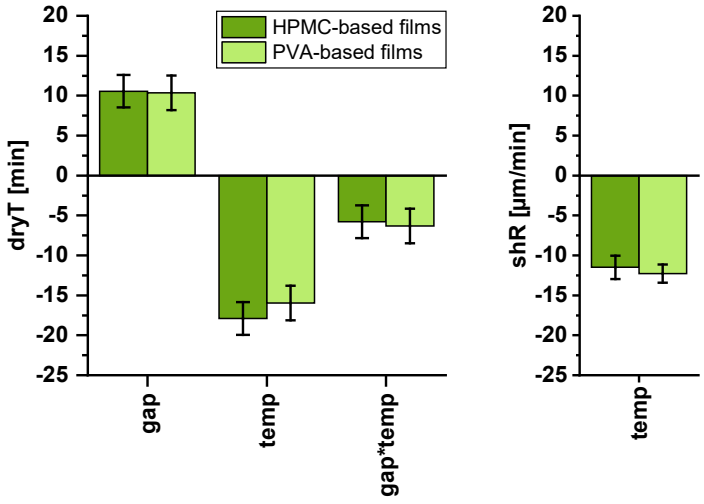

Figure 75: Coefficient plots for significant effects on drying time (dryT) and shrinking rate (shR), scaled and centred (± CI: 95%)

If the WFT is known, it is possible to predict how long the drying process of the observed system will take using the determined shrinking rates. Recent publications demonstrated that a prediction of final dry film thickness is possible by modelling a two-component system consisting of polymer and water [230, 240, 241]. However, the experimental approach using the optical sensor has the advantage that real data of a multi-component system is captured.

Only the drying temperature was significantly influencing the shrinking rate (Figure 75). With higher temperature of the heating plate shR increased. Due to the falling slope, the shR appears to be in the negative range. The film thickness decreased linearly with respective rates depicted in Table 15 whereby the values of HPMC and PVA were almost equal. Since the WFT of both polymers was almost equal (Figure 70) at respective settings, the diffusion distance for the water molecules was the same.

Table 15: Shrinking rates (shRs) of the polymer solutions at different temperatures (mean ± SD, n = 8, *n = 3)

Polymer	shR [µm/min]		
	30 °C	40 °C	50 °C
HPMC	-6.5 ± 0.4	-13.4 ± 0.4*	-29.5 ± 2.0
PVA	-7.2 ± 0.3	-16.5 ± 0.5*	-31.8 ± 1.8

3.3.4 Summary and Conclusion

In the present study, a screening of absorbing additives for the incorporation into film substrates for inkjet printing was performed. The results indicated that the selected additives are most effective in water-based ink absorption and internalisation when they are not surrounded by the polymer. A dense particulate surface such as in tablets or powder-coated films was beneficial in comparison to common ODFs. Furthermore, it was shown that not every polymer-solid particle combination is processable. HPMC and silica particles were not compatible so that PVA had to be used alternatively. The latter combination showed, however, the most promising absorption behaviour due to existing particle-rich film side. Since it was still challenging to quantitatively measure the absorption capacity, the used methods have to be developed further.

The drying profiles of film substrates based only on HPMC and PVA were successfully monitored by an optical sensor and evaluated in small-scale. The XYZ-frame built for this purpose has fulfilled its function well. Process-relevant effects and interactions could be

determined. The cast polymer solution reached the set temperature of the heating plate within 10 s. The adjusted gap width of the coating knife had the greatest effect on the WFT and with that on the DFT and grammage. However, it was made apparent that the use of the gap width of coating knife as setting tool for the real WFT is not sufficient because the gap width and real WFT deviated from each other. The difference was between 12.7% and 38.5% for both polymer types. With that it could be shown that the recommended generalised excess of 30% would not be precise enough especially in case of drug-containing film substrates. An implemented in-line measuring system provides a helpful feedback control and should be used in the future during film production.

3.4 Generalised Concept for Pharmaceutical Inkjet Printing onto Film Substrates

3.4.1 Introduction and Objectives

The objective of this chapter is to summarise all the findings obtained in the previous studies and to elaborate a flow chart for optimising drug printing via inkjet technology onto film preparations. Thereby, the focus was on appropriate individualised drug therapy. Overviews describing a pre-formulation approach, possible technical issues or important process steps have already been attempted in literature [156, 242, 243]. However, a generalised concept that includes the main factors and rational interconnections has yet to be developed. This would facilitate the formulation and process development in this still young field and could be expanded in the future to include further insights.

For that purpose, critical process steps and controllable or monitorable parameters were identified and discussed against the background of the Quality by Design (QbD) concept according ICH guideline for Pharmaceutical Development Q8 (R2) [244]. This implies that the quality of pharmaceutical products has to be built into the product during the development process, as quality cannot be analysed into it subsequently. This primarily includes deep understanding of the functionality of product composition and the manufacturing process. Critical quality attributes (CQAs) of the product as well as critical process parameters (CPPs) must be identified and brought under control [244].

As pharmaceutical inkjet printing still is in its early stage, the QbD approach is applied here, even the individualised therapy defined here aimed at a small-scale application in hospitals or public pharmacies. The quality demand does not change with the batch size.

3.4.2 Workflow for Pharmaceutical Inkjet Printing

The elaborated workflow comprising the development of a film dosage form based on pharmaceutical inkjet printing is depicted as flow chart in Figure 76. The starting point is the case of a prescribed individualised drug therapy. At this early stage, it can be already assessed if inkjet printing is a suitable manufacturing process. The decision criterion is whether the API is indicated in a low-dose regimen or not. Depending on the solubility of the API, the base for

the ink formulation can be selected. The choice is between aqueous or organic solvents. If the solubility is poor, a nano-particulate ink suspension has to be developed. Especially with suspensions, care has to be taken to prevent nozzle clogging. It is recommended that the particle size shall be smaller than 1/10 or even 1/50 of the nozzle diameter of the target print head [245]. Besides, the particle size distribution as identified major CQA should be monitored as well as the suspension stability during the storage and processing time of the bulk ink. If required, addition of dispersing agent, increasing of ink viscosity or an adjustment of the particle size distribution have to be carried out [218]. In any case, an adjustment of the physicochemical properties surface tension, dynamic viscosity and density should be performed in accordance with the target printing equipment. For a water-based ink formulation, the microbial stability over shelf-life is crucial for the patient safety and may require the addition of a preservative system. Even though it is an oral dosage form, this could be critical for immunocompromised patients as well as newborns with an insufficiently developed immune system [246]. If the ink is to be distributed in bulk or is not completely utilised during production, adequate preservation has to be ensured. If this is not possible for rational reasons like contraindication, chemical or physical incompatibilities with the API or excipients, then the ink must be processed within 24 h (section 3.1.3.1). For an organic-solvent ink formulation, the quantity and toxicity of the residues in the final product are decisive. The ICH Q3C (R8) guideline, also replicated in Ph. Eur. 2.4.24 [247], distinguishes three classes [164]. Class 1 is not suitable as solvent component at all due to its pronounced health hazards. Class 2 and 3 are applicable but subject to defined limits. If the deposited solvent quantity exceeds the permitted daily or single dose when undried, the remaining residue must be monitored. If the drying conditions are insufficient, they have to be adjusted as CPPs so that the residual solvent content is below the acceptance limit, but the API and the substrate quality are not affected. Particularly in case of water-based inks, the residual water content should monitored, otherwise the film substrate can become too flexible and tacky [110, 115].

The drying or absorption and immobilisation of further liquid components contained in the ink by the substrate has to be ensured in such a way that no stability issues occur. If this is not the case, either the formulation of the ink or, if necessary, also of the substrate has to be adjusted. In section 3.1.3.3, it was shown which consequences a remaining liquid layer and with that dissolved API on the surface can have.

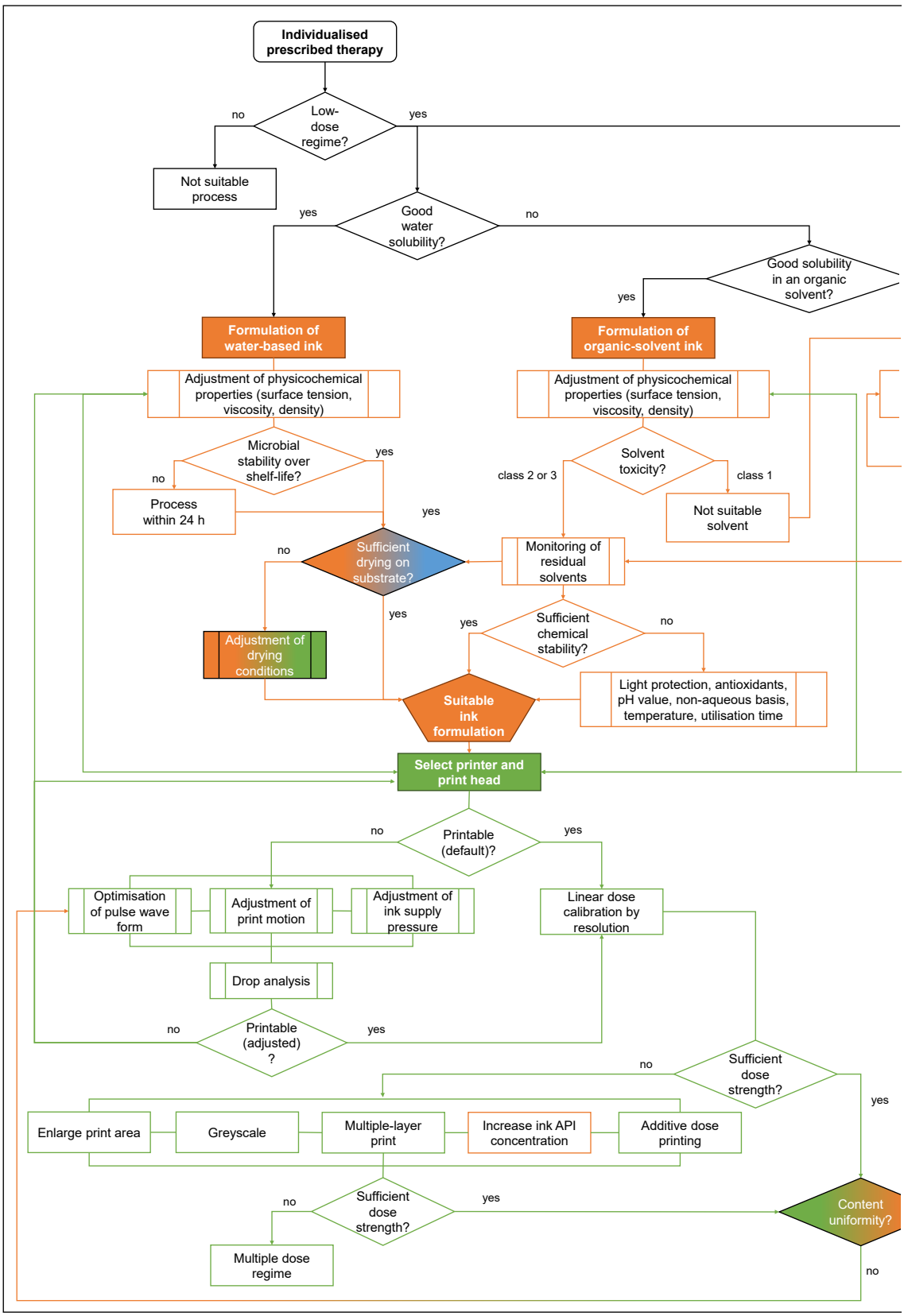

Figure 76: Flowchart of the generalised concept for pharmaceutical inkjet printing onto film substrates

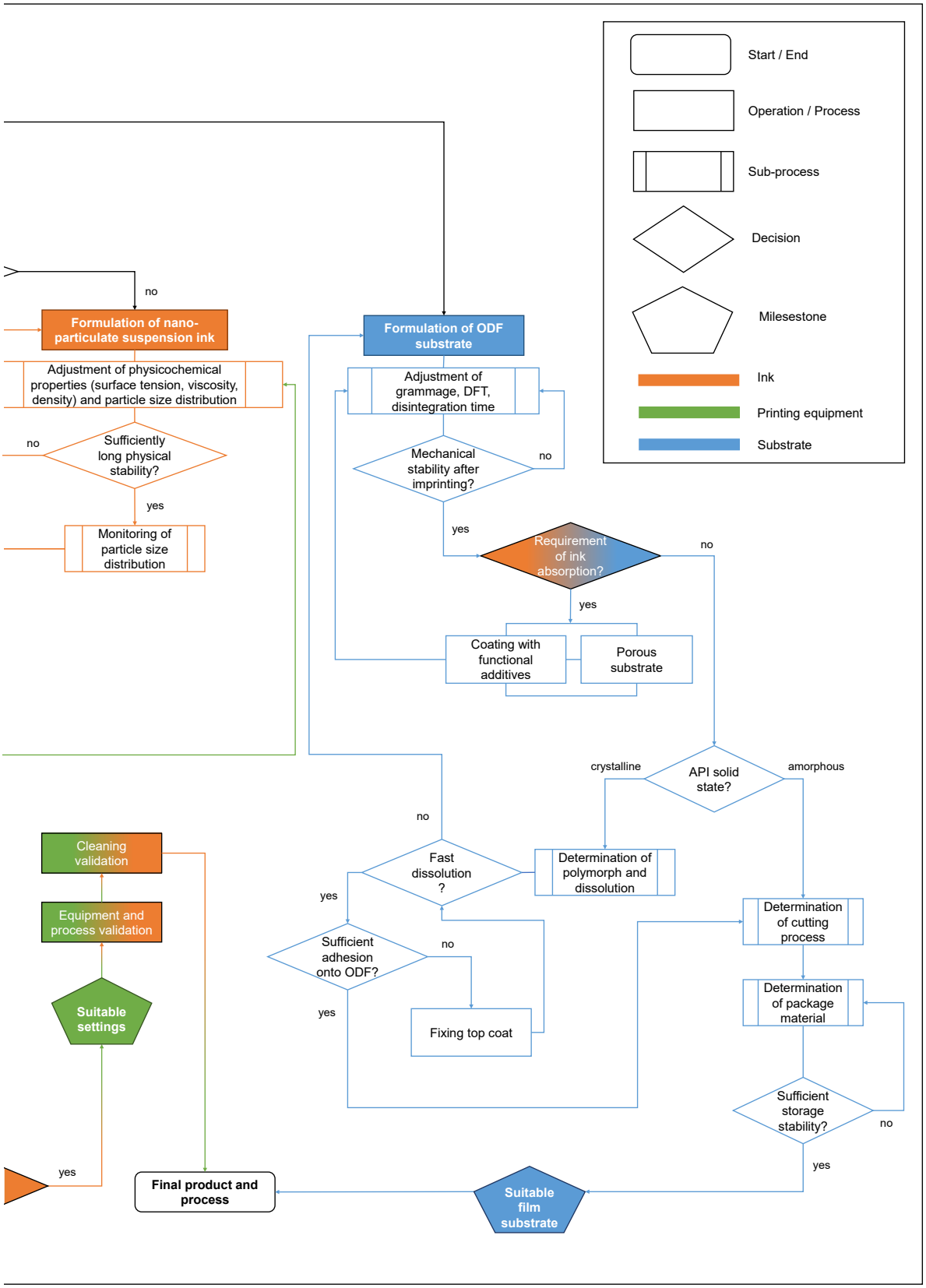
Start / End
Operation / Process
Sub-process
Decision
Milesestone
Ink
Printing equipment
Substrate
no
Formulation of nano-particulate suspension ink
Adjustment of physicochemical properties (surface tension, viscosity, density) and particle size distribution
no
Sufficiently long physical stability?
yes
Monitoring of particle size distribution
Formulation of ODF substrate
Adjustment of grammage, DFT, disintegration time
Mechanical stability after imprinting?
no
yes
Requirement of ink absorption?
no
yes
Coating with functional additives
Porous substrate
crystalline
API solid state?
amorphous
no
Fast dissolution ?
Determination of polymorph and dissolution
yes
Sufficient adhesion onto ODF?
no
yes
Fixing top coat
Determination of cutting process
Determination of package material
Sufficient storage stability?
no
yes
Cleaning validation
Equipment and process validation
Suitable settings
yes
Final product and process
Suitable film substrate

Furthermore, the chemical stability of the API and excipients as identified CQA has to be assured. To achieve a sufficient ink shelf-life, sensitive APIs may require light protection of the ink supply and area of printing, humidity control, decrease in print head and substrate table temperature or the limitation of utilisation time. The ink formulation can also be adapted by adding suitable antioxidants, changing from aqueous to organic base or adjustment of the pH.

These cycles of adaptation have to be followed until a suitable formulation is developed. As already mentioned, this cannot be done separately from the printing equipment. Therefore, the pharmaceutical ink development is always in interaction with the selected equipment and its settings. Before blindly adjusting the print settings, the printability of the ink candidate, a further CQA, should be tested using the default settings. If these are not working for the developed ink, the CPPs negative pressure of the ink supply, the piezoelectric pulse waveform and printing movement should be systematically optimised (section 3.2.2). The printability has to be monitored by drop analysis using an appropriate drop viewing system. Depending on its technical features, the drop image and calculation of drop properties are closer or further from reality. Should the printability still not be given and when all possibilities for formulation development have been exhausted, the exchange of the target equipment must be considered.

If ink printability is given, linear resolution ranges have to be identified with which the individual dose strengths can be achieved independent from the dose regime (section 3.2.4.1 and 3.2.4.2). When printing with all nozzles of a print head, the free selection of the print resolution is limited by their spacing and thus the native print head resolution. Using only one nozzle, however, the printing time increases with decreasing number of activated nozzles. For a specified concertation of the API in the ink, a linear equation can be established to calculate the resolution to be set. However, it could be shown that the robustness of the linear dose calibration over print head life time has to be analysed to verify the reliability on the linear equation (section 3.2.5).

If the increase in print resolution in the linear range is not sufficient, there are further options to achieve the target dose. Selected options were tested in the present work, so the additional ones are only discussed theoretically for completeness. As far as the solubility of the API allows, the concentration in the ink can be increased. However, recrystallisation of the API at the nozzle plate or blockage of the nozzles due to large number of nano-particles can disrupt the printing process. Another possibility is to print multiple layers or use the greyscale mode

of the print head. The greyscale mode allows to print successively several drops from one nozzle so that the single drops form one large drop [245]. Additionally, the print area could be enlarged to deposit a higher dose on the substrate. This is limited by the oral cavity dimensions of the target patient. Furthermore, the additive dose printing could be used (section 3.2.4.4). An individual dose can be added to a fixed API dose already incorporated in a cast film using inkjet printing. If all these options do not result in the desired dose, several pieces must be administered. Finally, it has to be ensured that each dose contains an equivalent quantity of API investigating the content uniformity according Ph. Eur. 2.9.40 [198]. Once the appropriate print settings are found with which uniform dose units can be produced, a validation of the equipment and process as well as a cleaning validation of the parts in contact with the product (section 3.2.6) must be carried out.

Parallel to the ink, the suitable formulation of the film substrate, in the case of the present work ODF, must be developed. These should have sufficient mechanical stability after imprinting without losing its target dosage form characteristics. If the films are mechanically sensitive to force, the grammage and final film thickness measured as DFT or MST (section 3.3.3.3) can be adjusted. If this is not sufficient enough, the ODF has to be re-formulated by changing the polymer and/or plasticiser. If the films are only deformed by the deposited ink, the absorption of the ink at the film surface should be ensured. This can be done by coating the film substrate with absorbing particles (section 3.3.2) or if insufficient, create a porous structure by foaming and/or freeze drying [126].

The solid state of the printed API on the substrate must be investigated. If it is crystalline, the polymorphs should be determined and the dissolution tested. If the dissolution is fast, it should be tested if the API crystals have a sufficient adhesion on the ODF substrate. As already showed by Genina et al., insufficient adhesion can lead to remaining API on the packaging [98]. To avoid this, a fixing top coat can be applied similar to varnishes used in the print media. If the API release is not sufficient, the solid state of the API and the disintegration time of the ODF have to be adapted. The latter can be achieved by reducing the grammage and the film thickness and by optimisation of the film formulation. The control of the solid state is more challenging. Both inkjet printing and drying process as well as the type of substrate have an effect on this [157, 248].

In the next step, the precise cutting process of the printed areas has to be determined. Especially if the pharmaceutical ink is transparent, the visual secondary control or colorimetric measurements [97] is not applicable. Exact coordinate correspondence of the printed areas and the cut-out ODF pieces must be given. Otherwise, the target dosage will not be met and/or an inappropriate content uniformity will result. An integrated PAT instrument that can locate and quantify the printed dose using infrared spectroscopy and/or Raman chemical imaging could be considered [91, 94, 105, 249, 250].

Finally, the stability of the imprinted ODF should be ensured by determination of a suitable packaging material and design. Since ODFs are sensitive to humidity [234, 235] and the API could have further stability issues, the package and storage conditions must offer sufficient protection to achieve an appropriate shelf-life for by the patient. When this has been verified and confirmed, the final developed product and production process has been achieved.

3.4.3 Summary and Conclusion

With the help of the performed experiments and literature research, it was feasible to develop a generalised concept for pharmaceutical inkjet printing. The CQAs and CPPs were elaborated and integrated in the developed workflow. This may help guide future formulation developers, providing a decision support and contributing to the further understanding of the process.

4 Summary and Outlook

The aim of the present work was to use inkjet printing as liquid dosing technique to prepare customised orodispersible films on demand. By combining this innovative dosage form with the new flexible API loading technology, a prospective solution has been established that enables an individualised drug therapy. With the utilisation of metoprolol tartrate and L-thyroxine as APIs, a broad patient group range was intended to be addressed.

First, different pharmaceutical ink formulations were developed. It turned out that the choice of suitable excipients is limited. Drug-free inks were used to gain prior knowledge of printing behaviour and were used for comparison purposes. Mixtures of the organic solvent ethanol and polyethylene glycol 400 as viscosity enhancer and humectant initially proved promising. After printing onto hypromellose-based films, however, it was found that quantities of polyethylene glycol 400 of 50% (w/w) and higher lead to insufficient evaporation and absorption of the ink solutions. Furthermore, glycerol, like polyethylene glycol 400, has been shown to be unsuitable as excipient in quantities of 10% (w/w) and even to accumulates the soluble metoprolol tartrate on the substrate surface within liquid drops. This was a serious impairment of the pharmaceutical product quality and has to be avoided. Dimethyl sulfoxide, used as solvent in L-thyroxine containing ink, in contrast, showed no residual liquid film on the substrate despite poor evaporation. These finding have not been mentioned in the literature until now, although polyethylene glycol 400 and glycerol has been used as excipients in pharmaceutical inks. Finally, for acceptable ink formulations, it was sufficient to use water with surfactants or organic solvents to achieve a uniform dosage. Polyethylene glycol or glycerol were not required even though the recommended range of dimensionless Ohnesorge number was not reached.

Inks containing metoprolol tartrate and L-thyroxine were used to test different drug dosing strategies. It was found that an effective increase in dose of the final product by means of increased ink concentration is limited due to resulting significant change in physicochemical properties. Moreover, recrystallisation of the API on the substrate surface may occur. More studies on the solid state characteristics and drying process of printed units should be performed in the future. Print resolution proves to be a useful parameter for dose control. Nozzle aging necessitates a calibration step prior to each batch manufacturing to ensure

accurate dosing. The print head's number of nozzles and their arrangement can limit the print resolution range and thus the possible dosages at a given ink concentration. Since in the present work mostly conceptually one nozzle was used, the exact impact has to be investigated in further studies.

Confocal Raman microscopy, optical high-shear viscosimetry based on microfluidic chip-system and stroboscopic drop view were implemented as analytic methods for ink characterisation. Together with the quantification of the API content by HPLC, these provide a more tangible overview for pharmaceutical purposes than the dimensionless numbers commonly used to merely predict the printability of inks.

Two different industrial print heads, KM512SHX and Spectra SE-128 AA, were compared with regard to their suitability for pharmaceutical applications. A design of experiments was conducted to identify the key factors on resulted quantities and to evaluate the performance of the print heads. Print heads with lower native resolution but larger nozzle diameter, such as Spectra SE-128 AA, are not disadvantageous per se, although it has been found that lower negative pressure is required to hold the ink meniscus. Contrary to the assumption that print heads with smaller nozzles like KM512SHX lead to more precise dosing, it has been shown that smaller nozzles are more susceptible to clogging. In addition, it may be challenging and time-consuming to achieve target dosage strength with such small drop volumes. Therefore, the latter was excluded for further investigations. Cleaning investigations showed, however, that the print head together with the ink supply are the most critical parts. To decrease the cross-contamination risk, the use of dedicated print head units is advised. In the second step, special designed pharmaceutical equipment adapted to GMP requirements should be developed.

Fundamental studies on the solvent-casting process of orodispersible films were conducted generating new mechanistic insights. The chromatic confocal optical sensor proved to be a useful tool for monitoring film thickness not only during coating, as shown previously, but also during the drying process. In order to optimise orodispersible film formulations for inkjet applications in terms of absorption capacity, various additives and incorporation techniques were investigated. It was found that a particle-enriched surface independent from the additive type is advantageous. After contact with the ink drop, the polymer-coated areas slowly began to swell, forming a diffusion barrier for the residual drop remaining on the surface, rather than

rapidly absorbing the ink. However, the mouthfeel of functional orodispersible films with preferable particulate surface should be tested to ensure the patients′ adherence.

The acquired knowledge could be used to conceptualise a general workflow for the development of ink formulations and film substrates as well as pharmaceutical inkjet printing process.

In conclusion, inkjet printing for API deposition on orodispersible films was successfully examined in the present thesis. Deepening process understanding in the pharmaceutical field contributes to the advances in individualised medicines. Nevertheless, multi-disciplinary collaborations between pharmacists, pharmaceutical technologists, engineers and inkjet printing experts are crucial for the further progress and success of this innovative approach.

5 Experimental Part

Parts of this section have already been published at conferences and in peer-reviewed journals. The content was adopted unchanged or linguistically modified and partly extended.

5.1 Materials

Table 16: Model drug substances

Substance	Batch No.	Manufacturer / Distributer
metoprolol tartrate (MPT)	MTP02409	Microsin, Romania
metoprolol tartrate, secondary standard	LRAC1767	Sigma Aldrich, Germany
L-thyroxine (LT)	LOD226	United States Pharmacopeia (USP), USA

Table 17: Substances used for ink preparation

Substance	Grade	Manufacturer / Distributer
dimethyl sulfoxide (DMSO)	p.a.	Sigma Aldrich, Germany
ethanol (EtOH), absolute	Ph. Eur.	Merck, Germany
glycerol 85%	Ph. Eur.	Caesar & Loretz, Germany
hydroxypropyl cellulose (HPC)	HPC-L	Nisso, Japan
hydroxypropyl methylcellulose (HPMC), hypromellose	Pharmacoat® 615	Shin-Etsu Chemical, Japan
Millijet® blue 28 (MB28)	SG30May2017	Milliken Chemical, USA
poloxamer 407 (P407)	Lutrol® F 127	BASF, Germany
polyethylene glycol (PEG), macrogol	Polyglycol 400	Clariant, Germany
polysorbate (PS20)	Tween® 20	Caesar & Loretz, Germany
polyvinylpyrrolidone (PVP), povidone	Kollidon® 30	BASF, Germany
propylene glycol (PG)	Ph. Eur.	Caesar & Loretz, Germany
triethylene glycol monoethyl ether (TGME)	technical	Sigma Aldrich, Germany
water, deionised (H_2O)	-	freshly tapped

Table 18: Substances used for polymer film preparation

Substance	Grade	Manufacturer / Distributer
glycerol 85%	Ph. Eur.	Caesar & Loretz, Germany
hydroxypropyl methylcellulose (HPMC), hypromellose	Pharmacoat® 606 Pharmacoat® 615	Shin-Etsu Chemical, Japan
polyvinyl alcohol (PVA)	PVA 4-88 PVA 18-88 PVA 26-88	Merck, Germany
water, deionised (H_2O)	-	freshly tapped
ethanol (EtOH), absolute	technical	in-house

Table 19: Substances used as fillers for functional films

Substance	Grade	Manufacturer / Distributer
dicalcium phosphate anhydrous (DCPA)	Fujicalin®	Fuji Chemical Industry, Japan
α-lactose monohydrate (fLAC)	FlowLac® 100	Meggle Pharma, Germany
microcrystalline cellulose (MCC105)	Vivapur® 105	JRS Pharma, Germany
microcrystalline cellulose, silicified (sMCC)	Prosolv® SMCC 50	JRS Pharma, Germany
powdered cellulose (PC)	Arbocel® P290	JRS Pharma, Germany
silica gel (SG60)	Silica gel 60	Merck, Germany
silica gel (pSLC)	Parteck® SLC	Merck, Germany

Table 20: Substances used as excipients for tablet manufacturing

Substance	Grade	Manufacturer / Distributer
crospovidone (xPVP)	Kollidon® CL	BASF, Germany
α-lactose monohydrate (tLAC)	Tabletose® 80	Meggle Pharma, Germany
microcrystalline cellulose (MCC102)	Vivapur® 102	JRS Pharma, Germany
mannitol + sodium croscarmellose (MxCMC)	Parteck® ODT	Merck, Germany
fumed silica (SiO_2)	Aerosil® 200	Evonik, Germany

Table 21: Substances used for the analytics

Substance	Grade	Manufacturer / Distributer
acetonitrile	p.a.	VWR, France
orthophosphoric acid	p.a.	Fisher Scientific, UK
sodium dihydrogen phosphate monohydrate	Ph. Eur.	AppliChem, Germany
L(+)-tartaric acid	Ph. Eur.	AppliChem, Germany
thiourea	p.a.	Acros Organics, UK
water, purified	p.a.	freshly prepared by Barnstead™ NanoPure™, Thermo Scientific, USA

5.2 Manufacturing Methods

5.2.1 Film Preparations

5.2.1.1 Polymer Solutions

For the preparation of polymer solutions, the components were weighed individually. In case of drug-free films, water and glycerol 85% were premixed and heated to 80 °C for HPMC-based films and to 90 °C for PVA-based films on a magnetic stirrer (MR Hei-Standard, Heidolph Instruments, Schwabach, Germany). Subsequently, the polymer was dispersed while stirring at high rotation speed. The resulting solution was let cool down to ambient temperature and reweighed. Evaporated water was added and the solution was gently stirred until no more air bubbles were present. In case of API containing films, no heat was used. The API was dissolved in the water-glycerol blend and the polymer was dissolved at ambient temperature under stirring. Batches of 100–600 g were produced.

5.2.1.2 Suspensions

Batches of 100 g were produced, with 5 g of the appropriate filler dispersed in 95 g of a pre-fabricated drug-free polymer solution. The suspension was stirred on a magnetic stirrer IKA COMBIMAG RCO (IKA, Staufen, Germany) at ambient temperature until the powder was wetted, homogeneously distributed and no more air bubbles were present. It was always stirred until just before casting so that the particles had little time to sediment.

5.2.1.3 Casting of Film Preparations

The films were produced on lab-scale equipment using the solvent-casting method. The automated film applicator Coatmaster 510 (Erichsen, Hemer, Germany) equipped with an electrically heated vacuum suction plate was used to cast the polymer solutions or suspensions on the siliconized process liner consisting of a polyamide/polyester mixture (Mediflex® XM AMWL 45/105, Amcor Flexibles, Gent, Belgium). The adjustable coating knife (Figure 77, Multicator 411/220 mm, Erichsen, Hemer, Germany) was set to a gap width of 500 µm at a casting speed of 6 mm/s. Subsequently, the drug-free solution films were dried at 50 °C due to time reasons and the suspension films as well as films containing API at 25 °C. One exception was the experiment described in section 3.3.3.2 where deviating settings were used. The total size of the final film sheet was 880 cm² (22 × 40 cm).

Figure 77: Coating knife (Erichsen) (a) and detailed side view of the wedge-shaped blade geometry (b)

5.2.1.4 Cutting

Printed film sheets were left on the process liner and cut manually with a scalpel (Aesculap®, Braun, Tuttlingen, Germany), leaving an edge of 0.5 cm around the printed areas. Unprinted film sheets were positioned on a self-adhesive mat and cut in pieces using a desktop cutting machine (Silhouette Cameo® 3, Silhouette America, USA). Rectangular cutting patterns of 1 cm² (section 3.2.4.4), 4 cm² (section 3.3.3) and 6 cm² (section 3.3.2.3) were designed using the Silhouette Studio® software (version 4.1.201ss, Silhouette America, USA). The AutoBlade of 1 mm was used for HPMC-based films and the deep-cut blade of 2 mm (both: Silhouette America, USA) for PVA-based films. The blade length was adjusted depending on the substrate thickness and stickiness.

5.2.2 Ink Solutions

For the preparation of the inks, the API or dye was weighed (Table 22) and dissolved in the appropriate volume of the solvent or solvent mixture while stirring at ambient temperature. A screw glass sealed by Parafilm® M (Bemis Company, Neenah, USA) was used for storage to avoid evaporation and the associated change in concentration.

Table 22: Overview of the used balance types

API	Balance	Manufacturer
metoprolol tartrate (MPT)	Practum 224S-1 CP224 S	Sartorius, Göttingen, Germany
Millijet® blue 28 (MB28)	Chyo MJ-3000	YMC, Kyoto, Japan
L-thyroxine (LT)	Excellence Plus XP56 MC1 RC 250 S	Mettler Toledo, Columbus, USA Sartorius, Göttingen, Germany

5.2.2.1 Drug-free Inks

For the initial ink formulation screening (section 3.1.2.2) different inks were prepared.

Table 23: Compositions (w/w %) for ink formulations screening

Ink	EtOH [%]	H_2O [%]	G85% [%]	PEG 400 [%]	PG [%]	HPC-L [%]	HPMC606 [%]	PVP-K30 [%]	PS20 [%]
T1	100.0	-	-	-	-	-	-	-	-
T2	-	100.0	-	-	-	-	-	-	-
T3	-	-	100.0	-	-	-	-	-	-
T4	-	-	-	100.0	-	-	-	-	-
T5	-	-	-	-	100.0	-	-	-	-
T6	33.33	33.33	33.33	-	-	-	-	-	-
T7	33.33	33.33	-	33.33	-	-	-	-	-
T8	33.33	33.33	-	-	33.33	-	-	-	-
T9	33.33	-	33.33	33.33	-	-	-	-	-
T10	33.33	-	-	33.33	33.33	-	-	-	-
T11	-	97.0	-	-	-	3.0	-	-	-
T12	-	97.0	-	-	-	-	3.0	-	-
T13	-	90.0	-	-	-	-	-	10.0	-
T14	-	50.0	-	50.0	-	-	-	-	-
T15	-	49.95	-	49.95	-	-	-	-	0.1
T16	60.0	-	-	40.0	-	-	-	-	-
T17	75.0	-	-	25.0	-	-	-	-	-

For the drug-free lead formulations of drug-free inks, the carrier fluids of specified EtOH-PEG 400 ratios were prepared (Table 27). 2% (w/v) MB28 was dissolved in 100.0 ml of each carrier fluid mixture (M1–M3). Since a follow-up DoE was planned in context of the comparison of print heads (section 5.4.1.1), F2 was produced three times (F2.1, F2.2, F2.3) as centre point.

Table 24: Lead formulations of drug-free model inks

Ink	Carrier fluid (ratio EtOH : PEG 400)	MB28 [w/v %]
F1	M1 (1:0)	2.0
F2 (F2.1, F2.2, F2.3)	M2 (1:1)	2.0
F3	M3 (2:3)	2.0

In the development of inks containing MPT (section 3.1.3), drug-free formulations were produced for comparison purposes (Table 25).

Table 25: Composition (w/w %) of investigated drug-free inks (I1–I4)

Ink	P407 [%]	G85% [%]	HPMC615 [%]	H_2O [%]	EtOH [%]
I1	0.1	-	-	99.9	-
I2	0.1	10.0	-	89.9	-
I3	0.1	-	1.0	98.9	-
I4	0.1	10.0	1.0	88.9	-

In the development of an ink containing LT (section 3.1.4), a drug free formulation was produced for comparison (Table 26).

Table 26: Composition (v/v %) of investigated drug-free ink L1

Ink	DMSO [%]	EtOH [%]	H_2O [%]
L1	30.0	30.0	40.0

5.2.2.2 Drug-containing Inks

To develop an MPT-containing ink (section 3.1.3), different compositions were manufactured (Table 27).

Table 27: Composition (w/w %) of investigated MPT-containing ink formulations (I5–I9, E)

Ink	P407 [%]	G85% [%]	HPMC615 [%]	MPT [%]	H_2O [%]	EtOH [%]
I5	0.1	-	-	10.0	89.9	-
I6	0.1	-	1.0	10.0	88.9	-
I7	0.1	10.0	1.0	10.0	78.9	-
I8	0.1	-	-	20.0	79.9	-
I9	0.1	-	-	41.0	58.9	-
E	-	-	-	10.6	49.9	39.5

For the LT-containing ink (section 3.1.4), LT was added to the mixture of DMSO, EtOH and H_2O in a concentration of 1 mg/ml (Table 28) under exclusion of light using ultrasonic bath to speed up the solution process.

Table 28: Composition of investigated LT-containing ink formulation L2

Ink	DMSO [v/v %]	EtOH [v/v %]	H_2O [v/v %]	LT [w/v %]
L2	30.0	30.0	40.0	1.0

5.2.3 Tableting

The direct compression of drug-free tablet substrates was conducted by the uniaxial tableting instrument Styl'One Evolution (Medelpharm, Beynost, France) with implemented flat-faced EU-B punches of 11.28 mm diameter (Ritter Pharma-Technik, Stapelfeld, Germany). The components of the different compositions (Table 29) were weighed and blended for 15 min by a Turbula® mixer (T2F, W.A. Bachofen, Basel, Switzerland). The die-filling with the powder blend was performed by the integrated gravity feed shoe. The tablets were manufactured at three different compression forces (4.5 kN, 8 kN and 15 kN) adjusting the die-filling height to 10 mm and varying the compression thickness. External lubrication by magnesium stearate was used. To calculate the corresponding compression pressure p, Equation 11 was used. Here F is the compression force and A is the area of the punch tip.

$$p\ [MPa] = \frac{F\ [N]}{A\ [mm^2]} \qquad \text{(Equation 11)}$$

Per formulation, 50 tablets were produced. The ambient conditions were kept constant at of 21 °C and 45% RH.

Table 29: Compositions (w/w %) of produced drug-free tablets

Formulation	tLAC 80 [%]	MCC 102 [%]	xPVP [%]	SiO_2 [%]	MxCMC [%]
C1	30.0	68.0	2.0	-	-
C2	-	97.0	3.0	-	-
C3	-	99.8	-	0.2	-
C4	-	-	-	-	100.0

5.3 Inkjet Printing

Inkjet printing was performed using the desktop inkjet system PixDro LP50 (Figure 78, Meyer Burger, Eindhoven, The Netherlands) controlled by the LP50 HMI software (version 4.4.5.0, Meyer Burger, Eindhoven, The Netherlands).

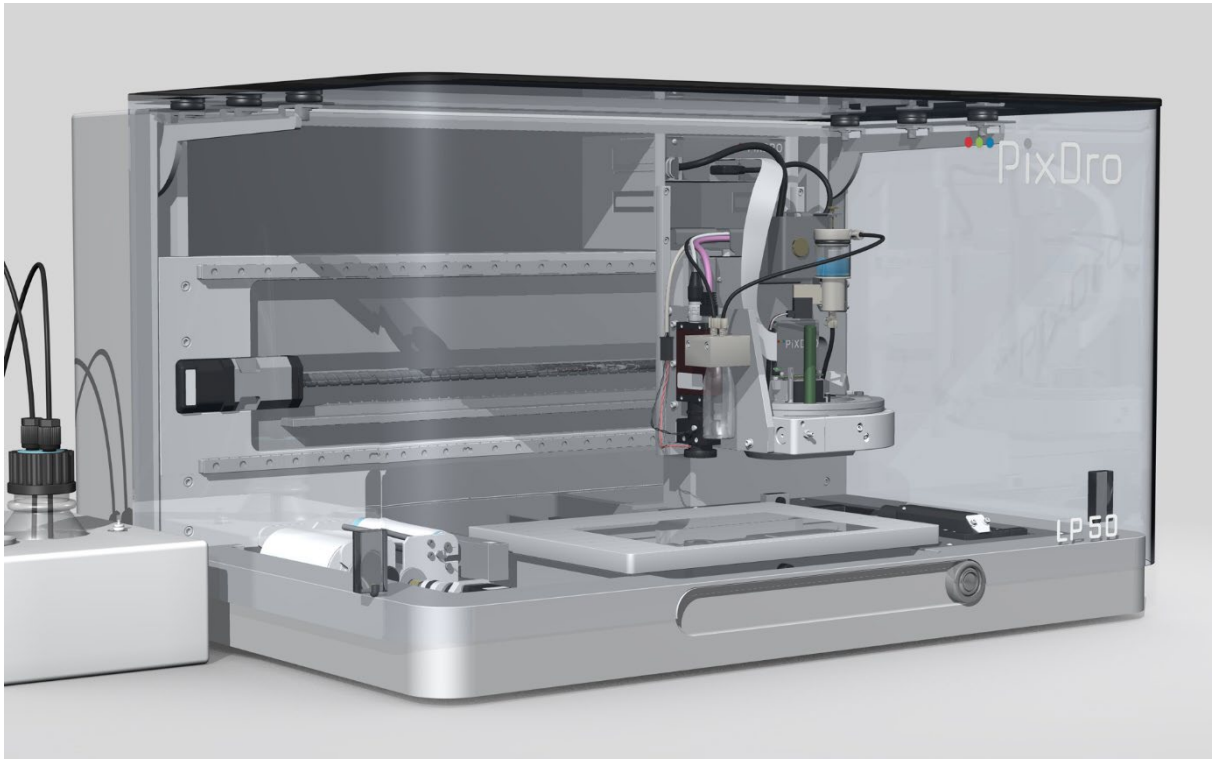

Figure 78: Overview 3D illustration of inkjet printer PixDro LP50 (Meyer Burger)

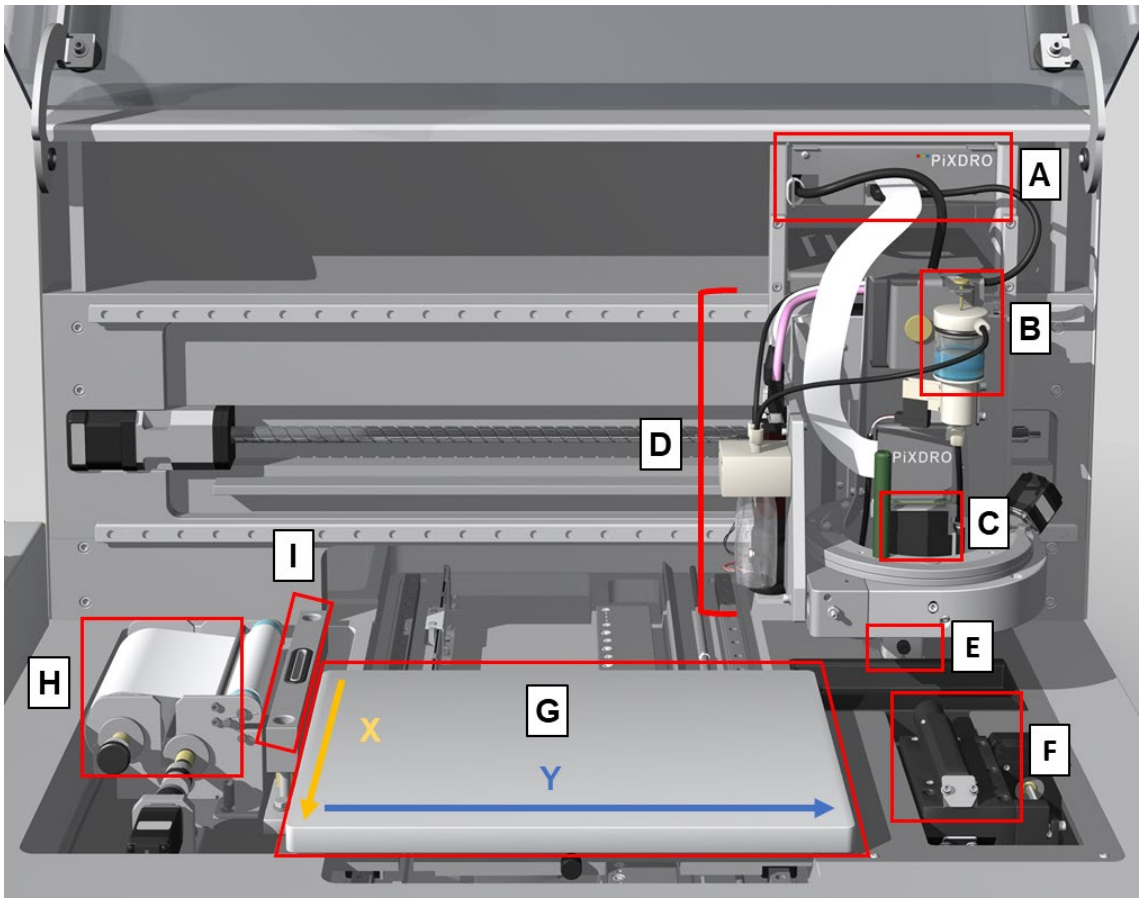

Figure 79: Detailed 3D insight into the inkjet printer with opened cover and exemplary mounted KM512SHX print head located in the service position. A: head personality boards (HPB), B: ink supply, C: print head, D: print head assemblies (PHA), E: stroboscopic LED, F: CCD camera, G: substrate table, H: wiping station, I: capping station

Piezo-driven drop-on-demand (DoD) print heads Spectra SE-128 AA (SP, Fujifilm Dimatix, Santa Clara, USA) and KM512SHX (KM, Konica Minolta, Tokyo, Japan) were used. The print heads (Figure 79, C) were mounted in exchangeable specific print head assemblies (PHA) to ensure the compatibility with the printer (Figure 79, D). The individual head personality boards (HPB) convert the generic information from the drive electronics into the specific signals that is required by the particular print head type (Figure 79, A).

Print templates with a pre-defined area were created by editing software Photoshop CS2 (Adobe, San José, USA) and uploaded into the HMI software. The temperature of the print heads was set to 30 °C to create conditions independent of the environment. The substrate table (Figure 79, G) had a temperature of 20–25 °C. Only one nozzle of different numbers was used for the printing process. An exception was the study in section 3.2.2.3 whereby also ten nozzles were used. The voltage and associated waveform as well as the negative pressure applied to the ink supply to hold the ink meniscus (Figure 79, B) were adjusted depending on the used ink formulations and print heads (section 5.3.1). The ink was filtered into the ink

supply through a membrane polypropylene filter with pores of 0.45 µm before each printing campaign. Cleaning of the print heads was conducted either by manually wiping with special lint-free cloths or, in case of serious blockage, by using the integrated capping station (Figure 79, I).

5.3.1 Selection of Waveform

5.3.1.1 Konica Minolta KM512SHX (KM)

Figure 80 displays the typical waveform of the KM print head and defines its single parts. Default time settings were used. The ON pulse width represents the time the pulse has high voltage (ON V) and was set to 6.0 µs. The OFF pulse width represents the time the pulse has low voltage (OFF V) and was set to 3.0 µs. In the present work, pulse voltage combinations (ON/OFF V) of 12/6 V, 16/8 V and 20/10 V were used to print MB28-containing inks (section 3.1.2 and 3.2.2), equally for both nozzle rows right (R) and left (L). For simplification, only the ON pulse voltage is mentioned. The delay between ON and OFF pulse was always set to 0 µs. The drop period describing the time of one-drop-cycle was 10.0 µs and the phase length defining the complete time of the complete three-drop-cycle was accordingly 30.0 µs.

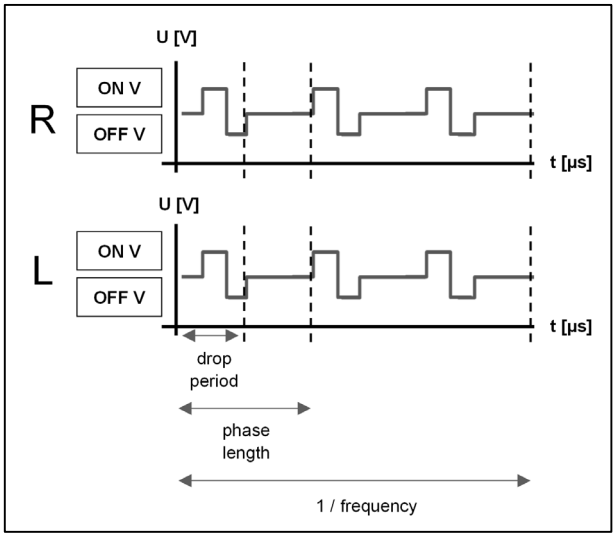

Figure 80: Schematic waveform of KM print head

5.3.1.2 Spectra SE-128 AA (SP)

Figure 81 displays the waveform of the SP print head, typically of a trapezium shape, and defines its single parts. The waveform was applied equally to both PZT slices A and B. In the present work, pulse voltages of 80–100 V were adjusted. The maximum amplitude voltage

(max) was set to 90% by default which means that the actual applied voltage was 72–90 V. This provides a buffer for a possible voltage overshoot to prevent damage to the print head by exceeding the maximum permissible voltage limit. The minimum amplitude voltage (min) was set to 0%. The rising and falling time of the voltage was set to 2.0 µs respectively, only the dwell time defining the voltage plateau was varied between 4.0 and 5.8 µs depending on the used ink.

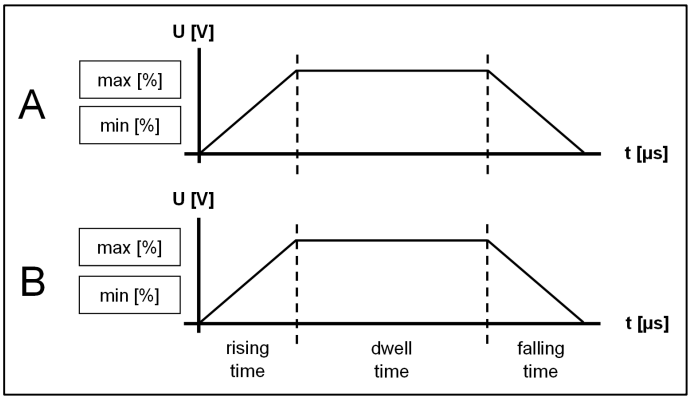

Figure 81: Schematic waveform of SP print head

5.3.2 Printing Movement

The print direction was bi-directional and the print angle Y-normal unless otherwise stated. After each swath the movement of the print head to the right (Y-direction) was one pixel. The speed of the substrate table in X-direction was predefined as 200 mm/s or adjusted to keep a certain jetting frequency.

To investigate the influence of printing settings on surface structure of ODFs (section 5.3.1), print speed as well as direction and angle were varied (Table 30). For that purpose, an area of 1 in^2 (= 2.54 × 2.54 cm) was printed, adjusting the print resolution to 500 dpi. These dimensions were selected to simplify the calculation of number of drops per area or line, as the resolution is measured in dots per inch (dpi).

In this context, print speed is defined as speed of the substrate table below the print head. Print angle describes according to Meyer Burger the coordinate direction of the print head movement. Finally, print direction determines the swaths printed by the print head (Figure 82).

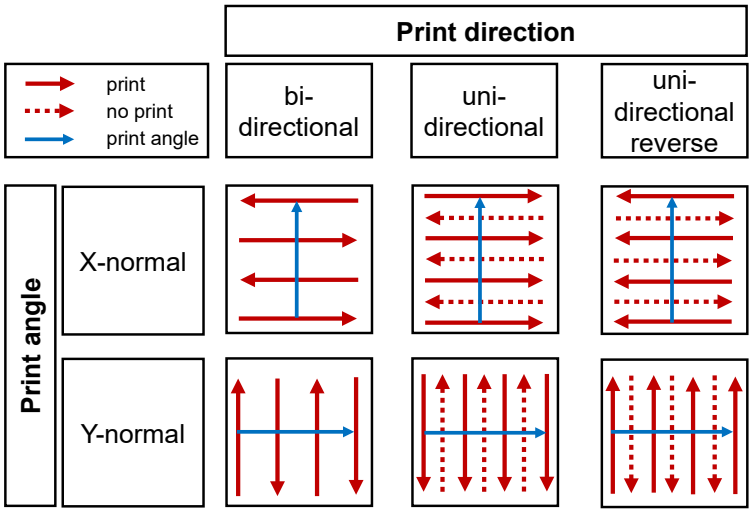

Figure 82: Illustration of used combinations of print direction (red) and angle (blue) [41], modified according to PixDro LP50 manual [251]

Table 30: Overview on print settings

Sample	Print speed [mm/s]		Print angle		Print direction		
	50	100	X-normal	Y-normal	bi-directional	uni-directional	uni-reverse
M1	X		X		X		
M2		X	X		X		
M3	X			X	X		
M4		X		X	X		
M5	X		X			X	
M6		X	X			X	
M7	X			X		X	
M8		X		X		X	
M9	X		X				X
M10		X	X				X
M11	X			X			X
M12		X		X			X

5.3.3 Static Jetting

In the present work, static jetting is defined as the ejection of drops in the drop view position of the inkjet printer PixDro LP50 (Meyer Burger, Eindhoven, The Netherlands) at a set frequency. A watch glass was placed underneath the print head for a specified period if collection of the ejected ink was necessary.

5.4 Statistical Evaluation

5.4.1 Designs of Experiments

To identify influences of the process parameters and establish factor and response relationships, design of experiments (DoE) was used as statistical tool. Experiment planning and analysis were carried out with the software MODDE® Pro (version 12.1, Umetrics® Sartorius Stedim Biotech, Malmö, Sweden). To minimise the effect of experimental error, a randomisation of the experiment run order was performed. The confidence interval (CI) was set to 95%.

5.4.1.1 Printing Parameters

A balanced fractional factorial screening design of resolution V was performed including five factors at two levels, thus $2^{5-1} = 16$ factor level combinations, plus three repetitions of the centre point (section 3.2.2.4) (Table 31). This resulted in total of 19 experimental runs (N1–N19). Main effects and two-factor interactions were not confounded.

Table 31: Experimental matrix of the DoE performed with MB28 inks by printing

Factors (abbreviation)	Units	Levels		
		-1	0	+1
dynamic viscosity (η)	mPa·s	1.0	4.2	6.7
pulse voltage (V) KM ǀ SP	V	12 ǀ 60 (90%)	16 ǀ 80 (90%)	20 ǀ 100 (90%)
resolution (dpi) KM ǀ SP	dpi	600 ǀ 220	900 ǀ 330	1200 ǀ 440
number of layers (lay)	-	1	3	5
print head distance (phd)	mm	0.22	5.11	10.00

5.4.1.2 Film Thickness

A full factorial two level screening design with four factors, thus $2^4 = 16$ factor level combinations, was performed to investigate the effects and interactions of process parameters during the casting of drug-free ODFs based on HPMC and PVA (section 3.3.3.3) (Table 32). Due to the time-consuming heat up and cool down of the film applicator, a split-plot-design was applied. Consequently, the experimental plan was divided in three parts corresponding to the three drying temperatures. The centre point was repeated three times. This resulted in

total of 19 experimental runs per polymer type (N1–N19) which were randomised within the respective parts.

Table 32: Experimental matrix of DoE performed with drug-free polymer solutions based on HPMC or PVA

Factors (abbreviation)	Units	Levels		
		-1	0	+1
polymer grade (g)	[qualitative]	HPMC 606 PVA 4-88	HPMC 606 PVA 4-88	HPMC 615 PVA 18-88
gap width (gap)	µm	300	500	700
casting speed (v)	mm/s	6	12	18
drying temperature (temp)	°C	30	40	50

5.4.2 Analysis of Variance (ANOVA)

The analysis of variance (ANOVA) was performed by the graphing and data analysis software Microsoft Excel® (version 16.0, Microsoft Corporation, Redmond, USA) and OriginPro® (version 2020, OriginLab Corporation, Northampton, USA). The significance level was set to $\alpha = 0.05$.

The two-way ANOVA with replication was conducted to investigate the influence of different geometries and ink formulations on the printed MB28 quantity (section 3.2.2.3).

The mean contents of printed units at different days and at the same operation day were compared in each case to determine whether or not there is a statistically significant difference (section 3.2.5). For that purpose, the one-way ANOVA with subsequent post hoc Tuckey was performed.

5.5 Analytical Methods

5.5.1 Rheology

Rheological properties were measured with the help of the rotational rheometer Kinexus pro controlled by the software rSpace of version 1.61 (both: Malvern Instruments, Worcestershire, UK).

5.5.1.1 Rotational Tests

To determine the dynamic viscosity rotational tests were performed using a cone (1°/ Ø 60 mm; CP1/60 SR2482 SS) and plate geometry (Ø 65 mm; PL65 S0520 SS).

In case of inks (section 3.1), the measurements were carried out at a temperature of 30 °C and a shear rate of 1000 s^{-1}. Each sample was measured in triplicate. Per measurement 60 values were recorded, arithmetic mean and standard deviation were calculated.

In case of polymer solutions (section 3.3), the cone geometry was exchanged to a smaller one (1°/ Ø 20 mm, CP1/20 SC004 SS) and a shear ramp was recorded from 0.01 to 100 s^{-1} at logarithmic intervals. The temperature of the measuring geometries was adjusted regarding to the casting and drying temperature of the film 25 to 50 °C. 10 values were recorded per set shear rate.

5.5.1.2 Optical High-Shear Tests

The flow properties of inks were additionally determined by the optical high-shear rheometer Fluidicam RHEO (Formulaction, Toulouse, France) based on microfluidic chip-system (section 3.1.2.3 and 3.1.3.1). The sample ink and a reference liquid with known dynamic viscosity were pumped through the Y-shaped flow cell of the microchip and flow laminar next to each other (Figure 83). The ink was pumped at different flow rates to reach different shear rates while the position of the interface between the liquids was monitored by a camera. The flow rate of the reference was adjusted by the software until the interface was centred. With this information the dynamic viscosity of the samples was calculated by the instrument. Water was used as reference liquid for low viscous inks and a mixture of PEG 200 (Rotipuran® Ph. Eur., Carl Roth, Karlsruhe, Germany) and water (50:50, w/w %) for more viscous inks. Per flow rate one measurement was performed recording 10 values, arithmetic mean and the analytical standard deviation were calculated.

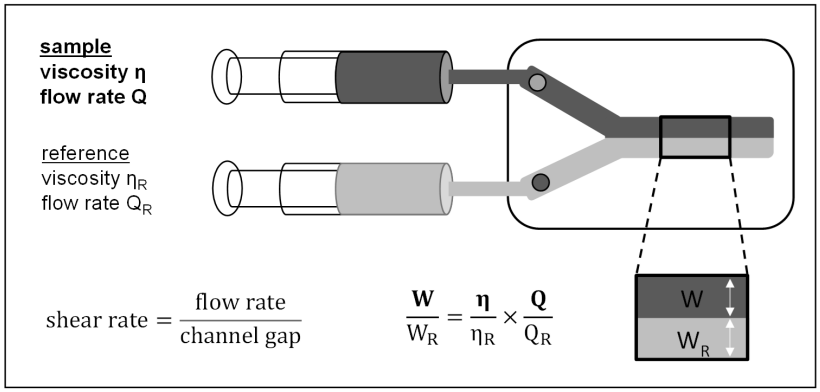

Figure 83: Measuring principle of Fluidicam RHEO, modified with permission from manufacturer`s website [252] (used from Kiefer et al. [176], by courtesy of Elsevier)

5.5.1.3 Oscillatory Tests

Oscillatory tests of the polymer solutions were performed using a cone (1°/ Ø 20 mm; CP1/20 SC004 SS) and plate with solution trap (Ø 55 mm; PLS550030 SS) as measuring geometries. The temperature was adapted to the casting and drying temperature of the films. First, an amplitude sweep was performed over a shear strain range of 0.01 to 100% to determine the limit of the linear viscoelastic region (LVER) at an angular frequency of 1 Hz. A deviation of ± 5% over 5 points according to ISO 6721-10 and EN/DIN EN 14770 was defined as tolerance for G′, G′′ and G*. Finally, a strain-controlled frequency sweep was carried out at frequency range of 0.01 to 10 Hz. The cross-over point of G′ and G′′ was determined automatically by the software. It indirectly provides information about flexibility and mobility of polymer molecules.

5.5.2 Surface Tension

Surface tension of the ink solutions was determined by the automatic force tensiometer K100 (Krüss, Hamburg, Germany) using a platinum probe (PL01, Krüss, Hamburg, Germany) for the Wilhelmy plate method at 30 °C. The samples were measured in triplicates. Per measurement run 10 values were recorded, arithmetic mean and standard deviation were calculated.

5.5.3 Density

Density was measured by filling a defined sample volume in a volumetric flask and weighing it on an analytical balance (CP224 S, Sartorius, Göttingen, Germany) in triplicates. In case of ink solutions, the measurements were performed at 30 °C whereas the polymer solutions were investigated at ambient conditions of 22 °C. The arithmetic mean and standard deviation were calculated.

5.5.4 Contact Angle

Contact angle measurements were performed by Drop Shape Analyzer DSA100 (Krüss, Hamburg, Germany) at ambient conditions. A syringe with a volume of 500 µl equipped with a blunt needle was used for drop deposition. The needle diameter was selected according to the viscosity of the sample and was in the range of 0.4 to 1.2 mm. The drop volume of polymer solutions was 10 µl, the drop volume of inks was 0.5 to 1 µl. As the drop deposition took place volumetrically and liquids are generally sensitive to temperature and humidity, absolute deviations cannot be excluded. Therefore, results were compared relatively to each other.

The illumination, zoom and focus were adjusted to create sharp images. Videos were recorded by the integrated CCD camera in order to capture all stages of the drop within the set time period. Then frames at selected time points were saved and analysed by the software DSA1 (version 1.90.014, Krüss, Hamburg, Germany). There is no universally suitable method for the analysis of all drop sizes and shapes. Nevertheless, care was taken to use the same methodology for comparability wherever possible.

For the purpose of observing only the drop shape or absorptive behaviour, images were evaluated visually.

5.5.5 Determination of Negative Pressure

A set negative pressure is applied to the ink storage container to prevent the ink leaking through the nozzles during the printing. To find out suitable values for both print heads (section 3.2.2.2), the target ink mixtures were jetted by one selected nozzle over a watch glass for 3 min at a frequency of 3000 Hz. The ejected fluid was quantitatively transferred and diluted by deionised water.

In the print head manual [251], it is recommended to calculate the necessary negative pressure by using following equation (Equation 12):

$$p_{set} = -(p_{meniscus} + \rho \cdot h) \quad \text{(Equation 12)}$$

Here p_{set} is the adjusted ink negative pressure, $p_{meniscus}$ the required negative meniscus pressure (2.5–10 mbar). The density of fluid is described by ρ and the height of ink level above the nozzle plate (here: 18–20 cm) is represented by h.

Negative pressures between -15 and -30 mbar were tested. The driving voltage was set to 80 V (90%) for SP and to 16/8 V for KM. Additionally, the jetted drops were observed by the drop view camera of the inkjet system (section 5.5.7).

5.5.6 Drying of Ink

For investigation of the drying behaviour of inks (3.1.2.5), 2 g of each ink was stored open in a weighing pan with a diameter of 4.5 cm in an oven (Tv40u, Memmert, Schwabach, Germany) at 30 °C. At selected time points (0, 20, 40 min, 1, 2, 3, 24, 48, 72 h) the samples were weighed on an analytical balance (CP224 S, Sartorius, Göttingen, Germany).

5.5.7 Analysis of Jetted Drops

The integrated drop view system of the inkjet printer PixDro LP50 (section 5.3) was used for visualisation and analysis of the jetted drops in real time.

The installed LED sent high speed strobe light so that the drop shadows could be watched by the CCD camera on the opposite site in-flight (Figure 84). The time delay of the strobe light, further referred as LED delay, enables to display the drops at a certain moment in time and with that at a certain distance to the nozzle plate.

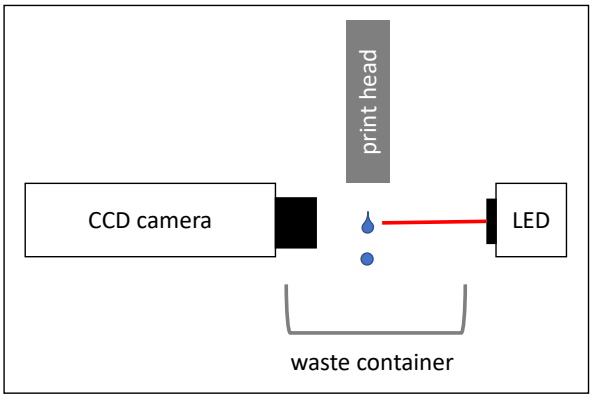

Figure 84: Schematic illustration of PixDro LP50 drop view system, side view

The drop volume was calculated by the printer software assuming the drop is a stack of cylinders with height 1 px and the width is the given number of pixels (Figure 85). The drop speed and angle were determined automatically by comparing the image to a second image at a greater LED delay. To fix the position of the drop, a coordinate system is used by the software. The X-centre as well as the Y-centre of the drop is defined as the point where 50% of the pixels from that droplet are on the opposite side.

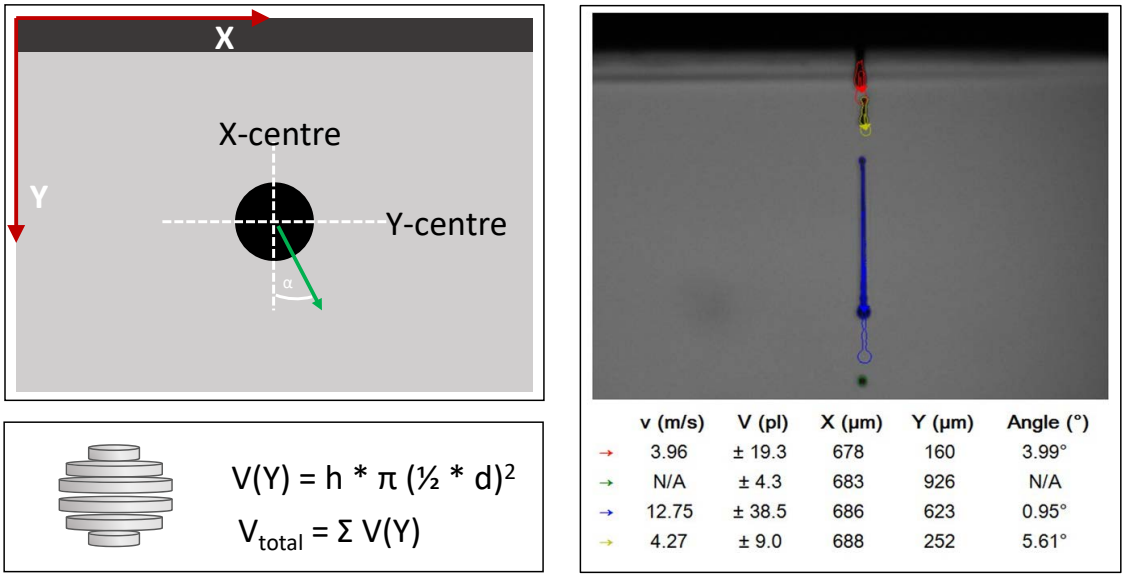

Figure 85: Calculation basis of the drop properties, modified from PixDro LP50 manual [251] (left) and an exemplary result screen of a real recorded drop (right); coloured arrows and drop borders mark the flight vectors and change in drop position after 10 µs

Additionally, the aspect ratio (AR) of the main drop defined as major axis divided by the minor axis of an approximated ellipse was determined by the image processing software Fiji (ImageJ2/Fiji, version 1.46r) [253].

The Advanced Drop Analysis (ADA), an automated software tool (v2.4.2, Meyer Burger, Eindhoven, The Netherlands), was used to investigate the printability of inks, to optimise the waveform (section 5.3.1) and to create merged drop images at systematically varied jetting settings. Per ink formulation, 100 measurements with a time duration of 10 s at a frequency of 1000 Hz were conducted to test the long-term jetting stability.

5.5.8 Print Performance Test

To ensure the target nozzle is not clogged or otherwise disabled, a print test was performed activating all nozzles before printing. For this purpose, the individual print head signature (Figure 86) was printed by each print head on copy paper and then checked for errors. This was only feasible if the ink was coloured. Using transparent fluids, the functional tests of the nozzles were limited to drop watching before each printing (section 5.5.7).

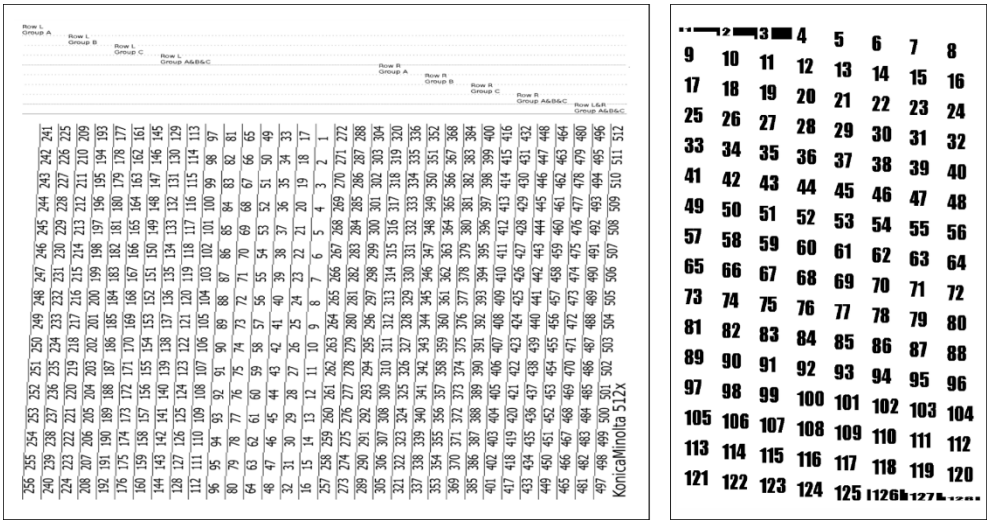

Figure 86: Print head signature templates of KM512SHX (left) and Spectra SE-128 AA (right) [251]

5.5.9 Determination of Weight

To determine the weight of dry films an analytical balance (MC1 RC 250 S, Sartorius, Göttingen. Germany) was used. At least six film pieces of the same area were weighed. The arithmetic mean and standard deviation were calculated. The area weight, so-called grammage, was calculated in g/m² based on EN ISO 536 for comparison purposes.

5.5.10 Refractive Index

Refractive index n of polymer solutions was measured once using the automatic digital refractometer AR200 (Reichert® Technologies, Unterschleißheim, Germany). A drop of polymer solution was placed on the sapphire prism. The results were automatically calculated for 20 °C.

5.5.11 Thickness

5.5.11.1 Mechanical Thickness Measurement

Thickness of dry films was determined non-destructively with a digital micrometre screw gauge (IP65, Mitutoyo, Kawasaki, Japan) complemented with two jaws of 6 cm^2. The resulting values correspond to the thickest part of the film piece. At least six samples were measured and the arithmetic mean of the micrometre screw thickness (MST) as well as standard deviation were calculated.

5.5.11.2 Chromatic Confocal Thickness Measurement

Thickness of the polymer solution during the casting process was measured contactless by a chromatic confocal sensor (CHRocodile S, Precitec Optronik, Gaggenau-Bad Rotenfels, Germany). The chromatic confocal optical sensor consists of a sensor unit connected to an optical probe with a measuring range of 3 mm and a spot diameter of 12 µm. The sensor unit contains an LED white light source and the spectrometer (Figure 87). The light is transmitted along the optical fibre to the probe whereby it is focused with pronounced chromatic aberration onto the sample. In case of the used thickness operation mode, two peaks at different wavelengths (λ_1, λ_2) appear in the spectrum of the reflected beam. These peaks correspond to two distances (D1, D2) from which the optical thickness of the polymer layer was calculated. The physical thickness can be determined from the spectral distance, also called optical thickness, and the refractive index (RI) n of the sample.

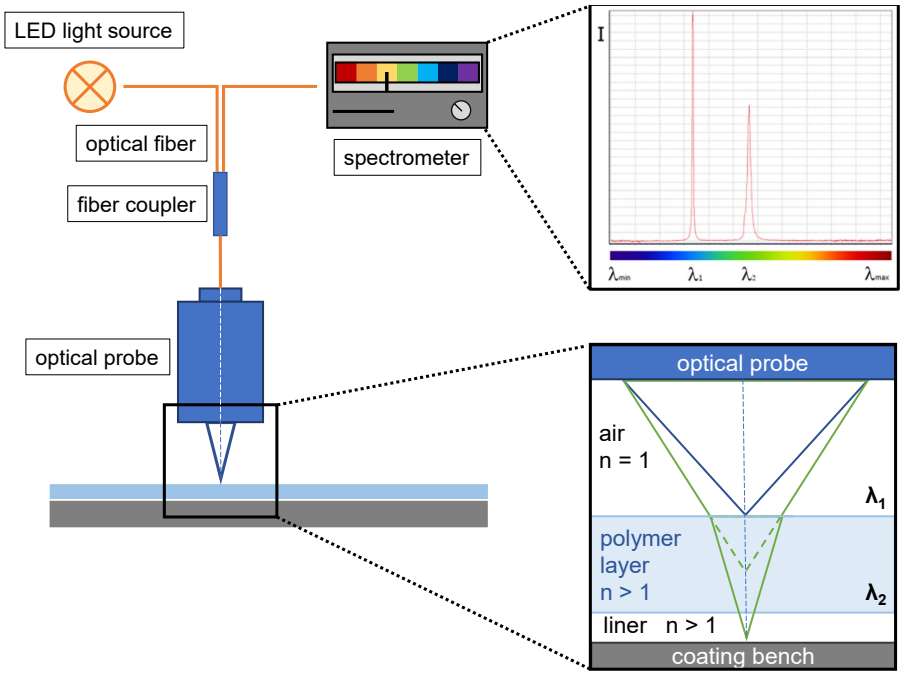

Figure 87: Schematics of chromatic measuring principle (modified from Precitec [254])

The probe was mounted perpendicular to the film applicator with the help of the customised adjustable XYZ-frame (Figure 88, section 3.3.3.1). The sensor unit was monitored by the software CHRocodileExplorer (version 0.98.0.0, Precitec Optronik, Gaggenau-Bad Rotenfels, Germany). A scan rate of 2000 Hz was used. An average over 200 data points was calculated by the software so that 10 values per second were recorded.

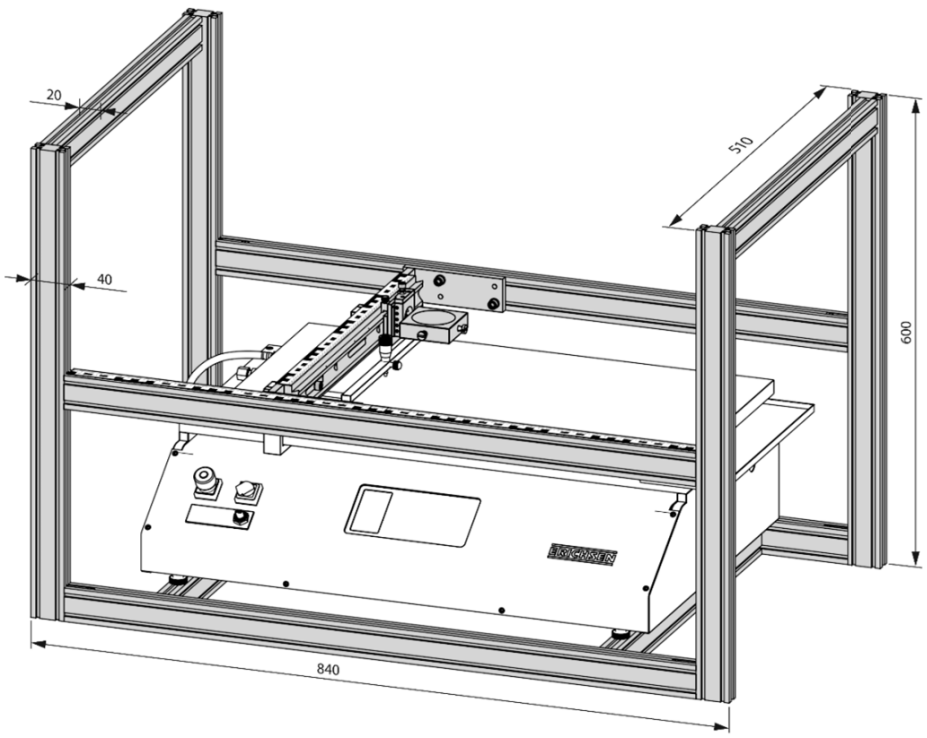

Figure 88: Overview drawing of XYZ-frame and integrated film applicator, dimensions in mm

In addition to the cast polymer solution, the process liner was located within the measuring range (Figure 89). Therefore, the optical thickness of the process liner (oTH_{liner}) (Equation 13) must be subtracted to assess the polymer film thickness (oTH_{film}) (Equation 14):

$$oTH_{liner} = D2_{total} - D1_{liner} \quad \text{(Equation 13)}$$

$$oTH_{film} = oTH_{total} - oTH_{liner} \quad \text{(Equation 14)}$$

However, due to dynamically changing refractive index (RI) of the sample during the drying (section 3.3.3.2), the physical thickness could not be calculated just by Equation 15 inserting the measured RI of the polymer solutions.

$$pTH = oTH_{film} \cdot RI \quad \text{(Equation 15)}$$

The distance difference between optical probe and polymer layer interface as well as probe and process liner had to be calculated retroactively to determine the physical thickness pTH_{film} (Figure 89). The process liner was measured for a period of 60 s before the casting process was started. Each measured value of distance to the polymer film $D1_{total}$ was subtracted from the arithmetic mean of process liner distance $D1_{liner}$ (Equation 16).

$$pTH_{film} = D1_{liner} - D2_{total} \quad \text{(Equation 16)}$$

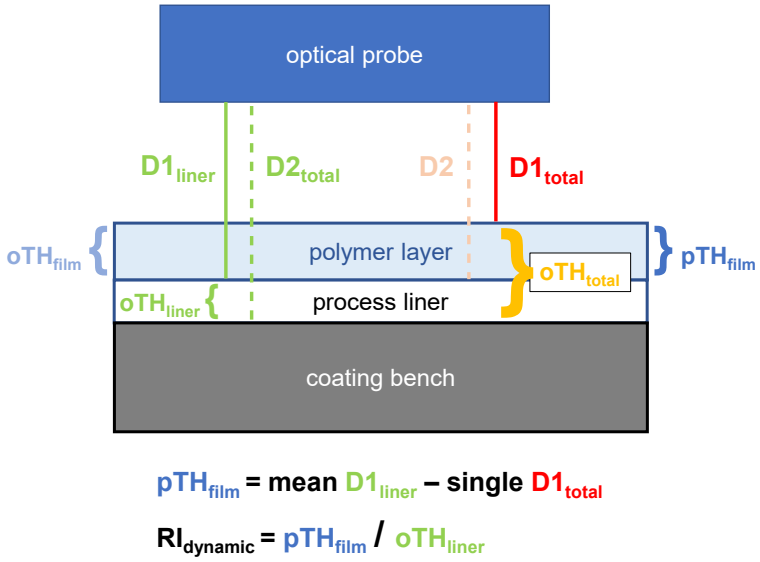

Figure 89: Schematic illustration of the recorded distances (D1, D2) by the optical probe and equation to calculate the physical polymer film thickness (pTH_{film})

D2 as distance to the second interface measured through the transparent material was not used as the real dynamic RI was not known. However, the dynamic RI could be retroactively calculated for each single pTH_{film} value (Equation 17).

$$RI = pTH_{film} - oTH_{liner} \quad \text{(Equation 17)}$$

5.5.12 Dynamic Vapour Sorption

To examine the moisture absorption behaviour of films a vapour sorption analyser (SPS11-10µ, ProUmid, Ulm, Germany) was used at 25 °C. Two film pieces of 6 cm², respectively, were placed in per sample dish and were first weighed at 0% relative humidity until the mass constant was reached. Then the relative humidity was gradually increased in 10%-steps to 90% and then decreased again to 0%. A weight change of < 0.01%/15 min was set as target equilibrium condition. Each sample was investigated at least for 60 min and maximum for 60 h.

5.5.13 Ambient Conditions

The ambient temperature and relative humidity (RH) were monitored by the data logger testo 175 H1 and read out by the software ComSoft Basic (both: Testo, Lenzkirch, Germany). The measuring rate was set to 1/h or 1/min depending on the experiment.

5.5.14 Thermography by IR Camera

To investigate the temperature distribution of the heated coating plate of the film applicator as well as of the drawn polymer solution the IR camera optris® PI 640 (Optris, Berlin, Germany) was used. The camera was mounted obliquely from above in front of the film applicator and controlled by the software Optris PI Connect (version 2.12, Optris, Berlin, Germany). A polygon that represented the region of interest was selected as measurement area. In this region, an emission level of ε = 0.90 was set. First, the temperature profile of the uncoated process liner and then the casting of the polymer solutions at process settings described in section 5.4.1.2 were recorded with a frame rate of 32 Hz. For the evaluation, single frames were extracted from the video and a rectangular measuring range along the film applicator width was selected.

5.5.15 Drying Kinetics of Polymer Films

The drying kinetics of films was indirectly determined by measuring the thickness (section 5.5.11.2) of polymer layer. Figure 90 shows an exemplary curve. For curve analysis, the first measured thickness value was defined as initial lamella (A). The drying time of cast polymer solutions was defined as the intersection of the inter- and extrapolated linear falling branch (C) and the parallel one to the x-axis (plateau, D). The intersection was calculated by means of Solver add-in of Excel® (Microsoft, Redmond, USA). A linear fit of the falling branch (C) was performed. The slope describing the shrinking rate (shR) and the coefficient of determination showing the goodness of fit were calculated. The mean of measured thickness in the first three seconds was defined as wet film thickness (WFT) and the mean of last 20 values of the plateau as dry film thickness (DFT).

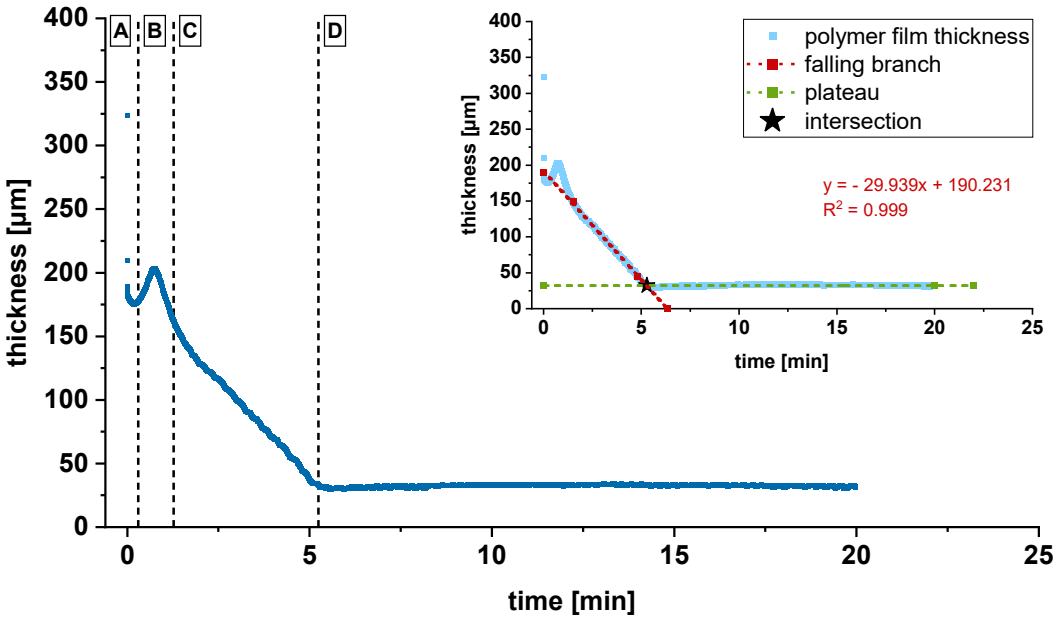

Figure 90: Example thickness curve of HPMC 615 solution cast at 50 °C with subdivided segments initial lamella (A), wave (B), falling branch (C) and plateau (D); linear fit of falling branch (red) and plateau (green)

5.5.16 Mechanical Characteristics

Mechanical characteristics of films were tested performing a penetration test conducted by the texture analyser TA.XT*plus* (Stable Micro Systems, Godalming, UK) equipped with a cylindrical flat-faced aluminium probe of 5.0 mm diameter. The samples were clamped between two plates with a circular recess of 10.0 mm diameter (Figure 91). The probe was moved perpendicular to the sample at a speed of 1.0 mm/s. After a trigger force of 1 N was reached, a distance of 5.0 mm was covered [116]. Depending on the number of available

samples, triple or sixfold measurements were conducted. The force-distance profiles were recorded and analysed regarding puncture point and texture properties.

Puncture strength (Equation 18), the maximum reached force until break related to an area, and elongation at break (Equation 20) were calculated [116, 255].

$$puncture\ strength\ \left[\frac{N}{mm^2}\right] = \frac{F}{A} \quad \text{(Equation 18)}$$

$$L_s\ [mm] = \sqrt{R'^2 + d^2} \quad \text{(Equation 19)}$$

$$elongation\ at\ break\ [\%] = \left(\frac{(L_s + r) - R_0}{R_0}\right) \times 100 \quad \text{(Equation 20)}$$

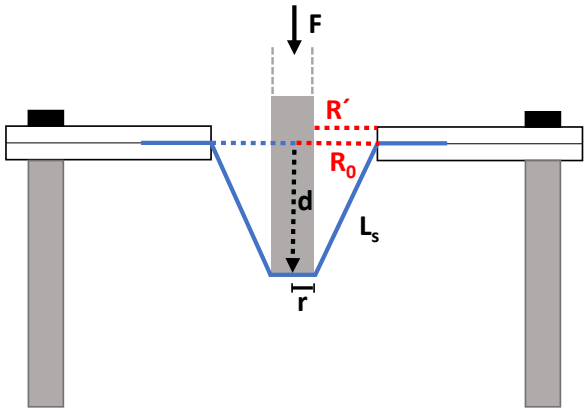

Figure 91: Schematic illustration of side view of the experimental setup, F: force, r: radius of probe, R_0: initial radius of film, R´: R_0-r, d: displacement of the probe, L_S: length of R´ after strain according to Radebaugh et al. and Preis et al. [116, 255]

5.5.17 Disintegration Time

Disintegration time of films was measured by clamping six samples into the PT-ODF6 test basket connected to the disintegration test apparatus PTZ Auto EZ (both: Pharma Test Apparatebau, Hainburg, Germany). The volume of the disintegration medium water was 900 ml and the temperature 37 ± 0.5 °C. Clamp weights of 3 g were fixed at each film and the disintegration time was detected automatically after they gained contact with the metal mesh.

5.5.18 Tensile Strength

The tablet tensile strength σ is defined as breaking force related to the tablet's dimensions and was calculated according to Equation 21 (section 3.3.2.5) [256]. The breaking force *F*, diameter *d* and height *h* of 10 tablets each were measured using the semi-automated tablet tester (Smart

Test 50, Sotax, Aesch, Switzerland). The arithmetic mean and standard deviation of the calculated tensile strength were determined.

$$\sigma\,[MPa] = \frac{2 \times F}{\pi \times d \times h} \qquad \text{(Equation 21)}$$

5.5.19 Laser Diffraction Analysis

To determine the particle size distribution of raw materials (section 3.3.2.1), Mastersizer 3000 connected to the dry dispersion system Aero S (both: Malvern Instruments, Worcestershire, UK) was used. The measuring principle is based on laser diffraction. Dispersion pressure of 0.8 bar was set and the feed rate was adjusted manually to keep optimum laser obscuration. The measurements were performed in triplicates and the data was collected and analysed by the Mastersizer software (version 3.10, Malvern Instruments, Worcestershire, UK).

5.5.20 Microscopic Investigations

5.5.20.1 Optical Microscopy

Light Microscope

To visualise the printed inks on films, the light microscope Leica DMLB equipped with the digital microscope camera DFC450 (both: Leica Microsystems, Wetzlar, Germany) and related analysis software Leica Application Suite (version 4.6) was used. Furthermore, polarisation and dark field mode were applied to determine the solid phase properties as well as crystal morphology.

Stereo Light Microscope

The absorption behaviour of functional films was observed using a stereo microscope (MZ7.5, Leica Microsystems, Wetzlar, Germany) equipped with the digital microscope camera DFC450 and a halogen cold light source KL 1500 LCD (both: Leica Microsystems, Wetzlar, Germany) (section 3.3.2.5). The films were fixed on a slide and a blue coloured 10 µl drop of water was placed onto the film surface. Images were taken with the help of the software Leica Application Suite (version 4.6, Leica Microsystems, Wetzlar, Germany) at a magnification of 3.2 every 30 s for a period of 30 min.

5.5.20.2 Scanning Electron Microscopy (SEM)

For visualisation purposes of surface and cross-section morphology of raw materials and films, the desktop scanning electron microscope Phenom G2 Pro (PhenomWorld, Eindhoven, The Netherlands) was used operating at an acceleration voltage of 5 kV. The samples were fixed to pin stubs by conductive double-sided adhesive carbon tabs (Ø 12 mm, EM-Tec CT12, Micro to Nano, Haarlem, The Netherlands) and mounted in the standard sample holder. A gold sputtering was not necessary as no charging of the samples took place during the measurement time.

5.5.20.3 Confocal Raman Microscopy

Microscopic Raman investigations on ODFs imprinted by MPT were performed using confocal Raman microscope alpha300 R (WITec, Ulm, Germany). A fibre coupled single mode DPSS laser with 532 nm excitation wavelength was used. The laser power on the samples was set to 20–23 mW. A Zeiss EC Epiplan-Neofluar HD 100x/0.9 NA and a Zeiss EC Epiplan-Neofluar HD 20x/0.5 were selected as microscope objectives. WITec UHTS 300 was used as spectrometer in combination with an Andor iDus Deep Depletion CCD detector, which was cooled to -60 °C. The Raman scattered light was spectrally dispersed at a reflection grating with 600 lines/mm. An average spectral resolution of about 3.8 cm^{-1}/pixel were achieved. The evaluation of the measurement data and the creation of the Raman images was performed using the software FIVE (version 5.2.4.81, WITec, Ulm, Germany), including a cosmic ray removal and background subtraction by the implemented shape function. After analysis of the spectra of main pure substances HPMC and MPT, the MPT peak at 1615 cm^{-1} (Figure 92) was selected as its characteristic one, unaffected by HPMC. All spectra were normalised related to the HPMC peak at 1370 cm^{-1} correcting scattering losses due to penetration depth.

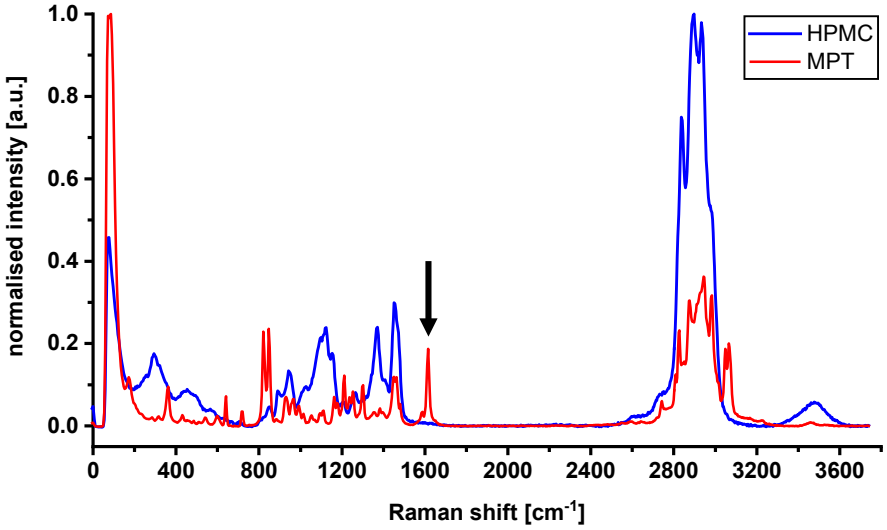

Figure 92: Raman spectra of pure substances HPMC and MPT with characteristic peak at 1615 cm^{-1}, spatial resolution and 10 s exposure time, normalised intensity in arbitrary unit (a.u.) (modified from Kiefer et al. [41])

Furthermore, the Raman microscope was used in dark field mode to investigate the surface structure of printed ODFs (section 3.1.3.3 and 3.2.3). Using the microscope objective Zeiss EC Epiplan-Neofluar HD 20x/0.5 stitching images were recorded and combined to an overview.

5.5.21 Assays

5.5.21.1 Millijet® Blue 28

Jetted inks containing MB28 were transferred quantitatively from the watch glass and diluted by deionised water. Imprinted films were weight and dissolved in appropriate amount of deionised water to fit the calibrated range of 1 to 51 µg/g water (Figure 93). Since the blue dye MB28 is a viscous liquid polymer dye, the stock solution was prepared gravimetrically for examination of the linearity range. Each sample was measured without filtering by UV/Vis spectrophotometer Spekol-1800 (Shimadzu, Kyoto, Japan) at wavelength of 641 nm three times. The concentration was calculated with the help of the calibration equation and multiplied by the sum of film and dissolution media weight to determine the dye quantity in mg.

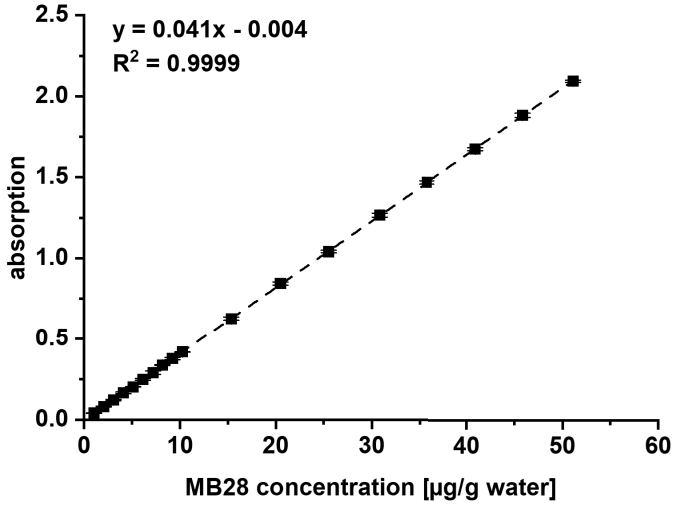

Figure 93: Calibration line of MB28 in deionised water, measured at a wavelength of 641 nm (mean ± analytical SD, n = 3)

5.5.21.2 Metoprolol Tartrate

MPT content of films was analysed using high performance liquid chromatography (HPLC). The analytical HPLC system Agilent 1260 Infinity (Agilent Technologies, Santa Clara, USA) consisted of binary pump G1312B, autosampler G1329B, temperature-controlled column compartment G1316A, degasser G4225A and diode array detector (DAD) G4212B. The C18-column ODS Hypersil™ with the dimensions 150 × 4 mm and particle size of 3 µm (Thermo Fisher Scientific, Waltham, USA) was used. 10 µl of sample were injected and analysed at a wavelength of 221 nm. A mixture of phosphate buffer (4.6 mM, pH 3 adjusted with phosphoric acid 85%) and acetonitrile (15:85) was used as eluent for the isocratic method. The flow rate was set to 2.0 ml/min at a column temperature of 25 °C. The films were dissolved in 10.0 ml or 100.0 ml water to remain within the calibration range and filtered through 0.45 µm polypropylene filter (VWR, Leuven, Belgium). The peaks were manually re-integrated with the help of control software OpenLAB CDS ChemStation (version C.01.07, Agilent Technologies, Santa Clara, USA).

Figure 94 shows exemplarily a chromatogram of the metoprolol peak at a retention time of 4.51 min and of the tartaric acid peak at 0.52 min.

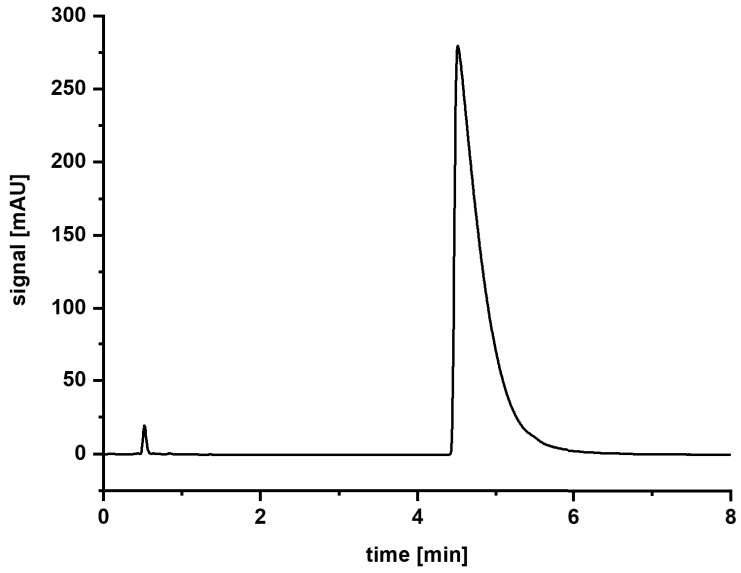

Figure 94: Chromatogram of MPT in deionised water (exemplary of c = 0.85 mg/ml)

The HPLC method was validated according to ICH guideline Q2 and Reviewer Guidance [257, 258] regarding to accuracy, linearity, precision, recovery, robustness and specificity. All investigations were performed in triplicates.

Accuracy was shown comparing the drug substance with secondary reference standard at 80%, 100% and 120% level of target dosage of 3.5 mg. The mean contents were 100.08%, 99.84% and 99.99% of label claim on the respective level. The RSD providing the analysis variation was between 0.03% and 0.41%. To analyse the matrix influence and with that the recovery, drug-free films were spiked with MPT to reach concentrations of 0.28 mg/ml, 0.35 mg/ml and 0.42 mg/ml. The mean contents were 100.56%, 100.07% and 101.07% of label claim at the respective concentration and the RSD was between 0.17% and 0.29%. Therefore, it can be considered that the film matrix had no remarkable influence on API peak shape.

Linearity was determined by measuring a calibration series prepared freshly at seven days spread over six months as well as at five consecutive days. At least six concentrations were distributed equidistantly over a range of 0.005 mg/ml to 1.0 mg/ml (Figure 95). The regression coefficient R was between 0.99988 and 0.99999 and thus every day $R > 0.999$. The slope as measure of sensitivity of the method was between 7796.1 and 7988.7 with RSD of 0.7%.

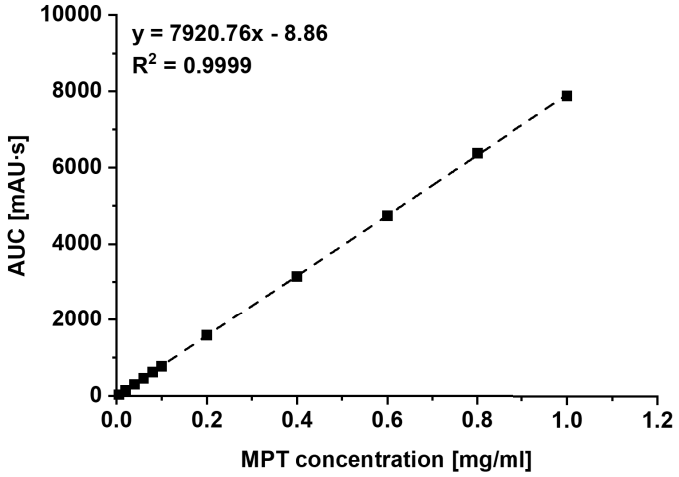

Figure 95: Calibration line of MPT in deionised water, measured at a wavelength of 221 nm (mean ± analytical SD, n = 3)

As part of the precision test, intermediate precision as well as injection repeatability and reproducibility were tested. For intermediate precision, samples of 0.35 mg/ml were prepared six times at one day and one time at five different days. The solutions were injected and analysed three times, respectively. The RSD was 0.67% and thus < 1%. The injection precision was shown by tenfold injection of one sample of a concentration of 0.35 mg/ml. The RSD was 0.15% and thus < 1%. The reproducibility was demonstrated by confirmation of linearity at 12 days spread over six months and additionally at one day by a second operator.

Filter adsorption was determined additionally as recovery parameter. For that purpose, 10 ml of 0.35 mg/ml sample were distributed into ten test vials 1 ml each. Except the first and last millilitre, all volumes were filtered through one 0.45 µm polypropylene filter. The recovery was between 99.2 and 100.2% for all filtrated volumes. For practical reasons, it was decided to use a discard of 1.5 ml for all measurements.

Robustness of the HPLC method was analysed varying the flow rate, pH value of the buffer and column temperature (Table 33). With regard to the signal area under the curve (AUC), the method can be classified as robust within the tested limits of buffer pH value and column temperature. The change in flow rate has the greatest influence on the AUC and retention time and should not deviate from the developed standard method.

Table 33: Robustness of HPLC method for MPT, tested concentration of 0.35 mg/ml (mean ± analytical SD, n = 3)

	Settings	Area [mAU·s]	Retention time [min]
standard method		2,742.1 ± 11.8	4.65 ± 0.00
flow rate [ml/min]	1.0	5,395.4 ± 22.4	9.45 ± 0.00
	1.5	3,585.5 ± 11.3	6.25 ± 0.00
pH value of buffer	2.5	2,731.9 ± 3.4	3.76 ± 0.03
	4.0	2,742.2 ± 10.0	4.03 ± 0.13
column temperature [°C]	20	2,722.0 ± 4.8	4.72 ± 0.00
	30	2,717.1 ± 3.5	4.63 ± 0.01

In addition, sample solution stability was investigated. For that purpose, the content of a calibration series (t_0) was measured after 24 h (t_1) and 96 h (t_2) stored in vials at ambient lab conditions. Comparing each measuring point of the calibration series at t_0, t_1 and t_2, an RSD of < 1% was calculated. Furthermore, a sample of 0.35 mg/ml was exposed to controlled white light source (L 18 W/940, Lumilux®, Osram, Munich, Germany) for 96 h. The signal AUC was 2728.2 ± 2.9 mAU·s and no degradation peak could be detected. In conclusion, the sample solutions are stable during five days, even under light exposure.

System suitability test was performed on the basis of daily linearity examination regarding the tailing factor T and capacity factor k'. The tailing factor was between 4 and 7 and thus exceeded the recommendation of $T \leq 2$. It was shown that the peak shape did not change and no degradation products appeared during the sample preparation and measurement period. As the HPLC method was only used to determine the content of one API and not to separate several peaks, the peak tailing was accepted as long as the linearity of $R > 0.999$ could be reached. The capacity factor describing the ratio to void volume was between 6 and 7 and thus $k' > 2$.

5.5.21.3 L-Thyroxine

LT content of films was analysed using HPLC. The analytical HPLC system Agilent 1260 Infinity (Agilent Technologies, Santa Clara, USA) consisted of the same parts as described in section 5.5.21.2. The C18-column ODS Hypersil™ with the dimensions 150 × 4 mm and particle size of 3 µm (Thermo Fisher Scientific, Waltham, USA) was used. 10 µl of sample were injected and analysed at a wavelength of 225 nm. A mixture of phosphate buffer (4.6 mM, pH 3 adjusted with phosphoric acid 85%) and acetonitrile was used as eluent. A gradient method

(Table 34) was necessary to shorten the retention time of LT peak. Flow rate of 1.0 ml/min was used at a column temperature of 30 °C. The film samples were dissolved in 10.0 ml water and filtered through 0.45 μm polypropylene filter (VWR, Leuven, Belgium). The peaks were manually re-integrated with the help of control software OpenLAB CDS ChemStation (version C.01.07, Agilent Technologies, Santa Clara, USA).

Table 34: HPLC gradient method for LT

Time [min]	A: phosphate buffer [%]	B: acetonitrile [%]
0.0–1.5	80	20
1.5–3.5	80 → 20	20 → 80
3.5–5.0	20	80
5.0–6.1	20 → 80	80 → 20
6.1–8.0	80	20

The drug substance was dissolved in DMSO-EtOH-water mixture (30:30:40 v/v %) for preparation of the stock solution. Water without additional organic solvents could not be used due to solubility issues of LT. DMSO peak appears in the chromatogram at a retention time of 1.32 min and LT peak at 6.11 min (Figure 96).

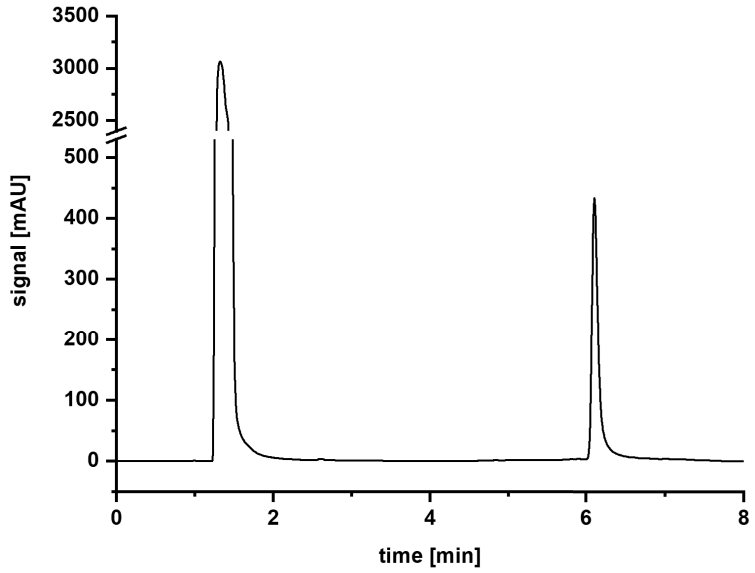

Figure 96: Chromatogram of LT in DMSO–EtOH–water (30:30:40 v/v %, exemplary of c = 80 μg/ml)

Linearity was shown by measuring a calibration series before each examination (Figure 97). At least six concentrations were distributed equidistantly over a range of 0.6 μg/ml to 100.0 μg/ml. The regression coefficient R was between 0.9991 and 0.9995 and thus R > 0.999 at each analysis. The slightest variation in high concentrations leads to large changes in the

course of the regression line in lower ranges. Since the target concentrations were in the range of the lower curve part (section 3.2.4.2), only the lower six points were used for calibration.

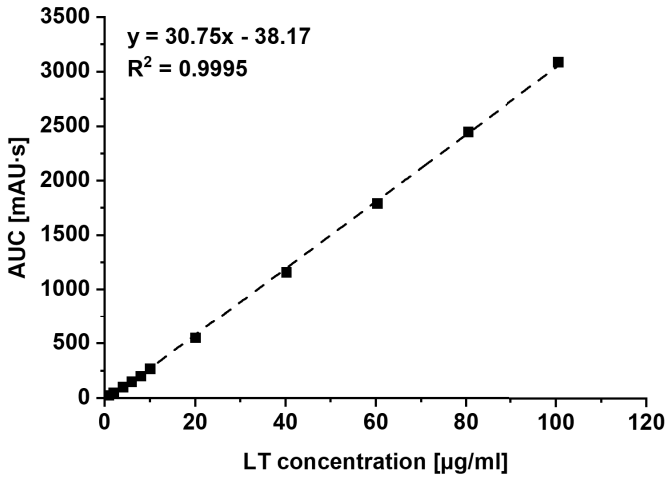

Figure 97: Calibration line of LT in DMSO–EtOH–water mixture, measured at a wavelength of 225 nm (mean ± analytical SD, n = 3)

The stability of the sample solutions was verified by storing a calibration series (t_0) in brown-glass HPLC vials at ambient lab conditions and re-measuring them one week later (t_1). Comparing each measuring point of the calibration series at t_0 and t_1 no significant changes in content could be detected.

5.5.22 Uniformity of Dosage Units

The content uniformity (CU) was determined according to Ph. Eur. monograph 2.9.40 at level 1 (L1) [198]. The content of 10 single doses was measured by HPLC (section 5.5.21.2). The mean of individual contents $\overline{X}$ expressed as percentage of the label claim was calculated and inserted into the equation (Equation 22) to determine the acceptance value (AV).

$$AV = |M - \overline{X}| + k\,s \qquad \text{(Equation 22)}$$

M is the reference value depending on the label claim set at the time of the production, the acceptability constant k is 2.4 (n = 10) and s is defined as sample standard deviation. The maximum allowed AV is 15.0 for L1.

5.6 Visualisation

The 3D computer graphics and digital simulations of the experimental setup of inkjet printing and film casting were constructed by the software Cinema 4D (R19, Maxon Computer, Friedrichsdorf, Germany). In case of film casting, additionally, the plug-in Navié Plants & Effex was used to simulate the polymer solution flow.

The individual components of the experimental setup were first photographed from four perspectives: frontal, from above, from side and from three-quarters angle. The dimensions of them and their details were taken to enable later a scale reproduction. However, in case of missing measured parts, a scale bar was prepared using a known length. Videos of partial processes were recorded to capture every important movement. To carry out the process simulation, a scene was built by modelling and texturing the equipment required for the experiment setup (Table 35). The lighting setup and camera position were arranged.

Table 35: Scene components and sub-processes for 3D process simulation

	Inkjet printing	**Film casting**
scene components	inkjet printer with the print and drop view system	XYZ-frame with the associated mounting and the sensor unit
	substrate table with polymer film on process liner	optical probe
	print heads in PHA	film applicator with temperature controller, heated plate and coating knife
	utility station	beaker with polymer solution
		process liner
sub-processes	cover opening	pour polymer solution from beaker onto process liner
	approach to service position by PHA	film casting
	printing	zoom into cross-section of coating knife with polymer solution

For polymer solution flow animation, the polymer solution was constructed creating first a particle cache node to store the geometry simulation for a particle system to file. The particle system was transferred to a coherent liquid system using the surface re-constructor including adjusted liquid dynamic properties. After finding optimal parameters for the Effex scene, the experimental setup was animated with the synchronous cache-recording and storage. Finally, the scenes were rendered, the complete video was assembled and produced.

6 Appendix

Table 36: Summary of factor combinations and corresponding response, the quantity of MB28, of the DoE performed with F1, F2 and F3 ink and KM print head (section 3.2.2.4)

Exp. name	η [m·Pa]	V [V]	dpi [dpi]	lay [dimensionless]	phd [mm]	MB28 [µg]
N1	1.0	60	600	1	10	0.00
N2	6.7	60	600	1	0.22	14.20
N3	1.0	100	600	1	0.22	48.54
N4	6.7	100	600	1	10	24.68
N5	1.0	60	1200	1	0.22	68.08
N6	6.7	60	1200	1	10	0.00
N7	1.0	100	1200	1	10	0.00
N8	6.7	100	1200	1	0.22	127.05
N9	1.0	60	600	5	0.22	101.90
N10	6.7	60	600	5	10	0.00
N11	1.0	100	600	5	10	163.09
N12	6.7	100	600	5	0.22	154.74
N13	1.0	60	1200	5	10	454.91
N14	6.7	60	1200	5	0.22	0.00
N15	1.0	100	1200	5	0.22	863.07
N16	6.7	100	1200	5	10	608.28
N17	4.4	80	900	3	5.11	158.51
N18	4.4	80	900	3	5.11	159.67
N19	4.4	80	900	3	5.11	165.41

Abbreviations: η = dynamic viscosity, V = pulse voltage, dpi = print resolution, lay = number of layers, phd = print head distance from substrate, MB28 = Millijet® blue 28

Table 37: Summary of factor combinations and corresponding response, the quantity of MB28, of the DoE performed with F1, F2 and F3 ink and SP print head (section 3.2.2.4)

Exp. name	η [m·Pa]	V [V]	dpi [dpi]	lay [dimensionless]	phd [mm]	MB28 [µg]
N1	1.0	60	220	1	10.00	0
N2	6.7	60	220	1	0.22	5.41
N3	1.0	100	220	1	0.22	55.53
N4	6.7	100	220	1	10.00	24.52
N5	1.0	60	440	1	0.22	50.77
N6	6.7	60	440	1	10.00	0
N7	1.0	100	440	1	10.00	172.01
N8	6.7	100	440	1	0.22	99.08
N9	1.0	60	220	5	0.22	79.76
N10	6.7	60	220	5	10.00	0
N11	1.0	100	220	5	10.00	243.2
N12	6.7	100	220	5	0.22	117.44
N13	1.0	60	440	5	10.00	0
N14	6.7	60	440	5	0.22	141.88
N15	1.0	100	440	5	0.22	601.77
N16	6.7	100	440	5	10.00	521.11
N17	4.4	80	330	3	5.11	121.87
N18	4.4	80	330	3	5.11	118.89
N19	4.4	80	330	3	5.11	126.17

Abbreviations: η = dynamic viscosity, V = pulse voltage, dpi = print resolution, lay = number of layers, phd = print head distance from substrate, MB28 = Millijet® blue 28

Table 38: Summary of factor combinations and corresponding responses of the DoE performed with HPMC-based solutions (section 3.3.3.2)

Exp. name	grade	gap [µm]	v [mm/s]	T [°C]	WFT [µm]	DFT [µm]	lamella [µm]	dryT [min]	shR [µm/min]	WH [µm]	WL [min]
N1	606	300	6	30	203.8	31.4	1208.8	26.0	-6.8	200.7	0.64
N2	615	300	6	30	210.0	35.1	649.1	29.5	-6.0	204.5	0.78
N3	606	700	6	30	524.0	86.2	994.5	67.9	-6.4	515.5	0.77
N4	615	700	6	30	498.1	77.6	1106.1	60.8	-6.9	493.5	0.77
N5	606	300	18	30	205.1	35.4	1092.9	28.5	-5.9	199.9	0.59
N6	615	300	18	30	261.8	43.5	1325.6	35.5	-6.1	259.3	0.50
N7	606	700	18	30	498.5	83.1	658.0	60.0	-7.0	495.7	0.50
N8	615	700	18	30	497.0	94.7	880.7	61.7	-6.6	495.2	1.02
N9	606	300	6	50	207.8	37.4	548.4	5.6	-31.9	222.6	0.79
N10	615	300	6	50	180.2	32.0	323.4	5.3	-29.9	203.5	0.75
N11	606	700	6	50	581.3	90.7	995.7	18.5	-26.0	598.9	0.90
N12	615	700	6	50	485.2	113.2	492.2	13.7	-28.4	531.7	0.74
N13	606	300	18	50	190.8	37.3	288.3	5.2	-32.2	214.2	0.98
N14	615	300	18	50	223.6	38.2	257.4	6.5	-29.9	228.8	0.91
N15	606	700	18	50	496.1	90.5	1688.9	14.9	-27.8	521.9	1.07
N16	615	700	18	50	472.3	89.8	672.7	13.6	-29.5	504.3	0.98
N17	606	500	12	40	369.8	65.5	615.8	22.9	-13.3	368.4	0.77
N18	606	500	12	40	359.4	71.2	650.6	21.1	-13.8	357.2	0.78
N19	606	500	12	40	359.4	61.9	570.6	22.9	-13.1	354.9	0.86

Abbreviations: grade = HPMC grade, gap = gap width, v = drawing speed, T = drying temperature, WFT = wet film thickness, DFT = dry film thickness, lamella = initial lamella, dryT = drying time, shR = drying rate, WH = wave height, WL = wave length

Table 39: Summary of factor combinations and corresponding responses of the DoE performed with PVA-based solutions (section 3.3.3.2)

Exp. name	grade	gap [µm]	v [mm/s]	T [°C]	WFT [µm]	DFT [µm]	lamella [µm]	dryT [min]	shR [µm/min]	WH [µm]	WL [min]
N1	18-88	300	6	30	205.8	30.5	363.7	23.9	-7.2	202.4	0.5
N2	26-88	300	6	30	205.5	33.6	436.7	23.7	-7.2	195.8	0.6
N3	18-88	700	6	30	520.0	100.7	802.2	56.0	-7.5	512.7	0.7
N4	26-88	700	6	30	505.1	93.6	736.4	61.1	-6.7	495.3	0.6
N5	18-88	300	18	30	207.6	36.0	435.8	22.4	-7.6	201.8	0.5
N6	26-88	300	18	30	240.3	41.5	283.3	27.2	-7.3	237.0	0.5
N7	18-88	700	18	30	501.6	85.9	717.1	55.2	-7.5	493.3	0.5
N8	26-88	700	18	30	497.7	86.7	670.3	58.4	-7.0	499.3	0.5
N9	18-88	300	6	50	191.6	36.6	287.7	5.0	-33.9	205.5	0.8
N10	26-88	300	6	50	184.4	33.3	284.1	4.9	-32.0	191.1	0.8
N11	18-88	700	6	50	503.3	95.3	817.8	13.1	-31.6	511.8	0.9
N12	26-88	700	6	50	481.0	90.5	714.0	13.2	-30.0	487.6	0.8
N13	18-88	300	18	50	193.8	41.2	299.3	4.9	-34.8	201.3	0.8
N14	26-88	300	18	50	194.5	38.7	234.9	5.3	-31.5	200.1	1.0
N15	18-88	700	18	50	478.0	86.1	817.5	12.9	-31.2	482.4	1.0
N16	26-88	700	18	50	469.3	88.3	630.6	13.2	-29.4	471.7	1.0
N17	18-88	500	12	40	351.4	78.6	457.8	17.7	-15.9	352.4	0.8
N18	18-88	500	12	40	352.0	69.4	481.7	17.4	-16.5	343.5	0.9
N19	18-88	500	12	40	348.4	62.5	546.6	16.8	-17.0	336.4	0.7

Abbreviations: grade = HPMC grade, gap = gap width, v = drawing speed, T = drying temperature, WFT = wet film thickness, DFT = dry film thickness, lamella = initial lamella, dryT = drying time, shR = drying rate, WH = wave height, WL = wave length

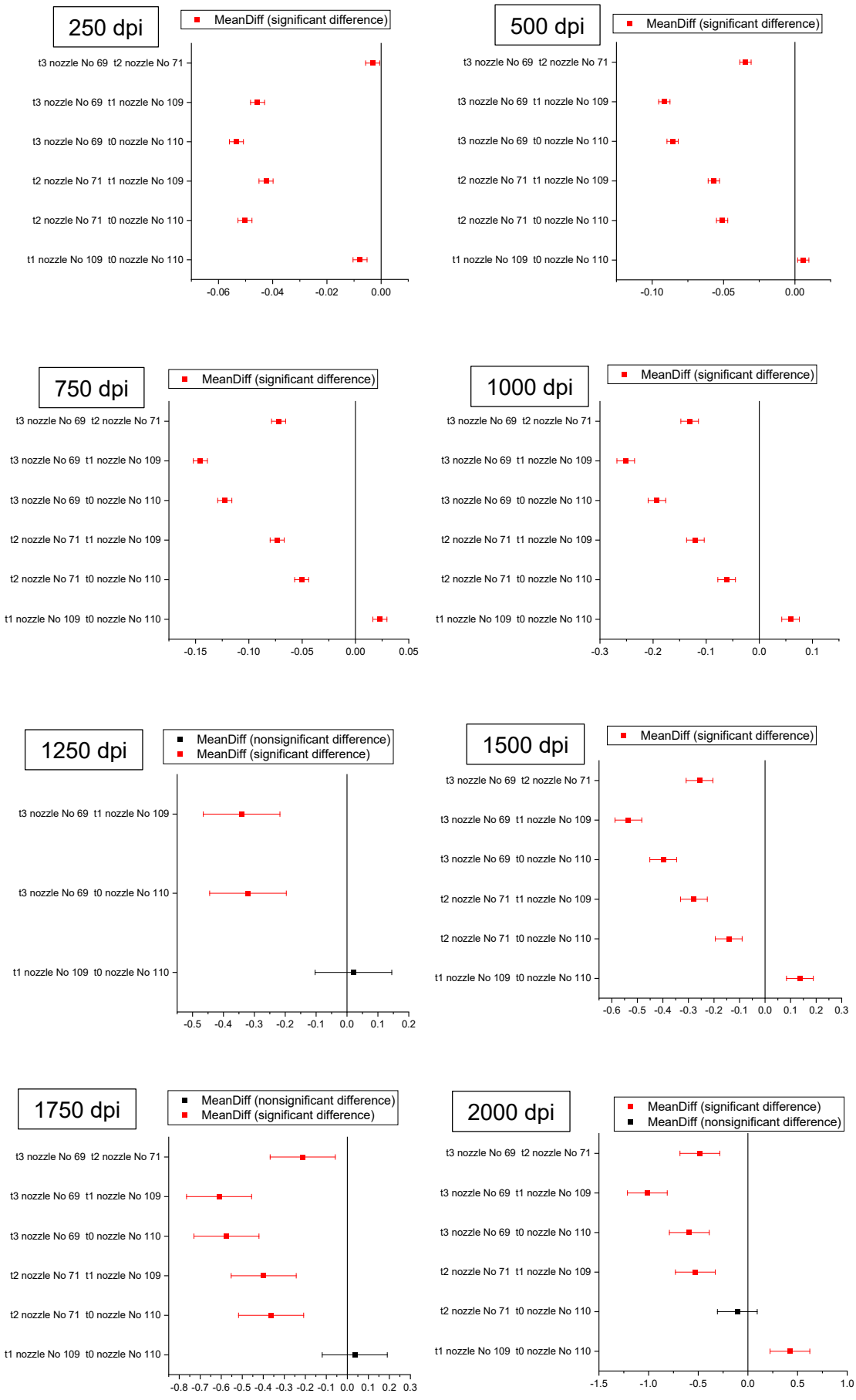

Figure 98: Comparison of means by Tuckey test during a time period of five months (section 3.2.5)

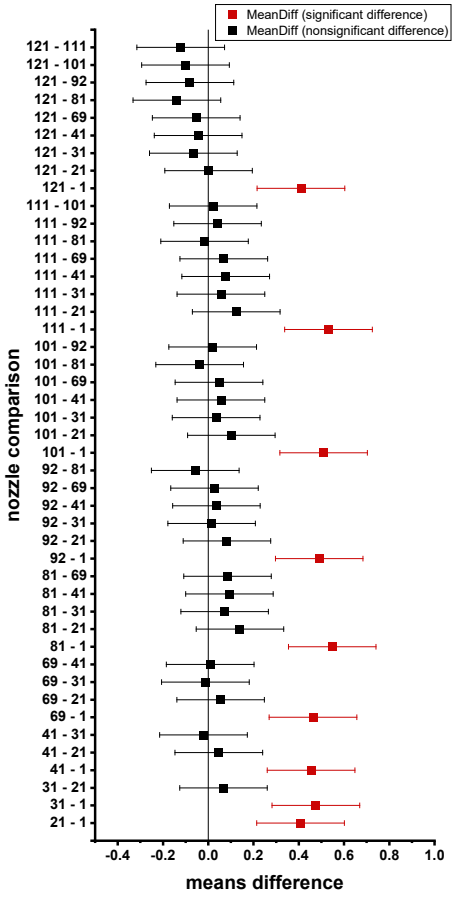

Figure 99: Comparison of means by Tuckey test at on operation day (section 3.2.5)

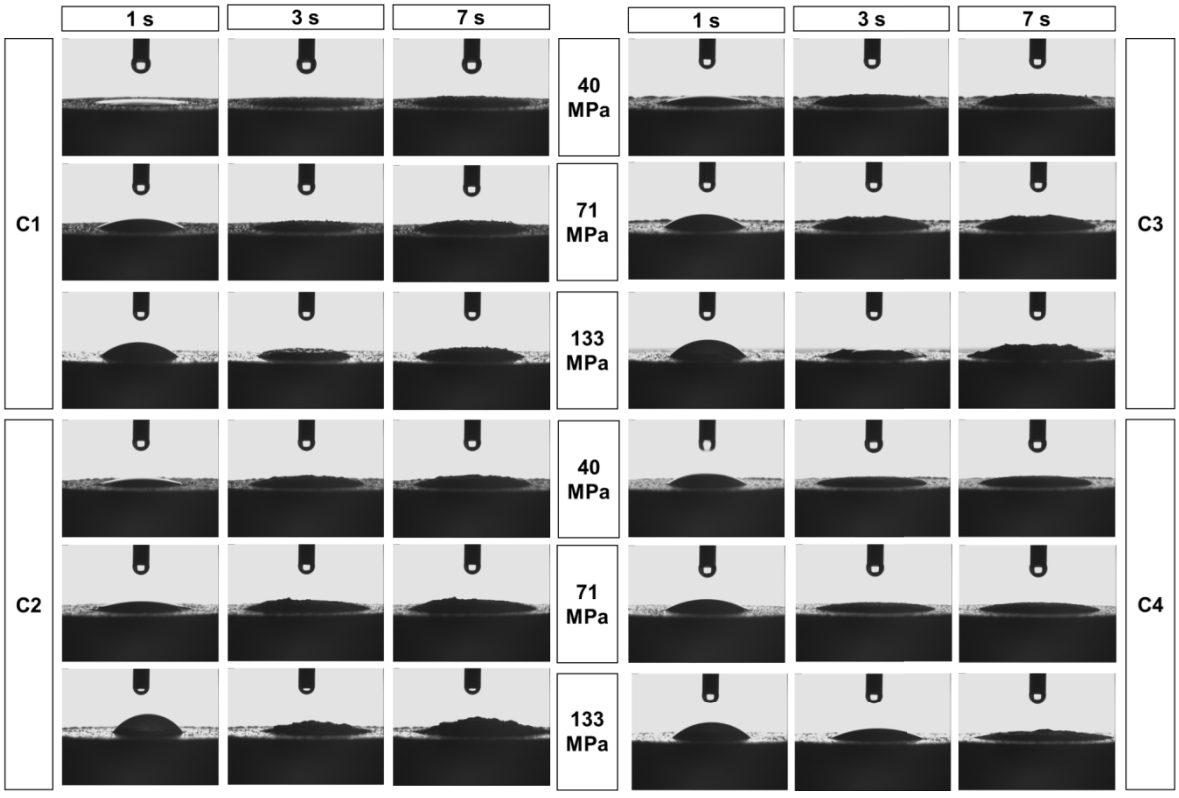

Figure 100: DSA images of tablets with applied drop of water (5 µl) at different time points and compression pressures (section 3.3.2.5)

7 Bibliography

[1] Srivastava, P., Drug metabolism and individualized medicine. *Curr Drug Metab,* 2003, *4* (1), 33-44.

[2] Evans, W. E.; Relling, M. V., Moving towards individualized medicine with pharmacogenomics. *Nature,* 2004, *429* (6990), 464-468.

[3] Abrahams, E.; Silver, M., The case for personalized medicine. *J Diabetes Sci Technol,* 2009, *3* (4), 680-684.

[4] Erikainen, S.; Chan, S., Contested futures: envisioning "personalized,""stratified," and precision" medicine. *New Genet Soc,* 2019, *38* (3), 308-330.

[5] Hood, L., A personal journey of discovery: developing technology and changing biology. *Annu Rev Anal Chem,* 2008, *1*, 1-43.

[6] Juengst, E.; McGowan, M. L.; Fishman, J. R.; Settersten Jr, R. A., From "personalized" to "precision" medicine: the ethical and social implications of rhetorical reform in genomic medicine. *Hastings Cent Rep,* 2016, *46* (5), 21-33.

[7] WHO (World Health Organization), *Priority medicines for Europe and the world "A public health Approach to innovation" - Background Paper 7.4 Pharmacogenetics and stratified medicine*, 2013.

[8] Drumond, N.; van Riet-Nales, D. A.; Karapinar-Çarkit, F.; Stegemann, S., Patients' appropriateness, acceptability, usability and preferences for pharmaceutical preparations: Results from a literature review on clinical evidence. *Int J Pharm,* 2017, *521* (1-2), 294-305.

[9] Wahlich, J.; Orlu, M.; Mair, A.; Stegemann, S.; van Riet-Nales, D., Age-related medicine. *Pharmaceutics* 2019, *1* (4), 172.

[10] Stegemann, S.; Ternik, R. L.; Onder, G.; Khan, M. A.; van Riet-Nales, D. A., Defining patient centric pharmaceutical drug product design. *AAPS J,* 2016, *18* (5), 1047-1055.

[11] Collins, F. S.; McKusick, V. A., Implications of the human genome project for medical science. *JAMA,* 2001, *285* (5), 540-544.

[12] Breitkreutz, J.; Boos, J., Paediatric and geriatric drug delivery. *Exp Opin Drug Deliv,* 2007, *4* (1), 37-45.

[13] Stegemann, S.; van Riet-Nales, D.; de Boer, A., Demographics in the 2020s - Longevity as a challenge for pharmaceutical drug development, prescribing, dispensing, patient care and quality of life. *Br J Clin Pharmacol,* 2020, *86* (10), 1899-1903.

[14] Madla, C. M.; Gavins, F. K. H.; Merchant, H.; Orlu, M.; Murdan, S.; Basit, A. W., Let's talk about sex: Differences in drug therapy in males and females. *Adv Drug Deliv Rev,* 2021.

[15] Doestzada, M.; Vila, A. V.; Zhernakova, A.; Koonen, D. P. Y.; Weersma, R. K.; Touw, D. J.; Kuipers, F.; Wijmenga, C.; Fu, J., Pharmacomicrobiomics: a novel route towards personalized medicine? *Protein Cell,* 2018, *9* (5), 432-445.

[16] Schleidgen, S.; Klingler, C.; Bertram, T.; Rogowski, W. H.; Marckmann, G., What is personalized medicine: sharpening a vague term based on a systematic literature review. *BMC Med Ethics,* 2013, *14* (1), 55.

[17] Cohen, J. S., Ways to minimize adverse drug reactions. *J Postgrad Med,* 1999, *106* (3), 163-172.

[18] Shariff, Z.; Kirby, D.; Missaghi, S.; Rajabi-Siahboomi, A.; Maidment, I., Patient-centric medicine design: Key characteristics of oral solid dosage forms that improve adherence and acceptance in older people. *Pharmaceutics,* 2020, *12* (10), 905.

[19] Minghetti, P.; Pantano, D.; Gennari, C. G. M.; Casiraghi, A., Regulatory framework of pharmaceutical compounding and actual developments of legislation in Europe. *Health Policy,* 2014, *117* (3), 328-333.

[20] ABDA (Arbeitsgemeinschaft der Berufsvertretungen Deutscher Apotheker), *Die Apotheke - Zahlen, Daten, Fakten 2021*, 2021.

[21] Gudeman, J.; Jozwiakowski, M.; Chollet, J.; Randell, M., Potential risks of pharmacy compounding. *Drugs R D,* 2013, *13* (1), 1-8.

[22] Tawab, M. In: *Verbesserung der Rezepturkompetenz durch ZL-Ringversuche - Besser als jedes Audit*, expopharm, 2020.

[23] European Parliament, *Regulation (EC) No 1901/2006 of the European Parliamant and of the Council of 12 December 2006 on medicinal products for paediatric use*, 2006.

[24] FDA (Food and Drug Administration), The FDA modernization act of 1997. https://www.fda.gov/regulatory-information/food-and-drug-administration-modernization-act-fdama-1997/fda-backgrounder-fdama (accessed 04 July 2021).

[25] Tomasi, P. A.; Egger, G. F.; Pallidis, C.; Saint-Raymond, A., Enabling development of paediatric medicines in Europe: 10 years of the EU paediatric regulation. *Pediatr Drugs,* 2017, *19* (6), 505-513.

[26] Strickley, R. G., Pediatric oral formulations: An updated review of commercially available pediatric oral formulations since 2007. *J Pharm Sci,* 2019, *108* (4), 1335-1365.

[27] Heitman, T.; Day, A.; Bassani, A. S., Pediatric compounding pharmacy: taking on the responsibility of providing quality customized prescriptions. *Children,* 2019, *6* (5), 66.

[28] EMA (European Medicines Agency), *EMA geriatric medicines strategy EMA/CHMP/137793/2011*, 2011.

[29] EMA (European Medicines Agency), *Reflection paper on the pharmaceutical development of medicines for use in the older population*, 2020.

[30] Wening, K.; Breitkreutz, J., Oral drug delivery in personalized medicine: Unmet needs and novel approaches. *Int J Pharm,* 2011, *404* (1), 1-9.

[31] FDA (Food and Drug Administration), Kymriah (tisagenlecleucel). https://www.fda.gov/media/107296/download (accessed 20 September 2021).

[32] Bundesministerium für Gesundheit, E-Health – Digitalisierung im Gesundheitswesen. https://www.bundesgesundheitsministerium.de/e-health-initiative.html (accessed 20 September 2021).

[33] Preis, M.; Breitkreutz, J.; Sandler, N., Perspective: Concepts of printing technologies for oral film formulations. *Int J Pharm,* 2015, *494* (2), 578-84.

[34] Genina, N.; Fors, D.; Vakili, H.; Ihalainen, P.; Pohjala, L.; Ehlers, H.; Kassamakov, I.; Haeggstrom, E.; Vuorela, P.; Peltonen, J.; Sandler, N., Tailoring controlled-release oral dosage forms by combining inkjet and flexographic printing techniques. *Eur J Pharm Sci,* 2012, *47* (3), 615-23.

[35] Janßen, E. M.; Schliephacke, R.; Breitenbach, A.; Breitkreutz, J., Drug-printing by flexographic printing technology — A new manufacturing process for orodispersible films. *Int J Pharm,* 2013, *441* (1–2), 818-825.

[36] Wickström, H.; Koppolu, R.; Mäkilä, E.; Toivakka, M.; Sandler, N., Stencil printing—A novel manufacturing platform for orodispersible discs. *Pharmaceutics,* 2020, *12* (1).

[37] Sandler, N.; Maattanen, A.; Ihalainen, P.; Kronberg, L.; Meierjohann, A.; Viitala, T.; Peltonen, J., Inkjet printing of drug substances and use of porous substrates-towards individualized dosing. *J Pharm Sci,* 2011, *100* (8), 3386-95.

[38] Voura, C.; Khinast, J. G.; Zimmer, A.; Brenn, G.; Bauer, W.; Eitzinger, B.; Strohmeier, D.; Schroedl, N.; Gruber, M. M., Printable medicines: a microdosing device for producing personalized medicines. *Pharm Technol Eur,* 2011, *23* (1), 32-36.

[39] Alomari, M.; Mohamed, F. H.; Basit, A. W.; Gaisford, S., Personalised dosing: printing a dose of one's own medicine. *Int J Pharm,* 2015, *494* (2), 568-577.

[40] Thabet, Y.; Sibanc, R.; Breitkreutz, J., Printing pharmaceuticals by inkjet technology: Proof of concept for stand-alone and continuous in-line printing on orodispersible films. *J Manuf Processes,* 2018, *35*, 205-215.

[41] Kiefer, O.; Fischer, B.; Breitkreutz, J., Fundamental investigations into metoprolol tartrate deposition on orodispersible films by inkjet printing for individualised drug dosing. *Pharmaceutics,* 2021, *13* (2), 247.

[42] UKHD (Universitätsklinikum Heidelberg), Arzneimittel in exakter Dosierung „drucken". https://www.klinikum.uni-heidelberg.de/newsroom/arzneimittel-in-exakter-dosierung-drucken/ (accessed 28 August 2021).

[43] Dachtler, M.; Huber, G.; Pries, T., 2D & 3D-Print-Technologien in der pharmazeutischen Industrie. In: *Digitale Transformation von Dienstleistungen im Gesundheitswesen VII: Impulse für die Pharmaindustrie*, Pfannstiel, M. A.; Da-Cruz, P.; Rederer, E., Eds. Springer Fachmedien Wiesbaden: Wiesbaden, 2020; pp 53-66.

[44] Merck, Transform your clinical trials supply from complex to easy. https://www.merckgroup.com/en/research/innovation-center/highlights/onezeromed.html (accessed 28 August 2021).

[45] Öblom, H.; Sjöholm, E.; Rautamo, M.; Sandler, N., Towards printed pediatric medicines in hospital pharmacies: Comparison of 2D and 3D-printed orodispersible warfarin films with conventional oral powders in unit dose sachets. *Pharmaceutics,* 2019, *11* (7), 334.

[46] Zipdose® technology. https://www.aprecia.com/technology/zipdose (accessed 28 August 2021).

[47] DFE Pharma, New research in 3D printing shows benefits of powder bed printed tablets. https://dfepharma.com/Corporate/News-and-Events/News/New-research-in-3D-printing-shows-benefits-of-powder-bed-printed-tablets (accessed 13 September 2021).

[48] Le, H. P., Progress and trends in ink-jet printing technology. *J Imaging Sci Technol,* 1998, *42* (1), 49-62.

[49] Rayleigh, L., On the instability of jets. *Proceedings of the London Mathematical Society,* 1878, *1* (1), 4-13.

[50] Hoath, S. D., *Fundamentals of inkjet printing: The science of inkjet and droplets*. Wiley-VCH Verlag Weinheim, Germany: 2016.

[51] Wijshoff, H., The dynamics of the piezo inkjet printhead operation. *Phys Rep,* 2010, *491* (4), 77-177.

[52] Derby, B., Inkjet printing of functional and structural materials: fluid property requirements, feature stability, and resolution. *Annu Rev Mater Res,* 2010, *40*, 395-414.

[53] Morita, N.; Khalate, A. A.; van Buul, A. M.; Wijshoff, H., Inkjet printheads. In: *Fundamentals of inkjet printing: the science of inkjet and droplets*, Hoath, S. D., Ed. Wiley-VCH Verlag Weinheim, Germany: 2016; pp 57-92.

[54] Brünahl, J.; Grishin, A. M., Piezoelectric shear mode drop-on-demand inkjet actuator. *Sens Actuator A Phys,* 2002, *101* (3), 371-382.

[55] ImageXpert, The history of (and differences between) piezo, thermal, and continuous inkjet printing. https://imagexpert.com/the-history-of-and-differences-between-piezo-thermal-and-continuous-inkjet-printing/ (accessed 20 September 2021).

[56] Bale, M., A system approch to develop new platforms of industrial inkjet inks. In: *Handbook of industrial printing - A full system approach*, Zapka, W., Ed. John Wiley & Sons: 2018; pp 25-58.

[57] Fromm, J. E., Numerical calculation of the fluid dynamics of drop-on-demand jets. *IBM J Res Dev,* 1984, *28* (3), 322-333.

[58] Derby, B.; Reis, N.; Seerden, K.; Grant, P.; Evans, J., Freeform fabrication of ceramics by hot-melt ink-jet printing. *Mater Res Soc Symp Proc,* 2000, *625*.

[59] Jang, D.; Kim, D.; Moon, J., Influence of fluid physical properties on ink-jet printability. *Langmuir,* 2009, *25* (5), 2629-2635.

[60] Derby, B.; Reis, N., Inkjet printing of highly loaded particulate suspensions. *MRS Bull,* 2003, *28* (11), 815-818.

[61] Stow, C. D.; Hadfield, M. G., An experimental investigation of fluid flow resulting from the impact of a water drop with an unyielding dry surface. *Proc R Soc Lond A,* 1981, *373* (1755), 419-441.

[62] Mundo, C.; Sommerfeld, M.; Tropea, C., Droplet-wall collisions: experimental studies of the deformation and breakup process. *Int J Multiph Flow,* 1995, *21* (2), 151-173.

[63] Schmidt, W. A., Paper and paper-based substrates for industrial inkjet printing. In: *Handbook of industrial inkjet printing - A full system approach*, Zapka, W., Ed. John Wiley & Sons: 2018; pp 363-372.

[64] EU (European Union), *Directive 2011/62/EU of the European Parliament and of the Council*, 2011, pp 74-87.

[65] FDA (Food and Drug Administration), *Code of Federal Regulations (CFR) Title 21 Part 206: Imprinting of solid oral dosage form drug products for human use*, 2020.

[66] Qualicaps, Imprinting machines. https://www.qualicaps.com/en/Equipment/ouroffering/Tablets/imprintingmachines (accessed 21 September 2021).

[67] Ackley Machine, Machines - Laser drilling and printing machines for pharmaceutical, nutraceutical and confectionery applications. https://ackleymachine.com/machines/ (accessed 21 September 2021).

[68] Packiging World, Hewlett-Packard: Pharma ink-jet print cartridge. https://www.packworld.com/home/product/13342916/hewlettpackard-pharma-inkjet-print-cartridge (accessed 21 September 2021).

[69] Yamanouchi, T.; Mizoguchi, M.; Kinoshita, N.; Saeki, T.; Sadamoto, K.; Takai, Y.; Tanaka, M.; Sadamoto, T. In: *Idea for Unit-Dose Packaging in Japan*, 17th IAPRI World Conference on Packaging, 2010.

[70] Latest model of inkjet tablet press developed to automate production systems. http://labelandpackaging.4your.biz/index.php/print/digitalprinting/7056-latest-model-of-inkjet-tablet-press-developed-to-automate-production-systems (accessed 29 December 2021).

[71] Schena, M.; Heller, R. A.; Theriault, T. P.; Konrad, K.; Lachenmeier, E.; Davis, R. W., Microarrays: biotechnology's discovery platform for functional genomics. *Trends in Biotechnol*, 1998, *16* (7), 301-306.

[72] Lemmo, A. V.; Rose, D. J.; Tisone, T. C., Inkjet dispensing technology: applications in drug discovery. *Curr Opin Biotechnol,* 1998, *9* (6), 615-7.

[73] Tarcha, P. J.; Verlee, D.; Hui, H. W.; Setesak, J.; Antohe, B.; Radulescu, D.; Wallace, D., The application of ink-jet technology for the coating and loading of drug-eluting stents. *Ann Biomed Eng,* 2007, *35* (10), 1791-1799.

[74] Nganga, S.; Moritz, N.; Kolakovic, R.; Jakobsson, K.; Nyman, J. O.; Borgogna, M.; Travan, A.; Crosera, M.; Donati, I.; Vallittu, P. K., Inkjet printing of chitlac-nanosilver — a method to create functional coatings for non-metallic bone implants. *Biofabrication,* 2014, *6* (4), 041001.

[75] Boehm, R.; Miller, P.; Hayes, S.; Monteiro-Riviere, N.; Narayan, R., Modification of microneedles using inkjet printing. *AIP Adv,* 2011, *1* (2), 022139.

[76] Melendez, P. A.; Kane, K. M.; Ashvar, C. S.; Albrecht, M.; Smith, P. A., Thermal inkjet application in the preparation of oral dosage forms: dispensing of prednisolone solutions and polymorphic characterization by solid-state spectroscopic techniques. *J Pharm Sci*, 2008, *97* (7), 2619-36.

[77] FDA (Food and Drug Administration), Highlights of prescribing information. https://www.accessdata.fda.gov/drugsatfda_docs/nda/2015/207958Orig1s000lbl.pdf (accessed 28 August 2021).

[78] Edinger, M.; Iftimi, L.-D.; Markl, D.; Al-Sharabi, M.; Bar-Shalom, D.; Rantanen, J.; Genina, N., Quantification of inkjet-printed pharmaceuticals on porous substrates

using Raman spectroscopy and near-infrared spectroscopy. *AAPS PharmSciTech,* 2019, *20* (5), 207.

[79] Turković, E.; Vasiljević, I.; Drašković, M.; Obradović, N.; Vasiljević, D.; Parojčić, J., An investigation into mechanical properties and printability of potential substrates for inkjet printing of orodispersible films. *Pharmaceutics,* 2021, *13* (4), 468.

[80] Genina, N.; Fors, D.; Palo, M.; Peltonen, J.; Sandler, N., Behavior of printable formulations of loperamide and caffeine on different substrates-effect of print density in inkjet printing. *Int J Pharm,* 2013, *453* (2), 488-97.

[81] Öblom, H.; Cornett, C.; Bøtker, J.; Frokjaer, S.; Hansen, H.; Rades, T.; Rantanen, J.; Genina, N., Data-enriched edible pharmaceuticals (DEEP) of medical cannabis by inkjet printing. *Int J Pharm,* 2020, 119866.

[82] Cheow, W. S.; Kiew, T. Y.; Hadinoto, K., Combining inkjet printing and amorphous nanonization to prepare personalized dosage forms of poorly-soluble drugs. *Eur J Pharm Biopharm,* 2015, *96*, 314-21.

[83] Buanz, A. B.; Belaunde, C. C.; Soutari, N.; Tuleu, C.; Gul, M. O.; Gaisford, S., Ink-jet printing versus solvent casting to prepare oral films: effect on mechanical properties and physical stability. *Int J Pharm,* 2015, *494* (2), 611-618.

[84] Eleftheriadis, G. K.; Monou, P. K.; Bouropoulos, N.; Fatouros, D. G., In vitro evaluation of 2D-printed edible films for the buccal delivery of diclofenac sodium. *Materials,* 2018, *11* (5), 864.

[85] Thabet, Y.; Lunter, D.; Breitkreutz, J., Continuous inkjet printing of enalapril maleate onto orodispersible film formulations. *Int J Pharm,* 2018.

[86] Wickström, H.; Hilgert, E.; Nyman, J. O.; Desai, D.; Şen Karaman, D.; de Beer, T.; Sandler, N.; Rosenholm, J. M., Inkjet printing of drug-loaded mesoporous silica nanoparticles—A platform for drug development. *Molecules,* 2017, *22* (11), 2020.

[87] Kollamaram, G.; Faucher, A.; Croker, D. M.; Walker, G. M., Valvejet technology for the production of a personalised fixed dose combination of ramipril and glimepiride: An investigative study on the stability of ramipril. *Pharm Res,* 2018, *35* (9), 181.

[88] Arshad, M. S.; Shahzad, A.; Abbas, N.; AlAsiri, A.; Hussain, A.; Kucuk, I.; Chang, M.-W.; Bukhari, N. I.; Ahmad, Z. J. P. d.; technology, Preparation and characterization of indomethacin loaded films by piezoelectric inkjet printing: a personalized medication approach. 2020, *25* (2), 197-205.

[89] Kollamaram, G.; Hopkins, S. C.; Glowacki, B. A.; Croker, D. M.; Walker, G. M., Inkjet printing of paracetamol and indomethacin using electromagnetic technology: Rheological compatibility and polymorphic selectivity. *Eur J Pharm Sci,* 2018, *115*, 248-257.

[90] Alomari, M.; Vuddanda, P. R.; Trenfield, S. J.; Dodoo, C. C.; Velaga, S.; Basit, A. W.; Gaisford, S., Inkjet printing of T3 and T4 oral drug combinations as a novel strategy for hypothyroidism. *Int J Pharm,* 2018.

[91] Vakili, H.; Wickström, H.; Desai, D.; Preis, M.; Sandler, N., Application of a handheld NIR spectrometer in prediction of drug content in inkjet printed orodispersible

formulations containing prednisolone and levothyroxine. *Int J Pharm,* 2017, *524* (1–2), 414-423.

[92] Palo, M.; Kogermann, K.; Laidmäe, I.; Meos, A.; Preis, M.; Heinämäki, J.; Sandler, N., Development of oromucosal dosage forms by combining electrospinning and inkjet printing. *Mol Pharm,* 2017.

[93] Khor, Y. M.; Gaisford, S.; Carpenter, G. H.; Raimi-Abraham, B. T., Inkjet printed melatonin on poly(vinyl alcohol) oral films: Uptake in an ex vivo oral mucosal pellicle model. *Mat High,* 2020.

[94] Stranzinger, S.; Wolfgang, M.; Klotz, E.; Scheibelhofer, O.; Ghiotti, P.; Khinast, J. G.; Hsiao, W.-K.; Paudel, A., Near-infrared hyperspectral imaging as a monitoring tool for on-demand manufacturing of inkjet-printed formulations. *AAPS PharmSciTech,* 2021, *22* (6), 1-10.

[95] Planchette, C.; Pichler, H.; Wimmer-Teubenbacher, M.; Gruber, M.; Gruber-Woelfler, H.; Mohr, S.; Tetyczka, C.; Hsiao, W. K.; Paudel, A.; Roblegg, E.; Khinast, J., Printing medicines as orodispersible dosage forms: Effect of substrate on the printed microstructure. *Int J Pharm,* 2016, *509* (1-2), 518-27.

[96] Wimmer-Teubenbacher, M.; Planchette, C.; Pichler, H.; Markl, D.; Hsiao, W. K.; Paudel, A.; Stegemann, S., Pharmaceutical-grade oral films as substrates for printed medicine. *Int J Pharm,* 2018, *547* (1), 169-180.

[97] Vakili, H.; Nyman, J. O.; Genina, N.; Preis, M.; Sandler, N., Application of a colorimetric technique in quality control for printed pediatric orodispersible drug delivery systems containing propranolol hydrochloride. *Int J Pharm,* 2016, *511* (1), 606-618.

[98] Genina, N.; Janssen, E. M.; Breitenbach, A.; Breitkreutz, J.; Sandler, N., Evaluation of different substrates for inkjet printing of rasagiline mesylate. *Eur J Pharm Biopharm,* 2013, *85* (3 Pt B), 1075-83.

[99] Buanz, A. B.; Saunders, M. H.; Basit, A. W.; Gaisford, S., Preparation of personalized-dose salbutamol sulphate oral films with thermal ink-jet printing. *Pharm Res,* 2011, *28* (10), 2386-2392.

[100] Vuddanda, P. R.; Alomari, M.; Dodoo, C. C.; Trenfield, S. J.; Velaga, S.; Basit, A. W.; Gaisford, S., Personalisation of warfarin therapy using thermal ink-jet printing. *Eur J Pharm Sci,* 2018, *117*, 80-87.

[101] Visser, J. C.; Wibier, L.; Kiefer, O.; Orlu, M.; Breitkreutz, J.; Woerdenbag, H. J.; Taxis, K., A pediatrics utilization study in the netherlands to identify active pharmaceutical ingredients suitable for inkjet printing on orodispersible films. *Pharmaceutics,* 2020, *12* (2), 164.

[102] Scoutaris, N.; Alexander, M. R.; Gellert, P. R.; Roberts, C. J., Inkjet printing as a novel medicine formulation technique. *J Control Release,* 2011, *156* (2), 179-85.

[103] Scoutaris, N.; Hook, A. L.; Gellert, P. R.; Roberts, C. J.; Alexander, M. R.; Scurr, D. J., ToF-SIMS analysis of chemical heterogenities in inkjet micro-array printed drug/polymer formulations. *J Mater Sci Mater Med,* 2012, *23* (2), 385-391.

[104] Wickström, H.; Palo, M.; Rijckaert, K.; Kolakovic, R.; Nyman, J. O.; Maattanen, A.; Ihalainen, P.; Peltonen, J.; Genina, N.; de Beer, T.; Lobmann, K.; Rades, T.; Sandler, N.,

Improvement of dissolution rate of indomethacin by inkjet printing. *Eur J Pharm Sci,* 2015, *75*, 91-100.

[105] Edinger, M.; Bar-Shalom, D.; Rantanen, J.; Genina, N., Visualization and non-destructive quantification of inkjet-printed pharmaceuticals on different substrates using Raman spectroscopy and Raman chemical imaging. *Pharm Res,* 2017, 1-14.

[106] Bonhoeffer, B.; Kwade, A.; Juhnke, M., Impact of formulation properties and process parameters on the dispensing and depositioning of drug nanosuspensions using micro-valve technology. *J Pharm Sci,* 2017, *106* (4), 1102-1110.

[107] Clarke, A.; Doughty, D., Development of liquid dispensing technology for the manufacture of low dose drug products. In: *Continuous manufacturing of pharmaceuticals*, Kleinebudde, P.; Khinast, J.; Rantanen, J., Eds. John Wiley & Sons: 2017; pp 551-557.

[108] Radcliffe, A. J.; Hilden, J. L.; Nagy, Z. K.; Reklaitis, G. V., Dropwise additive manufacturing of pharmaceutical products using particle suspensions. *J PharmSci,* 2019, *108* (2), 914-928.

[109] Ph. Eur. 9.3, *1807 Oromucosal preparations*, In: European Pharmacopoeia Comission (Ed.). European Pharmacopoeia, European Directorate for the Quality of Medicines & Healthcare (EDQM), Strasbourg, France, 2017.

[110] Borges, A. F.; Silva, C.; Coelho, J. F.; Simões, S., Outlining critical quality attributes (CQAs) as guidance for the development of orodispersible films. *Pharm Dev Technol,* 2017, *22* (2), 237-245.

[111] Visser, J. C.; Dohmen, W. M. C.; Hinrichs, W. L. J.; Breitkreutz, J.; Frijlink, H. W.; Woerdenbag, H. J., Quality by design approach for optimizing the formulation and physical properties of extemporaneously prepared orodispersible films. *Int J Pharm,* 2015, *485* (1), 70-76.

[112] Borges, A. F.; Silva, C.; Coelho, J. F.; Simões, S., Oral films: current status and future perspectives: I - galenical development and quality attributes. *J Control Release,* 2015, *206*, 1-19.

[113] Ph. Eur. 10.0, *0478 Tablets - Orodispersible tablets*, In: European Pharmacopoeia Comission (Ed.). European Pharmacopoeia, European Directorate for the Quality of Medicines & Healthcare (EDQM), Strasbourg, France, 2020.

[114] FDA (Food and Drug Administration), *Guidance for industry: orally disintegrating tablets*, Center for Drug Evaluation and Research (CDER), 2008, pp 1-3.

[115] Hoffmann, E. M.; Breitenbach, A.; Breitkreutz, J., Advances in orodispersible films for drug delivery. *Expert Opin Drug Deliv,* 2011, *8* (3), 299-316.

[116] Preis, M.; Knop, K.; Breitkreutz, J., Mechanical strength test for orodispersible and buccal films. *Int J Pharm,* 2014, *461* (1), 22-29.

[117] FDA (Food and Drug Administration), Zuplenz (ondansetron) oral soluble film, 4 mg and 8 mg. https://www.accessdata.fda.gov/drugsatfda_docs/nda/2010/022524_zuplenz_toc.cfm (accessed 22 September 2021).

[118] Borges, A. F.; Silva, C.; Coelho, J. F. J.; Simões, S., Oral films: Current status and future perspectives II — Intellectual property, technologies and market needs. *J Control Release,* 2015, *206*, 108-121.

[119] Visser, J. C.; Wibier, L.; Mekhaeil, M.; Woerdenbag, H. J.; Taxis, K. J. I. J. o. C. P., Orodispersible films as a personalized dosage form for nursing home residents, an exploratory study. *Int J Clin Pharm,* 2020, 1-9.

[120] Visser, J. C.; Woerdenbag, H. J.; Crediet, S.; Gerrits, E.; Lesschen, M. A.; Hinrichs, W. L. J.; Breitkreutz, J.; Frijlink, H. W., Orodispersible films in individualized pharmacotherapy: The development of a formulation for pharmacy preparations. *Int J Pharm,* 2015, *478* (1), 155-163.

[121] Orlu, M.; Ranmal, S. R.; Sheng, Y.; Tuleu, C.; Seddon, P., Acceptability of orodispersible films for delivery of medicines to infants and preschool children. *Drug Deliv,* 2017, *24* (1), 1243-1248.

[122] Klingmann, V.; Pohly, C. E.; Meissner, T.; Mayatepek, E.; Möltner, A.; Flunkert, K.; Breitkreutz, J.; Bosse, H. M., Acceptability of an orodispersible film compared to syrup in neonates and infants: A randomized controlled trial. *Eur J Pharm Biopharm,* 2020, *151*, 239-245.

[123] Steiner, D.; Finke, J. H.; Kwade, A., Instant ODFs–Development of an intermediate, nanoparticle-based product platform for individualized medication. *Eur J Pharm Biopharm,* 2017.

[124] Steiner, D.; Finke, J. H.; Kwade, A., Efficient production of nanoparticle-loaded orodispersible films by process integration in a stirred media mill. *Int J Pharm,* 2016, *511* (2), 804-813.

[125] Speer, I.; Lenhart, V.; Preis, M.; Breitkreutz, J., Prolonged release from orodispersible films by incorporation of diclofenac-loaded micropellets. *Int J Pharm,* 2019, *554*, 149-160.

[126] Iftimi, L.-D.; Edinger, M.; Bar-Shalom, D.; Rantanen, J.; Genina, N., Edible solid foams as porous substrates for inkjet-printable pharmaceuticals. *Eur J Pharm Biopharm,* 2019, *136*, 38-47.

[127] Łyszczarz, E.; Brniak, W.; Szafraniec-Szczesny, J.; Majka, T.; Majda, D.; Zych, M.; Pielichowski, K.; Jachowicz, R., The impact of the preparation method on the properties of orodispersible films with aripiprazole: Electrospinning vs. casting and 3D printing methods. *Pharmaceutics,* 2021, *13 (8)*, 1122.

[128] Low, A. Q. J.; Parmentier, J.; Khong, Y. M.; Chai, C. C. E.; Tun, T. Y.; Berania, J. E.; Liu, X.; Gokhale, R.; Chan, S. Y., Effect of type and ratio of solubilising polymer on characteristics of hot-melt extruded orodispersible films. *Int J Pharm,* 2013, *455* (1), 138-147.

[129] Tian, Y.; Bhide, Y. C.; Woerdenbag, H. J.; Huckriede, A. L. W.; Frijlink, H. W.; Hinrichs, W. L. J.; Visser, J. C., Development of an orodispersible film containing stabilized influenza vaccine. *Pharmaceutics,* 2020, *12* (3), 245.

[130] Gupta, M. S.; Kumar, T. P., The potential of ODFs as carriers for drugs/vaccines against COVID-19. *Drug Dev Ind Pharm,* 2021, *47* (2), 179-188.

[131] Sjöholm, E.; Mathiyalagan, R.; Prakash, D. R.; Lindfors, L.; Wang, Q.; Wang, X.; Ojala, S.; Sandler, N., 3D-printed veterinary dosage forms–A comparative study of three semi-solid extrusion printers. *Pharmaceutics,* 2020, *12* (12), 1239.

[132] Traas, A. M.; Fleck, T.; Ellings, A.; Mahabir, S.; Stuebner, K.; Brown, D. C.; Durso, D.; DiGregorio, M.; Bode, L.; Kievit, K. I., Ease of oral administration and owner-perceived acceptability of triglyceride oil, dissolving thin film strip, and gelatin capsule formulations to healthy cats. *Am J Vet Res,* 2010, *71* (6), 610-614.

[133] Heumann Pharma, *Fachinformation Metoprolol Heumann*, 2021.

[134] Gelbe-Liste Pharmindex, Metoprolol. https://www.gelbe-liste.de/wirkstoffe/Metoprolol_455 (accessed 23 September 2021).

[135] Ph. Eur. 10.0, *1028 Metoprolol tartrate*, In: European Pharmacopoeia Comission (Ed.). European Pharmacopoeia, European Directorate for the Quality of Medicines & Healthcare (EDQM), Strasbourg, France, 2020.

[136] FDA (Food and Drug Administration), *Waiver of in vivo bioavailability and bioequivalence studies for immediate-release solid oral dosage forms based on a biopharmaceutics classification system - Guidance for industry*, 2017.

[137] Albers, S.; Elshoff, J. P.; Völker, C.; Richter, A.; Läer, S., HPLC quantification of metoprolol with solid-phase extraction for the drug monitoring of pediatric patients. *Biomed Chromatogr,* 2005, *19* (3), 202-207.

[138] Hsien, L.; Breddemann, A.; Frobel, A.-K.; Heusch, A.; Schmidt, K. G.; Läer, S., Off-label drug use among hospitalised children: identifying areas with the highest need for research. *Pharm World Sci,* 2008, *30* (5), 497-502.

[139] Nachtwey, J. *Stabilitätsuntersuchungen einer oralen Metoprololtartratlösung zur Anwendung in der Pädiatrie*. Diploma thesis, Friedrich-Schiller-Universität Jena, 2013.

[140] Weis, M. In: *Perorale Liquida für die Pädiatrie in deutschen Krankenhäusern – Status quo 2016*, 16. Symposium Herstellung in der Krankenhausapotheke - Eigenherstellung von Parenteralia und Oralia, 10-11 November 2016; ADKA: Berlin, Germany, 2016.

[141] Blake, C. M.; Kharasch, E. D.; Schwab, M.; Nagele, P., A meta-analysis of CYP2D6 metabolizer phenotype and metoprolol pharmacokinetics. *Clin Pharmacol Ther,* 2013, *94* (3), 394-399.

[142] Frobel, A.-K. *Untersuchung der Pharmakokinetik von Bisoprolol bei Kindern in einer klinischen Studie und mit physiologiebasierter Simulation als Konsequenz aus einem systematischen Cochrane-Review und als Beitrag zur Optimierung zukünftiger Studien*. Doctoral thesis, Heinrich-Heine-Universität Düsseldorf, 2010.

[143] *Metoprololtartrat*, In: ABDA – Bundesvereinigung Deutscher Apothekerverbände (Ed.). Rezepturhinweise - Deutscher Arzneimittel-Codex®/Neues Rezeptur-Formularium® (DAC/NRF), Govi-Verlag/Avoxa – Mediengruppe Deutscher Apotheker, Eschborn, Germany, 2021.

[144] Hellekson, K. L. U.S. Department of Health and Human Services, *The forth report on the diagnosis, evaluation, and treatment of high blood pressure in children and adolescents*, 0002-838X; 2005, p 1014.

[145] *NRF-Rezepturvorschriften 10.3. Metoprololtartrat-Lösung 1 mg/mL*, In: ABDA – Bundesvereinigung Deutscher Apothekerverbände (Ed.). Rezepturhinweise - Deutscher Arzneimittel-Codex®/Neues Rezeptur-Formularium® (DAC/NRF), Govi-Verlag/Avoxa – Mediengruppe Deutscher Apotheker, Eschborn, Germany, 2020.

[146] Sanofi-Aventis, *Fachinformation L-Thyroxin Henning®*, 2018.

[147] Fliers, E.; Demeneix, B.; Bhaseen, A.; Brix, T. H., European Thyroid Association (ETA) and Thyroid Federation International (TFI) joint position statement on the interchangeability of levothyroxine products in EU countries. *Eur Thyroid J,* 2018, *7* (5), 238-242.

[148] *Levothyroxin-Natrium*, In: ABDA – Bundesvereinigung Deutscher Apothekerverbände (Ed.). Rezepturhinweise - Deutscher Arzneimittel-Codex®/Neues Rezeptur-Formularium® (DAC/NRF), Govi-Verlag/Avoxa – Mediengruppe Deutscher Apotheker, Eschborn, Germany, 2016.

[149] Lindenberg, M.; Kopp, S.; Dressman, J. B., Classification of orally administered drugs on the World Health Organization Model list of Essential Medicines according to the biopharmaceutics classification system. *Eur J Pharm Biopharm,* 2004, *58* (2), 265-278.

[150] Gelbe Liste Pharmindex, Levothyroxin. https://www.gelbe-liste.de/wirkstoffe/Levothyroxin_18511 (accessed 25 September 2021).

[151] Grandt, D.; Lappe, V.; Schubert, I. BARMER Institut für Gesundheitsforschung, *BARMER Arzneimittelreport 2021 - Arzneimitteltherapie in der Schwangerschaft und bei Frauen im gebärfähigen Alter*, 2021, p 41.

[152] Free U.S. outpatient drug usage statistics - The top 200 drugs of 2019. https://clincalc.com/DrugStats/ (accessed 25 September 2021).

[153] Abrantes, C. G.; Duarte, D.; Reis, C. P., An overview of pharmaceutical excipients: safe or not safe? *J Pharm Sci,* 2016, *105* (7), 2019-2026.

[154] Sicherheitsdatenblatt Millijet® blue 28. *Milliken Chemical,* v. 1.0. 2015, pp 1-8.

[155] Hsu, H. y.; Toth, S. J.; Simpson, G. J.; Taylor, L. S.; Harris, M. T., Effect of substrates on naproxen-polyvinylpyrrolidone solid dispersions formed via the drop printing technique. *J Pharm Sci,* 2013, *102* (2), 638-648.

[156] Raijada, D.; Genina, N.; Fors, D.; Wisaeus, E.; Peltonen, J.; Rantanen, J.; Sandler, N., A step toward development of printable dosage forms for poorly soluble drugs. *J Pharm Sci,* 2013, *102* (10), 3694-704.

[157] Hirshfield, L.; Giridhar, A.; Taylor, L. S.; Harris, M. T.; Reklaitis, G. V., Dropwise additive manufacturing of pharmaceutical products for solvent-based dosage forms. *J Pharm Sci,* 2014, *103* (2), 496-506.

[158] Vakili, H.; Kolakovic, R.; Genina, N.; Marmion, M.; Salo, H.; Ihalainen, P.; Peltonen, J.; Sandler, N., Hyperspectral imaging in quality control of inkjet printed personalised dosage forms. *Int J Pharm,* 2015, *483* (1-2), 244-9.

[159] Elele, E.; Shen, Y.; Khusid, B., Electrodeless electrohydrodynamic printing of personalized medicines. *Appl Phys Lett,* 2010, *97* (23), 233501.

[160] Takala, M.; Helkiö, H.; Sundholm, J.; Genina, N.; Kiviluoma, P.; Widmaier, T.; Sandler, N.; Kuosmanen, P. In: *Ink-jet printing of pharmaceuticals*, Proceedings of the 8th International DAAAM Baltic Conference, 2012.

[161] Montenegro-Nicolini, M.; Miranda, V.; Morales, J. O., Inkjet printing of proteins: an experimental approach. *AAPS J,* 2017, *19* (1), 234-243.

[162] Elele, E.; Shen, Y.; Susarla, R.; Khusid, B.; Keyvan, G.; Michniak-Kohn, B., Electrodeless electrohydrodynamic drop-on-demand encapsulation of drugs into porous polymer films for fabrication of personalized dosage units. *J Pharm Sci,* 2012, *101* (7), 2523-2533.

[163] WHO (World Health Organization), *Toxicological evaluation of certain food additives with a review of general principles and of specifications - Seventeenth report of the Joint FAO/WHO Expert Committee on Food Additives*, 1974.

[164] ICH (International Council for Harmonisation of Technical Requirements for Pharmaceuticals for Human Use), *Q3C (R8): Impurities: guideline for residual solvents*, 2021.

[165] FDA (Food and Drug Administration), Inactive ingredient search for approved drug products. https://www.accessdata.fda.gov/scripts/cder/iig/index.cfm (accessed 25 September 2021).

[166] WHO (World Health Organization), *Evaluation of food additives: specifications for the identity and purity of food additives and their toxicological evaluation: some extraction solvents and certain other substances; and a review of the technological efficacy of some antimicrobial agents*, 14; Geneva, 1971, p 36.

[167] Mulla, M. A.; Yow, H. N.; Zhang, H.; Cayre, O. J.; Biggs, S., Colloid particles in ink formulations. In: *Fundamentals of inkjet printing: the science of inkjet and droplets*, Hoath, S. D., Ed. Wiley-VCH Verlag Weinheim, Germany: 2016; pp 141-168.

[168] EMA (European Medicines Agency), *Assessment report. Propylene glycol in medicinal products for children. Committee for Medicinal Products for Human Use (CHMP)*, EMA/175205/2014; 2014.

[169] Wheeler, J. S. R.; Yeates, S. G., Polymers in inkjet printing. In: *Fundamentals of inkjet printing: the science of inkjet and droplets*, Hoath, S. D., Ed. Wiley-VCH Verlag Weinheim, Germany: 2016; pp 117-139.

[170] S-class jetting assembly product manual. *Dimatix,* 2006, pp 1-86.

[171] Corall, J., Konica Minolta`s inkjet printhead technology. In: *Handbook of industrial inkjet printing: a full system approach*, Zapka, W., Ed. Wiley-VCH Verlag: 2017; pp 253-284.

[172] Kwon, K.-S.; Choi, Y.-S.; Go, J.-K., Inkjet jet failures and their detection using piezo self-sensing. *Sens Actuators A Phys,* 2013, *201*, 335-341.

[173] Breitkreutz, J. *Molecular Modeling-Studien und experimentelle Untersuchungen zur molekularen Struktur von Polyethylenglykolen und zu deren Wechselwirkungen mit Wasser und Phenol*. Doctoral thesis, University of Münster, 1996.

[174] Christopher, D. P.; Russel, R. P.; John, R. C. An ink suitable for ink jet printing. WO1999061533A1, 1999.

[175] Croucher, M. D.; Hair, M. L., Design criteria and future directions in ink-jet ink technology. *Ind Eng Chem Res,* 1989, *28* (11), 1712-1718.

[176] Kiefer, O.; Breitkreutz, J., Comparative investigations on key factors and print head designs for pharmaceutical inkjet printing. *Int J Pharm,* 2020, *586*, 119561.

[177] Merck, *Safety Data Sheet - Polyethylene glycol 400*, 2017, pp 1-14.

[178] Vazquez, G.; Alvarez, E.; Navaza, J. M., Surface tension of alcohol + water from 20 to 50 °C. *J Chem Eng Data,* 1995, *40* (3), 611-614.

[179] Khattab, I. S.; Bandarkar, F.; Fakhree, M. A. A.; Jouyban, A., Density, viscosity, and surface tension of water + ethanol mixtures from 293 to 323K. *Korean J Chem Eng,* 2012, *29* (6), 812-817.

[180] Kell, G., Precise representation of volume properties of water at one atmosphere. *J Chem Eng Data,* 1967, *12* (1), 66-69.

[181] Wijshoff, H., Drop formation mechanisms in piezo-acoustic inkjet. *Proc Nanotech2007*, 2007, *3*, 448.

[182] USP - U.S. Pharmacopeial Convention, *Safety Data Sheet - Levothyroxine*, 2018.

[183] Verheijen, M.; Lienhard, M.; Schrooders, Y.; Clayton, O.; Nudischer, R.; Boerno, S.; Timmermann, B.; Selevsek, N.; Schlapbach, R.; Gmuender, H., DMSO induces drastic changes in human cellular processes and epigenetic landscape in vitro. *Sci Rep,* 2019, *9* (1), 1-12.

[184] Madsen, B. K.; Hilscher, M.; Zetner, D.; Rosenberg, J., Adverse reactions of dimethyl sulfoxide in humans: a systematic review. *F1000Research,* 2018, *7*.

[185] Sigma-Aldrich, *Sicherheitsdatenblatt - Dimethylsulfoxid*, 2019, p 5.

[186] Konica Minolta, KM512 Series. https://www.konicaminolta.com/inkjet/inkjethead/512/spec.html (accessed 30 May 2021).

[187] Shandong Yuteng Industrial, Spectra Printhead Spectra S-Class SE-128 AA. https://www.yuten-digiprinter.com/spectra/251-spectra-printhead-spectra-s-class-se-128-aa-print-head.html (accessed 30 May 2021).

[188] Kerr, W.; Kelly, J.; Geddes, D., The areas of various surfaces in the human mouth from nine years to adulthood. *J Dent Res,* 1991, *70* (12), 1528-1530.

[189] Beurer, G.; Kretschmer, J. In: *Function and performance of a shear mode piezo printhead*, IS&T`s NIP 13: International Conference on Digital Printing Technologies, Seattle, 1997; pp 621-625.

[190] Rodriguez-Rivero, C.; Castrejón-Pita, J. R.; Hutchings, I. M., Aerodynamic effects in industrial inkjet printing. *J Imaging Sci Technol,* 2015, *2015* (1), 29-38.

[191] Alomari, M. H. A. *Application of thermal inkjet systems: Personalised dosing of medicines*. Doctoral thesis, University College London, 2016.

[192] Takeuchi, Y., Konica Minolta, Improvement of drive energy efficiency in a shear mode piezo-inkjet head. https://www.konicaminolta.com/inkjet/technology/report.html (accessed 22 May 2020).

[193] Deegan, R. D.; Bakajin, O.; Dupont, T. F.; Huber, G.; Nagel, S. R.; Witten, T. A., Capillary flow as the cause of ring stains from dried liquid drops. *Nature,* 1997, *389* (6653), 827-829.

[194] Talbot, E.; Bain, C.; De Dier, R.; Sempels, W.; Vermant, J., Droplets drying on surfaces. In: *Fundamentals of inkjet printing: the science of inkjet and droplets*, Hoath, S. D., Ed. Wiley-VCH Verlag Weinheim, Germany: 2016; pp 251-279.

[195] Scriven, L.; Sternling, C., The marangoni effects. *Nature,* 1960, *187* (4733), 186-188.

[196] Soltman, D.; Subramanian, V., Inkjet-printed line morphologies and temperature control of the coffee ring effect. *Langmuir,* 2008, *24* (5), 2224-2231.

[197] Kadonaga, M., Recent progress of inkjet simulations. *J Imag Soc Japan,* 2018, *57* (6), 685-691.

[198] Ph. Eur. 9.1, *2.9.40 Uniformity of dosage units*, In: European Pharmacopoeia Comission (Ed.). European Pharmacopoeia, European Directorate for the Quality of Medicines & Healthcare (EDQM), Strasbourg, France, 2017.

[199] FDA (Food and Drug Administration), *Highlights of prescribing information: Levothyroxine sodium tablets*, 2019, pp 1-19.

[200] Paoli, P.; Rossi, P.; Macedi, E.; Ienco, A.; Chelazzi, L.; Bartolucci, G. L.; Bruni, B., Similar but different: The case of metoprolol tartrate and succinate salts. *Cryst Growth Des,* 2016, *16* (2), 789-799.

[201] Rossi, P.; Paoli, P.; Chelazzi, L.; Conti, L.; Bencini, A., Metroprolol fumarate: Crystal structure from powder X-ray diffraction data and comparison with the tartrate and succinate salts. *Cryst Growth Des,* 2018, *18* (11), 7015-7026.

[202] FDA (Food and Drug Administration), *Validation of cleaning processes (7/93) - Guide to inspections validation of cleaning processes*, 1993.

[203] EMA (European Medicines Agency), *Guideline on setting health based exposure limits for use in risk identification in the manufacture of different medicinal products in shared facilities*, 2015.

[204] APIC (Active Pharamceutical Ingredients Comittee), *Guidance on aspects of cleaning validation in active pharmaceutical ingredient plants*, 2021, pp 1-62.

[205] Product Monograph - TEVA Metoprolol tartrate. *Teva,* 2018.

[206] Pardeike, J.; Strohmeier, D. M.; Schrodl, N.; Voura, C.; Gruber, M.; Khinast, J. G.; Zimmer, A., Nanosuspensions as advanced printing ink for accurate dosing of poorly soluble drugs in personalized medicines. *Int J Pharm,* 2011, *420* (1), 93-100.

[207] Hoffmann, E. M. *Flexible Arzneistoffbeladung orodispersibler Filme durch Bedrucken*. Doctoral thesis, Heinrich-Heine-Universität Düsseldorf, 2012.

[208] Garsuch, V. *Preparation and characterization of fast-dissolving oral films for pediatric use*. Doctoral thesis, Heinrich-Heine-Universität Düsseldorf, 2009.

[209] Preis, M.; Pein, M.; Breitkreutz, J., Development of a taste-masked orodispersible film containing dimenhydrinate. *Pharmaceutics,* 2012, *4* (4), 551-562.

[210] Film applicators TBE 284/286/288/358/360/411/421 - V/16. *Erichsen,* 2016.

[211] Betriebsanleitung - Microcontroller Trocknungs- und Filmziehgerät - Multicator 511. *Erichsen,* 2007.

[212] Wörtz, C. *Entwicklung und Charakterisierung von orodispersiblen Polymerfilmen mit suspendiertem Arzneistoff*. Doctoral thesis, Heinrich-Heine-Universität Düsseldorf, 2015.

[213] Krampe, R. *Orodispersible Filme mit schwerlöslichem, hochdosiertem Arzneistoff: Herstellungstechniken und biorelevante Beurteilung*. Doctoral thesis, Heinrich-Heine-Universität Düsseldorf, 2016.

[214] Niese, S.; Quodbach, J., Application of a chromatic confocal measurement system as new approach for in-line wet film thickness determination in continuous oral film manufacturing processes. *Int J Pharm,* 2018, *551* (1), 203-211.

[215] Visser, J. C.; Woerdenbag, H. J.; Hanff, L. M.; Frijlink, H. W., Personalized medicine in pediatrics: The clinical potential of orodispersible films. *AAPS Pharm Sci Tech,* 2017, *18* (2), 267-272.

[216] Meggle, *Technical brochure FlowLac®*, 2020, pp 1-7.

[217] Takami, K.; Machmura, H.; Takado, K.; Inagaki, M.; Kawashima, Y., Novel praparation of free flowing spherically granulated dibasic calcium phosphate anhydrous for direct tabletting. *Chem Pharm Bull,* 1996, *44* (4), 868-870.

[218] Tadros, T. F., *Dispersion of powders: in liquids and stabilization of suspensions*. John Wiley & Sons: 2012.

[219] Prasad, L. K.; McGinity, J. W.; Williams, R. O., Electrostatic powder coating: Principles and pharmaceutical applications. *Int J Pharm,* 2016, *505* (1), 289-302.

[220] Khan, M. K. I.; Schutyser, M. A.; Schroën, K.; Boom, R. M., Electrostatic powder coating of foods – State of the art and opportunities. *J Food Eng,* 2012, *111* (1), 1-5.

[221] Kinloch, A. J., The science of adhesion. *J Mat Sci,* 1980, *15* (9), 2141-2166.

[222] Speer, I.; Steiner, D.; Thabet, Y.; Breitkreutz, J.; Kwade, A., Comparative study on disintegration methods for oral film preparations. *Eur J Pharm Biopharm,* 2018, *132*, 50-61.

[223] Brunauer, S.; Emmett, P. H.; Teller, E., Adsorption of gases in multimolecular layers. *J Am Chem Soc,* 1938, *60* (2), 309-319.

[224] Villalobos, R.; Hernández-Muñoz, P.; Chiralt, A., Effect of surfactants on water sorption and barrier properties of hydroxypropyl methylcellulose films. *Food Hydrocoll,* 2006, *20* (4), 502-509.

[225] Debeaufort, F.; Voilley, A., Methyl cellulose-based edible films and coatings I. Effect of plasticizer content on water and 1-octen-3-ol sorption and transport. *Cellulose,* 1995, *2* (3), 205-213.

[226] Edinger, M.; Bar-Shalom, D.; Sandler, N.; Rantanen, J.; Genina, N., QR encoded smart oral dosage forms by inkjet printing. *Int J Pharm,* 2018, *536* (1), 138-145.

[227] Lenhart, V.; Quodbach, J.; Kleinebudde, P., Fibrillated cellulose via high pressure homogenization: Analysis and application for orodispersible films. *AAPS PharmSciTech,* 2019, *21* (1), 33.

[228] Conder, E. W.; Cosbie, A. S.; Gaertner, J.; Hicks, W.; Huggins, S.; MacLeod, C. S.; Remy, B.; Yang, B.-S.; Engstrom, J. D.; Lamberto, D. J.; Papageorgiou, C. D., The pharmaceutical drying unit operation: an industry perspective on advancing the

science and development approach for scale-up and technology transfer. *Org Process Res Dev* 2017, *21* (3), 420-429.

[229] Abbott, S.; Kapur, N.; Sleigh, P.; Thompson, H.; Summers, J., Industrial film drying. *Convertech & e-Print,* 2011, *1*.

[230] Velaga, S. P.; Nikjoo, D.; Vuddanda, P. R., Experimental studies and modeling of the drying kinetics of multicomponent polymer films. *AAPS PharmSciTech,* 2018, *19* (1), 425-435.

[231] Vanderhoff, J.; Bradford, E.; Carrington, W. In: *The transport of water through latex films*, J Polym Sci Polym Symp, Wiley Online Library: 1973; pp 155-174.

[232] Steward, P.; Hearn, J.; Wilkinson, M., An overview of polymer latex film formation and properties. *Adv Colloid Interface Sci,* 2000, *86* (3), 195-267.

[233] Rösch, M. *Potenziale und Strategien zur Optimierung des Schablonendruckprozesses in der Elektronikproduktion*. Doctoral thesis, Friedrich-Alexander-Universität Erlangen-Nürnberg, 2011.

[234] Garsuch, V.; Breitkreutz, J., Comparative investigations on different polymers for the preparation of fast-dissolving oral films. *J Pharm Pharmacol,* 2010, *62* (4), 539-545.

[235] Niese, S.; Quodbach, J., Formulation development of a continuously manufactured orodispersible film containing warfarin sodium for individualized dosing. *Eur J Pharm Biopharm,* 2019, *136*, 93-101.

[236] Chou, W.-H.; Galaz, A.; Jara, M. O.; Gamboa, A.; Morales, J. O., Drug-loaded lipid-core micelles in mucoadhesive films as a novel dosage form for buccal Aadministration of poorly water-soluble and biological drugs. *Pharmaceutics,* 2020, *12* (12), 1168.

[237] Precitec, Line Sensor. https://www.precitec.com/optical-3d-metrology/products/line-sensors/ (accessed 17 July 2021).

[238] Precitec, Area Scan Sensor. https://www.precitec.com/optical-3d-metrology/products/area-scan-sensor/ (accessed 17 July 2021).

[239] Mezger, T. G., Oszillationsversuche. In: *Das Rheologie Handbuch*, Vincentz Network: 2016.

[240] Naseri, A. T.; Cetindag, E.; Bilgili, E.; Davé, R. N., A predictive transport model for convective drying of polymer strip films loaded with a BCS Class II drug. *Eur J Pharm Biopharm,* 2019, *137*, 164-174.

[241] Naseri, A. T.; Cetindag, E.; Forte, J.; Bilgili, E.; Davé, R. N., Convective drying kinetics of polymer strip films loaded with a BCS class II drug. *AAPS PharmSciTech,* 2019, *20* (2), 40.

[242] Edinger, M.; Jacobsen, J.; Bar-Shalom, D.; Rantanen, J.; Genina, N., Analytical aspects of printed oral dosage forms. *Int J Pharm,* 2018.

[243] Scarpa, M.; Stegemann, S.; Hsiao, W.-K.; Pichler, H.; Gaisford, S.; Bresciani, M.; Paudel, A.; Orlu, M., Orodispersible films: Towards drug delivery in special populations. *Int J Pharm,* 2017.

[244] ICH (International Council for Harmonisation of Technical Requirements for Pharmaceuticals for Human Use), *Q8 (R2): Pharmaceutical development*, Step 4; 2009.

[245] Hutchings, I. M.; Martin, G. D., *Inkjet technology for digital fabrication*. John Wiley & Sons: 2012.

[246] Levy, O., Innate immunity of the newborn: basic mechanisms and clinical correlates. *Nat Rev Immunol,* 2007, *7* (5), 379-390.

[247] Ph. Eur. 10.1, *2.4.24 Identification and control of residual solvents*, In: European Pharmacopoeia Comission (Ed.). European Pharmacopoeia, European Directorate for the Quality of Medicines & Healthcare (EDQM), Strasbourg, France, 2020.

[248] Engström, E. *Printing and spectrometric detection of active pharmaceutical ingredients on different surfaces*. Master thesis, Åbo Akademi University, 2021.

[249] Palo, M.; Kogermann, K.; Genina, N.; Fors, D.; Peltonen, J.; Heinämäki, J.; Sandler, N., Quantification of caffeine and loperamide in printed formulations by infrared spectroscopy. *J Drug Deliv Sci Technol,* 2016, *34*, 60-70.

[250] Inoue, M.; Kiefer, O.; Fischer, B.; Breitkreutz, J., Raman monitoring of semi-continuously manufactured orodispersible films for individualized dosing. *J Drug Deliv Sci Technol,* 2020, 102224.

[251] PixDro LP50 user manual. *Meyer Burger*, v. V5.1. 2015.

[252] Formulaction, Microfluidics by optical imaging. https://www.formulaction.com/en/products-and-technologies/technologies/microfluidics-by-optical-imaging (accessed 24 September 2021).

[253] Schindelin, J.; Arganda-Carreras, I.; Frise, E.; Kaynig, V.; Longair, M.; Pietzsch, T.; Preibisch, S.; Rueden, C.; Saalfeld, S.; Schmid, B., Fiji: an open-source platform for biological-image analysis. *Nat Methods,* 2012, *9* (7), 676-682.

[254] Optischer Sensor CHRocodile S - Bedienungsanleitung. *Precitec Optronik,* v. 02/2016. pp 2-18, 2-19.

[255] Radebaugh, G. W.; Murtha, J. L.; Julian, T. N.; Bondi, J. N., Methods for evaluating the puncture and shear properties of pharmaceutical polymeric films. *Int J Pharm,* 1988, *45* (1-2), 39-46.

[256] Fell, J.; Newton, J., Determination of tablet strength by the diametral-compression test. *J Pharm Sci*, 1970, *59* (5), 688-691.

[257] CDER (Center for Drug Evaluation and Research), *Reviewer guidance - validation of chromatographic methods*, 1994.

[258] ICH (International Council for Harmonisation of Technical Requirements for Pharmaceuticals for Human Use), *Q2 (R1): Validation of analytical procedures: text and methodology*, 2005.

8 Danksagung

Die vorliegende Arbeit entstand unter der Leitung von Herrn Prof. Dr. Jörg Breitkreutz und der Betreuung von Herrn Prof. Dr. Dr. h.c. Peter Kleinebudde im Rahmen meiner Tätigkeit als wissenschaftliche Mitarbeiterin am Institut für Pharmazeutische Technologie und Biopharmazie der Heinrich-Heine-Universität Düsseldorf.

Meinem Doktorvater Herrn Prof. Dr. Jörg Breitkreutz danke ich herzlich für die Aufnahme in seinen Arbeitskreis und die damit gegebene Möglichkeit ein interessantes, ungewöhnliches und innovatives Promotionsthema zu bearbeiten. Ich möchte Ihnen besonders für die gute Betreuung, Ihre Diskussionsbereitschaft und immerzu aufbauenden Worte danken. Wenn man Ihr Büro verlässt, weiß man gar nicht mehr, mit welcher Sorge man hineingegangen ist.

Frau Prof. Anne Seidlitz danke ich für die spontane Übernahme des Koreferats.

Herrn Prof. Dr. Peter Kleinebudde danke ich für die gute Mitbetreuung, die kritischen Fragen sowie hilfreichen Denkanstöße während der Fokusgruppen und Doktorandenseminaren. „Keep it simple!“

Herrn Jun.-Prof. Dr. Michael Hacker danke ich für die voranbringenden Ideen in und außerhalb der Fokusgruppen.

Bei allen Professor*innen möchte ich mich ganz besonders für Ihre stetige Ansprechbarkeit, die offene, kollegiale und lernbegierige Atmosphäre am Institut und die Möglichkeit der Teilnahmen an zahlreichen internationalen Konferenzen, Fort- und Weiterbildungen bedanken.

Dr. Klaus Knop danke ich für seine Hilfsbereitschaft und das Korrekturlesen dieser Arbeit.

Dr. Björn Fischer danke ich für die Konstruktion des XYZ-Rahmens, die Messungen am konfokalen Raman-Mikroskop in seiner Firma und die fachliche Unterstützung bei deren Auswertung.

Meinem Vater Dimitri Kapelnikov danke ich für seine virtuosen 3D-Animationen. Diese haben meine Doktorandenvorträge und Präsentationen auf Konferenzen mehr als bereichert. Vielen Dank, dass ich einige Darstellungen in der vorliegenden Arbeit verwenden konnte.

Ard Lura, dem besten Büronachbar der Welt, gilt mein herzlicher Dank für die tägliche besondere musikalische Begleitung, die moralische Unterstützung in jeglichen Phasen der

Promotionsarbeit, die zahlreichen Gespräche über dies und für unseren Papp-Bürokollegen John (auch wenn seine Anschaffung ich übernommen habe). Es war die beste Idee mit dir in den Keller zu ziehen. #famebüro

Dr. Hannah Lou Keizer danke ich von ganzem Herzen für die tolle U2-Nachbarschaft, die vielen motivierenden Fach- und Nichtfach-Gespräche sowie die wundervolle Freundschaft, die in Granada auf der Polizeistation mit einer Tüte Lakritz-Pandas begann.

Anja Göbel danke ich besonders für die aufschlussreichen Film-Fachsimpeleien, die schöne gemeinsame Zeit im und außerhalb des Filmlabors sowie für das Korrekturlesen des Film-Kapitels dieser Arbeit. Eine filmtastische Freundschaft entstand!

Laura Falkenstein danke ich für Alice in London, die gute HPLC-Nachbarschaft, die tollen Kaffeepäuschen und den Notsüßigkeitenvorrat. Er hat mich nicht nur einmal gerettet!

Den Office-Boys initial bestehend aus Philipp Kiefer, Bastian Hahn und Dr. Martin Günter Müller, danke ich für eure immerzu offene Büro-Tür. Marcel Kokott danke ich für die nicht abreißende Milchschnitte- und Kinderriegel-Versorgung. Stefan Klinken danke ich für die tapfere Mitbetreuung der E-tongue und sein offenes Ohr für alle Arten von Statistikfragen.

Bei Dr. Svenja Niese und Dr. Yasmin Thabet möchte ich mich für die Einführung in die Film- und Druckwelt in meiner Anfangszeit bedanken.

Dorothee Eikeler, Dorothee Hetkämper-Flockert, Andrea Michel, Simone Mönninghoff-Pützer und Stefan Stich danke ich für die fachliche und technische Unterstützung sowie Organisation bei den Studierendenpraktika und meiner eigenen Promotionsarbeit.

Lisa Man und Vanessa Weggen danke ich für euer unglaubliches Organisationstalent und immer fortwährende moralischen Beistand.

Den Studierenden Lukas Bollmann und Rebecca Schiffer, Arne Schulzen und Simon Schulte-Herbrüggen, Shahzad Sayyed und Hadia Ahmad danke ich für die produktive und gute Mitarbeit während der Wahlpflichtpraktika.

Dr. J. Caroline Visser, thank you very much for the opportunity to collaborate and for the fruitful scientific exchange.

Dr. Motoki Inoue, thank you very much for the good cooperation and the introduction in the manifold Japanese culture.

Ein ganz besonderer Dank geht an meine Eltern. Danke, dass ihr mir all das ermöglicht habt und mich in jeglicher Lebens- und Promotionslage mit immerzu guten Ratschlägen und eurem Glauben an mich unterstütz. Ihr schenkt mir Rückhalt und Kraft.

Philipp, vielen Dank für deinen unendlichen Optimismus, deine Geduld und Unterstützung in jeglicher Hinsicht. Ohne dich hätte ich diesen Wahnsinn nicht auf mich genommen und schon lange nicht durchgehalten. Danke dir, dass du ein Teil meines Lebens geworden bist!

9 Eidesstattliche Erklärung

Hiermit versichere ich an Eides Statt gemäß § 5 Abs. 1 der Promotionsordnung der Mathematisch-Naturwissenschaftlichen Fakultät der Heinrich-Heine-Universität Düsseldorf, dass die Dissertation von mir selbständig und ohne unzulässige fremde Hilfe unter Beachtung der „Grundsätze zur Sicherung guter wissenschaftlicher Praxis an der Heinrich-Heine-Universität Düsseldorf“ erstellt worden ist. Die vorliegende Arbeit wurde in dieser oder ähnlicher Form noch bei keiner anderen Fakultät eingereicht.

_____

Olga Kiefer